College of Optical Sciences

THE UNIVERSITY OF ARIZONA®

College of Optical Sciences

THE UNIVERSITY OF ARIZONA.

The booklet of the *College of Optical Sciences*, University of Arizona, Tucson (2014)

Edited by Masud Mansuripur

Cover Photo (Courtesy of Chris Summitt): The Optical Sciences Building

The west wing of the Optical Sciences building is one of the most striking and beautiful on campus. The west wing has received many architechtural awards, and it is not uncommon to see architechture students in the courtyard sketching the building, or modern dance students during an in-class recital on the grassy knoll just outside the building. Inside and out, the west wing of the college is a wonderful and comforting place to work and study.

Beautiful glass sculptures can be found outside and inside the building. The Optical Sciences building is also home to the Museum of Optics, containing a collection of optical instruments such as antique and histroic telescopes, microscopes, lenses, and cameras dating from the 18th century to the present.

Desert Flower, a glass sculpture in the lobby of the West Wing of the College of Optical Sciences, by Christopher Ries, 2006. (Donated by *SCHOTT North America, Inc.*)

Photo Courtesy of Chris Summitt

The College of Optical Sciences 2014 Booklet

Table of Contents

Brief Introduction to the College of Optical Sciences

Welcome to the *College of Optical Sciences* at the University of Arizona. As we celebrate the 50th anniversary of the founding of the college in 1964, it is rewarding to reflect on the growth and tremendous impact the college has had on education and research in the field of Optics.

On behalf of the faculty and staff of the college, I am thrilled that we can bring so many opportunities to students as they enter such a dynamic and exciting field. From its inception as the *Optical Sciences Center* our focus was on graduate education, and the college has now produced nearly 700 Ph.D. and 1200 M.S. students. Some 20 years ago we expanded our mission to include undergraduates and have produced nearly 500 B.S. professionals to date. Together, these represent a significant fraction of today's world-wide professional talent in this field.

Our students benefit from an unparalleled breadth of courses now numbering over 100, and many have enjoyed unusual opportunities to gain experience in real, deployed optical systems. In our engineering areas, many of our faculty have substantial industry experience, and are able to effectively convey the essential tradeoffs and integration of design, materials, and fabrication. In the fundamental science areas, we pursue high-risk, provocative new ideas, and we are proud to count three Nobel prize winners among our faculty. Many of our faculty have been recognized in the National Academies and professional societies both with awards for their accomplishments and in leadership roles.

From the very beginning, by attracting the nation's top talent in optics to our faculty, the initial focus on optical design and engineering quickly blossomed to include exceptional research programs in the most fundamental of optical physics, image science, and the rapidly growing technologies of photonics and fiber optics. Today our students and faculty are making research advances that enable breakthroughs in science, ranging from astronomy and exo-planet research to quantum information and control. Their research programs and collaborations are improving the world around us every day, enabling exciting and often lucrative new applications of optics and photonics in fields ranging from medicine to optical communications, and from critical defense technologies to entertainment.

This booklet provides a glimpse into the *College of Optical Sciences* research programs for our prospective students. Here you will learn about the science and technology that is the focus of attention of many of our faculty members. You will also see many pictures of the U.A. campus, our buildings and laboratories, our faculty and students at work, and also the beautiful scenes in and around Tucson where our students, faculty, and staff live and work.

Thomas L. Koch, Dean
College of Optical Sciences

Our Academic Program

John Koshel, Associate Dean for Academic Affairs

When the *Optical Sciences Center* was formed in 1964, its mission statement included the directive to "provide an internationally preeminent program in education," which has been steadfastly maintained as the Center evolved into the *College of Optical Sciences*. The college boasts one of the best educational programs in the field and, being the largest, teaches more students in various disciplines of Optics than any other institution in the United States. As the College approaches its 50th anniversary in 2014, more than 2200 degrees in Optical Sciences & Engineering have been awarded at all levels. Initially the program conferred only Master's and Doctoral degrees. However, over the years the program has evolved and grown in response to changing national and international needs. Our College provides a comprehensive education in the burgeoning field of Optics, such that our graduates are in great demand and are employed at the international level by governments and laboratories, by businesses, and by universities in the United States and abroad.

Our Optics academic program is comprised of a world-class faculty, an international student body, an undergraduate Optical Sciences & Engineering degree program, and Optical Sciences Master's and Doctoral degree programs. Distance-learning classes provide students thoughtout the world with opportunities to undertake Master's degrees and graduate certificates.

Undergraduates at pre-commencement (2014)

By 2014, there are over one hundred graduate and undergraduate courses, with more than 35 of these courses offered in conjunction with our distance-learning program. Classes are offered in four primary areas: *Optical Engineering*, *Optical Physics*, *Photonics*, and *Image Science*. In the distance-learning program, students are part of the on-campus instruction, watching streamed videos of the lectures, completing the same assignments as campus students, taking the class examinations, and engaging in course projects. Projects generally involve written as well as oral presentations; for the latter, the students participate in classroom activities through "virtual meeting" software, enabling them to both present their work and to ask questions from instructors and fellow students.

The *College of Optical Sciences* presently offers the following degree programs:

Undergraduate Degrees

- *Bachelor of Science in Optical Sciences & Engineering*. Our B.S. in OS&E program, jointly administered with the UA College of Engineering, gives our graduates skills needed to succeed in the modern Optics workforce. The OS&E degree is accredited by ABET, which means it has an actively reviewed curriculum that meets approved national standards. The senior-year activities include a team Capstone project involving students from several engineering and science disciplines. Additionally, there are numerous tracks (optics, opto-electronics, optical materials, opto-mechanics) in the B.S. OS&E degree program that enable students to specialize in their desired area.
- *Optics Minor.* Interested undergraduates can supplement their major with upper-level classes in Optics. The Optics minor prepares undergraduates for a career in Optics that requires primarily knowledge and expertise in other disciplines; it also encourages students to pursue graduate studies in Optical Sciences.

Graduate Degrees

- *Professional Graduate Certificate in Optical Sciences.* The Graduate Certificate provides post-undergraduate eduction for those needing insight into the field of Optics for their professional career. Professionals who have Bachelor's, Master's, or even Doctorate degrees in science and technology, while actively working for the industry or for government labs, are perfect candidates for this degree program. Thus, it is an ideal scholarly pursuit for those seeking to extend their education through distance learning; however, resident students on campus are also allowed to take the relevant courses and obtain a professional certificate.
- *Professional Graduate Certificate in Photonic Communications Engineering.* Similar to the Certificate in Optical Sciences, this Graduate Certificate program provides a unique opportunity for those working in the comunications industry. Along with the *Center for Integrated Access Networks* (*CIAN*), the College administers this program for individuals with similar backgrounds to those who pursue the Certificate in Optical Sciences. Interested students are also encouraged to take additional courses in entrepreneurship and marketing.
- *Master of Science in Optical Sciences.* The M.S. in Optical Sciences degree equips its graduates with the tools to undertake fulfilling careers in industry or for continued academic studies. This degree program is offered both on-campus and on-line via distance learning. The program curriculum is flexible, allowing the student to tailor his/her own plan of studies. Three options are available: thesis, non-thesis with a final report, and non-thesis with comprehensive course evaluation. The students receiving a Master's degree in Optical Sciences typically pursue careers in industry, go on to doctoral studies, or work in research centers such as government laboratories.
- *M.S. in Optical Sciences and MBA Dual Degree.* This one-of-a-kind degree program offers students an opportunity to gain two prestigious degrees concurrently—one from the *College of Optical Sciences* and one from the *UA Eller College of Management*. This gives the student a powerful advantage for entrepreneurial success. At the conclusion of their studies, students in this program present their Optics master's report and their MBA summer project.
- *Master of Science in Photonic Communications Engineering.* The M.S. in PCE, presented in conjunction with the *College of Engineering* and the *College of Optical Science*'s CIAN, educates engineers for modern photonic engineering challenges with an emphasis on industrial relevance in the burgeoning field of telecommunications. The M.S. PCE degree may be pursued by campus students, or online through distance learning, with both thesis and non-thesis options available.

- *Doctor of Philosophy in Optical Sciences.* The Ph.D. in Optical Sciences opens windows to extraordinary careers in Optics, whether in academia, research institutes, or industry. A set of required core topics gives all students a firm foundation in applied math and physics, particularly electromagnetic theory, geometrical optics, physical optics, quantum optics and optical physics, and solid-state optics. The curriculum has some degree of flexibility that enables students to tailor their studies to their areas of technical interest. Comprehensive exams, both written and oral, test the students' knowledge early in their doctoral student careers, while the thesis proposal and the final dissertation defense ensure that the students can conduct independent research and present their findings in professional forums. Doctoral students work on state-of-the-art optics projects with their chosen advisors. The College provides opportunities for independent research in diverse areas of optical science and engineering.
- *Optics Minor.* Graduate students from other programs can supplement their education with courses from the *College of Optical Sciences*. The minor in Optics allows these students to add to their research experience and understanding of Optics.

Associate Dean Dr. John Koshel with pre-commencement valedictorian Dr. Laura Coyle (2014)

Laser Fun Day (2014)

Pre-commencement (2014)

The degrees comprise the formal aspects of Optics education, but the College also engages in an active outreach program by presenting and instructing Optics to students and teachers of all ages, especially from elementary to high-school levels. This outreach not only teaches about the field, but also provides an excellent introduction to the College and to the exciting world of Optics.

Look but don’t touch: cactus flowers are some of the most beautiful and surprising elements of the desert.

Photo Courtesy of Brian Anderson

Turbulent Times in Quantum Physics: Exploring Fluid Dynamics at Absolute Zero

Brian P. Anderson

The *College of Optical Sciences* is home to the coldest spot in Arizona. My research group uses laser light to trap dilute vapors of rubidium atoms, cool them to temperatures below 100 billionths of a degree above absolute zero, and then manipulate these gases to study the relationships between fluid dynamics, turbulence, and quantum mechanics in weakly interacting systems. At the end of a typical cooling sequence that involves numerous stages, about one million rubidium atoms remain levitated inside a vacuum chamber by magnetic and laser fields, and comprise an ultracold droplet of dilute atomic superfluid called a Bose-Einstein condensate (BEC). The BEC droplets created in my lab are about 50 microns in diameter, and are about the same shape as a human white blood cell although about five times larger—big enough to study using novel imaging techniques. To produce these BECs, a 14-foot optical table packed full of optics and lasers, shelves full of electronics, and an intricately timed sequence of events are needed.

While atomic BECs are now routinely created in laboratories throughout the world, they were only first produced in 1995, the achievement of a significant milestone of physics that had been pursued for 70 years, and which was honored with the 2001 Nobel Prize in Physics. The techniques used to bring the gases to such low temperatures in these earlier BEC experiments and now in my lab utilize laser cooling, a now-common method for reducing the kinetic energy of a small sample of atoms in a vapor by transferring that energy to laser light. After laser cooling brings the temperature of a dilute atomic vapor down to the micro-Kelvin scale, other techniques are then used to reach the nano-Kelvin scale needed for BEC creation. The record-breaking temperatures reached in experiments with ultracold gases are indeed the coldest temperatures that we are aware of in the universe, and to our knowledge, they can only be created in a laboratory. But well beyond this attention-grabbing claim, these gases are important platforms for exploring a wide array of interesting and significant outstanding problems in basic physics, such as the nature of turbulence, due to their unique properties and their amenability to probing, manipulation, and observation with laser light. Such fundamental physics studies thus fit in well among the broad range of scientific topics pursued at the *College of Optical Sciences*.

At the extreme low end of the energy spectrum, atomic BECs display behaviors that are not found in classical systems of everyday familiarity, such as the air we breath or drops of rain. For example, the methods that have been developed for understanding the flow of water or air fail to accurately account for the flow dynamics of a BEC. This is because a BEC is an example of a superfluid—a fluid that can move without losing energy to its container due to the conversion of kinetic energy to heat by friction. A superfluid, in principle, can therefore continue to flow indefinitely without slowing down. Superfluids also have regions of circulating fluid that are characterized by quantum vortices. Vortices in classical fluids are common—the circulation of air masses around the eye of a hurricane is one such example of an enormous vortex—but a quantum vortex is substantially different. We can picture the fluid-free core of a quantum vortex as the smallest possible “eye of the hurricane” that can exist in a quantum fluid. Because of the existence of a single wavefunction that can be used to characterize the entire BEC, a vortex is quantized in the sense that it cannot gradually and continually spin up or spin down, like a hurricane or an eddy in a pool of water can. Rather, if a superfluid is somehow set spinning, one would observe a regular array of individual vortices rather than one large vortex core: the

number of vortices that would be observed in this case is related to how much angular momentum there is in the superfluid.

More generally, complex dynamics of quantum vortices in a superfluid serve as indicators of complex fluid dynamics, such as turbulence. By examining the motion of the cores of the quantum vortices in a superfluid, one can thus learn about the motion of fluids that have a quantum-mechanical nature, such as BECs. Unfortunately these cores are tricky to observe in an experiment, due to the fragility of the BEC (simply shining laser light on it can destroy it), and due to the small size of the vortex cores (typically they have diameters on the order of the wavelength of imaging light).

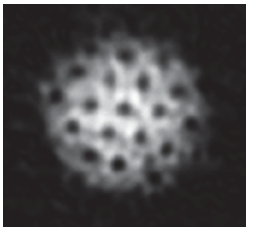

Fig. 1. A triangular lattice of vortices in a BEC is the primary signature that the droplet of atomic superfluid is uniformly rotating. In other words, by looking at the distribution of vortex cores, we can tell that the BEC is rotating.

In prior work at the University of Arizona, my group showed that a laser beam that is gently pushed through a BEC can produce a pair of vortices within the BEC, with the direction of fluid circulation about each vortex opposite that of the other vortex. Such a pair of vortices is called a vortex dipole, due to the equal and opposite fluid circulation directions. The vortices orbit two halves of the BEC in opposite directions, motion that can be observed by acquiring snapshots of vortices produced in sequential BECs using the same gentle stirring procedure. This experiment demonstrates that by using laser beams to gently stir a BEC, the energy of stirring can be gently placed into fluid circulation without destroying the fragile BEC or heating it up significantly.

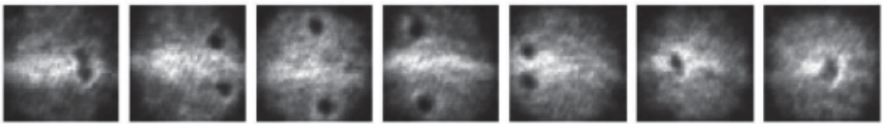

Fig. 2. A stroboscopic sequence of images shows the motion of two vortices of opposite circulation. The vortices are created by sweeping a laser beam through the BEC, setting up dipolar fluid flow, with circulation carried by the vortices. The fluid flow is laminar: that is, it is regular, predictable, and the vortex nucleation process is repeatable.

My experimental team and theory collaborators currently focus on stirring up BECs with much more vigor: we are now exploring the laws and manifestations of two-dimensional turbulence in BECs, a very different regime from that of dipolar fluid flow. Research on two-dimensional turbulence in classical fluids has been studied for decades and has led to tremendous strides in understanding the complex dynamics in various systems whose flows are nominally confined to two dimensions, such as small portions of planetary atmospheres like Earth's or Jupiter's, or stratified flows within the ocean. As with three-dimensional turbulence, which is commonly encountered in a fast-flowing river or when water is rapidly stirred, there are numerous scientific challenges left to solve in this field. One of the central issues of turbulence is to relate microscopic flow dynamics to the stability of average quantities, such as how the energy density is distributed among flows of different characteristic length or momentum scales, and how the dynamics and these average quantities together change in time and space as energy is forced into the fluid or as kinetic energy dissipates and heats the fluid.

Although the creation of a BEC in a laboratory is a technical challenge, and although a BEC is a fragile microscopic droplet of dilute vapor that must be stirred with light, some of the

problems of two-dimensional turbulence are nevertheless dramatically simplified in BECs due to the laws of quantum mechanics and the weakness of the interactions between the atoms in the gas. In a BEC, the modeling of turbulence is rendered quantitatively accurate at a level that allows for the association of microscopic flow dynamics and vortex core distributions with average quantities such as energy spectra in analytically and numerically tractable ways. The equations used to study BECs and the motions of vortices permit theoretical approaches that are directly relevant to BEC experiments and observations, but not classical fluids. Condensates thus afford an entirely new approach to some of the most significant and challenging problems of fluid dynamics.

We recently experimentally demonstrated the production of two-dimensional turbulence and the characterization of its dynamics in a quantum-mechanical fluid for the first time. Our first step was to confine the BEC in a toroidal trap, one that makes the BEC acquire a shape similar to that of a digital video disc (DVD).

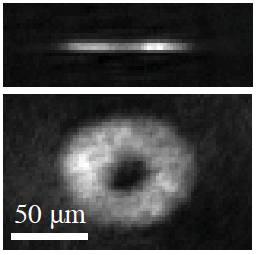

Fig. 3. A toroidally trapped BEC is seen from two orthogonal directions. The BEC has a shape much like that of a DVD: it is flat, as can be seen from the side-view of the upper image. Looking down the axis of the toroid in the lower image, we see that the BEC is round, and has a large region in the center where there is no atomic fluid. This hole in the BEC is not a vortex, but rather exists due to the presence of a laser beam that repels the atomic fluid.

After using a tightly focused laser beam to stir the BEC, a disordered distribution of numerous vortices within the BEC was observed, signifying the onset of two-dimensional quantum turbulence. As the system was left to evolve, the BEC started to uniformly rotate, signifying the transfer of fluid energy from small to large spatial scales, one of the characteristics of two-dimensional turbulence. Interestingly, it is this transfer of energy from small to large scales that may also provide the mechanism for the existence and longevity of Jupiter's Great Red Spot, a possible scenario for the mechanisms of two-dimensional turbulence in a classical fluid.

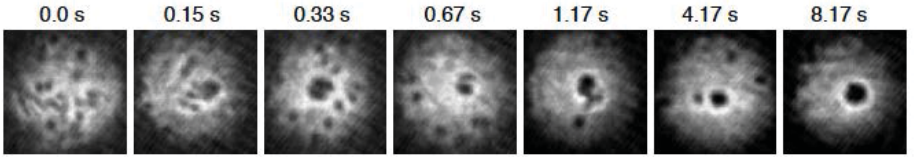

Fig. 4. In the left-most image, a disordered distribution of vortices in a BEC is observed after a laser beam rapidly stirs the BEC. The BEC then remains in the trap for a period of time indicated above the images. It is then released from the trap, it ballistically expands, and is then imaged. During expansion, vortices are observed as the holes in the fluid, and the hole in the middle of the BEC fills. As time evolves, the vorticity ends up being concentrated in the middle of the BEC, and the large hole that grows with time and is observed in the right-most image signifies the accumulation of kinetic energy at the largest length scales of the system. This growth of large-scale kinetic energy is a characteristic of the dynamics of two-dimensional quantum turbulence, previously observed in classical fluids, and observed here for the first time in a quantum fluid.

Numerous experiments on the creation, decay, and dynamics of two-dimensional quantum turbulence are now possible. For example, in a highly turbulent pancake-shaped BEC, vortices that have the same sign of circulation are predicted to cluster together. Making such an observation is one of the current goals of researchers in the field of two-dimensional quantum

turbulence. Many of these experiments, however, demand the real-time tracking of quantum vortices in a BEC. The challenge now is to find ways to observe these dynamics. To this end, my group is also now focused on pushing the limits of optical detection of vortices by pursuing real-time imaging and tracking of vortices, and our location at the *College of Optical Sciences* allows us to readily interact with numerous imaging experts. Techniques based on novel applications of dark-field imaging are currently in development, along with new methods for creating vortices on-demand and manipulating their positions with tightly focused laser beams. Someday soon, the marriage of all of these experimental techniques will permit novel approaches to probing, measuring, and even manipulating the characteristics of quantum turbulence in order to fully explore and better understand this one corner of the large puzzle of turbulence.

For more information on these and other research projects from my group and collaborators, please see the following publications:

1. *Characteristics of Two-Dimensional Quantum Turbulence in a Compressible Superfluid*, T.W. Neely, A.S. Bradley, E.C. Samson, S.J. Rooney, E.M. Wright, K.J.H. Law, R. Carretero-González, P.G. Kevrekidis, M.J. Davis, and B.P. Anderson, *Phys. Rev. Lett.* **111**, 235301 (2013).
2. *Observation of Vortex Dipoles in an Oblate Bose-Einstein Condensate,* T.W. Neely, E.C. Samson, A.S. Bradley, M.J. Davis, and B.P. Anderson, *Phys. Rev. Lett.* **104**, 160401 (2010).
3. *Spontaneous vortices in the formation of Bose–Einstein condensates,* C.N. Weiler, T.W. Neely, D.R. Scherer, A.S. Bradley, M.J. Davis, and B.P. Anderson, *Nature* **455**, 948 (2008).
4. *Energy Spectra of Vortex Distributions in Two-Dimensional Quantum Turbulence,* A.S. Bradley and B.P. Anderson, *Phys. Rev. X* **2**, 041001 (2012).

Doctoral Student Kali Wilson working in Professor Anderson's Laboratory

Associate Professor Brian P. Anderson has been a faculty member involved with Bose-Einstein condensate research at the University of Arizona since 2001. Prior to joining the faculty at the *College of Optical Sciences*, he earned his B.A. in Physics from Rice University in 1992, his M.S. and Ph.D. in Applied Physics from Stanford University in 1999, and he was a National Research Council Postdoctoral Scholar at NIST/JILA at the University of Colorado from 1999 to 2001. Anderson was the recipient of a 2004 Presidential Early Career Award for Scientists and Engineers, and is a fellow of the American Physical Society.

The Tucson region is home to an enormous variety of bird life, from golden eagles and great-horned owls (top photograph, pair of owls in neighboring palm trees) to hummingbirds (bottom photograph, a newly hatched hummingbird is pictured).

Photos courtesy of Brian Anderson

Optics for more efficient solar photovoltaic generation

Roger Angel

Photovoltaic modules are remarkable quantum machines. Made from thin slices of pure silicon stuck behind a sheet of glass, and with no moving parts, they silently convert sunlight directly into electricity. How different this is from 19th century generation, with rotating engines and electromagnetic machinery. A quality 3×5 foot standard panel yields over 300W when directly illuminated by the Sun. Globally, hundreds of millions of these panels were built and installed last year, mostly in large-scale generating plants. Yet PV modules are far from perfect. At best, they convert only around 20% of sunlight energy into electricity, while the rest simply warms up the panel. How can efficiency be improved? I lead a group which is exploring ways to use optics to make PV generation more efficient while at the same time reducing its cost, to ensure its use as a major source of carbon-free electricity.

Sunlight, as Newton showed, contains a spectrum of different colors—in fact, the range of photon energies extends well beyond that seen by the eye, into both the infrared and ultraviolet. In photovoltaic conversion, the energy of individual optical photons is transferred to electrons in a semiconductor, raising their electrical potential to a level set by the semiconductor bandgap. The electrons then release their energy in an external electrical circuit powered by the cell. From Einstein's equation $E = h\nu$, we know that blue photons (higher frequency, ν) carry more energy than red, and this energy can be harvested by a cell with a wide bandgap. The electrons are raised to a higher potential, and therefore deliver more energy. But a high bandgap cell will be transparent to lower energy (redder) photons, and thus unable to convert their energy.

The semiconductor used to make most solar cells is silicon. Its bandgap is 1.1 electron volt (eV), matched to infrared photons of wavelength 1.0 micron, which are converted to electrical energy with about 50% efficiency. However, the actual conversion efficiency of the best commercial PV modules to the *full solar spectrum* is much less, around 20%. This is because most of the Sun's energy is carried by bluer photons, whose full energy payload is not captured.

Photovoltaic conversion of sunlight with twice this efficiency is already achieved by photovoltaic cells developed for space power, which divide sunlight by color, and convert each color band separately by a PV cell with matched bandgap. These "multi-junction" cells are made commercially as a stack of several cells. The top cell has the highest bandgap, converting the blue part of the spectrum and transmitting longer wavelengths for conversion by red and infrared sensitive cells below. Stacks of four or more cells are under development, with commercial products of 50% and higher projected over the next decade. But multi-junction cells, made by successive deposition of many different thin film layers, are generally too expensive for terrestrial use in natural sunlight—they are only used in solar racing cars and aircraft, where there is a high premium of getting the highest power from fixed area.

There is the potential to exploit the very high efficiency of multi-junction cells at low cost, if sunlight from a large area is focused onto a very small cell area. This general strategy is called Concentrating Photovoltaic, or CPV. Per unit area, multi-junction cells cost around 200 times as much as standard PV modules. Therefore, operated at 1000× concentrated sunlight, and with double the conversion efficiency, their cost per watt of output will be ten times less. But if there are to be overall cost savings, the large area of optics to catch and concentrate light onto the cells must be inexpensive, as must be the mechanism to aim the configuration of optics and cells at the Sun as it moves through the sky. These challenges are being addressed by my group and a spin-off company, *REhnu*.

The optical concentrators being developed by the group are built around large dish reflectors. The figure above shows one made recently at the University of Arizona Mirror Lab from a flat sheet of glass. The glass is set over an accurately machined steel plate, and after heating to 650°C, it slumps to take on the shape of a paraboloidal dish. When silvered on the back, like a bathroom mirror, and aimed at the Sun, this mirror will bring 2.5 kW of sunlight to a sharp focus. Mirrors like this, but cylindrically curved, have been used for decades in utility solar thermal plants, in which sunlight is focused onto black pipes carrying hot oil to power a steam generator. The paraboloidal mirrors made in our new process bring the light to a more intense point focus, where multi-junction cells convert the concentrated sunlight energy with twice the efficiency of the steam-based process.

In operation, “mirror modules”, each comprising a mirror and converter at the focus, will be arrayed on tracking mounts to aim them at the Sun throughout the day. The figure above shows an architect’s rendition of several eight-module units in a small-scale desert generator. In this design concept, the modules are set high, so the natural desert vegetation does not have to be cleared.

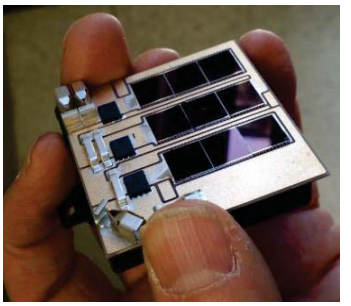

Production units to go at each mirror focus have been designed by *REhnu*, and are now being tested on-sun at the UA Solar Lab. The focused sunlight enters the unit, shown upper left, through a ball lens of fused silica. The lens stabilizes the light in a sharp, square image of the mirror. This image is relayed to the cells by a folded metal reflector—origami optics—designed to deliver the light precisely onto the cells at 1000× concentration. The cells inside the unit are mounted on four circuit cards, shown upper right. Under test, shown on the left, the output from each card is measured at 200W, for a full mirror module rating of 800W.

Already, the improvement in performance compared to standard PV modules is striking. The illustration below compares the performance of a standard PV module with a mirror module, today and projected to 2020. The mirror module is 60% larger in area than a standard PV module, shown to scale, yet provides far more electricity (800W vs 240–340W for the standard module, depending on manufacturer and cost). A further advantage of the mirror module is that the heat is captured by liquid coolant circulated through the converter unit, and is available for use if desired. Currently with 40% efficient cells, the heat available is 1200W per module (red in the figure). By 2020, when cell efficiency is projected at 50%, the electrical and heat outputs of a module will be equal, both at 1 kW.

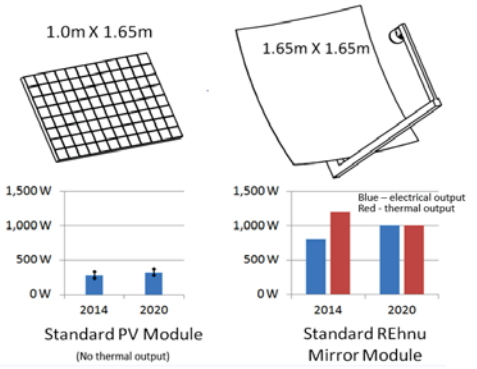

Electricity Generated by Standard PV Module	Electricity and Heat Generated by Standard *REhnu* Mirror Module

Will this technology really take over from standard PV and play a big role in the trillion-dollar electricity production industry? It has a good chance. In essence, the trade is one in which complexity is used to increase efficiency and thereby reduce use of materials and land. While simple PV systems with fixed modules have the advantage of no moving parts, they are inefficient not only because of low light to electricity conversion, but because light is not efficiently delivered to the modules—in the early morning and evening the Sun's rays strike the cells at a low angle or not at all. By contrast, mirror modules rely on moving parts for their improved efficiency: a fan and pump to recirculate coolant, as in an automobile, plus a tracking mount with motors, gears, and drive system to aim the concentrating optics directly at the Sun from sunrise to sunset. But these moving parts don't use much material and can be made highly reliable, with lifetime longer even than the projected 25 years of standard PV modules. In fact, a 40-year lifetime seems realistic, with output that can be increased over the years by upgrading with ever more efficient multi-junction cells.

Team members:

Dr. Roger Angel is Regents' Professor of Astronomy and Optical Sciences. He founded the University of Arizona Mirror Lab, which makes mirrors for the world's largest astronomical telescopes. He is a member of the National Academy of Sciences, a Fellow of the Royal Society, a MacArthur Fellow and a Kavli Laureate. He founded *REhnu* in 2008.

Dr. Tom Stalcup (PhD, UA Optical Sciences) is *REhnu*'s Chief Engineer. Prior to joining *REhnu*, he led opto-mechanical systems development at the W. M. Keck and MMT Observatories. At *REhnu* he leads the development of the commercial mirror module.

Dr. Blake Coughenour recently completed his PhD in Optical Sciences. His research focused on the spectral modeling and hardware integration of solar cells. His dissertation detailed the optical design and modeling of the power conversion unit placed at the focus of the mirrors. His contributions were instrumental in converting the UA's prototype CPV system into a low-cost unit for the commercial mirror module. He is a Carson Scholar.

Brian Wheelwright is pursuing a PhD in Optical Sciences. His dissertation research tests new methods to achieve high solar concentration using small-scale mechanical tracking. His areas of interest include large optic metrology, freeform optical fabrication, and non-imaging optical design. He is an NDSEG Fellow, ARCS Scholar, Carson Scholar, and Kidger Scholar.

Sunset over the Tucson Mountains.

Photo Courtesy of Brian Anderson

Steward Observatory Mirror Laboratory

(Adapted from http://mirrorlab.as.arizona.edu/)

At the University of Arizona's Steward Observatory Mirror Laboratory, a team of scientists and engineers is making giant, lightweight mirrors of unprecedented power for a new generation of optical and infrared telescopes.

These mirrors represent a radical departure from the conventional solid-glass mirrors used in the past. They have a honeycomb structure on the inside; made out of Ohara E6-type borosilicate glass that is melted, molded and spun cast into the shape of a paraboloid in a custom-designed rotating oven. Honeycomb mirrors offer the advantages of their solid counterparts - rigidity and stability—but they can be significantly larger, and dramatically lighter. With their lightweight structure, air can be circulated through the honeycomb structure forcing the glass to reach thermal equilibrium with the air temperature in a relatively short time, on the order of 20-30 minutes.

The Mirror Lab team has also developed a revolutionary new method to polish the honeycomb mirrors with a deeply curved, parabolic surface that results in much shorter focal lengths than conventional mirrors. Such fast mirrors not only improve telescope performance, but they can fit into a much shorter telescope body that requires a smaller, less expensive enclosure. The typical focal ratios are of order $f/1.25$ to $f/1.14$.

The pioneering work being done today at the Steward Observatory Mirror Lab had its beginning around 1980 with a backyard experiment by Dr. Roger Angel, the lab's founder and scientific director. Curious about the suitability of borosilicate glass (the kind used in glass ovenware) for making honeycomb structures, he tested the idea by fusing together two custard cups in an improvised kiln. The experiment was a success and led to a series of bigger kilns and small furnaces and, eventually, the spin casting of three 1.8 meter mirrors.

By 1985, with financial support primarily from the US Air Force, the National Science Foundation, and the University of Arizona, Roger Angel (in photo at left) and a talented Mirror Lab team moved to the current facility under the east wing of the UA football stadium. A large, rotating furnace was built and a series of mirrors as big as 3.5 meters in diameter were successfully cast.

By 1990, the rotating furnace was expanded to its current size, and a new wing was added to the Mirror Lab to house two mirror polishing stations and a test tower. The new furnace, which is large enough to cast mirrors up to 8.4 m in diameter, was first used in 1992 to make a 6.5-m mirror. In January 1997 the first 8.4-m mirror for the Large Binocular Telescope (LBT) was completed.

As part of the technology development process, the Mirror Lab has successfully produced fourteen mirrors with diameters of 1.2, 1.5, 3.5, 6.5, and 8.4 m. Nearly all of these mirrors are now operating in telescopes including: the SAO 1.2-m $f/1.9$ on Mt. Hopkins, the Lennon 1.8-m $f/1.0$ on Mt. Graham, the ARC 3.5-m $f/1.75$ on Apache Point, NM, the WIYN 3.5-m $f/1.75$ on Kitt Peak and the Phillips Lab 3.5-m $f/1.5$ at Starfire Optical Range, NM. The 3.5-m mirrors and larger ones have been polished at the Mirror Lab using the stressed-lap polishing technique to produce a surface figure ~15 to 20 nm r.m.s.

The Mirror Lab continues its impressive history of successful, ground breaking mirror castings. After a series of 1.2 m and 3.5 m mirrors proved the casting and polishing techniques,

the oven was enlarged for the casting of 8-m class mirrors in 1991. In April 1992, the first 6.5-m $f/1.25$ honeycomb blank was successfully cast. This mirror went into operation in May 2000 as the MMT Conversion Project on Mt. Hopkins. In February 1994, the second 6.5-m $f/1.25$ honeycomb blank was cast. This mirror, for the Magellan Project, was installed at Las Campanas Observatory, Chile in 2001.

GMT - Giant Magellan Telescope

The Giant Magellan Telescope will be one of the next class of super giant earth-based telescopes that promises to revolutionize our view and understanding of the universe. It will be operational in about 10 years and will be located in Chile.

The GMT has a unique design that offers several advantages. It is a segmented mirror telescope that employs seven of today's largest stiff monolith mirrors as segments. Six off-axis 8.4 meter or 27-foot segments surround a central on-axis segment, forming a single optical surface with a collecting area of 24.5 meters, or 80 feet in diameter. The GMT will have a resolving power 10 times greater than the Hubble Space Telescope. The GMT project is the work of a distinguished international consortium of leading universities and science institutions.

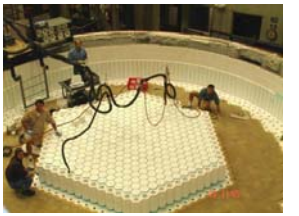

Some 1750 alumina-silica cores are being installed to spin cast GMT M1. This first off-axis paraboloid is one of seven 8.4-m mirrors for GMT.

LSST: The Large Synoptic Survey Telescope

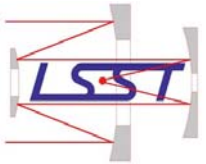

The LSST is a new kind of telescope. With a light-gathering power among the largest in the world, it can detect faint objects with short exposures. Its uniquely wide field of view allows it to observe large areas of the sky at once; compact and nimble, it can move quickly between images. Taking more than 800 panoramic images each night, it can cover the sky twice each week.

A powerful data system will compare new with previous images to detect changes in brightness and position. Hundreds of images of each part of the sky will be used to construct a movie of the sky. As just one example, this movie can be used to detect and track potentially hazardous asteroids—asteroids that might impact the Earth and cause significant damage.

Data from LSST will be used to create a 3D map of the Universe with unprecedented depth and detail. This map can be used to locate the mysterious dark matter and to characterize the properties of the even more mysterious dark energy. As with past technological advances that opened new windows of discovery, such a powerful system for exploring the faint and transient universe will undoubtedly serve up surprises.

Plans for sharing the data from LSST with the public are as ambitious as the telescope itself. Anyone with a computer will be able to fly through the Universe, zooming past objects a hundred million times fainter than can be observed with the unaided eye. The LSST project will provide analysis tools to enable both students and the public to participate in the process of scientific discovery. LSST will be unique: no existing telescope or proposed camera could be re-designed to cover ten square degrees of sky with a collecting area of forty square meters. The science that it will pursue had to wait for this new capability—the ability to reach faint objects twenty times faster than currently possible over the entire visible sky.

Gates Pass, reached after a 20-minute drive to the west of campus into the Tucson Mountains, marks a portion of the western border of the Tucson basin. The road up and over the pass is a winding scenic drive that is reached at the western end of *Speedway Boulevard*, which also extends across the entire city to the eastern edge of the Tucson basin. The short drive over the pass provides access to some of the most densely populated regions of Saguaro cactus in the world, protected in and around the western unit of Saguaro National Park. At the top of Gates Pass, at an elevation of about 3000 feet, there is an easily accessible scenic outlook nestled between mountain ridges. It is a Tucson favorite for sunset watching, with views extending for tens of miles. Multiple trailheads and the popular *Arizona-Sonora Desert Museum* are also nearby.

Photo Courtesy of Chris Summitt

Computational Imaging

Amit Ashok

Imaging refers to the process of forming a visual replica (i.e. an isomorphic representation) of a scene. This near isomorphic relation between the scene and the image has been the driving principle of optical imaging system design for many centuries. The first imaging systems simply imaged a scene onto a screen for viewing purposes. For example one of the earliest imaging devices, "camera obscura," invented in the 10^{th} century, relied on a pinhole and a screen to form an inverted image [1]. The next significant step in the evolution of imaging systems was the development of a photosensitive material, i.e., photographic film, which allowed an image to be recorded for later viewing. The perfection of the photographic film gave birth to a multitude of new applications, ranging from medical imaging using x-rays for diagnosis purposes to aerial imaging for surveillance. Development of the charge-coupled device (CCD) sensor in 1969 by George Smith and Willard Boyle at Bell labs [2] combined with advances in communication theory revolutionized imaging system design and its applications. The electronic recording of an image allowed it to be stored digitally and transmitted over long distances reliably using modern digital communication systems. These revolutionary advances in digital sensor and electronic processing technology have culminated in the modern digital camera. Furthermore, advances in optical materials and fabrication technology coupled with computer-aided optical design have lead to a significant improvement in modern imaging system cost-to-performance ratio. These revolutionary changes have enabled the proliferation of modern digital cameras, as we know them in a wide range of consumer and scientific devices.

It is interesting to note that typically the role of electronic image-processing in most modern imaging systems, such as the point-and-shoot or the digital SLR camera, is limited to image-processing tasks such as de-noising, color balance, contrast stretching and image compression. Modern electronic processors or computers have followed Moore's law, doubling in computational capability every eighteen months. This exponential growth in electronic processing combined with modern optical design has led to a new paradigm in imaging referred to as *computational imaging* or *computational photography*. While in a traditional imaging system, optics has the sole burden for image formation, computational imaging employs digital processing in conjunction with optics for image formation. As a result, in a computational imager the optical field in the detector plane does not necessarily resemble a focused image as in the case of a traditional optical imager. In fact, the detector plane in a computational imager captures an intermediate image, as shown in Fig.1, which is subsequently digitally processed to form the final focused image. In computational imaging the shared role of digital processing in the image formation process relaxes some of the demanding requirements/constraints placed on the optical design in traditional imaging. This enables a larger design space that is unique to computational imaging, as illustrated in Fig. 2.

The concept of computational imaging is perhaps best illustrated with a concrete example. In an optical imaging system the depth-of-field describes the range of object distances over which the image is considered to be sharp or focused. In a traditional optical system the depth of field or depth of focus is roughly inversely proportional to the f-number or $f/\#$ (i.e. ratio of focal length to aperture size), a well-known fact in photography. If we want to increase the depth-of-field of a camera, say, to accommodate a subject and the background, we have to "stop-down" the lens, i.e., reduce the lens's aperture size. While this does increase the depth-of-field, it

also adversely affects the spatial resolution and light collection capability of the camera. This can be especially disadvantageous when one is trying to capture an image in low-light conditions.

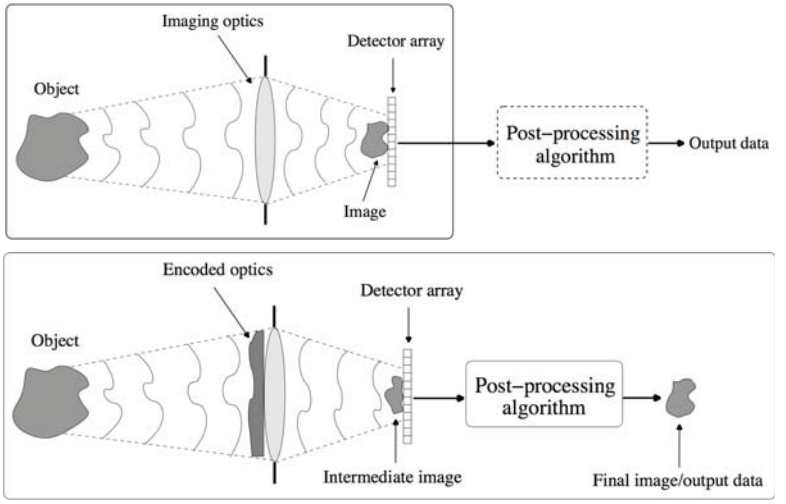

Figure 1. Traditional imaging system employs digital processing/post-processing to enhance images (top). In a computational imaging system (bottom) digital processing is a critical part of the image-formation process.

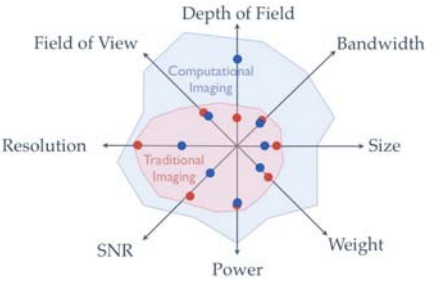

Figure 2. Expanded system design space of computational imaging enables system design with new capabilities that are not achievable with traditional imaging.

Cathey and Dowski [3], proposed a computational imager design to extend the depth-of-field without reducing the $f/\#$ and as such without effectively lowering the spatial resolution and/or the light-collection capability of the camera. Their ingenious design employed a carefully designed cubic phase-plate in the aperture-stop of the imaging system rendering the optical point spread function (PSF) nearly invariant to focus. The modified optical PSF, due to its extended structure, also blurred the optical image in the detector plane. However, as the optical PSF is nearly focus-invariant, the image blur problem can be effectively eliminated by digitally processing the image with a carefully designed image-sharpening filter. This yields a focused image with an extended depth-of-field (EDoF) as illustrated in Fig. 3. Note that here the digital processing is a critical part of image-formation, in contrast to traditional imaging where digital processing may be optional.

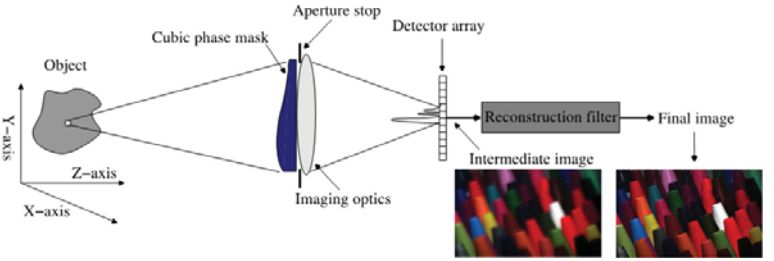

Figure 3. Computational imager using a cubic phase-plate and a digital image-sharpening filter to achieve extended depth-of-field imaging [3].

At University of Arizona (UA) we have made significant advances in EDoF imaging-system design that has led to improved image quality and larger depth-of-field. Figure 4 shows our new Zernike phase-plate design that improves upon the original cubic phase-plate design in terms of improved system modulation transfer function [4]. We have employed this new phase-plate design along with sophisticated digital image processing to extend the depth-of-field of a thermal (long-wave infrared) camera for night-vision applications.

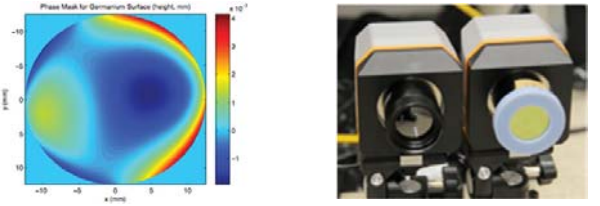

Figure 4. The Zernike phase-plate profile (left). A traditional thermal camera (left side) and EDoF thermal camera (right side) with the phase-plate attachment.

A traditional thermal camera and the EDoF thermal camera are also shown side-by-side in Figure 4. The traditional thermal camera is capable focusing on object distances ranging from infinity to 12 meters, while the EDoF camera can focus on objects as close as 3 meters without need for re-focus. This extended depth-of-field is illustrated in Fig.5 using a scene with old-fashioned Christmas light string (with a thermal signature) laid out from 25 meters to 1 meter. As we can observe, the EDoF camera image maintains focus almost right up to the camera whereas the traditional camera image shows significant defocus for closer distances. One high-impact application of EDoF computational imager we are pursuing at UA is elimination of auto-focus mechanism for smart phone cameras, which would enable a thinner camera and phone designs.

Figure 5. An image from the traditional thermal camera that is blurred due to defocus from close objects such as the person (left). The EDoF computational thermal camera delivers crisp images including close objects (right).

Another example of imaging-system design within the computational imaging paradigm is compressive imaging. As most of us have experienced first hand, for nearly all modern digital cameras, such as point-and-shoot camera, smart phone camera, or even a digital SLR camera, the digital image is *compressed* for efficient storage and transmission. It is interesting to note that despite image compression, in most cases, there is little to no loss of visual quality in compressed images. This is especially true for natural images that tend to be smooth at various scales. An image compression algorithm exploits this *smoothness* to reduce the image file size by "throwing away" redundant data in the image. A compression ratio of 10× is commonly achieved for most images. The fact that natural images are redundant (and thus compressible) suggests that a traditional imaging system design is inefficient because it acquires redundant information. Thus from an engineering perspective it would make sense to move the "compression" into image acquisition step as opposed to a digital processing step. This is exactly what a compressive imaging system accomplishes, which is to effectively measure a compressed image directly and then employ digital processing to "decompress" the image. As expected, there are many potential benefits of compressive imaging such as lower detector count sensors, better measurement signal-to-noise ratio, and lower detector readout rate, to name a few. Compressive imaging is especially useful in cases where detector arrays are expensive or high-resolution detector arrays do not even exist (e.g., at infrared and THz frequencies).

At UA we have made significant advances in the design and implementation of optical compressive cameras in the visible and infrared spectral bands [5]. This work entails optical design, sophisticated statistical image processing, and system optimization. We have developed information-optimal compressive imaging system designs that maximize image quality for a given compression ratio. Figure 6 shows an optical compressive imaging prototype developed at UA in the Intelligent Imaging and Sensing Lab, capable of near real-time imaging operating at a compression ratio of 8×. This imaging system employs a digital mirror device (DMD), commonly used in projectors and projection TVs, to implement the optical compression. Figure 7 shows example images acquired from the compressive imager prototype at two compression ratios. Observe that even at 8× compression there is little degradation in image quality relative to the uncompressed image from a traditional imager.

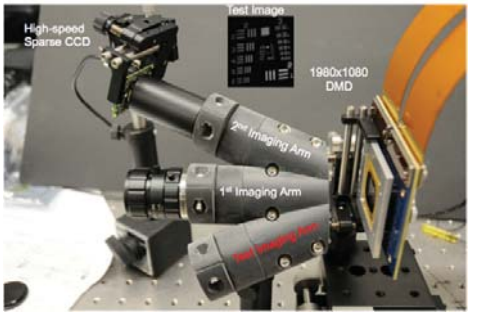

Figure 6. Optical compressive imager prototype developed at UA capable of producing mega-pixel images at 8× optical compression.

As we have learned from the aforementioned examples of computational imaging, this new imaging system design paradigm offers possibilities for imaging system design with novel capabilities. There are numerous applications of computational imaging, currently being explored for a variety of applications and optical/non-optical imaging modalities. For example, at

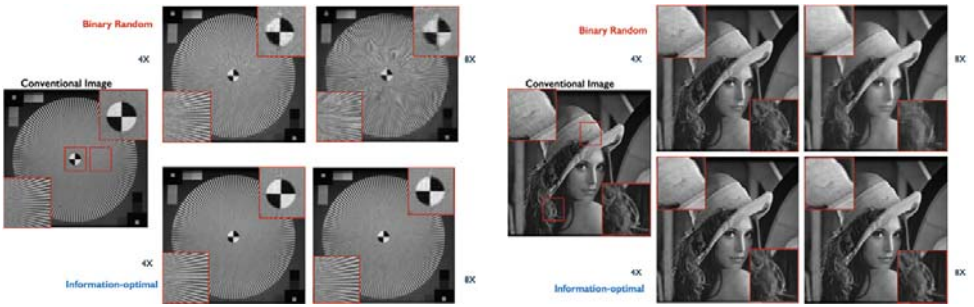

Figure 7. Example images from the compressive imager prototype developed at UA. A traditional imager with a 500,000 detector count CCD image-sensor is used to acquire the conventional images. The compressive images at 4× (middle column) and 8× (right column) compression ratio were acquired with a 50,000 detector count image-sensor. The binary random (top row) and information-optimal (bottom row) refer to two design choices for the compressive imager implementation. Note that the information-optimal design offers superior image quality.

UA we are pursuing novel computational imaging based system architectures for advanced explosive detection in checked and carry-on bags using x-rays for airport security. Other efforts include investigating the use of computational imaging for high-dimensional imaging such as three-dimensional imaging for depth, multispectral and hyperspectral imaging, and polarization imaging, to name a few. Computational imaging is inherently a multi-disciplinary area of research encompassing optical design, physical optics, statistical inference, optimization theory, and computer science. The computational imaging research at UA offers a unique and exciting opportunity to work at the intersection of these disciplines to translate the promise of computational imaging into real-world imaging devices that address important problems.

1. N. J. Wade and S. Finger, "The eye as an optical instrument: from camera obscura to Helmholtz's perspective," *Perception* **30**(10), 1157-1177 (2001).
2. W. Boyle and G. Smith, "Charge Coupled Semiconductor Devices," *Bell System Technical Journal* **49**, 587 (1970).
3. E. R. Dowski and W.T. Cathey, "Extended Depth of Field Through Wavefront Coding," *Applied Optics* **34**(11), 1859-1866 (1995).
4. R. Kerviche and A. Ashok, "A Joint-Design Approach for Extended Depth of Field Imaging," in *Imaging and Applied Optics*, OSA Technical Digest, paper CW4C.4 (2013).
5. R. Kerviche, N. Zhu, and A. Ashok, "Information-optimal Scalable Compressive Imaging System," in *Classical Optics*, OSA Technical Digest, paper CM2D.2 (2014).

Amit Ashok is an Assistant Professor with joint appointments in *College of Optical Sciences* and *Department of Electrical and Computer Engineering* (ECE) at the University of Arizona. He directs the Intelligent Imaging and Sensing Laboratory in the *College of Optical Sciences*. His nearly 15 years of research experience in both industry and academia spans the areas of computational/compressive imaging and sensing, Bayesian inference, statistical learning theory, and information theory. Dr. Ashok has made key contributions in task-based joint-design framework for computational imaging and information-theoretic system performance measures such as the task-specific information. He has numerous peer-reviewed publications and several patents, and has been invited to speak at various OSA, IEEE, SIAM and SPIE conferences.

The Universe of Semiconductor Optics

Rolf Binder

Semiconductor optics is everything. No, seriously! Those of us working in semiconductor optics will sooner or later be exposed to just about any subject you can imagine in modern science. In my Theoretical Semiconductor Optics Group at the *College of Optical Sciences*, we constantly come across a wide variety of general science issues that are somehow related to our specific semiconductor optics projects; see Fig. 1. The reason is that a semiconductor is not just a piece of material, but when excited, say, by light, it turns into a most versatile mini-laboratory. Chemists can work with hydrogen atoms and study the binding of these atoms to form hydrogen molecules, or they can study ionization of hydrogen atoms in a hydrogen plasma. Astrophysicists can observe hydrogen in interstellar space. But can anyone actually make hydrogen atoms? No, it cannot be done in practice, because creating matter requires a whole lot of energy. But now, consider a semiconductor, which is a crystal in which the valence band is filled with electrons and the conduction band is completely empty, as shown in Fig. 2. If we excite a semiconductor, for example with an optical laser beam, we promote electrons from the valence band to the conduction band. This creates a negatively-charged, rather freely mobile particle in the conduction band (we will just call it electron in the following), and a missing electron in the valence band, which is a positively-charged hole. For this process, we merely need a laser with frequency typically in the near infrared or visible range, which is fairly easy to obtain. When the laser beam hits the semiconductor, it is a little bit like the 'Big Bang,' because we basically create a certain kind of matter inside a semiconductor—okay, it is more like a small bang.

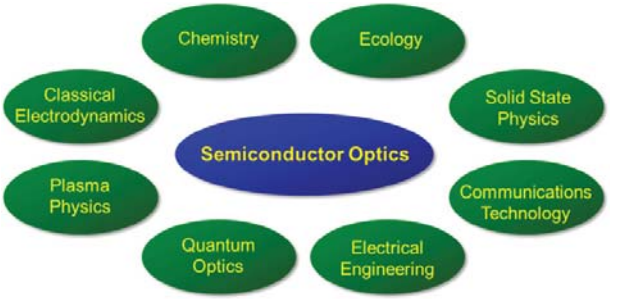

Figure 1. Scientific areas related to topics in modern semiconductor optics.

The optically-excited electrons and holes behave in many respects similarly to electrons and protons that form basic matter such as hydrogen atoms. This is because they interact via the Coulomb interaction just as ordinary charged particles do. And the Coulomb interaction makes things interesting. It is the basic source for many optical phenomena, including optical nonlinearities. Of course, electrons and holes in semiconductors do not move quite as freely as electrons and protons in vacuum, and they usually do not live very long. The movement is inhibited because the charge-carriers interact with lattice vibrations (phonons). The fact that charge-carriers, such as electrons, can scatter off of phonons gives rise to electrical resistivity in metals, a familiar effect. As for the lifetime of electron-hole pairs, in a typical III-V compound, such as GaAs, they live only for about a nanosecond. While that may not seem very long, on a typical time-scale of microscopic scattering processes, which is only tens or perhaps a few

hundred femtoseconds, a nanosecond seems like an eternity. And there are many things that can happen during that time interval.

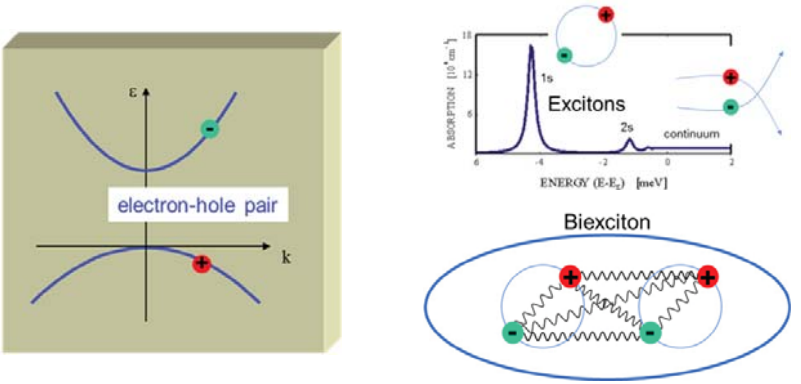

Figure 2: Left: Electronic band structure of a typical inorganic direct-gap semiconductor, such as GaAs. An electron-hole pair, which may be created through optical excitation, is indicated. Upper right: A typical absorption spectrum with an exciton resonance peak, corresponding to the creation of an electron-hole pair bound by the Coulomb interaction. Lower right: Schematic of a biexciton, a bound state of two excitons. The wiggly lines show the six different Coulomb interactions present in the biexciton.

As shown in Fig. 2, two excitons can form a bound state, a biexciton, where all four particles, two electrons and two holes, interact via the Coulomb force. In Ref. [1] we worked out these interactions for biexcitons in GaAs quantum-wells in detail. The details are quite complicated, but the principle is rather similar to the Heitler-London model, often taught in quantum mechanics and chemistry courses that cover the principles of covalent binding. The complication in the case of excitons stems from the fact that holes, unlike protons, are quite light and cannot be treated as particles that simply refuse to move because of their large mass. Creating biexcitons through nonlinear optical excitation leads to interesting phenomena. (The excitation must be nonlinear, as linear excitation creates a single exciton, but two are needed.)

One of those phenomena is the so-called four-wave mixing, whereby a pump and a probe pulse create an excitation grating, and due to the nonlinear interaction, a diffracted four-wave mixing signal appears; see Fig. 3. The direction of that signal depends on the geometry of the system. For example, in a semiconductor microcavity, which consists of two mirrors with a semiconductor quantum-well in the middle, the four-wave mixing signal comes out along the same direction as the probe beam goes in. One can study the many-body interactions in the cavity by looking at the four-wave mixing signal using various polarization states (linear x, linear y, circular σ_+, circular σ_-); see Fig. 4. Doing this we found evidence for Coulomb correlated continuum electron-hole states, that is, states where electrons and holes have such high energies that they are not bound as excitons [2]; see Fig. 2. For such states Coulomb correlations usually cannot be observed; only incoherent Coulomb scattering is readily observable.

One might ask: can a four-wave mixing signal take part in a four-wave mixing scattering process, that is, can the four-wave mixing signal itself play the part of the probe (which originally generates the four-wave mixing signal). The answer is yes, and the result can be in a way catastrophic, because this opens a feedback loop that could lead to optical instabilities. We

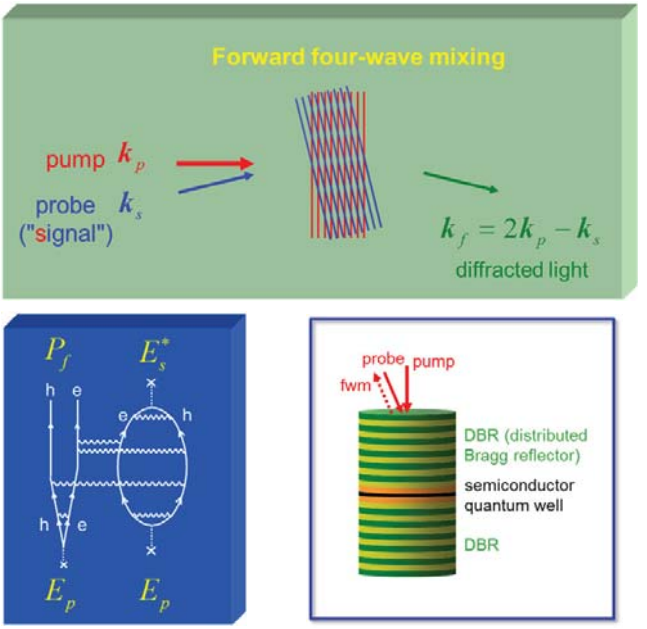

Figure 3: Top: Schematic of a four-wave mixing process, brought about by a pump and a probe beam. Lower left: Example of a Feynman diagram that would be part of the description of the four-wave mixing process (with *E* denoting the light field amplitudes and *P* the induced excitonic polarization). Lower right: Four-wave mixing configuration involving a semiconductor microcavity, in which a semiconductor quantum well (a very thin semiconductor layer) is sandwiched between two DBR mirrors.

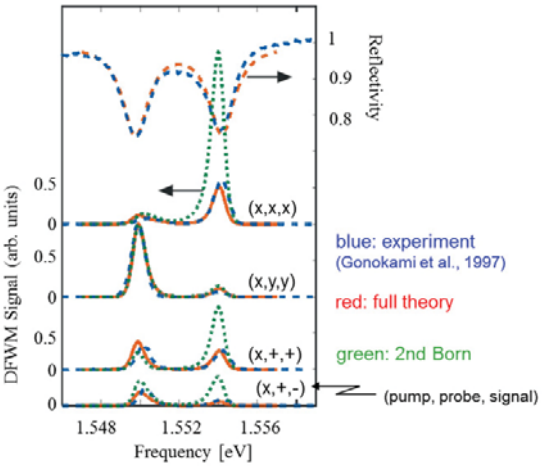

Figure 4: Degenerate four-wave mixing spectra from a semiconductor microcavity for various linear and circular polarization states of the pump, probe, and four-wave mixing signal. From Ref. [2].

have studied four-wave mixing instabilities in many different systems, but the system of a semiconductor microcavity turned out to be particularly interesting. In a microcavity, we usually do not distinguish between light (photons) and material polarization (excitons), but consider the true eigenmodes of the coupled system, the polaritons. Polaritons form a quantum fluid with many interesting properties. For example, pumping the system at normal incidence, but choosing the frequency to be above the lowest polariton mode, can create a situation where the pumped polaritons, which have zero in-plane momentum, scatter onto the polariton branch, thus creating polaritons that do have in-plane momentum; see Fig. 5.

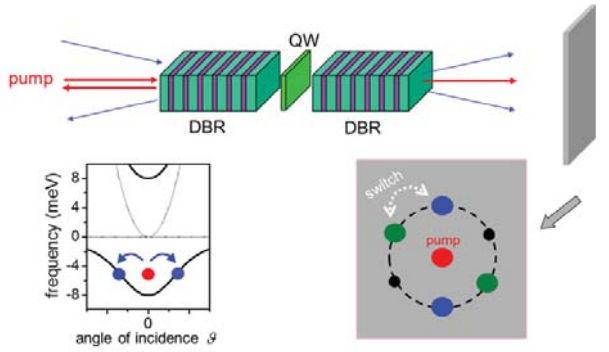

Figure 5: Schematic of a semiconductor microcavity, pumped in normal incidence at a frequency above the lowest polariton mode. Off-axis fields can be created through scattering of the pump onto the polariton eigenmodes at non-zero in-plane momentum (here indicated by the angle of incidence). The possibility of a two-spot far-field pattern and switching the beams' direction is indicated. From Ref. [3].

We predicted that, under certain circumstances, two off-axis beams can emerge, that are related to the two polaritons with non-zero in-plane momentum [3]. Following an idea originally realized in a Rubidium gas [4], we found that the direction of the off-axis beams can be switched with a relatively weak control field. This can be viewed as an all-optical switch or all-optical transistor [5]. But what physical principles are behind these spontaneously-formed off-axis beams and the possibility of switching them?

It turns out that the spontaneous formation of a two-spot far-field pattern, which corresponds to stripes in the near-field (Fig. 6), is closely related to patterns in other areas of science, for example, zebra stripes, or the emergence of fingers on our hands (luckily, once we are beyond the embryonic stage, that pattern is pretty much fixed, and a small perturbation will not change the number or orientation of our fingers!), and also ecological patterns in predator-prey systems (e.g., foxes and rabbits). Now, the patterns the biologists and chemists discuss in the context of morphogenesis, and ecologists in the context of ecological or population patterns, are often viewed as so-called Turing patterns. In Turing's original model of morphogenesis, two chemical substances, an auto-catalytic activator and an inhibitor, diffuse spatially and the nonlinear chemical reaction, together with the diffusion, could lead to spatially stable patterns. In ecological systems, an example for a species that acts analogously to an auto-catalytic chemical, would be rabbits, which tend to particularly enjoy multiplying themselves, while foxes, which hunt rabbits, play the role of inhibitors; see Fig. 7.

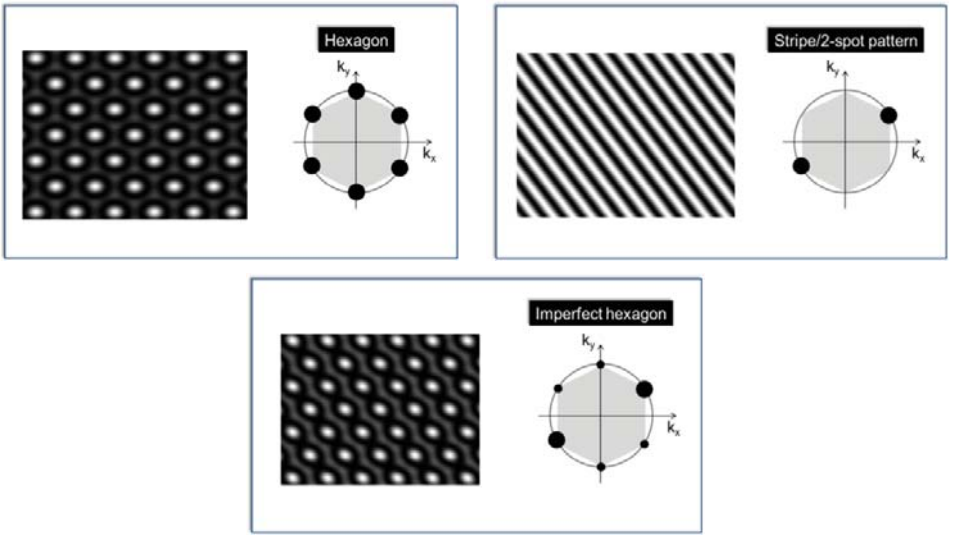

Figure 6: Schematic of simple patterns in real space and the corresponding patterns in momentum (or *k*) space. The *k*-space patterns correspond to far-field patterns. The dot thickness in the *k*-space patterns indicates the intensity. The stripe consists of two counter-propagating fields, and hence two opposite spots in the *k*-space.

Figure 7: Left: Schematic of a fox and rabbit population that can exhibit, under certain circumstances, stationary patterns (Turing patterns). Right: If diffusive transport is replaced by diffractive transport, as found in quantum fluids, one could imagine wave-like quantum foxes and quantum rabbits.

Coming back to polaritons and quantum fluids, just like rabbits, four-wave mixing can reinforce or multiply itself, but we do not have diffusive transport in these systems; rather, we have diffractive transport. Other than that, the nonlinear reactions are formally quite similar to those in the original Turing model, and, therefore, the idea of Turing patterns has been extended to nonlinear optical systems in the past, while we took the next step and extended it to quantum fluids. Loosely speaking, replacing diffusive by diffractive transport changes rabbits and foxes to quantum rabbits and quantum foxes, as shown in Fig. 7, or more seriously, in our case to polaritons. Our experimental collaborators in Paris have indeed observed patterns that we predicted [6,7]. Figure 8 shows a calculated hexagonal pattern, while Fig. 9 shows an experimentally observed (imperfect) hexagonal pattern—compare this with the schematic of an imperfect hexagon in Fig. 6. Moreover, our experimental collaborators were able to switch two-spot patterns in a reversible fashion; see Fig. 10 [7].

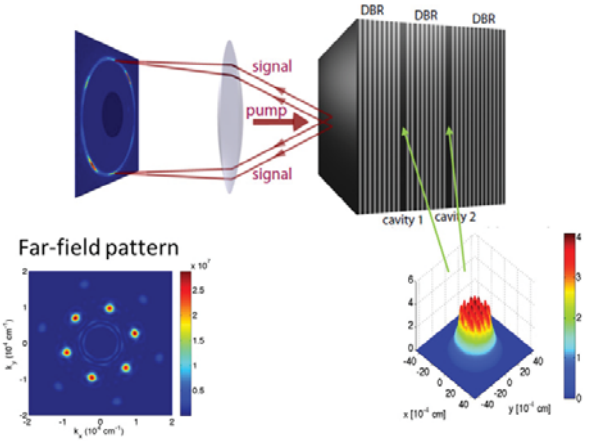

Figure 8: Computed patterns in a polariton quantum fluid in a double microcavity. The reflective far-field pattern shows six spots, corresponding to a hexagonal near-field pattern of polariton-density inside the cavities. From Ref. [6].

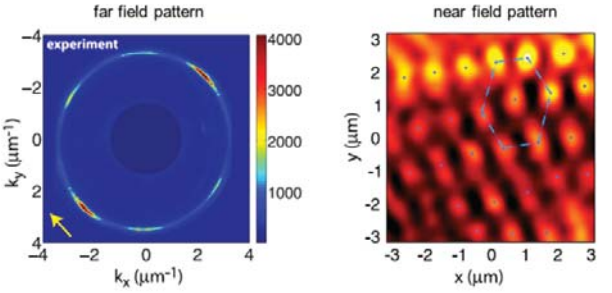

Figure 9: Experimentally observed patterns from the double microcavity. From Ref. [7].

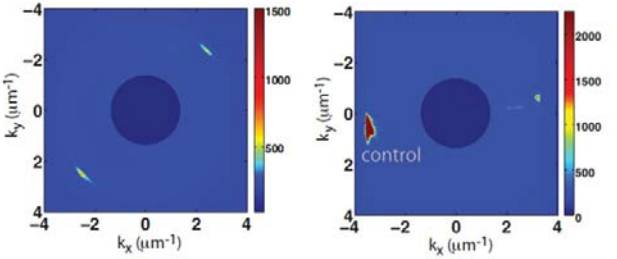

Figure 10: Experimentally observed switching of two-spot patterns. From Ref. [7].

As mentioned above, electrons and holes can interact with lattice vibrations (phonons), which creates fundamental limits to the material's electrical conductivity. A material system that has been extensively investigated over the last decade is graphene, a two-dimensional honeycomb lattice of carbon atoms. Graphene is unlike an ordinary semiconductor, and unlike an

ordinary metal, because the conduction and valence bands are not parabolic, and they 'touch' at the *K*-point (Dirac point) in the Brillouin zone (i.e. there is no bandgap); see Fig. 11. The electrons and holes close to the *K*-point are said to be massless (similar to photons). The charge-carrier mobility in graphene is much higher than in, say, silicone, which makes it an interesting material for electrical applications. However, do we really know in detail how the electrons interact with phonons? This is an area of ongoing research, and optical spectroscopy can help to shed light on the electron-phonon interactions.

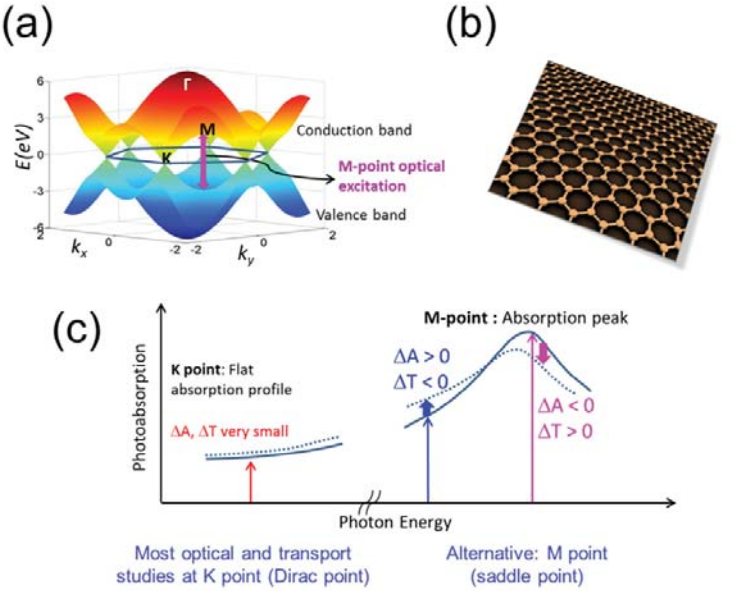

Figure 11: (a) Graphene bandstructure. (b) Schematic of real-space honeycomb lattice. (c) Schematic of the absorption spectrum close to the *K*-point (THz frequencies), and close to the *M*-point (ultraviolet frequencies). After Ref. [8].

Instead of focusing on the *K*-point, we have looked at the *M*-point (or saddle point), where graphene's absorption spectrum exhibits a peak. While not being as spectrally narrow as an exciton peak in a GaAs spectrum, the *M*-point absorption peak offers an opportunity to do very sensitive spectroscopy. We have calculated delay-time resolved differential absorption spectra and, from comparison with data obtained by our experimental collaborators, deduced values for the effective acoustic and optic deformation potentials, which are quantities of fundamental importance, as they characterize the strength of the electron phonon interaction; see Fig. 12.

In addition to the aforementioned projects, some other projects that our group is or has been involved in include slow light [9,10], optical refrigeration of semiconductors [11] and fiber lasers [12], optical switching through polarization rotation [13], excitonic effects in semiconductor nano-membranes [14], and electromagnetically-induced transparency [15]. A more complete list of publications can be found at fp.optics.arizona/binder, and an overview of four-wave mixing and its relation to many-body interactions can be obtained by downloading the IQEC 2009 Tutorial talk from fp.optics.arizona.edu/binder/research.

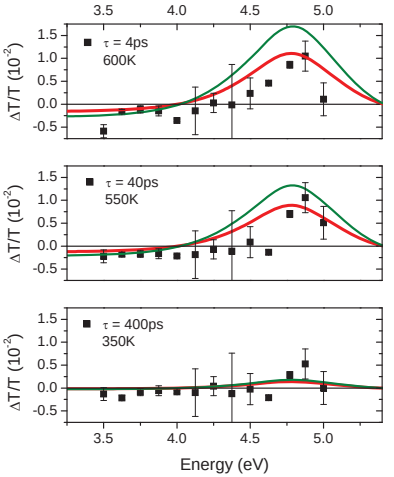

Figure 12: Calculated and experimentally observed differential transmission signals in the vicinity of the saddle point (*M*-point) absorption. Red line: only electron-acoustic phonon interaction taken into account. Green line: both electron-acoustic phonon and electron-optic phonon interactions taken into account. The theory reproduces the order of magnitude of the observed signal, the basic lineshape, and the zero-crossing. From Ref. [8].

1. R. Takayama, N.H. Kwong, I. Rumyantsev, M. Kuwata-Gonokami, and R. Binder, "T-matrix analysis of biexcitonic correlations in the nonlinear optical response of semiconductor quantum wells," Eur. Phys. Journal B **25**, 445-462 (2002).
2. N.H. Kwong, R. Takayama, I. Rumyantsev, M. Kuwata-Gonokami and R. Binder, "Evidence of Nonperturbative Continuum Correlations in Two-Dimensional Exciton System in Semiconductor Microcavities," Phys. Rev. Lett. **87**, 027402(4) (2001).
3. S. Schumacher, N.H. Kwong, R. Binder, and Arthur L. Smirl, "Low intensity directional switching of light in semiconductor microcavities," phys. stat. sol. (RRL) **3**, 10-12, (2009).
4. A.M.C. Dawes, D.J. Gauthier, S. Schumacher, N.H. Kwong, R. Binder, and Arthur L. Smirl, "Transverse optical patterns for ultra-low-light-level-all-optical switching," Laser & Photon. Rev.4, No.2 221-243 (2010).
5. A.M.C. Dawes, "Towards a single-photon all-optical transistor," phys. stat. sol. (RRL) **3**, A17-A19 (2009).
6. M.H.Luk, Y.C. Tse, N.H. Kwong, P.T. Leung, P. Lewandowski, R. Binder, and S. Schumacher, "Transverse optical instability patterns in semiconductor microcavities: Polari ton scattering and low-intensity all-optical switching," Phys. Rev. B **87**, 205307 (2013).
7. V. Ardizzone, P. Lewandowski, M.H. Luk, Y.C. Tse, N.H. Kwong, A. Lucke, M. Abbarchi, E. Baudin, E. Galopin, J. Bloch, A. Lemaitre, P.T. Leung, P. Roussignol, R. Binder, J. Tignon and S. Schumacher, "Formation and control of Turing patterns in a coherent quantum fluid," Scientific Reports 3,3016 (2013).
8. A.T. Roberts, R. Binder, N.H. Kwong, D. Golla, D. Cormode, B.J. LeRoy, H.O. Everitt, and A. Sandhu, "Optical characterization of electron-phonon interactions at the saddle point in graphene," Phys. Rev. Lett. 112.187401 (2014).
9. B. Gu, N.H. Kwong, R. Binder, and Arthur L. Smirl, "Slow and fast light associated with polariton interference," Phys. Rev. Rev. B **82**, 035313 (2010).
10. Z. S. Yang, N. H. Kwong, R. Binder, and A. L. Smirl, "Stopping, storing and releasing light in quantum-well Bragg structures," J. Opt. Soc. Am. B **22**, 2144-2156 (2005).
11. G. Rupper, N.H. Kwong, and R. Binder, "Large excitonic enhancement of optical refrigeration in semiconductors," Phys. Rev. Lett. **97**, 117401 (2006).
12. D.T. Nguyen, J. Zong, D. Rhonehouse, A. Miller, Z. Yao, G. Hardesty, N.H. Kwong, R. Binder, and A. Chavez-Pirson, "All Fiber Approach to Solid-State Laser Cooling," Proc. of SPIE, **8275**, 827506-1 (2012).

13. D.T. Nguyen, N.H. Kwong, Z.S. Yang, R. Binder, and A.L. Smirl "Mechanism of all-optical spin-dependent polarization switching in Bragg-spaced quantum wells," Appl. Phys. Lett., **90**, 181116-1 (2007).
14. B. Gu and R. Binder, "Theoretical approach to the excitonic response of GaAs nanomembranes in the averaged-strain approximation," J. Opt. Soc. Am. B **29**, A60-A68 (2012).
15. M.C. Phillips, H. Wang, I. Rumyantsev, N.H. Kwong, R. Takayama and R. Binder, "Electromagnetically Induced Transparency in Semiconductors via Biexciton Coherence," Phys. Rev. Lett. **91**, 183602(4) (2003).

Dr. Rolf Binder is a Professor at the College of Optical Sciences and the Department of Physics, University of Arizona. He received his PhD in Theoretical Physics from the University of Dortmund, Germany, in 1989. Dr. Binder is a Fellow of the Optical Society of America, and has been named Outstanding Referee of the American Physical Society. He has been involved in the organization of various international scientific conferences, including the SPIE Photonics West conference, CLEO/QELS, and the conference on Fundamental Optical Processes in Semiconductors (FOPS), which he co-chaired in 2007. He has co-authored more than 110 peer-reviewed scientific publications, one conference proceedings book, and seven book chapters, and has given numerous invited talks. Dr. Binder has taught at both graduate and undergraduate levels at the College of Optical Sciences, Department of Physics, and Department of Mathematics at the University of Arizona, and as a guest lecturer at the Technical University of Berlin, Germany.

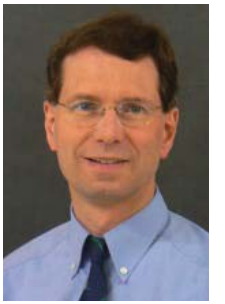

Student Optics Chapter (SOCk) Spring Camping Trip on Mount Lemmon (2013).

Photo Courtesy of Laura Coyle

The Early Days of 4D Technology

John Hayes

After I left WYKO in 1999, Jim Wyant invited me to join the faculty of the *College of Optical Sciences* as a research professor. At the time, I was interested in vibration insensitive interferometry and I began work on a contract from NASA to develop an interferometer that would actively cancel vibrations using an idea originally proposed by Jim Burge. We built the equipment, got it working, and went to a conference in Huntsville to present a paper on it late in 2001. There I met a guy named James Millerd from California, who had developed a very clever idea for high speed interferometry using a holographic beam splitter and some phase plates to grab all the data needed to compute phase in a single frame. I was immediately impressed with his approach and could see that it had a lot of advantages over what we were working on. Not only that, but it solved some of the problems that we had with our interferometers at WYKO over the years. Vibration was always a problem with interferometry and this looked like a very clever way to solve the problem.

About a week later, I met with Jim Wyant and suggested that we go visit James and his partner Neal Brock in California, where they had started a little company called 4D Vision Technology to make and sell interferometers. Their office was basically just a few rooms, and we could tell that they were working hard to convince us that they had a lot more employees besides themselves, but the place was pretty empty. Still, their interferometer actually worked pretty well and Jim seemed as impressed as I was by the whole idea. It was one of those super clever and yet incredibly simple ideas that made us look at each other and say, "why didn't we think of that!" Later in the day, we were sitting around the table talking about technical issues, and the state of their business (which wasn't very good), when Jim Wyant suddenly looked at James and Neal and asked, "So, how much do you want?" James stammered around and replied, "For one interferometer or do you want more than one?" Jim smiled and simply replied, "For the whole company..." and the room went quiet. Gosh, we hadn't exactly talked about this idea on our way over, so Jim and I weren't exactly on the same page at that moment. Neal and James fumbled around without really answering the question, and we left promising to work it out. Afterwards, Jim and I had a long discussion, and we finally agreed to start a new company, become partners again, and loan the company the funds to buy 4D Vision and to get things going. It had never been easy but we had had a lot of fun with WYKO, and we both agreed that maybe we could do it again. I agreed to run the company but the one thing that I told Jim was that I wasn't sure that I had another 15 years in me (which is about how long I was at WYKO), so I committed to give it at least five years and then evaluate what I'd do next.

Early in 2002 we incorporated and called the new company "4D Technology Corporation." It took a bit of convincing but James and Neal moved to Arizona and we rented office space near the Tucson airport. I can still remember opening the front door for the first time and walking into the office by myself. It takes a moment like that to realize that you are really starting all over again—almost completely from scratch. Fortunately, James and Neal were supplying a lot of the early development work, which really helped with sales in those early days. Still, the more mundane things like buying lab equipment, setting up payroll, hiring people, talking to customers, establishing credit lines along with a lot of other tasks can seem overwhelming. There is no doubt that when you start a company, it's fun, it's scary, it's exciting, and there are a million things to do, but in the end, it is a LOT of hard work! The hours are long, the headaches can be big ones, and nothing (I really mean nothing) is easy, so it is extremely satisfying to see it finally take off. Within the first few months, Steve Martinek came over from Veeco to help with sales and he was very successful. Over time, we gradually gathered a lot of loyal customers and we all worked very hard to make them happy with our products and our services.

In the first five years, we won many awards—the *Photonics Spectra Circle of Excellence* award, the R&D 100 award (multiple times), citations of merit from NASA, and a few more I can't even remember. It took a while but we built up a world-class staff of engineering talent including many OSC graduates and former WYKO employees. I lost track of the number of patents we were awarded, and our interferometers could do things unmatched by anyone else. We were also lucky to hire a very experienced

production manager, Chris Lesadd, who taught us about lean production methods and demonstrated that if you do things right, you don't need to have Ph.D.s assembling complicated optical instruments!

We did a lot of work to develop our products. Along the way, we improved our first product (the PhaseCam), we developed a way to make a couple of different, single-frame Fizeau phase shifting systems, we built and demonstrated a single-frame PDI system, and developed a Mach-Zehnder wavefront metrology system. James Millerd turned out to be one of the most clever optical engineers I've ever worked with, and he was always coming up with new, amazing ideas. One of the ideas that many of us worked on was a completely new method to measure optical phase using a structured wire-grid polarization mask similar to a Bayer mask used in color cameras. It took a lot of development work to be able to produce these sensors, and they are still the basis for many of the 4D systems. Eventually NASA trusted us with some very important and interesting development contracts to supply equipment to measure the primary segments of the James Webb Space Telescope (JWST) and a very high speed, high powered speckle system to measure the backplane support structure for the telescope. The structure was very large, it was not smooth, and it was very black, so it was a difficult thing to measure using light. We solved the problem with a 100+ MW pulsed laser with a coherence length of only a couple of feet. That laser was so powerful that we all had a lot of respect for it when it was running! We also developed a sophisticated multiple wavelength system for measuring mirror phasing for the JWST during ground tests. Michael North-Morris, an OSC graduate, was the lead engineer on these projects and did an outstanding job.

As the guy running the company, I wasn't able to do very much technical work but I still enjoyed visiting customers to help install or adjust systems and a few visits really stand out. On one visit to Ball Aerospace, I helped setup a PhaseCam for testing the Hi-Rise telescope that is now orbiting Mars. I also got to stand next to the Deep Impact spacecraft before it was launched to intercept and impact comet Tempel 1 in deep space. Once while helping one of our customers set up a test, I asked what they were doing and they joked with us that they could tell us what they were using the equipment for, but that they would have to kill us afterwards! On one such visit, my cell phone rang in a secure area and everyone froze. They had forgotten to ask for everyone to turn in their phones and my phone created a LOT of paperwork (and probably more trouble behind the scenes than I ever realized!). I also enjoyed my many visits to the large mirror laboratory where many of our systems are still used to measure some of the largest monolithic telescope mirrors in the world.

After 5 years of running 4D, I decided that it was time to pursue other interests and I left my full-time position at the company. I continue to sit on the board and it has been very satisfying to see the company continue to succeed. James Millerd has now been at the helm for nearly seven years and the company has grown quite a bit. Over the years, a number of OSC students have been supported and done their Ph.D. work at 4D. The company recently completed a move into a new office and manufacturing space, the product lines have grown, and there are many new employees. The products are known all over the world and the company has become a leading supplier of dynamic interferometers. Starting a new company isn't for everyone, but I sure had a lot of fun with it and it was a real pleasure to work with Jim Wyant, James Millerd, Neal Brock, and all the good folks at 4D.

John Hayes received his BS in Physics and Astronomy from the University of Arizona in 1975. He received MS (1981) and Ph.D. (1984) degrees from the Optical Sciences Center at the University of Arizona. Dr. Hayes spent 15 years as a member of senior management on the corporate board of WYKO Corporation. During that time, he was responsible for the development of over a dozen product lines, designing numerous state-of-the-art interferometric metrology systems. As a Research Professor at the College of Optical Sciences, Dr. Hayes worked on interferometric vibration-compensated metrology. The author of many technical publications, Dr. Hayes also holds numerous patents in the areas of optical testing, atomic force microscopy, and suspension arm metrology. As an adjunct research professor at the College of Optical Sciences, he continues to teach courses on fast Fourier methods and optical engineering.

At Gates Pass, a different view begins when the sun goes down. The night sky in the areas around Tucson are surprisingly dark for a city of this size. Numerous spots less than ten miles out of town give access to skies dark enough to observe the Milky Way galaxy with the naked eye; Gates Pass is one such spot. There is prime meteor shower viewing to be had anywhere near Gates Pass.

Photo Courtesy of Chris Summitt

Holographic 3D Display

Pierre-Alexandre Blanche

Introduction. Imagine a world where the visual displays used by Tony Stark in the Ironman movies become a reality. In this world, your home television projects 3D images that change in response to your movements without the need for "3D" glasses or other eyewear. In this world, your cell phone displays floating pictures in thin air, where road directions are given to you by signage you see in front of your car. At the College of Optical Sciences, we are developing optical technologies that can make this futuristic world a reality by developing a holographic 3D display.

Figure 1*. Computer graphic imagery of a 3D display used for computer assisted engineering design. Image reproduced from Iron Man 2. Credit Marvel.*

A 3D display is not just a gimmick reserved for entertainment, it can save lives! In hospitals, it will help surgeons visualize injured patients and find the best strategy for an operation. On the battle field, it will help soldiers to avoid enemy fire by showing the elevation of the surrounding terrain and calculating lines of site. For first responders, it can display the entire building structure from rooftop to basement and allow the emergency team to find the safest approach to reach the occupants. If you are using a computer screen in your daily life, a 3D display will accelerate your work by making your interaction with your designs and data more collaborative, more intuitive, and more productive.

The improvement delivered by 3D technology has actually been proven in an Air Force study where the effectiveness of military troops has been evaluated with regular 2D paper maps versus holographic 3D battle maps.[1] For all the 14 specific tasks assessed, the troops performed significantly better with the holographic maps than with the regular 2D maps, even though all the troops had years of training with the 2D paper maps. These holographic terrain maps are now used by the US military to provide soldiers with advanced elevation information during their missions. Unfortunately, these 3D holographic maps are static holograms and are printed in advance of the mission and cannot be updated when new intelligence is gathered. A refreshable

holographic display would allow updated information on troop movement to be delivered to the battlefield in real time.

Currently, a plethora of displays and technologies claim to be holographic but in many cases these approaches use visual tricks rather than authentic optical holography. While these false holographic techniques can create dramatic effects involving images of recording artists, they often mislead the public about their capabilities, and the true benefit of holographic displays. At the College of Optical Sciences, our faculty and staff explore the science behind the human visual system and create genuine holographic displays that can one day turn today's science fiction into tomorrow's science reality.

Visual cues. Humans are meant to see in 3D, and there are different visual cues that help our brain to identify the relative distance to objects. Some can even be reproduced by classical 2D screens, like the relative size of objects, the occlusions (where the object in front masks the background), the perspective (used in tromp l'oeil paintings), or the shading as presented in Figure 2.

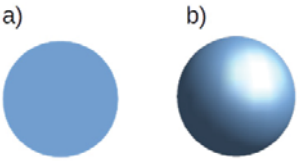

Figure 2*. 3D impression by shading. a) without shading. b) with shading.*

But some cues can only be reproduced by 3D displays, such as the lateral disparity where the image seen by the left eye is different from the image seen by the right eye. Disparity is used in today's stereoscopic 3D theaters and 3D televisions where a pair of glasses is worn by the viewer. The glasses separate the left image from the right image either by filter (usually red and blue as presented in Figure 3), cross polarizers, or shutters (active glasses). The term "stereoscopic" signifies that there are only two views projected to the audience, and this limitation has profound implications, as we will see.

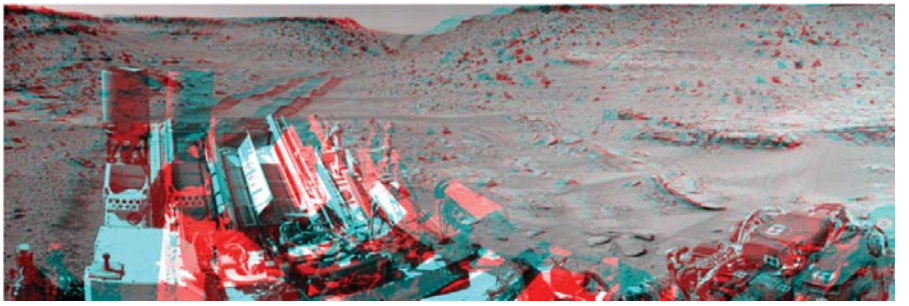

Figure 3*. 3D anaglyph image (red and blue). Curiosity rover on Mars. Credit NASA/JPL-Caltech.*

The human visual system employs multiple visual clues and stimuli that are not reproduced by current stereoscopic 3D displays. Two critical elements used by the human visual system to determine the 3D placement of objects are the motion parallax and the accommodation. Motion

parallax is the relative displacement of objects when the viewer changes position: objects closer to the viewer have a larger apparent translation than objects in the background. This cue is very important in the sense that the brain relies heavily on motion parallax to determine relative distances. Motion parallax is also used to display 360° objects, where the viewer can turn around the image and see all the different sides of a volume. With motion parallax, a scene suddenly becomes more interactive. You can see around corners, look at what is behind an object; your point of view matters, you are part of the visual experience, not someone looking at a scene from the outside.

Accommodation is a bit more complicated and involves the human eye physiology, but it is worth understanding. Inside the eye, there is a lens that helps focus the image on the retina, where the photo-receptors are located. To make the image appear sharp, the lens has to change its power to adjust for the object distance, this process is called accommodation. You can test your accommodation by looking at an object (your finger for example) increasingly closer to your eyes. When your finger is far away, it is easy for your eye to accommodate and bring the image into focus, but as the object moves closer and closer, you will begin to feel some eye strain. For most people, beginning approximately five inches from your face, it is not possible to focus to a sharp image anymore because your lens has reached its maximum power value.

The eye changes its accommodation thanks to the ciliary muscles. These muscles are attached all around the lens, they keep the lens centered in front of the pupil, and stretch the soft tissue of the lens when the focus needs to be changed (Figure 4). This process is automatic and you do not have to think about it, but it sends a feedback to the brain about the distance to the object and this accommodation cue helps your brain construct the 3D scene.

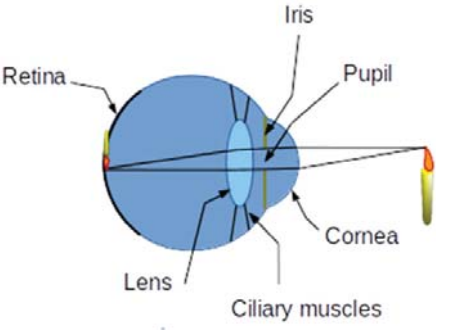

Figure 4. *Eye cross section presenting the different optical elements.*

Accommodation is considered as a secondary cue because a scene can be correctly interpreted without it. However, when people are viewing a display that does not reproduce the accommodation clues for a prolonged period of time, they can experience adverse effects such as dizziness, headache, eye strain, or motion sickness. These reactions occur because there is an unconscious conflict of visual information inside the viewer's brain.

The vergence-accommodation conflict has been very well studied and its principle is presented in Figure 5.[2] When looking at a scene, both eyes are rotating inward to align their optical axis toward the point of interest. This muscle tension exerted to rotate the eyeballs is interpreted by the brain as an optical cue, and is known as vergence. At the same time, and as was explained in the previous paragraph, the ciliary muscle tension stretches the inner lens to

accommodate at the correct focal distance. In the real world (Figure 5A) both vergence and accommodation send coherent and mutually reinforcing stimuli to the brain. But in the case of stereoscopic displays (Figure 5B), while the eyes are rotating toward two different images presented by the glasses, they accommodate to the screen where the images are projected. In this case the focal distance signals are in conflict with the vergence distance signal and the brain can get confused. This confusion is the fundamental reason why stereoscopic displays are not good enough for critical visualization tasks and a better 3D display is needed.

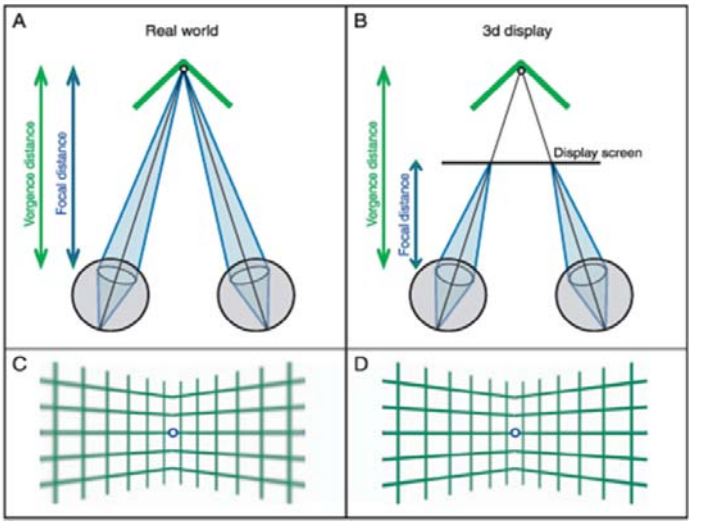

Figure 5. *The vergence-accommodation conflict. A) in the real world both distances are equal. B) For stereoscopic displays, the distances are different. C) In the real world, only objects at the focal distance are sharp. D) In stereoscopic display, the entire scene is sharp regardless of the distance. Credit: Journal of Vision.*

Technologies. There exist two very different display technologies that can provide the correct visual clues to overcome the vergence-accommodation conflict: volumetric displays and holographic displays.

In a volumetric display, the emitters (the pixels) are organized in a 3 dimensional volume instead of being limited to a 2D plane such as in the case of a regular television screen. Each pixel occupies a point in space and can be turned on or off to reproduce the 3D image. Scientists have created volumetric displays with rotating mirrors[3] (Figure 6a), focused laser[4] (Figure 6b), or light emitting diodes filling the volume. One advantage of such a technique is that the scene can be observed from anywhere. The viewer can walk all around the display to see the different perspectives of the object.

In a volumetric display, since the eye is actually looking at the location of the emitter, a real point in space, both the vergence and the accommodation are respected. Unfortunately, occlusions cannot be correctly reproduced since the front emitters do not (and should not) block the light from those at the rear. Technically, since the scene can be observed from any angle, there is no defined front and rear in a volumetric display.

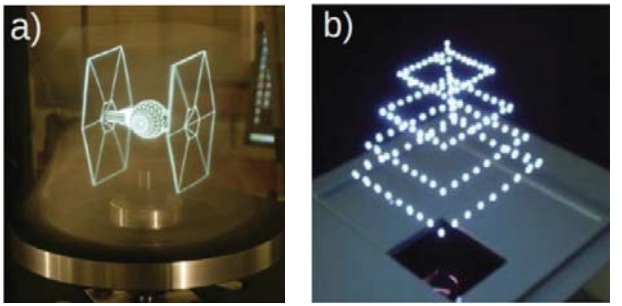

Figure 6*. Examples of volumetric displays. a) Rotating mirror. Credit ICT Graphics Lab at USC. b) Plasma bubbles by focusing laser in the air. Credit NAIST Japan/Omegatron.*

A solution found by researchers to display the correct image is to use a head-tracking device, presenting the correct occlusion for the position of the viewer. However, head-tracking technology works only for individual viewers. For a larger audience, one person will see the correct perspective while all the others will experience awkward perspective distortions.

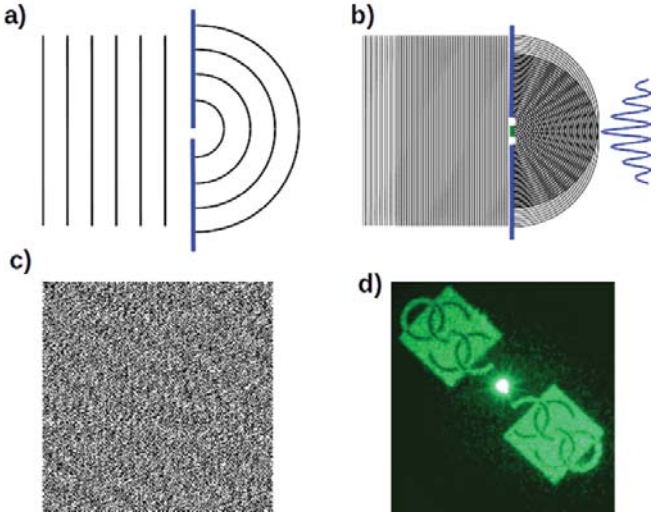

Figure 7*. Diffraction and holography. a) A pinhole transforms a plane-wave into a spherical wave. b) Two pinholes generate interference fringes. c) Carefully located pinholes diffract an image, in the present case the logo of the College of Optical Sciences (d).*

Holography, on the other hand, is a diffractive technique, meaning the light is redirected by very small structures.[5,6] In diffractive systems, apertures such as slits and pinholes change the propagation of light without mirrors (reflection) or lenses (refraction). Diffraction of light can be demonstrated with two pinholes placed close to each other, the Young's experiment. The light exiting the pinholes will interfere and generate fringes as presented in Figure 7b. By mastering diffraction, it is possible to carefully calculate the position of a large number of pinholes such

that the interference they produce generates an image and not just fringes. This calculation is what is presented in Figure 7c where the square mask with a two dimensional diffracting pattern will form the logo of the *College of Optical Sciences* (Figure 7d) when illuminated under the correct conditions (monochromatic collimated light).

The advantage of holography is that it is possible to generate not only the image (amplitude) of an object, but also the shape of the light associated with it, i.e., the wavefront. To understand how important this is, one needs to realize that it is the shape of the wavefront that differentiates the signal received from a point far away from you and one very close to you. In both cases, the image is the same, a point, but the light curvature is different as presented in Figure 8. This wavefront curvature is precisely what makes the eyes accommodate.

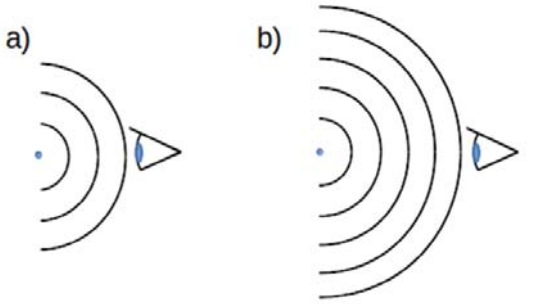

Figure 8. *Change of wavefront curvature according to the distance from an object.*

Not only can holography reproduce the wavefront of light from an object and solve the vergence-accommodation conflict; it is the only technique that can reproduce all the visual cues used by the human visual system. This has been extensively demonstrated with static holograms displaying images projected away from the media.

With holography, it is possible to make the image appear to be floating in thin air, either behind the hologram, like looking through a window, or in front of the hologram. But in any case, your eyes still need to look directly at the screen holding the diffraction pattern to see the image. When looking far to the side of the screen, the diffracted light does not reach your eye and the image just "disappears".

This property is demonstrated by a series of pictures presented in Figure 9: In Figure 9a, the hologram is illuminated from the back by a laser diode, the light is diffracted toward the camera and the image appears behind the plate. Note how the camera was focused on the image which is sharp, but the plate holding the diffraction pattern is out of focus since it is at a different depth. In Figure 9b, the camera has been rotated to the side and the image starts to be cropped outside the field of view of the plate. It is like looking through a window, when moving around the objects that were near the window frame are now hidden by the wall. In Figure 9c, the image is now totally outside of the field of view, and cannot be "seen." Figure 9d shows a picture of the same hologram on a white sheet of paper, the diffracting structure is so small that it cannot be distinguished with the naked eye. For the image to appear, the correct illumination must be used, in this case a monochromatic collimated light.

Static holograms have demonstrated the superiority of the technique over any others for reproducing 3D images with stunning realism, extended depth of field, and rich color gamut.[7] But what about holographic cinema and television, what about holographic moving images?

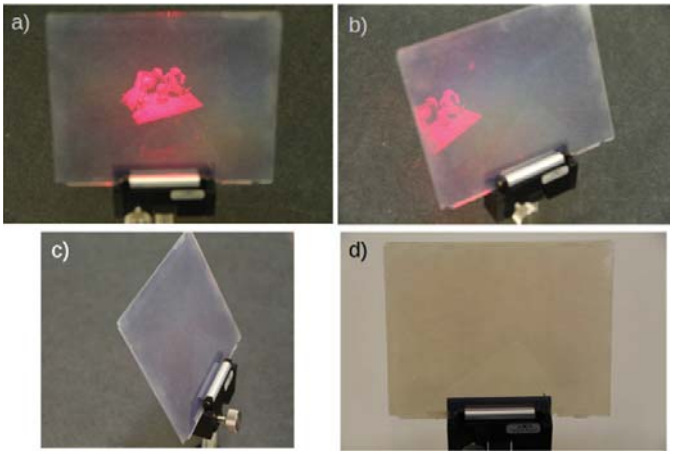

***Figure 9**. Pictures of a hologram. a) When correctly illuminated, the image appears behind the plate. b) When turning the camera around, the image starts to be cropped. c) The image is totally out of the field of view. d) Picture of the hologram on a white sheet of paper.*

Since the early days of holography (first demonstrated by Dennis Gabor in 1947), researchers have been looking toward making a video-rate display using holograms. But the task is not easy because of the numbers of diffractive elements (pixels) that need to be computed to generate an image. In the example in Figure 9, the hologram is composed of elements 300×300 nanometers in scale (half the wavelength of visible light). So for a comfortable 42 inches holographic television set, with a 93×52 cm^2 screen, there should be 5×10^{12} (i.e., 5 trillion) pixels! The values for both resolution and pixel-count are not yet possible to achieve. The best devices used for digital holography today have 5 micron pixels (16 times larger) and support only 2 million pixels. It would take 2.5 millions of these devices combined together to create such a holographic television.

Also, to have the images updated at video rate (30Hz), and to combine the 3 fundamental colors (red, green and blue), there should be 450 terabits per second of information directed to the display, which is 12 million times more information than the 36 megabits/s of the actual Blu-ray disc. 450 terabits per second is about a third of the entire internet capacity available in 2014,[8] and this capacity is needed to support a single display.

Looking at these numbers, one can appreciate the daunting task of building a holographic television. But the story does not end on this depressing impression. The brute force approach can be circumvented by different strategies and researchers all over the world are making progress that brings holographic display a step closer to reality every day.

At the College of Optical Sciences, we have developed a new refreshable recording material, called a photorefractive polymer, so the hologram can be recorded, erased, and updated at will. We are also working on methods to reduce the amount of information necessary to display the 3D image by approximating the wavefront rather than recreating the exact wavefront.

With their hundreds of terabits of information, holograms are so precise that they render details that the human eye is not capable of distinguishing. It is possible for example to detect changes in object shape down to the nanometer level with a technique called holographic

interferometry. But this level of precision is not needed to watch a 3D movie, and trade-offs can be made to dramatically reduce the size of data needed and still provide resolution beyond the capabilities of the human visual system. One of these techniques is holographic stereograms.

In holographic stereograms, the entire hologram is recorded block by block. These blocks are called hogels, a contraction of holographic pixel. Each hogel reproduces a structured cone of light that diffracts different intensities and colors in different directions (Figure 10b). When the viewer changes their position, they see different images or different parallaxes. The holographic display with parallax is in sharp contrast to the classical pixel use for 2D television, where the emitted cone of light is identical in all directions, and where the image does not change according to the viewer's position (Figure 10a).

Also, holographic stereograms do not reproduce a perfect wavefront as is the case with classical hologram (Figure 10c). Instead, the wavefront of the image is approximated by segments (Figure 10d). This segmentation significantly reduces the amount of information that needs to be recorded.

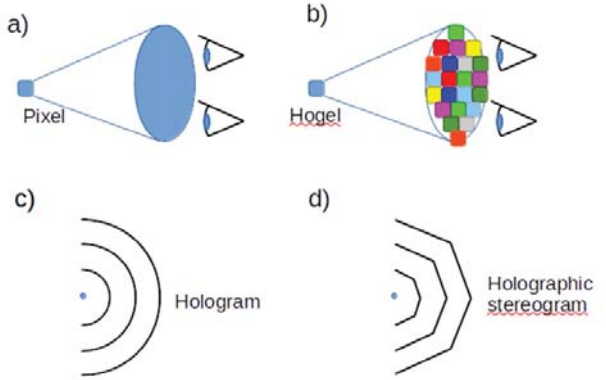

Figure 10. *a) Classic pixel emits a homogenous cone of light. b) Hogel emits a structured cone of light. c) Hologram reproduces the wavefront. d) Holographic stereogram approximates the wavefront.*

Combining the technique of holographic stereogram with new, refreshable, holographic recording material, the *College of Optical Sciences* has developed a holographic 3D display.[9] Figure 11 presents pictures of some holograms recorded with this system. The display can reproduce colors (Figure 11a), using 3D images from various sources, such as computer generated models (Figure 11b), or real pictures taken from different angles (Figure 11c). When viewers move left or right, they experience different parallaxes like for a real object (Figure 11c). The system is capable of a lateral resolution of 250 micrometer which is on par with the best actual 2D displays.

While the research has made significant progress, all the issues have not been solved, and we are not ready to sell millions of holographic 3D television sets in Best Buy and Walmart. The refresh rate of our system is still slower than video rate, and the laser used to print the hologram is rather bulky and expensive. But we are working hard to overcome these technical challenges, and it is our hope that someday in the near future we will present a holographic 3D display that can entertain at home, help at the office, and save lives in hospitals.

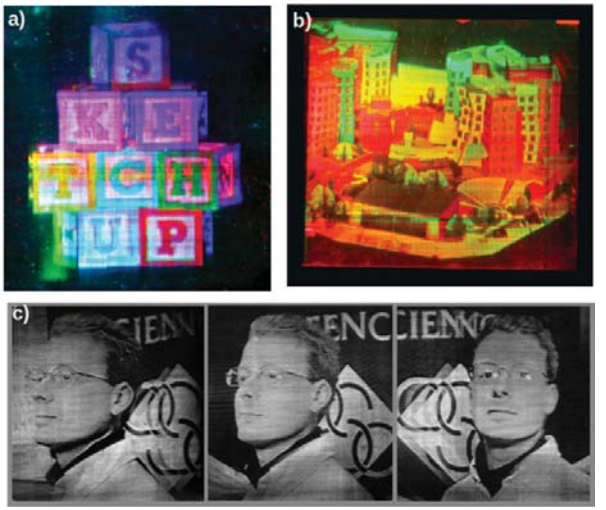

***Figure 11**. Pictures of holographic stereograms recorded with the College of Optical Sciences holographic display. a) Full color hologram. b) Computer generated architectural model. c) Pictures of the same hologram taken from different angles demonstrating the parallax.*

1. Martin, J. and Holzbach, M., "Evaluation of Holographic Technology in Close Air Support Mission Planning and Execution," Air Force Research Laboratory Human Effectiveness Directorate, Warfighter Readiness Research Division, Technical Report (2008).
2. Hoffman, D. M., Girshick, A. R., Akeley, K., & Banks, M. S., "Vergence-accommodation conflicts hinder visual performance and cause visual fatigue," Journal of Vision, **8**(3):33, 1-30 (2008).
3. A. Jones at al., "Rendering for an Interactive 360◦ Light Field Display," Proceeding SIGGRAPH, Emerging Technologies (2007).
4. H. Kimura et al., "Laser produced 3D Display in the air," Proceeding SIGGRAPH, Emerging technologies, 2006.
5. S. Benton and V. M. Bove Jr., "Holographic Imaging," Wiley-Interscience (April 2008).
6. P.-A. Blanche, "Field Guide to Holography," SPIE Field Guides Volume **31**, SPIE press (2014).
7. H. Bjelkhagen and D Brotherton-Ratcliffe, "Ultra-realistic imaging. Advanced techniques in analogue and digital colour holography," CRC Press, Taylor and Francis Group (2013).
8. CISCO, "The Zettabyte Era—Trends and Analysis" (May 2013).
9. P.-A. Blanche *et al.*, "Holographic three-dimensional telepresence using large-area photorefractive polymer," *Nature*, vol. **468**, issue 7320, pp 80-83, 4 (November 2010).

Pierre-Alexandre Blanche is an Assistant Research Professor at the College of Optical Sciences, University of Arizona. He received his Ph.D. In 1999 from the University of Liège (Belgium), and then held a post-doctoral position at the University of Arizona in the field of nonlinear optics. Back in Belgium, he developed a hologram production facility for diverse scientific applications using dichromated gelatine and photopolymers. In 2006 he joined the College of Optical Sciences to work on photorefractive materials, holographic 3D displays, and various diffractive optical systems.

Lizards are ubiquitous throughout Tucson, from the tops of the mountains down to the desert floor, from the wilderness areas to the center of the city. The Greater Earless Lizard, perched on a rock in this photo, is one of the most colorful lizards in the region.

Photo courtesy of Brian Anderson

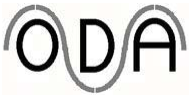

OPTICAL DATA ASSOCIATES, LLC

precision spectrophotometric measurements
5237 E. Seventh Street • Tucson, AZ 85711• Phone & Fax (520) 748-7333
optical@opdata.com • www.opdata.com

Optical Data Associates, LLC came into formal existence in December, 1991, but its origins lie clearly in Room 506 of what was then the *Optical Sciences Center* in the late 1970s. When the late Prof. Bernie Seraphin hired me as a Research Associate in 1977 to work with the Solar Energy Group, one of my responsibilities was the operation of the Optical Measurement Laboratory. That job remained in my portfolio till I left fourteen years later. During that period, we acquired and commissioned a new generation of spectrophotometric instruments, moving from optomechanical marvels, the Cary 14 UV-Vis-NIR and the Perkin-Elmer 137 IR spectrophotometers, to the first generation of digital instruments, the Cary/Varian 2415 and the Analect FTIR. Through the 1980s, research funding for optical coatings was strong, and the Measurement Lab supported not only the wide range of projects under the leadership of Prof. Macleod, but work conducted by groups throughout the Center and elsewhere on Campus and in the Tucson area. That funding then declined around 1990, and it was time for me to try something else.

I had always wanted my own full-time technically-oriented business, and I realized that establishing a totally independent spectrophotometry test laboratory might be feasible. My wife, Dr. Simone Jacobson, with a doctorate in chemistry from Cornell, eagerly agreed to be my business partner. When Security Pacific, since acquired by Bank of America, approved our business plan and provided an $80,000 loan, we formed *Optical Data Associates* in 1991 as a partnership. We converted our big two-car garage into a laboratory/office, purchased Varian Cary 500 UV-Vis-NIR and Perkin-Elmer 983G IR spectrophotometers and appropriate accessories as our first instruments, and jobs arrived immediately. The hunch that we could run a profitable independent lab has remained accurate; the stream of work has flowed reliably for 23 years. We paid off the loan in less than two years, and we have never needed to borrow significantly again.

In 1992, ODA won a major project as the Prime Contractor for silver coating development for the Gemini 8-M Telescopes Project. We hired two subcontractors for evaporation and sputtering of silver films and performed the management and measurement work across the spectrum. The contract ended successfully in 1995; we transferred the technology and Gemini began the shift from aluminum to silver coatings for major astronomical mirrors worldwide.

Tragedy arrived for Simone in 1998. Mammography detected trouble in June, and a small but nasty tumor was removed in July. Chemotherapy was recommended, and that ordeal began in September. Each cycle was worse, and a week after the fourth infusion, I took her to the hospital. She died there three days later, only 52 years old. Even though I have remarried and live nearby, the lab and her spirit remain where they were.

Since ODA's inception, over one thousand clients have been served, ranging in size from single-person enterprises like ODA to the world's largest companies, recently including Apple, Google, and Intel. Although I have measured the optical properties of rocks, roofing, pavement, shoes, horsehair, bones, prunes, beer, and other substances, the clients of ODA fall mainly into five categories:

- **Biotechnology:** ODA frequently calibrates filters employed in systems that monitor turbidity and other properties of blood.

- **Astronomy and Aerospace:** In addition to the Gemini Project mentioned above, ODA has performed measurements and consulted for many other telescope projects, including Large Synoptic Survey Telescope [LSST], Large Binocular Telescope [LBT], the Keck, SOFIA, Lick, Palomar, Discovery, MacDonald, and France-Canada-Hawaii Observatories, NASA-Wallops Flight Facility, NSBF, the National Scientific Balloon Facility [NSBF], and many projects at JPL. Related aerospace customers have included Lockheed-Martin, Boeing, Ball, Pilkington, and Goodrich Aerospace, and L3 Communications.
- **Military:** Through haze and transmittance evaluations, ODA has contributed to the development of massive armor glass windows for tanks and personnel carriers through a long project with BAE and other producers over the past ten years. Other involvement has been with General Dynamics and other satellite builders.
- **Energy Conservation:** ODA is the only independent lab in the USA that qualifies glazings for the International Glazing Database [IGDB] at the Lawrence Berkeley Laboratory [LBL]. This database permits engineers and architects to simulate low-emittance and other types of windows from listed glazing components. ODA can also characterize phase-change materials and take data at both cryogenic and elevated temperatures.
- **Information Technology:** Clients include organizations in the computer, entertainment, and museum areas.

ODA benefits profoundly from the *College of Optical Sciences* through the network of other spinoff companies in the Tucson area. ODA both supports the efforts of and seeks support from such companies as BRO, Photon Engineering, INOV, Optical Perspectives, and Composite Mirror Applications. The synergy inherent in these relationships strengthens all of us.

ODA selectively acquires cutting-edge instruments and accessories to provide the best possible services to its clients. The best recent example of such an effort has been ODA's participation in the development of the Universal Measurement Accessory [UMA] for Agilent's Cary 5000 UV-Vis-NIR over the past seven years. After serving as a beta-site and traveling to Australia twice to consult, ODA purchased the first UMA in the USA in August of 2013. The UMA provides unprecedented, versatile, fully-automated abilities to measure transmittance and reflectance at variable angles over the full spectral range of the instrument.

I am grateful to the *College of Optical Sciences* for serving as the incubator for ODA as for so many other companies, and also to the wonderful optical community in the Tucson Area, for allowing me to live my simple goal of operating an independent laboratory that supports academic, commercial, and government organizations throughout the USA and beyond.

Michael Ray Jacobson was born in Pittsburgh, Pennsylvania, on 1/11/1950. He graduated from Taylor Allderdice High School, Valedictorian, 1967, Harvard College, AB Cum Laude, Physics, 1971, Cornell University, MA, Astronomy, 1974, and Cornell University, PhD, Astronomy, 1977. At the *Optical Sciences Center* of the University of Arizona he was Research Associate to Associate Research Professor from 1977 to 1991. He is the Co-Founder and Associate of *Optical Data Associates, LLC* (1991-date). The photo on the right shows Dr. Jacobson and his late wife, Dr. Simone Ellen Jacobson, at ODA in 1993.

Astronomical Optics

James Burge

The University of Arizona is making the optics for the Giant Magellan Telescope, which will be the world's largest telescope when it is operational on a mountaintop in Chile around 2020. This telescope primary mirror is 25 meters across, made from seven 8.4-meter diameter segments. Telescope design and technology have come a long way since the time Galileo first turned his telescope to the sky. Galileo's observation of the moons of Jupiter and the phases of Venus changed the way we understand the universe. With modern telescopes, we are now imaging planets that orbit other stars!

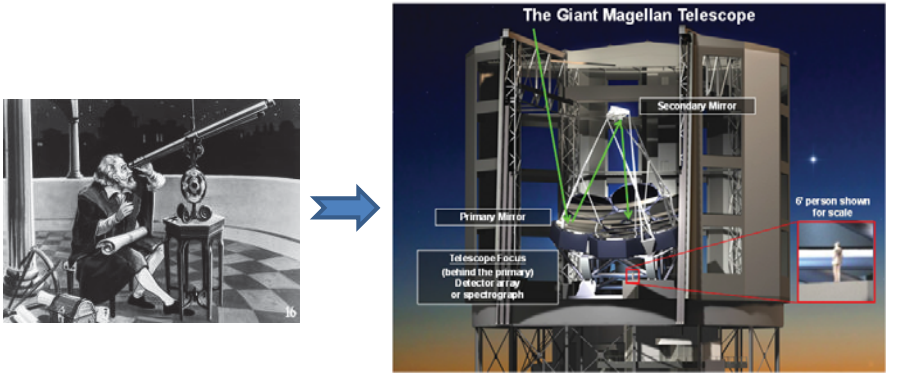

Figure 1. Optical technology for telescopes has advanced over the last 400 years of technological advances from Galileo's first 2-lens telescope[1] to the Giant Magellan Telescope[2] that uses an array of large mirrors.

Telescope observations require two main functions: the lenses or mirrors collect and focus the light, and the detector turns the light into a signal that can be used for processing. The use of larger and more precise optics creates a sharper, brighter focus that increases resolution (the ability to see small objects) and sensitivity (the ability to see dim objects). The technological advancement for the detection of light has improved from the human retina to film to electronic detectors that operate at nearly the performance limits of fundamental physics. We focus here on the recent technology advances that enable a leap in size and precision of telescope optics. Galileo's optical system improved his vision by an order of magnitude using a few small lenses. This design was expanded through the 1800's to use larger lenses. The largest telescopes use curved mirrors rather than lenses to collect and focus the light.

The science of astronomy has moved forward in large steps enabled by increased telescope capability. Fundamental limits on both resolution and sensitivity are directly connected to the size of the telescope aperture. Historically, the telescope resolution has been limited by defects in the telescope and by atmospheric fluctuations. But current telescopes achieve near perfection, using high-quality mirrors and adaptive optics systems that measure the atmospheric effects and compensate with ultra-thin deformable mirrors at the rate of 1000 times a second.

Modern telescopes achieve the ultimate possible resolution that is limited by the physics of diffraction, which couples the wave-like nature of light with the finite size of the collecting mirror. Rather than focusing light from a distant star to a point on the detector, diffraction causes the image to be blurred by an amount that corresponds to an angle on the sky of λ/D where λ is

the wavelength of the light and *D* is the diameter of the primary mirror. This effect is shown in Figure 2, where images from the smaller telescopes appear blurry compared to the simulated GMT image. The GMT will have resolution to read the headlines of a newspaper 50 miles away!

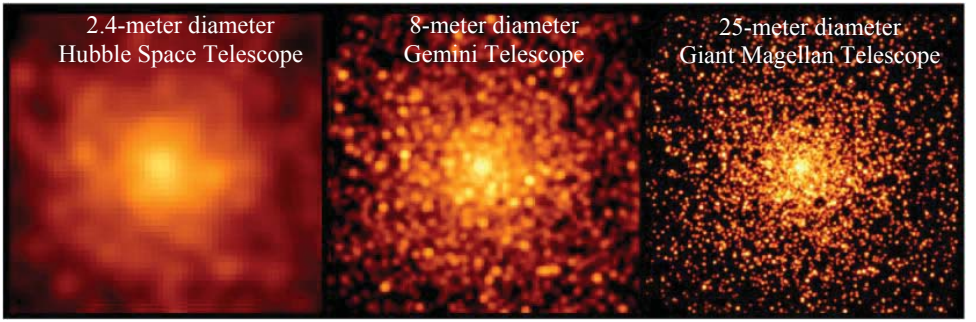

Figure 2. The resolution of all telescopes is limited by the physics of diffraction, providing enhanced performance with larger apertures. The improved image quality for the Giant Magellan Telescope with its adaptive optics atmospheric compensation is clearly seen in these simulated images of a globular cluster made over a 2 arcsecond field at 1.5 μm wavelength.[2]

The ultimate sensitivity is limited by the physics of quantum mechanics, which couples the particle-like nature of light with the statistics of detection. Detectors convert photons of light into photoelectrons that are counted to determine the amount of light. Modern detectors are extremely efficient and low-noise, turning each photon with the appropriate energy into a photoelectron without introducing stray electrons. But the photon stream is not continuous, so any measurement of a finite number of photoelectrons will follow Poisson statistics giving a random error that goes as the square-root of the total number of electrons. So the dynamic range is also equal to the square-root of the number of electrons. It takes a million photoelectrons per pixel to take images that have 0.1% noise or 1000:1 dynamic range. The only way to see dim objects is to collect a lot of photons, which requires larger collection area or more time. We achieve both by increasing the mirror size and the telescope's field of view. (The increased field of view allows simultaneous observation of multiple objects.)

Historically, telescope size has been limited by the technical abilities of making and supporting large collection optics. Lenses are limited to about 1 meter across, and suffer from the imperfections in the glass that absorb, scatter, disperse, and distort the light that goes through them. Mirrors that are made of glass and coated with reflective metal are now used for all large telescopes. Since the light does not penetrate the reflective coating, the only important property of the glass mirror underneath is its shape. Single mirrors up to 8.4 meters across are built into large telescopes. The 8.4-meter size represents a practical upper limit for manufacture, shipping, handling, and coating. Telescopes larger than 8.4 meters use multiple mirrors, such as the Large Binocular Telescope (LBT) and the Giant Magellan Telescope (GMT). The LBT, which is operational in Arizona, combines the light from two 8.4-meter diameter telescopes to achieve the resolution of a 23-meter telescope and the collecting area of a 12-meter telescope. The resolution and sensitivity of the LBT is sufficient to image planets that are circling distant stars.

The LBT and GMT provide sharp images and high-resolution spectral information by staring at particular science objects of interest. The Large Synoptic Survey Telescope (LSST) shown below in Figure 4 offers a wide field of view to take images of the full sky. This telescope

uses a more complex three-reflection design to achieve a 3.5° field of view in a compact structure that can be rapidly repointed. A single 8.4-meter glass mirror is being made at the University of Arizona which provides two different reflections in the telescope. The outer region provides the primary (1st reflection) and the inner region, which is more steeply curved, is the tertiary (3rd reflection).

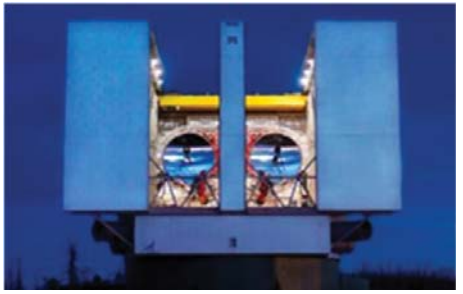

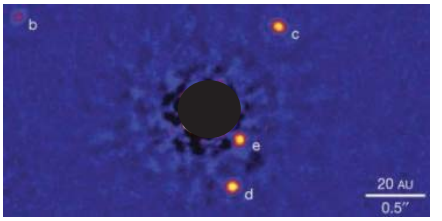

The multiple planet system orbiting HR8799, as resolved at LBT. The much brighter central star has been largely blocked, and four planets are labeled b, c, d and e.

Figure 3. The Large Binocular Telescope[3] on Mt. Graham, Arizona combines two 8.4-m diameter telescopes to achieve excellent resolution and sensitivity, enabling the acquisition of images of planets around other stars.[4]

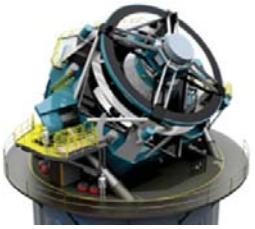

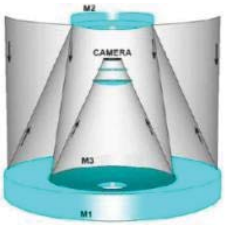

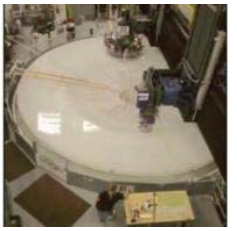

Figure 4. The Large Synoptic Survey Telescope uses three reflections to achieve a wide field of view. The combined 8.4-m diameter primary-tertiary mirror (M1 and M3) is being polished at the University of Arizona.[4]

The University of Arizona has developed unique capabilities for making large mirrors and building them into astronomical telescopes. Some of the key challenges and the University of Arizona solutions are shown in Table 1 and discussed further below.

Table 1. Issues for primary mirrors and the UA technical solutions

Issue	University of Arizona technical solution
Large mirror diameter	One-piece glass casting of 8.4-m diameter mirror blanks
Mirror shape change from wind pressure	Stiff, lightweight honeycomb mirror substrate
Mirror shape change from temperature variation	Low expansion glass, telescope thermal control
Mirror shape change from telescope motion	Support mirror with active supports
Air turbulence caused by mirror	Drive the mirror temperature to match the air
Small enclosure desired to reduce cost	Use steeply-curved mirrors with short focal length
Manufacture of steeply curved mirror blanks	Spin-cast the liquid glass, providing curved surface
Smooth steeply curved mirror surface	Computer-controlled stressed lap polishing tools
Accurate mirror shape measurement	Interferometry with computer-generated holograms

Light travels in waves. The diffraction-limited performance can only be achieved if the imperfections in the light's wavefront coming to focus are small compared to the light's wavelength of about 1 μm. Since any shape error in the reflective surface of the mirror will directly affect this wavefront, the optical surface must be manufactured accurately and the mirror must be supported such that this shape is maintained to a small fraction of a micron during the telescope operation.

The University of Arizona mirrors are specially designed for telescope operation. The large primary mirrors are cast and polished at the Steward Observatory Mirror Lab under the stands of Arizona Stadium. The mirrors are cast of low-expansion borosilicate glass in a spinning furnace to achieve a smooth curved surface on the top, supported by a lightweight honeycomb structure. Figure 5 shows the first of the 8.4-meter mirrors cast at the University of Arizona.

The stiffness of the UA mirrors provides excellent stability for the mirror shape in the operational telescope. An additional level of accuracy is applied using active support and thermal control. The mirrors are held in the telescope using a combination of 160 force-controlled actuators to maintain the shape, and six "hardpoint" stiff actuators that define the position. During the night, the telescope performance is monitored and the actuators are adjusted to maintain high-quality imaging. The mirror blanks are hollow, allowing temperature control by blowing controlled air into the empty voids.

Figure 5. The 8.4-meter diameter LBT primary mirror blank cast of low-expansion borosilicate glass in the spinning furnace at the University of Arizona's Steward Observatory Mirror Lab.

While the UA primary mirrors are made to be quite stiff, other primary mirrors are made to be thin and flexible. The primary mirror for the Daniel K. Inouye Solar Telescope, which is being polished at Large Optics Facility in the basement of the College of Optical Sciences, is 4.2 meters in diameter and only 75 mm thick. Since this telescope operates in the Sun, the thermal requirements are much different than those for night-time astronomy. The blank is made from Zerodur™, which does not distort due to temperature changes, and will be supported in the telescope with 118 force-controlled actuators.

Flexible mirrors are also used as secondary mirrors. The secondary mirrors for LBT and GMT are about 1 meter in diameter and are only 2 mm thick! These thin glass mirrors are supported with 672 actuators that deform the shape with millisecond response time to compensate for the effect of the atmosphere. Other telescopes use thin primary mirrors.

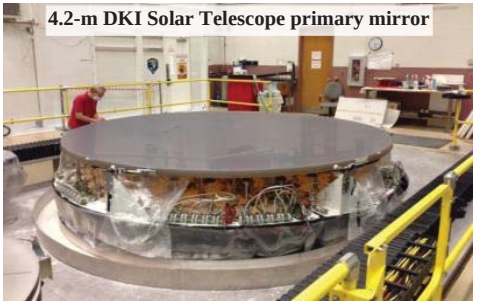

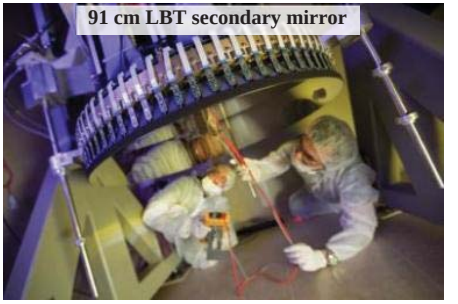

Figure 6. Thin flexible mirrors are used as the secondary mirror for LBT (2 mm thick with 672 actuators), and as the primary mirror for the DKI Solar Telescope (75 mm thick with 118 actuators).

Telescope cost is driven by the size of the enclosure, and the telescope length is defined by the focal length of its primary mirror. Primary mirrors that are more steeply curved have a shorter focal length allowing a smaller enclosure. However, it is much harder make mirrors as the focal ratio, defined as the ratio of focal length to diameter, is reduced. Steeply curved mirror blanks are cast by spinning the entire oven when the glass is molten so that it flows out naturally to the appropriate shape. But the most challenging aspect of the steeper mirrors comes from the complex shape of the optical surface. The required shapes for the primary mirrors are all nearly paraboloidal (a parabola of revolution), but the natural surface to polish and measure is part of the surface of a sphere. Optical surfaces are polished to be smooth and accurate by rubbing them with tools called laps using abrasive compounds that remove material to wear down the surfaces. A smooth surface results from a lap that fits the surface nearly perfectly. A spherical surface has the same curvature at all points on the surface, so the laps always fit. For this reason most optical surfaces are polished to be spherical. But the telescope designs require paraboloidal surfaces, which depart from this condition by an amount that is inversely proportional to the focal ratio to the third power. Classical techniques for making telescope mirrors allow only a few hundred microns of shape departure from spherical, which limits the focal ratio to ~2. University of Arizona's technologies enable steep paraboloids with focal ratios as low as 0.7, which are 20 times more difficult.

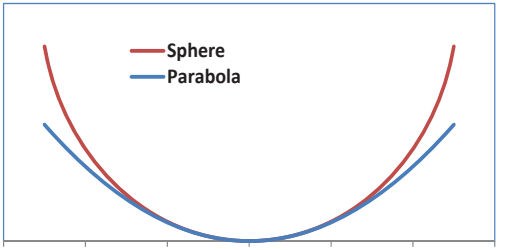

Figure 7. Telescope mirrors are difficult to polish and measure because of the large difference between the required paraboloidal shape of the mirrors and the natural spherical shape. The paraboloid (a parabola of revolution) is the natural geometric shape that brings rays of light to a sharp focus. The sphere is the natural shape that has the same curvature everywhere on the surface.

The telescope mirrors require steeply-curved optical surfaces that are accurate to a small fraction of a micron overall, and are smooth to better than 2 nm over scales of a millimeter. This near-perfection is achieved with advanced technologies for both polishing and measuring. The mirror accuracy and smoothness are achieved by processing the surface in several steps, each one providing a smoother and more accurate surface.

Steps for manufacturing the optical surface of a large mirror

1. **Generating:** The initial cast surface departs from ideal by many millimeters. We use the Large Optics Generator for initial shaping. This computer-controlled machine cuts the surface using a high-speed diamond cutting wheel driven to follow the desired mirror profile. This step is especially difficult for the primary mirror for the Giant Magellan Telescope. Each 8.4-meter diameter circular mirror segment is an off-axis portion of a 25-meter diameter paraboloid, so the deviation from spherical on the mirror segment follows a complex shape that varies by 14.5 mm across the mirror.

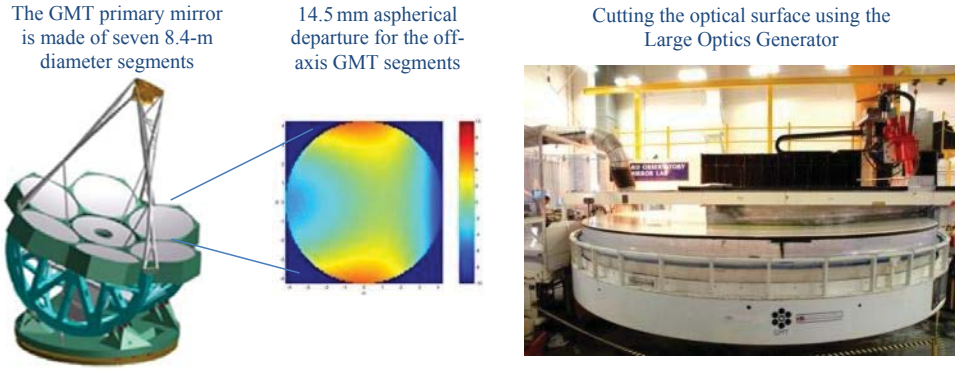

Figure 8. The Large Optics Generator uses diamond tools to cut the surface shape into one of the 8.4-meter diameter off-axis mirror segments for the Giant Magellan Telescope. These mirrors have 14.5 mm deviation from the natural spherical shape.

2. **Loose abrasive grinding:** The surface is stroked using a tool covered with hard tiles while abrasive grit is introduced. The grinding action of the abrasive material wears down the mirror surface according to the tool motion. The "stressed lap" grinding tool is deformed under computer control such that it always matches the desired aspheric shape of the mirror. In this stage of manufacture, the surface is measured to ~1 μm accuracy by scanning a ball across it and using a laser tracker system to measure the position of the ball. The laser tracker shoots a laser beam that follows a prism reflector inside the ball, using the reflection tom measure its position. The grinding runs are optimized to steadily improve the shape by rubbing more on the high regions and to create a finer surface using a succession of finer abrasives.

3. **Polishing:** The final operation uses the same stressed lap, but with very fine polishing compound to continue to wear down the surface to improve its shape and to leave a smooth, specular surface. The stressed lap insures that the polishing tool always fits the aspheric surface. We also polish with smaller tools that use viscoelastic materials to conform to the aspheric shape.

4. **Metrology:** In this polishing stage of processing, the mirror surfaces are measured to an accuracy of a few nanometers using laser interferometry. Since the mirrors are steeply aspheric, additional lenses, mirrors, and holograms are required to enable the measurements. These measurement systems are quite complex, so each mirror is measured with a combination of systems to insure that the measurements are correct and that the mirror is made right.

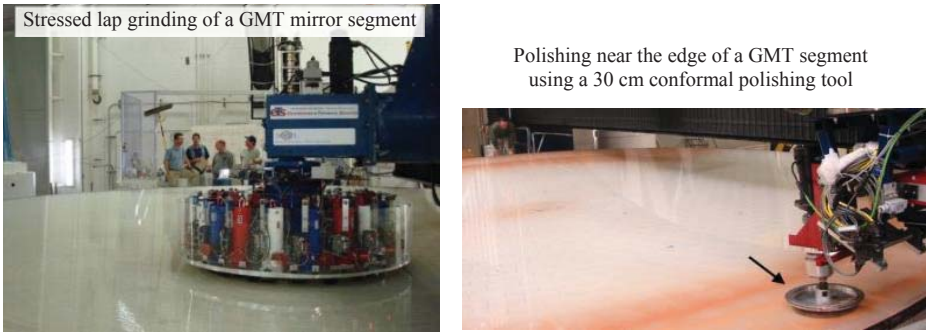

Figure 9. Accurate polishing of the GMT mirrors requires computer-controlled stroking of tools on the surface to wear down the desired regions of the optical surface. The tools are made to fit the aspheric surface by computer control for the stressed lap on the left, and using flow of a viscoelastic compound for the 30 cm tool on the right.

The surface measurements are especially challenging for these steeply aspheric mirrors. Optical systems are mounted above the mirror in the 28-meter tall isolated tower at the Mirror Lab. The GMT mirrors use a succession of different measurements. The laser tracker system is used to guide the grinding and initial polishing. The most accurate measurements are made using a laser interferometer with additional optics to compensate for the steep aspheric shape. The GMT interferometric test requires two large curved mirrors (one is 3.8 meters across!) and a computer-generated hologram. A final corroboration for the GMT mirrors uses a scanning pentaprism test that scans laser beams across the surface and measures their reflection. This combination of measurements provides the information needed to guide the manufacturing and to assure the quality of the final surface.

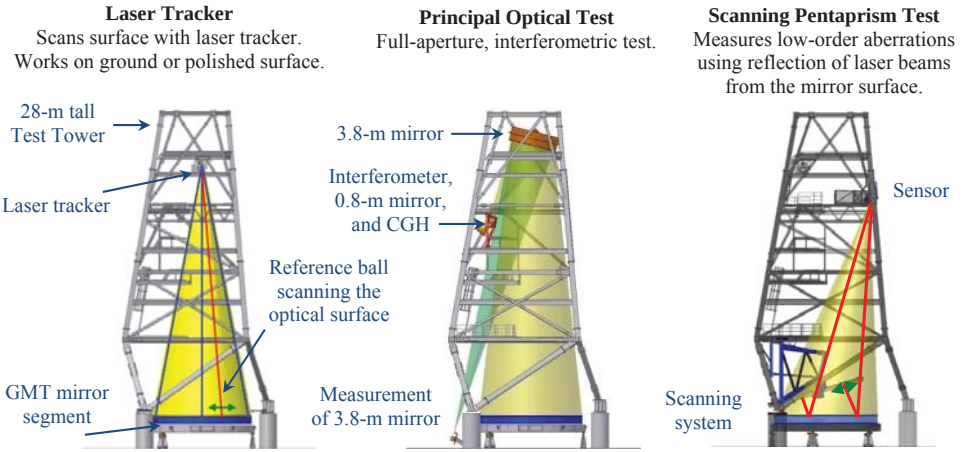

Figure 10. Three systems were developed for measuring the optical surface of the GMT mirror segments. The laser tracker is used to get the surface close, the principal optical test uses interferometry to guide the final polishing, and the scanning pentaprism test verifies the final shape.

The large telescope projects provide unique opportunities for University of Arizona students who join the LOFT (Large Optics Fabrication and Testing)[6] group and support the projects with research and development. LOFT students have provided the key elements of all of the items described above: computer-controlled polishing, viscoelastic laps, laser tracker metrology, CGH interferometry, and scanning pentaprism metrology. Students performed the fundamental research including initial exploration and prototyping. As the full-scale systems were engineered and deployed, students worked alongside seasoned UA staff, building professional skills and completing complex hardware projects. For each of these items, a student successfully completed a PhD dissertation that pushed the state of the art, and the student was a key member of a professional team that implemented the new technology at giant scale.

The University of Arizona provides the opportunity to do more than just cutting edge research. UA students make meaningful contributions to new telescopes that will make history. Shown on the following page are a few recent and current LOFT students.

1. "Galileo's telescope at 400: From Spyglasses to Hubble," *National Geographic*, August 2009.
2. www.gmto.org.
3. www.LBTO.org.
4. Skemer *et al.*, *ApJ* **753** 14 (2012).
5. www.LSST.org.
6. www.loft.optics.arizona.edu.

James Burge is a Professor at the University of Arizona with joint appointments in Optical Sciences, Astronomy, and Mechanical Engineering. He is the founding director of the Large Optics Fabrication and Testing group and the Optomechanical Engineering Laboratory at the College of Optical Sciences. Dr. Burge has published over 300 papers that span the fields of optical design, fabrication, testing, alignment, instrumentation, and optomechanical engineering. Dr. Burge is a fellow of both SPIE and OSA. He has also founded two companies, *Arizona Optical Systems* and *Arizona Optical Metrology* that manufacture a variety of high-technology optical systems.

Graduate students in the Large Optics Fabrication and Testing group perform fundamental research and apply it to real optical systems. See what a few LOFT students had to say about the College of Optical Sciences.

Wenrui Cai at the VLT Telescope site in Chile

"I am grateful to have been a part of the Large Optics Fabrication and Testing Group (LOFT). It is an important bridge connecting academic world and industry. As a graduate student, I had the opportunity to work on large projects, for example, testing the first segment of primary mirror of Giant Magellan Telescope (GMT). In addition, I really enjoyed the bi-weekly group meetings and the quad-chart presentations. LOFT is a big group with a large variety of research topics and hardware projects. In the group meeting, not only I can interact with my peers, but also practice my presentation skill."

Wenrui completed his PhD thesis in 2013, *Wavefront Analysis and Calibration for Computer Generated Holograms,* and was subsequently employed by a major semiconductor company.

Laura Coyle in the lab

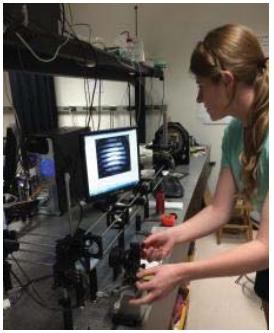

"Optical Sciences had everything I was looking for in a graduate program – world class facilities, faculty who are leaders in their field, specialized courses, and a thriving graduate student community. As a member of the LOFT group, I was able to make meaningful contributions to a number of large mirror projects, gain valuable experience with hardware—from table-top prototypes to multi-million dollar deliverable systems—and work with a group of passionate students, staff, and faculty. I was given responsibility for important tasks and worked to deadlines, helping me to not only develop technical skills, but also learn to work efficiently as a member of a team. Though I worked hard in classes and lab, there was still time to go camping with the Student Optics Chapter and play on the intramural soccer and basketball teams. The professional connections I developed through Optical Sciences, especially the bi-annual Industrial Affiliates event, provided valuable career development, and resulted in multiple exciting job opportunities upon graduation."

Laura is finishing her PhD thesis, *Alignment and calibration of optical systems using computer generated holograms*, and has already been hired by a major aerospace company.

Eric Frater with Wide Field Corrector for the Hobby Eberly Telescope

"The College of Optical Sciences has given me the opportunity to develop as a professional engineer with opportunities to do relevant work on important projects. The experience I have gained in the LOFT group and specifically within the large optics shop has given me practical skills with optics that cannot be learned in class. In addition, the level of responsibility I am given in my research has helped me develop as an effective team member and as a leader."

Eric is in his third year of the PhD program, preparing for a dissertation on precision mechanics and optical alignment.

Snow is common in the winter in the mountains around Tucson, but snow in the lower elevations is a rare event. When it occurs, the region can be transformed into an almost unrecognizable landscape. Walking on a trail though the ephemeral beauty of a blanket of snow on cacti, as shown here in a February snowfall in Sabino Canyon, is an otherworldly experience.

Photo courtesy of Brian Anderson

AdValue Photonics, Inc.

Shibin Jiang

AdValue Photonics develops and manufactures fiber lasers, amplifiers, broadband sources, and passive components. We introduce new products to the market that enable new capabilities for our customers' applications. Our mission is to serve as a value-adding and long-term partner to our customers, helping them achieve and preserve excellence and efficiency with our quality products and superior services.

The company's core competency and proprietary technology are in the areas of advanced rare-earth doped gain glasses, specialty fibers, and fiber laser/amplifier systems. It is by leveraging our expertise in these areas that we develop innovative products to our serving markets. Our proprietary non-silica gain fibers have the advantages of higher gain and higher output power over a shorter fiber length, broader gain bandwidth, and significantly lower optical nonlinearity as compared to silica-based gain fibers. These advantages make possible light generation and amplification at intensities otherwise beyond reach. These fibers are also immune to photo-darkening, which is a deficiency associated with heavily rare-earth-doped silica fibers. A wide variety of fiber types can be readily engineered for specific fiber-based device designs, including truly single-mode fibers with large mode area, double cladding fibers, triple cladding fibers, polarization maintaining (PM) gain fibers, and photonic crystal fibers. These specialty fibers are employed to build innovative lasers and amplifiers.

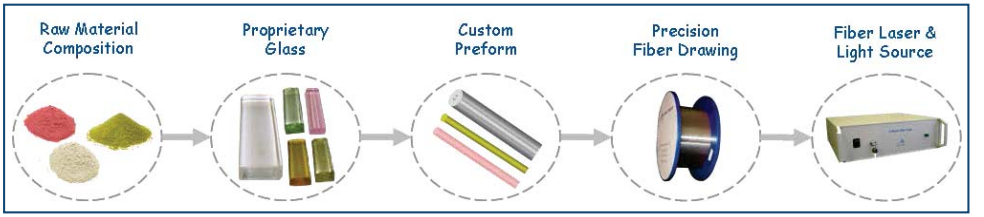

***AdValue Photonics*: From Raw Chemical Materials to Fiber Laser Systems.**

Current products have a focus on the wavelength region of 2 microns (~1.9-2.1 μm) including 2 micron mode-locked, Q-switched, continuous-wave (CW), single-frequency fiber lasers, 2 micron fiber amplifiers for both CW and Pulsed applications, and near 2 micron supercontinuum fiber sources. Application areas include LIDAR, sensing, frequency conversion, material processing, and laser surgery. Recently we also developed an all-fiber isolator at 1 micron wavelength, which can handle greater than 50 W backward power. This world-first all-fiber isolator enables the development and reliable operation of greater than 10 kW level, 1 micron wavelength fiber lasers.

The *AdValue Photonics'* outstanding employees include 12 senior engineers with Ph.D. degrees in optics, physics, chemistry, glass materials, and mechanics. Many of our engineers are graduates of the *College of Optical Sciences*. A great team produces great products. In the several years of the company's existence, we have obtained prestigious awards such as the 50th Anniversary 2012 R&D 100 award, and CLEO/Laser Focus World Innovation Award 2011 Honorable Mention.

Dr. Shibin Jiang, president and CEO of *AdValue Photonics*, founded the company in June 2007. Prior to that, Dr. Jiang had co-founded *NP Photonics* (1998), and successfully led the commercialization of single-frequency narrow-linewidth fiber lasers at 1.55 μm and 1.0 μm. Dr. Jiang also founded *AdValue Technology* in 2003, which presently is the leading supplier of alumina crucibles, zirconia crucibles, and fused-quartz crucibles for glass manufacturing, chemical processing, metal melting, semiconductor manufacturing, and lab ware applications. As an adjunct research professor of the *College of Optical Sciences*, Dr. Jiang is involved in developing joint projects with faculty members and interacting with students, which, among other things, has enabled him to identify and recruit some of the brightest Op-Sci graduates.

Polarization in Optical Design

Russell A Chipman

For many optical systems, designing and controlling the polarization properties present substantial challenges, and for systems like liquid crystal displays, obtaining good commercially competitive solutions can require man-years of dedicated polarization engineering. Such systems are called *polarization critical optical systems* because of the difficult polarization challenges. High resolution microscopes and microlithography projection optics are two more examples of polarization critical systems. Polarization engineering is the frequently difficult task of designing, fabricating, testing, and often mass producing with high yield, such polarization critical optical systems.

Polarized Light. Light is a transverse electromagnetic wave. The light's electric field oscillates in a direction transverse to the direction of propagation. Polarization refers to the properties of the light in this transverse plane.

The human eye is not sensitive to polarized light. Thus polarization effects escape our notice. Our eyes cannot tell that the light from rainbows and the glare reflecting from the road are highly polarized. Nor do we see how polarized light is scrambled by the stress in our eyeglasses and many other transparent plastic objects, such as clear plastic rulers and tape dispensers. Polarizers and polarimeters can make such polarization effects visible. Many animals do see the polarization of light, such as bees, ants, squid, and octopus, and use it to navigate, find prey, and communicate.

For monochromatic light, the polarization ellipse is the figure traced by the tip of the electric field vector over each period. Monochromatic light is by definition polarized, either linearly, elliptically, or circularly polarized. When the light's electric field only oscillates in a single direction, such as along the positive and negative *x*-axis as in Figure 1, left, the light is linearly polarized. The direction of oscillation is the *plane of polarization*. Polarization states are often represented by the polarization ellipse shown in Figure 2.

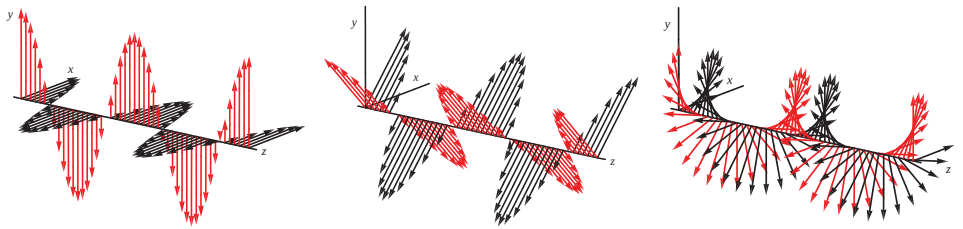

Figure 1. Electric (black) and magnetic (red) fields for (left) 0° polarized, (center) 45° polarized, and (right) right circularly polarized monochromatic light in space.

Polarization Elements and Polarization Properties. A *polarization element* is any optical element used to alter or control the polarization state of light and to transform light between polarization states. Polarization elements are classified into three broad categories—*polarizers, retarders*, and *depolarizers*—based on whether they operate on the amplitudes, phases, or coherence of the light. Mirrors, lenses, thin films, and nearly all optical elements alter polarization to some extent, but are not usually considered as polarization elements because that is not their primary role, but a side effect.

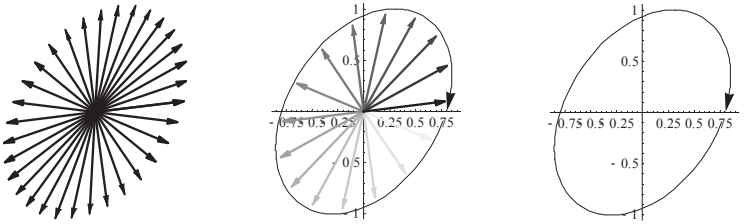

Figure 2. (a) The polarization ellipse for an elliptical polarization state is the ellipse drawn by the tip of the electric field vector during one period. (b) The electric field as a function of time is shown with the bounding ellipse. (c) Usually just the ellipse is drawn to indicate the polarization state.

Polarizers transmit a known polarization state independent of the incident polarization state. *Retarders* have two different optical path lengths associated with two special polarization states, the fast state and the slow state. The retardance is the difference in optical path lengths or phase between the two states as shown in Figure 3. *Depolarizers* scramble the state of polarization and convert polarized light into unpolarized light. Depolarization is usually associated with scattering, particularly multiple scattering. Integrating spheres will readily depolarize a beam of light. Most projection screens commonly used in classrooms and meeting rooms will effectively depolarize a beam of light. Try illuminating a screen with polarized light and observe that the scattered light cannot be extinguished with a polarizer.

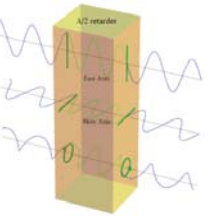

Figure 3. Three states of polarized light, propagating from the left in air, enter a half wave linear retarder (birefringent waveplate) with a vertical fast axis (lower refractive index). The vertical polarized mode (top, lower refractive index) has a longer wavelength inside the retarder so its optical path length is less, 2 waves, than the horizontally polarized mode (center) by ½ wave. (Bottom) Right circularly polarized light divides into the two modes which propagate separately, then combine exiting the retarder. This exiting beam is now left circularly polarized due to the half wave optical path difference (retardance) between the two modes.

Optical Design. Optical design is the engineering practice of finding good and useful combinations of optical elements. Imaging systems are designed to take input spherical waves and transform them into output spherical waves, since spherical waves form the best (smallest) images. Unfortunately it is not possible to transform the input waves from many different object points into perfectly spherical output waves. Some deviation from sphericity is inevitable with combinations of lenses and mirrors. These deviations from spherical wavefronts are called aberrations. One of the most important tasks in optical design is to minimize the optical system's aberrations over the desired range of wavelengths and object positions by optimizing the system. Control of wavefront aberrations is exquisite and the aberrations quite small in many types of optical systems such as camera lenses and astronomical telescopes. The situation for the control of polarization is quite different.

Figure 4 shows an example cell phone lens (US patent 7,453,654) and a set of ray paths calculated by ray tracing. Five collimated beams of light are shown entering on the left in *object space* and are represented by rays, lines normal to the wavefront. The ray tracing program, Polaris-M, calculates the intersection of each ray with the first surface, these are the *ray intercepts*. Using Snell's law the ray directions are calculated inside the first lens. Then the refracted ray is propagated until it intersects the second surface. The product of the ray length

and the refractive index is the optical path length for the *ray segment*. The process repeats, finding a ray intercept then refracting the ray, until the ray exits the last surface into *image space*.

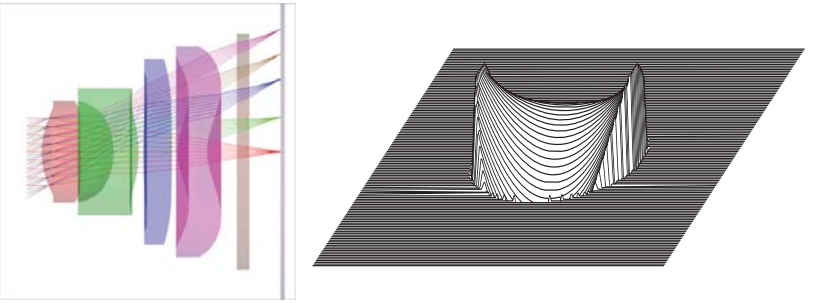

Figure 4. An example of a ray trace through a four element cell phone camera lens. On-axis rays are in red. Rays form an off-axis field are in green. A plane parallel IR-rejecting filter is located to the left of the image plane at the right. The wavefront aberration for the off-axis beam of the lens is shown as an oblique plot (right). This wavefront has about one wave of coma and one wave of astigmatism in addition to the half a wavelength of spherical aberration.

Ideally all the optical path lengths from object space to image space would be equal, and the exiting wavefront spherical. Variations of the optical path length are *aberrations*. The effect of these aberrations of Figure 4 on the image is calculated by the methods of Fourier optics. The image of a point source is called the *point spread function* or PSF. Figure 5 shows two views of the PSF for one of the cell phone's input beams, where due to the aberrations of Figure 4 the PSF is broadened by the aberrations and the peak intensity is reduced.

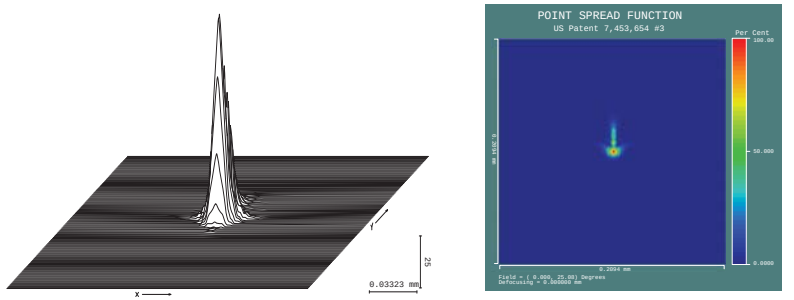

Figure 5. The off-axis point spread function in (left) oblique perspective plot and (right) false colored contour plot.

Polarization Ray Tracing. The objective of polarization ray tracing is to calculate the polarization states exiting from optical systems and to determine the polarization properties, diattenuation, retardance, and depolarization associated with the ray paths. In conventional optical design, only the effects of optical path length variation, the wavefront aberration, is calculated and analyzed.

The transmission and polarization state of the rays also varies from ray to ray because each ray has a different set of angles of incidence on each lens or mirror surface. These amplitude and polarization changes depend on the coatings used on each surface. Thus to calculate the polarization effect of the interfaces the coatings must be specified as well as the lens shapes and

refractive indices. Some coatings will cause much larger amplitude and polarization changes than others. In the last few years understanding and addressing the polarization effects due to coatings, polarization elements, liquid crystal cells, and many other devices lead to large changes in the art of optical design. Until recently the conventional assumptions that only optical path length needed to be calculated was adequate for a majority of optical design calculations. By 2010 polarization calculations were needed in many optical design problems to accurately simulate advanced optical system with high numerical aperture, tolerance polarization sensitive system, and understand the effects of optical coatings on the wavefront aberrations and polarization aberrations.

One of principal polarization effects in lens and mirror systems is due to s and p component reflection or transmission differences. The s and p components of the incident light are defined in Figure 6 left. The right side shows the fraction of light transmitted as a function of angle of incidence calculated from the Fresnel equations for air into uncoated surfaces with refractive indices of 1.5, 2, and 4. Coated interfaces have similar curves but with generally improved coefficients.

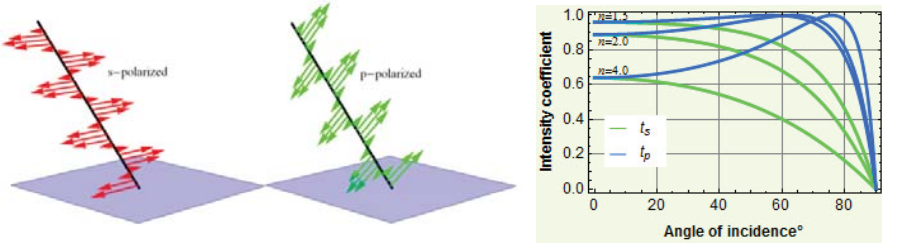

Figure 6. (left) The definition of s and p components at an interface. (right) The Fresnel coefficients for transmission from air into lenses of different refractive indices for s light (green) and p light (blue) is a function of the angle of incidence. The difference in transmission is a source of diattenuation or partial polarization.

Polarization ray tracing methods are based on the *polarization matrix propagation method*. A polarization matrix is calculated for each ray intercept and another for propagation along each ray segment. Matrix multiplication cascades the polarizing interactions. Finally a polarization matrix, such as a Jones matrix or Mueller matrix, is calculated for each ray path from object space to image space.

The polarization matrix propagation method can determine the output polarization state for all incident polarization states and describes the diattenuation and retardance for the ray paths. This is useful to understand why the polarization state changed and what might be done about it. The simplest way to describe the ray path's polarization is with Jones matrices, 2×2 matrices with complex elements shown in the following equation; matrix elements can be expressed in both Cartesian complex number form and polar form

$$\boldsymbol{J} = \begin{pmatrix} j_{1,1} & j_{2,1} \\ j_{1,2} & j_{2,2} \end{pmatrix} = \begin{pmatrix} x_{1,1} + i\,y_{1,1} & x_{1,2} + i\,y_{1,2} \\ x_{2,1} + i\,y_{2,1} & x_{2,2} + i\,y_{2,2} \end{pmatrix} = \begin{pmatrix} \rho_{1,1}\,e^{i\phi_{1,1}} & \rho_{1,2}\,e^{i\phi_{1,2}} \\ \rho_{2,1}\,e^{i\phi_{2,1}} & \rho_{2,2}\,e^{i\phi_{2,2}} \end{pmatrix}.$$

Stop and contemplate the consequences of the polarization matrix propagation method for the optical designer and the other engineers who need to use and understand his work. Conventional optical design describes the aberration with the wavefront aberration function, a

scalar function with one value, the optical path length, at each point on the wavefront in the exit pupil. The polarization matrix propagation method is replacing this scalar function with a Jones matrix at each point on the wavefront called the *polarization aberration function* or the *Jones pupil*. Going from a description with one variable for each ray (wavefront aberration) to a matrix with eight variables (polarization aberration function as a Jones matrix) at each ray is a very substantial complexification! It is no wonder that the early optical designers did not include the calculations for uncoated or coated lens surfaces and mirrors in their image quality calculations; it is not easy.

Typical polarization problems in optical systems. Polarization provides the basis of operation for many types of optical systems such as liquid crystal displays and the ellipsometers used in the microlithography industry which test the composition and thicknesses of the many layers which are deposited during chip fabrication. But polarization is also a problem in many systems, and so is frequently analyzed during the optical design process. A survey of the polarization aberrations of some simple optical systems will help understand the goals and methods for polarization ray tracing and analysis.

The polarization aberration of lenses arises due to the effect of the Fresnel and thin-film equations which describe how much light reflects and refracts at their surfaces. For an on-axis spherical wave at a spherical surface, the angle of incidence increases approximately linearly from the center of the pupil and the plane of incidence is radially oriented, as shown in Figure 7. For most coated and uncoated interfaces, the difference between the transmission for light polarized radially (in the p-plane) and tangentially (in the s-plane) increases approximately quadratically. Thus an uncoated lens surface acts as a weak linear polarizer with a radial transmission axis whose diattenuation increases approximately quadratically, as seen in Figure 7.

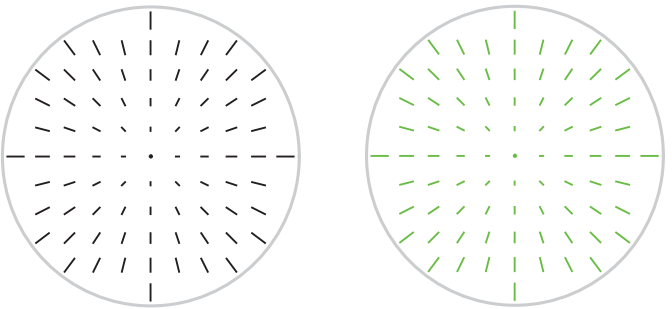

Figure 7. (Left) The plane of incidence and angle of incidence functions for an on-axis spherical wave incident at a spherical surface are shown. The angle of incidence is radially oriented and increases linearly from the center. (Right) The diattenuation orientation and magnitude (green) at a lens surface for an on-axis source is radially oriented and the magnitude increases quadratically.

Figure 8 shows the effect with a set of polarization pupil maps, series of polarization ellipses sampled around the pupil, of an uncoated lens when 0° linear, 45° linear, and right-circularly polarized beams enter the lens. In the left figure the beam is brighter at the top and bottom, dimmer on the right and left, and the polarization is rotated towards the radial direction in the four diagonals. The middle pattern has the same form but is rotated about the center by 45°. When circularly-polarized light is incident, the light becomes steadily more elliptical toward the

edge of the pupil, and the major axis is oriented radially. If the uncoated lens is placed between crossed polarizers, light is extinguished along the two polarizer axes, but leaks along the diagonals of the pupil as shown in Figure 9, a pattern known as the *Maltese Cross*. An interesting pattern is observed when a Maltese Cross beam is brought to focus. The point spread function (PSF) is dark in the center and along the *x*- and *y*-axes, but has four islands of light in one ring and dimmer islands of light further from the center, as shown in Figure 10. Thus coated and uncoated interfaces can cause degradation of the image and introduce polarization variations into the PSF itself.

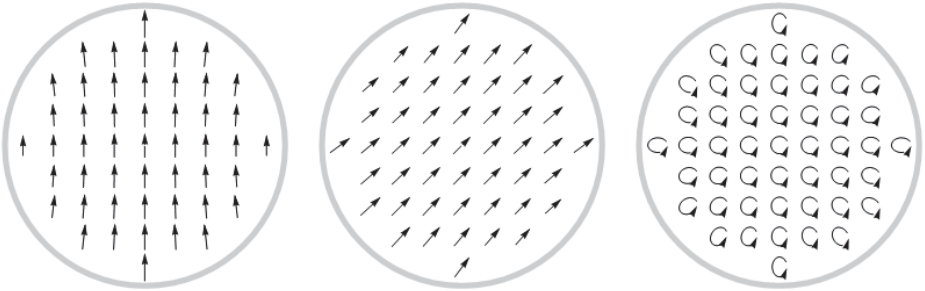

Figure 8. The effect of the diattenuation aberration of Figure 7 on incident (left) 90° linear, (center) 45° linear, and (right) left-circularly-polarized beams, causes a spatial variation of polarization state.

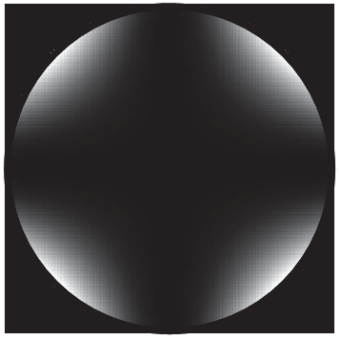

Figure 9. When an uncoated lens is viewed between crossed polarizers (*x* and *y*-oriented), light leaks through the edges of the four diagonals of the pupil in a pattern known as the *Maltese Cross*.

High Numerical Aperture Wavefronts. Numerical aperture characterizes the range of angles over which an optical system can accept or emit light; $f/\#$ describes the same property. Beams with high numerical aperture, a large cone angle, are valuable in optics because they can focus light into smaller images. So there is a constant push for systems with still higher and higher numerical aperture.

High numerical aperture beams must have polarization variations, because the polarization state cannot remain uniform in 3-dimensions, it must curve around the sphere. These intrinsic polarization state variations are frequently detrimental, broadening the image from the ideal Airy disk pattern.

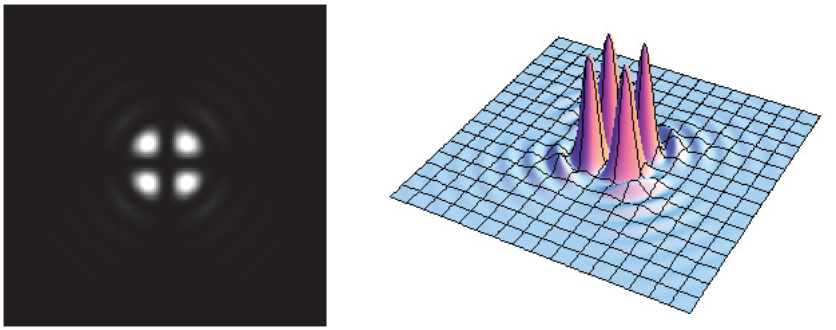

Figure 10. The point spread function of an uncoated lens between crossed polarizers (*x* and *y*-oriented) in (left) an intensity plot, and (right) oblique perspective plot.

Consider a hemispherical light beam subtending a solid angle of 2π steradians; its numerical aperture is one. When the beam is linearly polarized light with its *E*-field along *x*, the exiting polarization must curve around the hemisphere taking the form shown in Figure 11. Near the *z*-axis, the optical axis in the center of the beam, the polarization is nearly uniformly *x*-polarized in three-dimensions. Along the *y*-axis the light can remain polarized in the *x*-direction to the edge of the pupil, since these vectors are tangent to the sphere. Along the *x*-axis, however, the light has to tip downward to remain on the surface of the sphere. The polarization state of the light continues to rotate until at the right and left sides of the pupil shown in Figure 11 (center), the light becomes polarized in the $\pm z$-direction, since here the light is propagating in the $\pm x$-direction. Around the edge of the pupil, the polarization varies as shown in Figure 12. Because of these polarization variations, as the numerical aperture is increased, the image increasingly deviates from an Airy disk, and the improvements in resolution as the numerical aperture increases are not as good as would be hoped for.

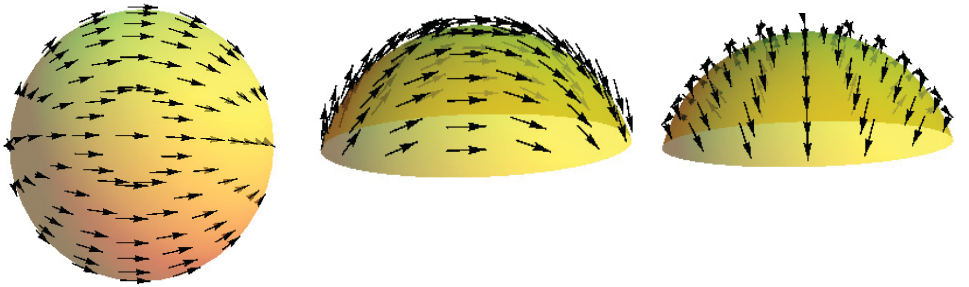

Figure 11. A high numerical aperture (NA) spherical wave linearly polarized in the *x*-direction and viewed along (left) the *z*-axis, (center) the *y*-axis, and (right) the *x*-axis. This polarization is aligned with latitude lines around a pole located on the *y*-axis.

There is great interest in microlithography and microscopy for other polarization distributions with useful imaging properties, particularly the radially- and tangentially-polarized beams shown in Figure 13. Note that these beams cannot be extended to the origin without discontinuity, thus are created with a dark spot in the center.

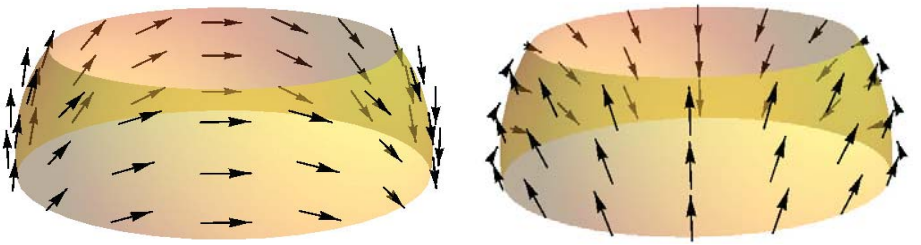

Figure 12. Distribution of linearly polarized light around the edge of a hemispherical wavefront.

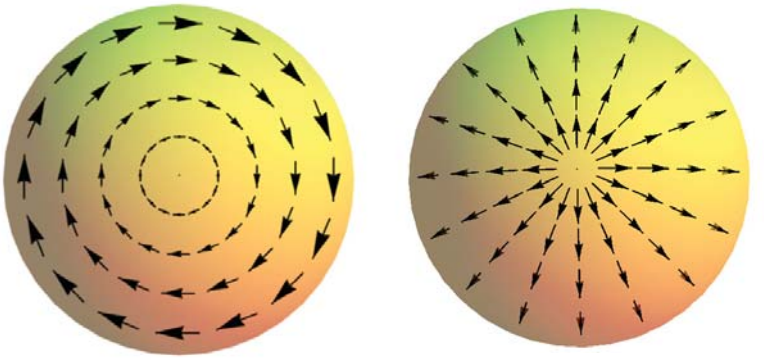

Figure 13. The polarization distributions in (left) a tangentially polarized wavefront, and (right) a radially polarized wavefront.

Stress Birefringence in Lenses. Another issue with polarized light and lenses, particularly injection molded lenses, is *stress birefringence.* Stress birefringence is a spatially varying birefringence resulting from forces within the lens material which compress or stretch the material's atoms causing birefringence. Stress birefringence becomes frozen into a glass blank or molded lens during fabrication as the lens material cools unevenly. Stress can also arise from externally applied stresses such forces on the lens from lens mounts. Stress birefringence is made visible by placing the lens between crossed polarizers and viewing the polarization leakage, as shown in Figure 14. Stress birefringence in lenses reduces image quality.

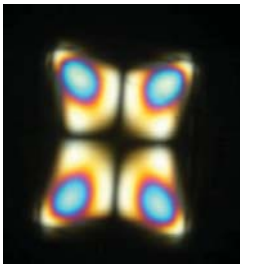

Figure 14. Large stresses frozen into a square piece of glass viewed between crossed polarizers exhibit the wavelength dependence of the stress-induced retardance.

Liquid Crystal Displays. Liquid crystal cells, displays, and projectors present some of the most challenging polarization aberration problems, because the eye is very sensitive to color variations across displays. Liquid crystals are a thick soup of birefringent molecules, typically rod shaped molecules chosen for their large dipole moment. These molecules rotate in response to applied electric fields changing the retardance of the cell. Figure 15 shows the molecular orientation in a

typical twisted nematic liquid crystal cell for several voltages, increasing towards the right. When placed between polarizers, the liquid crystal cell functions as a voltage controlled intensity modulator. Fabricate the electrodes in an addressable array, add an array of tiny red, green, and blue filters and voilà, a color display is created. One major issue with liquid crystal cells is the large variations of retardance with angle of incidence, a polarization aberration. An example of such retardance variation is shown in the far right of Figure 15.

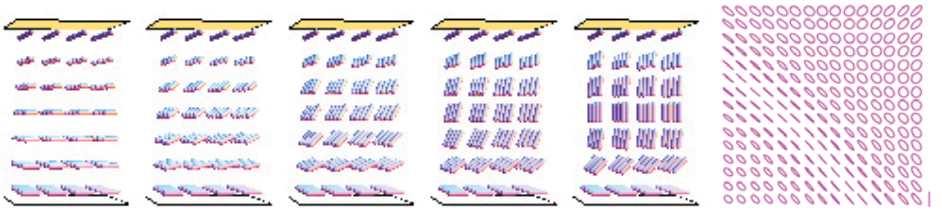

Figure 15. Orientation of liquid crystal molecules in a twisted nematic cell for several voltages, increasing from left to right. Light propagates in the vertical direction. Liquid crystal molecules are anchored to top and bottom horizontal planes. At zero volts (far left) the molecules rotate in the horizontal plane from top to bottom. As the voltage increases (moving right) the molecules begin to tip out of the horizontal plane in the center of the cell reducing their contribution to the retardance. (Right) At high voltages, the molecules at the center are rotated to the vertical plane, while molecules at the top and bottom remain anchored to the substrates. (Far right) A large retardance variation occurs, shown for one of the voltages due to propagation at different angles through the liquid crystal cell.

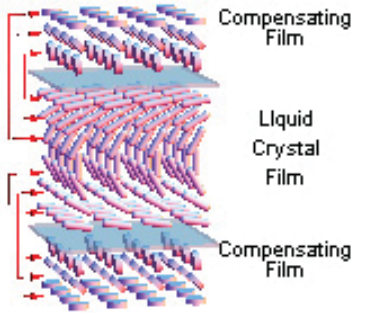

Figure 16. In all displays, liquid crystal cells are matched with compensating films to reduce the polarization aberrations. Here the film on the top compensated the top half of the liquid crystal cell, and the compensating film on the bottom compensates the lower half, greatly improving the color quality of the display by reducing undesired polarization state variation and leakage through polarizers.

This polarization variation can cause severe color and brightness problems in liquid crystal displays, which can be easily seen in many old displays. This is commonly *fixed* by adding additional films of fixed birefringent molecules, a biaxial multilayer film, typically with a disk shaped molecules, which can effectively compensate the rod shaped liquid crystal molecules birefringence with angle. Figure 16 shows a liquid crystal cell with two correcting films, one on each side of the liquid crystal cell. These are designed so that for the dark state of the display, each liquid crystal layer is compensated (cancelled) for all angles of incidence by molecules with opposite shape, rods versus disks.

Summary and conclusion. Polarization in optical design has recently become an important branch of optical design. As specifications for optical systems and products are constantly improved, what were once small effects become of paramount importance. Polarization ray tracing may be complicated, the polarization aberration function is eight times more complicated than the wavefront aberration function, but it is now becoming essential for many projects.

Russell Chipman is a Professor of Optical Sciences at the University of Arizona, Tucson. He runs the Polarization Laboratory which performs measurements and simulations of polarization elements, liquid crystals, and polarization aberrations. He recently developed the Polaris-M polarization ray-tracing code which analyzes optical systems with anisotropic materials, electro-optic modulators, diffractive optical elements, polarized scattered light, and many other effects. He is the Co-PI for the Jet Propulsion Laboratory's *Multi-Spectral Polarimetric Imager*, a candidate instrument for the global monitoring of aerosols from space, an instrument to support a more accurate measurement of the global energy balance for climate studies. Professor Chipman received his BS from MIT, and MS and PhD in Optical Sciences from the University of Arizona. Professor Chipman is a Fellow of OSA and SPIE. He won the SPIE's 2007 G. G. Stokes award for research in Polarimetry.

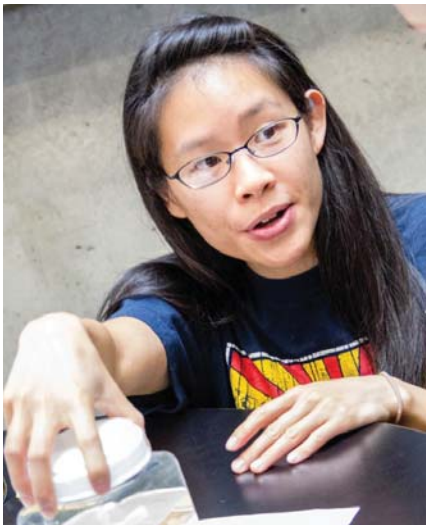

Optical Sciences doctoral student Victoria Chan during Laser Fun Day (March 2014).

Photo Courtesy of The University of Arizona College of Optical Sciences

The Tucson region has five distinct seasons. In addition to Autumn, Winter, and Spring, we experience the fore-summer of May and June, when temperatures are at their highest, rain is scarce and likely nonexistent, and moisture levels are low. However, if your impression is that the weather of a Tucson summer can be characterized as “a dry heat,” you may be surprised when you experience our fifth season: the Summer Monsoon. From mid-July to mid-September, thunderstorms may be frequent, and temperatures may quickly plummet. We receive half of our yearly rainfall during this season of relatively high humidity. This is the main season of growth for many of the regions plants, and the dry washes around the city can quickly and briefly turn into raging rivers. This is a dramatic, exciting, season, and the afternoon lightning shows are stunning. It is not uncommon to find Tucsonans who think of the Summer Monsoon season as their favorite time of year! In this photograph, a large storm cell drenches central Tucson.

Photo courtesy of Brian Anderson

Thin Film Center

Angus Macleod

Thin Film Center is a quite small company that specializes in support for optical coating design and manufacture. We supply software and training, all directed at thin-film optical coatings. Optical thin-film calculations use a beautiful matrix model that is aesthetically one of the most pleasing ever devised. Not only is it beautiful, but it is also exceptionally accurate. The sole defect is that manual numerical calculation of any but the most simple systems is excruciatingly tedious. Computers, of course, are the answer, and they have been used for thin-film calculations almost from the beginning, but in the old days thin-film calculation programs were mainly home-brewed and on mainframes. There was no real market for commercial programs until the personal computer had appeared.

I arrived at Optical Sciences in 1979 and almost the first thing I did was to write a teaching program for the university mainframe. To my surprise, Optical Sciences actually succeeded in selling a number of copies, although the money did not come to me. For my own personal use I had bought a Radio Shack TRS-80 machine and then around 1982 I was asked to write a thin-film program for a coating company, using a Radio Shack Model III, and this was my first real commercial venture in thin-film software. Then in 1984 the Macintosh computer appeared and I thought this was the finest machine I had ever seen. Although it was incredibly expensive I had to have one. Software development on it was a bit primitive, but I soon had a reasonable program running for optical coating design. At a meeting, I talked with Brian Newnam of Los Alamos National Laboratory. Brian, too, had a Macintosh and wondered if I might be able to supply him with a program.

If you look at the history of Science and Technology, the part played by supporting wives is rather neglected. James Clerk Maxwell's wife was his able assistant in his early work, before he became better known and could get an actual job. The hand in Roentgen's famous photograph is that of his wife. My wife's immediate reaction was enthusiastic encouragement. She was quite clear that we should form a company and sell a program to Brian. The first thing was to get a tax identity from the IRS, so she telephoned them. "What's the name of the company?" they asked. That was the one thing we had not thought of. "*Thin Film Center*," she said, with hardly a pause, and that is how the company got its name. It really didn't do very much for a while. It was a spare time activity with the aim mainly of funding my attendance at conferences. Then a year or two later, Michael Kidger, asked if Kidger Optics might represent us, and that got us better recognition. We had a good arrangement with Kidger Optics for some years, during which we gradually moved away from the Macintosh to the PC, and then we parted company but stayed friends.

My funding at Optical Sciences was really good throughout the 1980s but slightly more difficult in the 1990s. Nevertheless my group flourished and I had an incredibly able team of students who did all the work. I had a nice arrangement with the university that meant that almost all of my salary was hard money, so that the bulk of my soft money could go to students. However, the hard money distribution was revised in the early 1990s. I have to admit that the new arrangement was very much fairer than the old, but it left me with a problem. My contracts didn't include much for me, and so I could pay myself or my students, but not both at any reasonable level. Clearly I could take the money, or do something else. I thought something else was better. So I said to the university that I would take the hard money but no soft money, meaning that I was effectively on just over half time for the nine month academic year. The

university immediately rewrote my contract and *Thin Film Center*, that we had by then incorporated, had to pick up the rest. By 1995 it was clear that *Thin Film Center* was doing a lot better than the university and so, since I had done enough years to retire and become an emeritus, that is what I did. As an emeritus I can still teach at Optical Sciences and so I do.

I wish I could say that I had created a business plan that showed clearly the way forward and that my actions were in response to the plan. The truth is that luck played the major role. It was just at the time when the personal computer was making great inroads into industry. Companies were beginning to think that they would be better off by handing their software requirements to specialists. At first we supplied just the smaller enterprises, but gradually this extended even to the largest companies in the business. We have never had to borrow money. We have no idea of the market, if there is such a thing, but it supports three other principal companies in our field, all about the same size, or still smaller, than we. There are four of us who own, and who work full time at, *Thin Film Center*. Ann, my wife, and Eleanor look after the business side. Chris Clark is the genius who nowadays develops the software. I am involved with the theory of the algorithms and the operation of the software, especially when we are developing something new, and I work a lot on scripts. There is still code in the program that I actually wrote, but an important activity is looking after our customers, and training, and a little consultancy that we try to keep very limited. Our philosophy is that support is what we actually do and that the software is a tool that helps in support. We also try to write a reasonable number of papers to maintain visibility. We don't manufacture coatings ourselves. Never compete with your customers.

We entered the field at just the right time, which is always the main trick for success. The field is very specialized and small enough so that it has not attracted the attention of much bigger companies. We are great friends with our competitors. I spent a good part of my career in industry and the biggest problem was always the valuation of goods in progress and stock on the shelf. Software is an ideal product. Provided you don't capitalize your development (what has finished off a good number of companies) you never have trouble writing down inflated values. All we need are computers and brains. Optical coatings permeate the whole of optics and so are continually being developed with constant additional needs for design and analysis tools that keep us busy. The only downside is that Chris and I agree that we could never work for anyone else ever again.

Angus Macleod is President of *Thin Film Center, Inc.*, Tucson, and Professor Emeritus of Optical Sciences, University of Arizona. He was born in Scotland and after graduating from the University of Glasgow he worked in research, development, engineering, production and management for several UK companies. He was Reader in Thin-Film Physics at Newcastle-upon-Tyne Polytechnic (now University of Northumbria) from 1971 and professor of Optical Sciences at the University of Arizona from 1979. In 1995 he retired early from the University to devote his full attention to *Thin Film Center*. His technical interests are primarily in optical coatings, their design, analysis and production. He has over 200 publications in the area of optical coatings but is probably best known for his book "Thin-Film Optical Filters," now in its fourth edition.

What Optics Is Revealing About Art

Charles M. Falco

Have you ever wondered how some of the Great Master artists were able to create paintings that seem almost "photographic" in their level of detail? Working with the artist David Hockney, over the past decade we have found a variety of optical evidence that demonstrates some artists as early as c1425 used lenses or concave mirrors as direct aids for producing some features of some of their paintings.

Several years ago David Hockney observed features in a number of paintings that lead him to conclude some artists began using optical projections as aids as early as c1425. Together he and I subsequently found a variety of optical evidence in a number of paintings that demonstrate artists as important as Robert Campin, Jan van Eyck, Hans Holbein the Younger, Caravaggio, and others used projected images from lenses or concave mirrors as direct aids for producing some features of some of their paintings.

Fig. 1. Jan van Eyck, *The Arnolfini Marriage*, 1434.

Briefly, the necessary theoretical knowledge of optics as well as both refracting and reflecting optical elements were available by the early Renaissance. Sixty-one texts on Optics written between the years 1000, the time of Ibn al-Haytham, and 1425, that of Jan van Eyck, have survived, showing this 425-year period was one of remarkable scientific activity. Although only a few of these texts have been translated from Latin, those that have provide detailed descriptions for fabricating suitable concave mirrors from metal.

One of the earliest examples of a painting where we were able to extract optical evidence demonstrating the artist based portions of it on optical projections is shown in Figure 1. Several types of optical analysis show that the chandelier, enlarged in Figure 2, is based on an optical projection.

Fig. 2. Jan van Eyck, *The Arnolfini Marriage* (detail).

One painting, “Family Portrait” by Lorenzo Lotto (1523/1524), was particularly valuable in providing quantitative evidence for our thesis. As can be seen in Figure 3, this painting contains an octagonal pattern in the table covering. We were able to show to an accuracy of better than 1% that it consists of three segments, at three magnifications, resulting from the refocusing necessitated by the depth-of-field of a lens. This allowed us to calculate the focal length and

diameter of the lens Lorenzo Lotto would have had to use in order that these features should correspond so accurately to the laws of geometrical optics.

More recently we developed a portable high-resolution digital camera that allows us to acquire important information about paintings without needing to remove them from museums for detailed study. Infrared light penetrates many pigments further than does visible light, in many cases revealing "underdrawings" or other features not apparent in the visible. Figure 4 is an infrared (IR) "reflectogram" of the Lotto painting captured *in situ* where it was located on the wall of the Hermitage State Museum. Although too many features to discuss here are revealed by this IR reflectogram, one immediate observation is we can see that Lotto used a different pigment for the woman's dress than he used for the man's jacket, providing us with previously unknown information about the artist's working technique.

Figure 5 shows the octagonal pattern of the table covering in greater detail. As can be seen by comparison with Figure 3, the red and yellow pigments Lotto used are largely transparent in the IR, providing us with a clear view of the black lines he used to create this feature on the painting.

Fig. 3. Lorenzo Lotto, *Husband and Wife*, c1523-4.

Three distinct types of markings can be clearly seen for the lines making up the triangular pattern of the border of this feature: well defined lines in the region nearest the front of the image, consistent with tracing a projected image. These "traced" lines abruptly change to tentative lines in the middle region, where our previous analysis showed the magnification was reduced by $12.6 \pm 1.5\%$ due to having to refocus because of exceeding the depth-of-field. Because of this, Lotto would have had significant difficulty creating a plausible match for this geometrical pattern after refocusing. His abrupt change to tentative lines reflects this difficulty. The quality of the lines again abruptly changes to only short dashes in the region farthest into the scene, where our previous analysis shows the magnification was reduced by an additional $13.5 \pm 1.6\%$ due to having to refocus a second time after again reaching the limit of the depth-of-field. These results from IR reflectography provide important insights into the actual working practices of an artist, revealing quite specific details about how he made use of projected images over 150 years prior to the time of Galileo.

Fig. 4. Lorenzo Lotto, *Husband and Wife*, c1523-4. Infrared (IR) reflectogram.

Our earlier analysis of this painting found a change in the vanishing point that takes place part way back in the pattern in the border of the carpet to the right, quantitatively consistent with the change that is caused by the shift in position of a lens as it is refocused. Figure 5 shows the IR reflectogram of this portion of the painting. Overlaid to the left are seven units of a perfectly

repeating structure that replicates the geometrical pattern of the border. As can be seen, when corrected for optical perspective, this repeating structure is an excellent fit to the pattern near the front of the carpet, with a maximum deviation consistent with the degree of perfection found in the hand-made carpets of this type. Although an eighth unit of the structure does not fit at all, a small change in optical perspective makes the same repeating structure fit at the rear, again to within better than 2 mm. This change in perspective occurs at the same depth into the painting where our previous analysis found a shift in vanishing point, as happens when a lens is repositioned to focus further into a scene. In addition, not only does the perspective change where Lotto had to refocus, the pattern on the painting is missing a half-segment of the repeating pattern at this location. This is consistent with Lotto attempting to create a plausible match between two segments of a repeating structure after refocusing had caused the magnification to

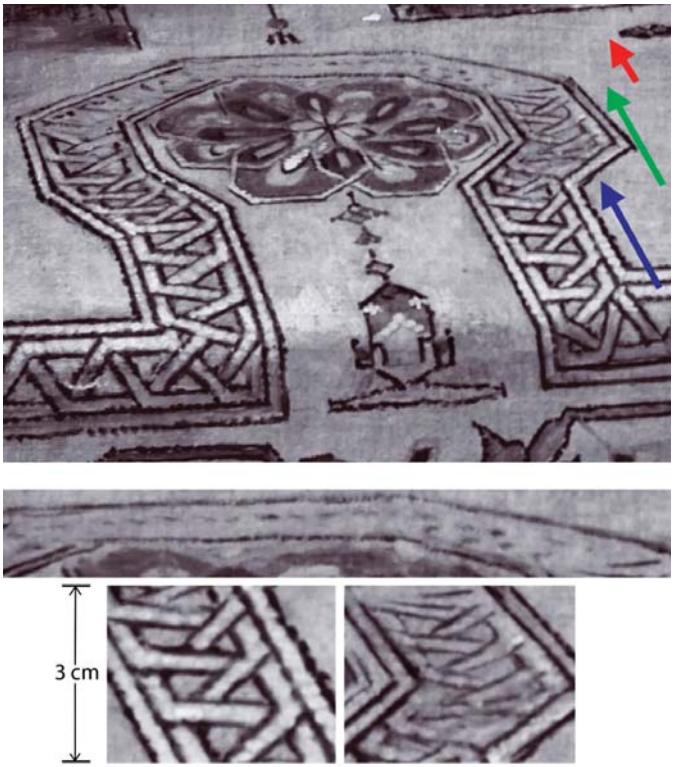

Fig.5. (Top) IR reflectogram of the octagonal pattern from Fig. 4. The arrows at the right indicate the three regions from which we were able to demonstrate this feature is based on an optical projection. (Bottom) The three insets are enlargements of the triangular patterns from the three regions at the right of the octagonal feature. Consistent with our previous analysis these IR reflectograms show Lotto abruptly changed between making lines that appear traced (lower left), to lines that are hesitant where he had to attempt to construct a plausible match to a geometrical pattern after the magnification had changed as a result of refocusing (lower right), to just a few dashed lines after the magnification had changed a second time after having to refocus a second time (upper inset).

change. Again, all of these detailed findings from IR reflectography are consistent with our earlier work that showed this portion of the painting is based on the optical projection of an actual hand-made carpet.

It is worth noting that we also have used 14th century optical technology, i.e., one lens of a pair of reading spectacles, as well as a metal concave mirror we fabricated following descriptions in texts of the time, to accurately reproduce all of the effects we have found in this carpet, and in all of the other paintings we have shown contain elements based on optical projections, including projecting such patterns directly on a screen of the same shade of red used in this painting. Even on such a colored screen, the projected images are quite distinct and easy to trace.

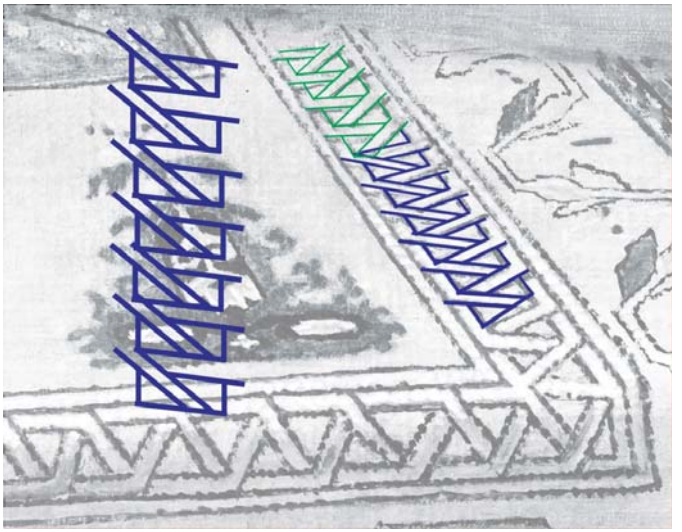

Fig. 6. IR reflectogram of the border pattern of Fig. 4. Overlay at left is seven segments of a repeating structure. When corrected for perspective, this is an excellent fit to the pattern at the front of the table covering. Changing the perspective, as happens when a lens is moved to refocus, gives an excellent fit to the pattern at the back.

These discoveries demonstrate that highly influential artists used optical projections as aids for producing some of their paintings early in the 15th century, at the dawn of the Renaissance, at least 150 years earlier than previously thought possible. In addition to van Eyck and Lotto, we also have found optical evidence within works by well-known later artists including Bermejo (c1475), Holbein (c1500), Caravaggio (c1600), de la Tour (c1650), Chardin (c1750) and Ingres (c1825), demonstrating a continuum in the use of optics by artists, along with an evolution in the sophistication of that use. However, even for paintings where we have been able to extract unambiguous, quantitative evidence of the direct use of optical projections for producing certain of the features, it does not mean that these paintings are effectively photographs. Because the hand and mind of the artist are intimately involved in the creation process, understanding these images requires more than can be obtained from only applying the equations of geometrical optics.

Acknowledgments: I am pleased to acknowledge my collaboration with David Hockney on all aspects of this research. Also, we have benefitted from contributions by Aimée L. Weintz Allen, David Graves, Ultan Guilfoyle, Martin Kemp, Nora Roberts (neé Pawlaczyk), José Sasián, Richard Schmidt, and Lawrence Weschler.

Bibliography

1. David Hockney and Charles M. Falco, “Optical insights into Renaissance art,” Optics & Photonics News, vol. **11**, 52 (2000).
2. David Hockney, *Secret Knowledge: Rediscovering the Lost Techniques of the Old Masters*, Viking Studio, 2001.
3. David Hockney and Charles M. Falco, “Quantitative analysis of qualitative images,” Proceeding of IS&T- SPIE Electronic Imaging, SPIE, **5666**, 326 (2005).
4. Charles M. Falco, "High Resolution Digital Camera for Infrared Reflectography," Review of Scientific Instruments, **80**, 071301-071309 (2009).
5. David Hockney and Charles M. Falco, "The Science of Optics: Recent Revelations About the History of Art," Proceedings of the SPIE **8480**, 84800A (2012).

Charles M. Falco has joint appointments in Optical Sciences and Physics at the University of Arizona where he holds the UA Chair of Condensed Matter Physics. He is a Fellow of four professional societies (the American Physical Society, the Institute of Electrical and Electronics Engineers (IEEE), the Optical Society of America, and the Society of Photo-optical Instrumentation Engineers (SPIE)), has published more than 250 scientific manuscripts, co-edited two books, has seven U.S. patents, and given over 400 invited talks at conferences, research institutions, and cultural organizations in 31 countries. In addition to his scientific research, he was co-curator of the Solomon R. Guggenheim museum’s *The Art of the Motorcycle* which, with over 2 million visitors in New York, Chicago, Bilbao, and the Guggenheim Las Vegas, was by far the most successful exhibition of industrial design ever assembled. More recently, he and the world-renowned artist David Hockney found artists of such repute as van Eyck, Bellini and Caravaggio used optical projections in creating portions of their work. Three international conferences have been organized around these discoveries, and recognition for them includes the 2008 *Ziegfield Lecture Award* from the National Art Education Association.

Tucson is justifiably famous for its sunsets, particularly during the Summer Monsoon season, and during the Winter. In this photograph taken from the east side of the city, brilliant sunset colors are seen over the Tucson Mountains and beyond.

Fortunately, rattlesnakes and scorpions are rarely found in the central parts of Tucson, although they are common in the outer areas of the city and in the foothills of the mountain ranges. While not typically considered desirable creatures to have around, scorpions can be fascinating to someone interested in Optics. When exposed to ultraviolet light, in the absence of other light sources, a scorpion's exoskeleton glows an eerie blue-green.

Photos courtesy of Brian Anderson

Molecular Imaging

Lars R. Furenlid

It is hard now to conceive of medical care in the days before the development of x-ray computed tomography (CT) and magnetic resonance imaging (MRI). These non-invasive imaging modalities make it possible for radiologists to read precise 3D images of the internal anatomy of patients, almost completely replacing *exploratory surgery* as a medical procedure. There's been another revolution in internal 3D imaging of increasing importance that is known as *molecular imaging*, where the objective is to illuminate biological function via the uptake of trace amounts of radio-labeled targeting molecules. These radio-tracers, or *radiopharmaceuticals* when used in the clinic, can be designed to reveal many scales of phenomena in living tissues – from the uniformity of perfusion of blood in the muscles of the heart down to the expression of receptors at the cellular level. When molecular imaging is used in the clinical setting, it is also known as *Nuclear Medicine*.

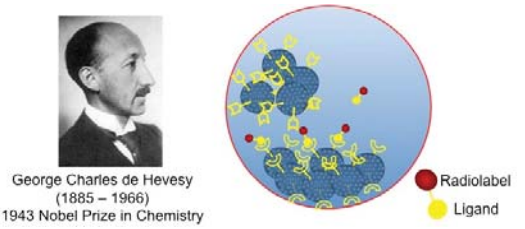

Figure 1. Molecular imaging is an extension of the *tracer principle* first expressed by George de Hevesy. The most sophisticated pharmaceuticals target specific receptors on individual cells.

Single Photon Emission Computed Tomography (SPECT) is a cross-sectional molecular imaging modality that makes use of gamma rays emitted *one-by-one* by radiopharmaceuticals introduced into the imaging subject. As a tomographic imaging technique, the resulting images represent the concentration of radio-tracer as a function of three-dimensional location in the subject. The designation *Single Photon* in the SPECT acronym is used to distinguish the technique from a related molecular imaging method known as Positron Emission Tomography (PET) in which a *correlated pair* of gamma-ray photons, arising from the matter-antimatter annihilation of a positron with an electron, together comprise the detected signal.

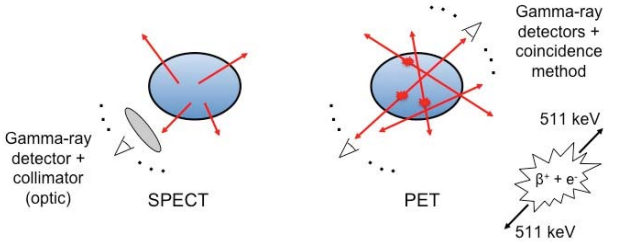

Figure 2. Illustration of the emission tomography principle for SPECT and PET. In SPECT, gamma-ray photons are emitted singly and an image-forming optic is required. In PET, pairs of gamma-ray photons are emitted simultaneously traveling in opposite directions, and no collimator is required to form an image.

SPECT and PET's strengths as diagnostic and scientific research tools derive from two key attributes: 1) properly designed radio-tracers can be very specific and thus bind preferentially or even exclusively at sites where particular molecular targets are present and 2) gamma-ray signals in detectors originate from radio-isotope tags on individual molecules, leading to potentially very high sensitivity in units of tracer concentration. Virtually all SPECT and PET systems are photon counting, i.e., they respond to and record signals from individual gamma-ray photons in order to extract the maximum possible information about the location and energy of emission.

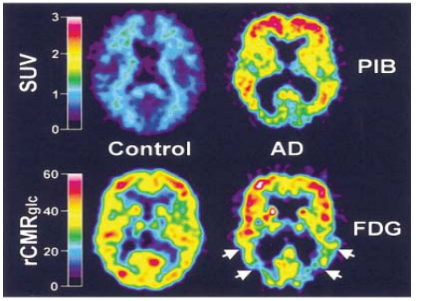

Figure 3. Brain PET scans with two tracers, Pittsburgh Compound B, which targets amyloid plaques, and ^{18}F-fluorodeoxyglucose, which reveals metabolic activity, showing clear differences between normal patients and those with Alzheimer's disease.

Gamma rays are photons that were emitted as a result of a nuclear decay and are thus distinguished from x-rays, which result from inner-shell electronic transitions, by the physical process from which they originate. Gamma-rays and x-rays used for imaging overlap in energy ranges, with x-rays as a rule of thumb covering the range between approximately $1\ keV$ to $100\ keV$, and gamma-rays covering the range of $10\ keV$ up to several MeV and higher. Most clinical SPECT imaging is performed with gamma-rays with energies of $80\ keV$ (^{201}Tl), $140\ keV$ (^{99m}Tc), $159\ keV$ (^{123}I), or $171\ keV$ and $245\ keV$ (^{111}In). Preclinical imaging of mice and rats can be carried with substantially lower energies, such as $30\ keV$ (^{125}I), due to the smaller amount of tissue that needs to be traversed with a low probability of scatter or absorption. PET, in contrast, always works with two $511\ keV$ photons, which corresponds to the rest masses of the positron and electron in Einstein's famous $E = mc^2$ relationship.

An ensemble of SPECT radioisotopes emit their photons isotropically, i.e., with equal probability in all directions. In order to form a useful projection image of an extended source on a two-dimensional detector, an image forming principle, generally based on a physical optic, must be employed. The purpose of the optic is to establish a relationship between locations in the object volume and pixels on the detector. In equation form, this can be expressed as

$$\bar{g}_m = \int h_m(\boldsymbol{r})\, f(\boldsymbol{r}) d^3 r\,,$$

where $f(\boldsymbol{r})$ is the gamma-ray photon emission rate (which is proportional to tracer concentration) as a function of 3D position $\boldsymbol{r}$, $h_m(\boldsymbol{r})$ is the sensitivity of pixel m to activity in different regions of the object volume, and $\bar{g}_m$ is the mean signal rate ultimately registered in pixel m. A variety of physical factors contribute to the three-dimensional shape (and magnitude) of the sensitivity functions, but the most important are the parameters of the image-forming optic, and the intrinsic resolution and detection efficiency of the detector.

All modern gamma-ray detectors convert the energy of individual gamma rays into electrical signals that are conditioned and digitized. Most clinical gamma cameras utilize an intermediate step in which the gamma-ray energy excites a burst of secondary lower-energy scintillation photons and are closely related to the scintillation camera designed by Hal Anger in the late 1950s. The design comprises a relatively large slab of inorganic scintillation crystal that is viewed by an array of photomultiplier tubes whose signals are processed to estimate gamma-ray interaction location and energy. Achieved detector resolutions are on the order of $2\text{-}3\,\text{mm}$. Research and preclinical SPECT imagers are making increasing use of semiconductor detectors. In these devices gamma-ray energy is converted directly into electron-hole pairs that migrate under the influence of a bias potential and induce signals in pixel or strip electrodes. Intrinsic resolutions can approach approximately $50\,\mu\text{m}$, consistent with the volume of detector material in which the energy of a gamma-ray is deposited when it interacts to produce a complicated cascade of secondary photons and energetic electrons.

For clinical SPECT applications, there is generally a significant probability that an emitted gamma ray scatters from electrons in the tissue of the imaging subject. If the angle of travel is changed significantly, which would lead to a blurring in the projection image, there is an accompanying energy loss described by the Compton formula,

$$\frac{1}{E'}-\frac{1}{E}=\frac{1}{m_e c^2}\left(1-\cos\theta\right),$$

where E' is the gamma-ray energy after scattering, E is the gamma-ray energy before scattering, m_e is the electron rest-mass, c is the speed of light in vacuum, and θ is the scattering angle. If detectors have good energy resolution, energy windows can be set to discriminate against Compton scatter. For preclinical SPECT applications, the likelihood of scatter is typically much lower due to the smaller dimensions of the imaging subjects, and energy resolution is desired principally to separate emissions in experiments with multiple isotopes. SPECT imagers generally incorporate multiple cameras to increase the efficiency of tomographic acquisition, which can involve the measurement of typically $60-100$ planar projections depending on the system and application.

Tomographic imaging almost always involves a reconstruction operation in which a collection of observations, projection images in the case of SPECT, are processed to recover an estimate of the underlying object. This can be expressed as

$$\hat{f}(\boldsymbol{r})=O(\boldsymbol{g}),$$

where O represents the reconstruction operation that acts on data-vector $\boldsymbol{g}$, and $\hat{f}(\boldsymbol{r})$ is the estimate of the object, generally in the form of activity in voxels. In SPECT, the reconstruction operation is currently most often either a *filtered backprojection* (FBP), which can be thought of as sending modified versions of the 2D images back through space and finding a representation of the object in the central region where the backprojections overlap. A more modern approach to reconstruction is use of an *iterative statistical algorithm* such as maximum-likelihood expectation maximization (MLEM) or ordered-subsets expectation maximization (OSEM). These latter reconstruction methods incorporate a forward model of the imaging process that makes it possible to compensate for imperfections in the imaging system, especially if careful calibration measurements are made, and also make it possible to approximately account for absorption and scatter occurring within the object.

Although it is possible, and sometimes advantageous, to perform SPECT imaging without ever forming intermediate projection images, most SPECT systems do acquire projection images at regular angular intervals about the imaging subject. Virtually any of the physical processes that redirect or constrain light, such as absorption, refraction, reflection, and diffraction, can in principle be used to form an image in the conventional sense—mapping light from an object source point or plane to an image plane. The need to map an object volume to an image plane, and the requirement to function at the short wavelengths characteristic of gamma rays, place severe restrictions on the types and geometries of optics that can be considered and used successfully for SPECT.

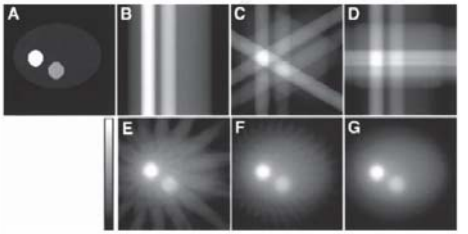

Figure 4. Illustration of the backprojection reconstruction method for a single 2D slice. A is the original object and B-G represent increasing numbers of backprojected angular views.

Conventional SPECT systems use pinholes and parallel-hole collimators, or closely related variations such as converging or diverging collimators, slits, and slats, to form images. By permitting only the fraction of light traveling through the open area of the aperture along a restricted range of angles to reach a detector pixel, pinholes and parallel-hole collimators define sensitivity functions that are non-zero in conical regions of the object volume. Parallel-hole collimators are the most commonly employed image-forming elements in clinical applications, in part because the projections they produce are the easiest to understand and process. Key features of parallel-hole collimators are that resolution degrades as a function of distance away from the collimator face while sensitivity is nearly unchanged. The parallel bores ensure that most gamma rays enter into the detector with nearly normal incidence angle, minimizing the parallax errors associated with uncertainty in depth of interaction in the detector. Parallel-hole collimators have no magnifying properties (the converging or diverging versions do) and require a tradeoff between distant-dependent loss of resolution and overall sensitivity as governed by the collimator aspect ratio. There is a further design tradeoff between resolution loss from leakage between collimator bores and sensitivity loss from reduced fill factor of open collimator area.

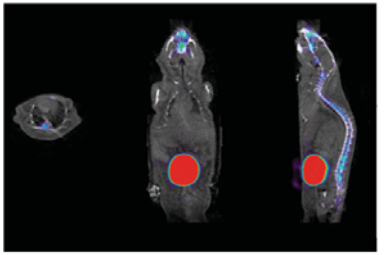

Figure 5. ^{99m}Tc-MDP SPECT image (color) coregistered with corresponding slices of the x-ray computed tomography image (grey-scale). Methylene diphosphonate (MDP) is used to visualize areas of increased bone deposition such as occurs when cancer spreads into bone.

SPECT imager design with pinhole apertures also involves a set of design tradeoffs involving resolution, sensitivity, and field of view. Pinhole cameras have magnifications that depend on the ratio of pinhole to detector and pinhole to source distances. Since a three-dimensional object necessarily has a range of pinhole to source distances, resulting in different magnifications for different parts of the object, and the sensitivity cones intersect the object volume with different angles that depend on individual detector pixel locations, pinhole SPECT projections can appear complicated to a human observer. There are also further design tradeoffs between blur from leakage through the pinhole boundaries versus loss of sensitivity from vignetting at oblique angles. Nonetheless, pinhole and multi-pinhole apertures are currently providing the highest resolution preclinical SPECT images, as reconstruction algorithms have no difficulty unraveling the geometric factors in the projections.

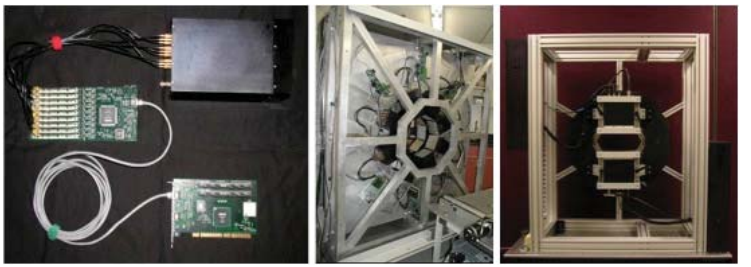

Figure 6. University of Arizona *Center for Gamma-Ray Imaging* modular gamma camera with list-mode electronics (left). Arrays of cameras are used with collimators to build SPECT systems (center) and with coincidence-timing to build PET systems (right).

SPECT and PET imaging are used in biomedical research for a variety of applications – among the most important being the development of new drugs that aid in the detection or treatment of cancer, cardiovascular disease, and neurodegenerative conditions such as Alzheimer's and Parkinson's diseases. Advances in molecular imaging are occurring rapidly as a result of new detector technologies, computational power, and knowledge gains in molecular biology. It is an exciting and rewarding research area that brings together optics, physics, mathematics, and biology.

1. Miles N. Wernick and John N. Aarsvold eds., *Emission Tomography: The Fundamentals of PET and SPECT*, Academic Press, 2004.
2. Matthew A. Kupinski and Harrison H. Barrett eds., *Small-Animal SPECT Imaging*,. New York: Springer, 2005.

Lars R. Furenlid is Professor in the *College of Optical Sciences* and the *Department of Medical Imaging* in the College of Medicine, where he has been a faculty member since 1998. He received a B.S. in Chemistry from the University of Arizona, and a Ph.D. in Physical Chemistry from the Georgia Institute of Technology. From 1990 to 1998, Dr. Furenlid was a staff physicist at the National Synchrotron Light Source at Brookhaven National Laboratory. In 2013, he received the IEEE Radiation Instrumentation Outstanding Achievement Award and was also named a Leading- Edge Researcher at the University of Arizona. He is the Associate Director of the NIBIB-funded Center for Gamma-Ray Imaging, a member of the University of Arizona Cancer Center, and a member of the Graduate Interdisciplinary Degree Program in Biomedical Engineering. He is a Fellow of the American Institute of Medical and Biomedical Engineers.

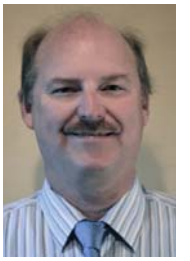

NP Photonics, Inc.

Nasser Peyghambarian

Company Information. Founded in 1998, *NP Photonics* develops and manufactures specialty fiber lasers, fiber amplifiers and transport fibers for the near- and mid-infrared (IR) wavelength bands. Our proprietary fiber technology is used across a broad family of products, including narrow line-width, low phase-noise fiber lasers designed for operation in industrial environments. Our core strengths are technology innovation, product development, quality engineering and manufacturing world-class products for applications in sensing, defense, metrology and research. We currently have over 1,400 lasers installed worldwide, and we continue to grow through technology development, strategic partnerships and engagement with markets in which the company has a clear sustainable advantage.

Competencies. NP Photonics' capabilities run the gamut from innovation in glass chemistry and development of rigorous processes for drawing fiber to the production of high-quality fiber laser systems. Our environmentally controlled facility, critical to the glass production process, houses unique and customized equipment designed for producing specialty materials and products. This vertical integration allows us to develop and deliver world-class fiber products to exceed customers' optical and mechanical requirements. We currently have 34 patents and more in process. These patents relate to glass composition, glass processing, fiber manufacturing, splicing, fiber lasers, fiber components and fiber amplifiers, all at multiple wavelengths across the near- and mid-IR.

Technology Library. Since inception, *NP Photonics* has successfully engaged in government-sponsored and customer-funded development programs to leverage core competencies and develop new technologies. Our engineering team has a deep background in glass, optics, and fiber lasers. The team has a wealth of experience developing innovative technologies and bringing products to market.

- Ultra-low-noise, single-frequency technology from continuous wave (CW) to high-energy pulsed lasers, free of non-linear effects.
- Distortion-free fiber amplifiers – unique high-gain-per-unit-length phosphate fiber enables significant distortion-free amplification of Q-switched and ultrafast pulses at 1.0 µm and 1.5 µm.
- A mid-IR supercontinuum laser source, with wavelength coverage from 1.0 µm to 4.5 µm.
- Ultra-low-loss mid-IR transport fibers, with transparency from visible to 5.0 µm.
- Mid-IR high-temperature oxide glasses.

Product Portfolio. *NP Photonics*' proprietary fiber technology is used across a broad family of innovative products. *NP Photonics* is a highly integrated company with capability to develop and manufacture high-performance fiber lasers. Fiber laser technology has the advantages of compactness, robustness, and efficiency – based on the fact that the laser is made from amplifying optical fiber in a way that there are no free space surfaces and no mechanical adjustments or alignments. *NP Photonics* fiber lasers have passed space-qualification standards, a testament to their reliability and robustness.

- Ultra-low-noise, single-frequency, tunable CW fiber lasers operating at 1.0 µm, 1.55 µm and 2.0 µm.
- Distortion-free fiber amplifiers – unique high-gain per unit length non-silica fiber enables ultra-compact, low-latency, distortion-free amplification of Q-switched and ultrafast pulses at 1.0 µm, 1.5 µm and 2.0 µm.
- A mid-IR supercontinuum fiber laser with wavelength coverage from 1-4.5 microns.
- Ultra-low-loss mid-IR transport fibers, UV to 5.0 µm.

The *NP Photonics*' ultra-narrow linewidth, 400 Hz to a few kHz, low-noise fiber lasers enable a wide variety of military and high-performance applications, where fiber lasers with extremely long coherence length are required. Our fiber-lasers are compact, deliver high output power (> 150 mW), and exhibit

narrow-linewidths of a few kHz and frequency drift of less than 10 MHz over hours. These fiber-lasers utilize NP's proprietary high-gain-per-unit-length fiber technology, and have proven to be the best performance narrow-linewidth fiber lasers in the market. These lasers have a coherence length of more than 100 km and are uniquely suited for long-range coherent acoustic detection via optical fiber. They have a small footprint (625 cm^3), low power consumption (< 3W) and can be ruggedized for harsh environments. Our fiber laser platform (ROCK laser) has been space-qualified.

Shown on the right-hand side is a photograph of *NP Photonics*' ROCK fiber laser. This OEM module includes the temperature controlled fiber laser, one or two semiconductor pump lasers and respective pump combiner, all drive and control electronics, an RS232 interface, an optical isolator, a monitoring photodetector, as well as a WDM to remove any residual pump light from the laser output. This laser is offered with a fast (10 kHz bandwidth) piezo tuning option with more than 300 MHz of frequency tuning for applications that require locking or stabilization to an external reference. The thermal and piezo tuning feature available in this laser is an important capability for mode-locked fiber lasers since locking to an external frequency is critical in some applications. A negative feedback circuit to the pump diode provides more than 20 dB suppression of the relative intensity noise (RIN) peak (around 1 MHz), and a power loop keeps the output laser power stable to better than 1%.

NP Photonics ROCK Fiber Laser OEM module

Active Fiber for High Fidelity Amplifier. Conventional erbium-doped fiber amplifiers (EDFA) use Er-doped silica fibers longer than one meter to achieve greater than 20 dB gain near the 1550 nm wavelength. More commonly, the length of the Er-doped silica fiber is ~10 to 20 meters. In applications where short length (~1-10cm) is necessary, high gain-per-unit-length of optical fiber becomes critical in order to obtain comparable amplifier performance in a reduced length. Standard Er-doped glass provides a gain per unit length of only 0.02 - 0.2 dB/cm, which does not support sufficient gain in the needed compact form-factor, and is not a viable choice for short-length optical amplifiers or lasers.

NP Photonics has developed high-gain-per-unit-length glass and fiber, and has extensive experience in using this fiber in commercial single-frequency fiber lasers and short-length optical amplifiers. To achieve the high-gain-per-unit-length, a new approach has been developed at *NP Photonics* using active core elements formed from a phosphate glass host co-doped with erbium and ytterbium. The phosphate glass composition improves the solubility to Er and Yb ions, thereby allowing order of magnitude higher dopant levels (i.e. 3-4% weight erbium concentration). This level of doping is higher than previously deemed practical without raising the up-conversion rate, which is deleterious to overall efficiency. The ytterbium co-doping greatly enhances the fiber's ability to absorb pump power while the elevated erbium levels enhance the gain-per-unit-length of the fiber. The development of this type of glass and optical fiber opens up new possibilities for extremely compact high performance optical lasers and amplifiers both for commercial and special applications where compact physical size and/or minimum signal latency are of paramount importance. Our high-gain-per-unit-length fiber has been integrated with micro-optic lenses and filters for signal-pump couplers and spectral gain flatteners, and packaged into one self-contained amplifier device with fiber pigtails for input and output signals as well as fiber pigtails for optically pumping the doped fiber. The figure below shows the gain spectrum of the Er-doped phosphate glass fiber and a schematic representation of one such device containing an 8 cm length of active fiber and completely packaged with micro-optic components within a 10 cm cylindrical tube. The active fiber is energized by commercially available, fiber pigtailed, semiconductor pump diodes (also included). Such a device can easily be scaled down in size to accommodate a much shorter length active fiber (~ 1cm).

NP Photonics fabricates its own glass and fiber, which gives it tremendous fiber design flexibility in terms of core diameter, NA, gain, dispersion, and nonlinearity. This is important for optimization of fiber amplifier and laser performance, and is particularly advantageous for designing an optimized mode-locked fiber laser. The *NP Photonics* Mini-EDFA comes in two types: one is the pre-amplifier Mini-EDFA which provides a spectrally flat gain of over 20 dB in the 1535nm - 1565nm wavelength region; the

other is the Mini-EDFA power amplifier which delivers more than 20 dBm output power in the 1535 nm-1565 nm wavelength region. Both devices have a short latency – equivalent to less than 20 ps relative to a 10 cm length of standard single-mode fiber. The figure shows the gain spectrum for the power amplifier version – indicating a high gain and high power over the full telecommunication band.

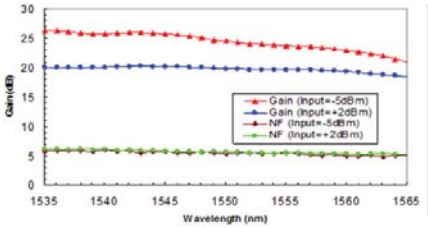

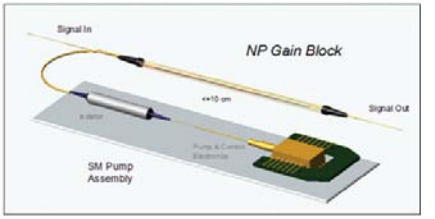

(Left) Gain and noise spectrum for power amplifier version of NP Mini-EDFA. Two input conditions are indicated: 2 dBm and 5 dBm. The active fiber length is 8 cm. (Right) Schematic representation of fully packaged short length amplifier device.

Manufacturing. NP Photonics upholds stringent process control in our state-of-the art Tucson manufacturing facility. Our laser products are manufactured in a clean-room environment. Our manufacturing operation is driven by product quality and consistency. This is achieved through rigorous process control and production metrics implemented by a highly skilled team of technicians.

Facilities/Equipment. Our company's facilities in the Optics Valley in Tucson include 14,000 sq. ft. research and development labs and manufacturing floor. It also houses a class 100 and two large class 1000 clean-rooms. The pictures below show *NP Photonics* clean-room, fiber-drawing tower, and house-made electronics.

NP Photonics clean room, fiber drawing tower, and house-made electronics.

We also possess the following equipment that is applicable to our research and development of pulsed fiber lasers and amplifiers:

- Fiber amplifiers/lasers development lab equipment (tunable source laser systems, pump laser driving power supplies, optical spectrum analyzers, power meters).
- Cascade amplifier system using the highly Yb and Er/Yb co-doped phosphate fibers which can be used to scale the pulse energy close to milli-joule level.
- Feedback loop controller and algorithms.
- Reliability test equipment (humidity chamber, temperature shock chamber).
- State of the art fusion splicer machines for standard and specialty fibers.
- General equipment (1000× microscope and other smaller microscopes, optical tables, etc.).
- Detectors, lock-in amplifiers, boxcar integrators, gold mirrors, oscilloscopes.
- Micro-Electro-Mechanical Systems.
- Glass fabrication equipment (ovens, furnaces, crucibles, weighing station, fume hood).
- Glass and crystal characterization equipment (spectrometer, thermal mechanical analyzer, differential scanning calorimeter, prism coupler).
- Fiber preform and crystal fabrication machineries (CNC , drilling , polishing machine).
- Custom-designed fiber drawing tower for non-silica glasses.

The Search for Exoplanets

Olivier Guyon

While the existence of exoplanets had long been suspected, astronomers have only recently become able to identify and study them. The first planets identified around other Sun-like stars were massive large "super-Jupiters" of about 10 Jupiter masses. Astronomers have now identified a few thousand exoplanets, showing that exoplanets are both abundant in the universe and also highly diverse. Many of the planets identified thus far have no analog in our solar system, such as the massive Jupiter-size planets that have been found orbiting very close to their stars, with a period of a few days. Thanks to the growing number of exoplanets discovered, the formation process for planetary systems (including ours) is now better understood.

Rapid progress in technology (in particular optics) allows us, for the first time in history, to answer one of humanity's long-standing questions: Are we alone in the universe?

Franck Drake expressed in 1960 the number of civilizations in our galaxy with which communication might be possible as the product of seven terms. In 1960, only the first of Drake's equation terms (the average rate of star formation per year in our galaxy) could be estimated. In 2014, we are measuring the second term in the equation (the fraction of those stars that have planets). A key recent finding is that approximately 10% of the stars in our galaxy have Earth-sized rocky planets in their habitable zones—the area around each star where liquid water can be sustained at the surface of a rocky planet.

Instruments that will measure the average number of planets that can potentially support life per star that has planets (Drake equation's third term) are now being designed. In the near future (at most 3 decades), we will be acquiring spectra of Earth-sized planets within habitable zones of nearby stars, allowing us to directly detect the presence of life on exoplanets.

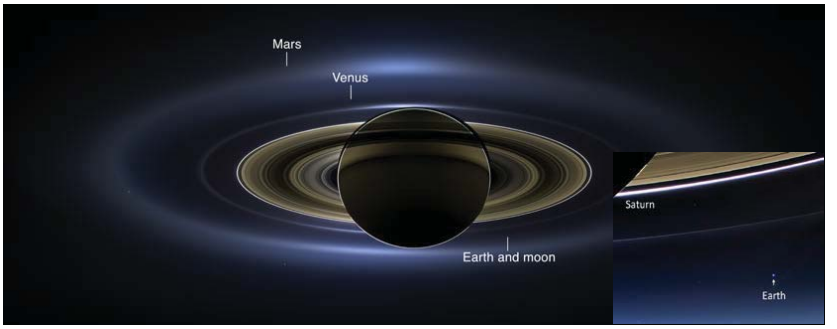

Image of Saturn taken by the Cassini spacecraft (wide angle and detail area around Earth's location). The spacecraft is in Saturn's shadow, and its camera is pointing toward the Sun. Our planetary system's inner rocky planets (Venus, Earth and Mars) are visible as faint sources, approximately 10 billion times fainter than the Sun. (Credit: NASA/JPL, Cassini mission.)

Detecting exoplanets: a formidable optical challenge. Exoplanets are much smaller than the stars they orbit in diameter, mass, and brightness. The Earth, for example, is 1/109 of the Sun's diameter, 1/333000 its mass, and 1.5×10^{-10} as bright. Detecting exoplanets is thus a high-precision optics problem: the exoplanet's signature is an extremely small perturbation over the star's light. Optical systems (telescopes and instruments) aimed at detecting and studying exoplanets are inevitably pushing the limits in measurement accuracy and precision.

Indirect detection techniques

Measuring tiny signals. All but a few of the exoplanets identified so far have never been directly seen: they have been detected indirectly, as a small perturbation over the star's light. Most of the first exoplanets identified around Sun-like stars were discovered by the radial velocity technique. Since both the star and the planet orbiting it are actually orbiting the center of mass of the star + exoplanet system, the exoplanet imprints a small periodic motion on the star. For example, the Earth pulls the Sun on a 4.5 km radius circular orbit at 9 cm/s. The line of sight component of this motion can be detected with a high-precision spectrograph using the Doppler shift technique: the star's spectral absorption lines are shifted slightly toward blue as it approaches, and toward red as it recedes. High-resolution spectrographs with cm/s-level precision (i.e., 1×10^{-10} of a wavelength) and long-term stability have been built for this purpose. The star Alpha Centauri B, one of the three stars in the most nearby stellar system, only 4.37 light years away from Earth, was recently found to harbor a 1.13 Earth-mass planet on a 3.2 day orbit using radial velocity measurements.

The small planet-induced stellar wobble can also be measured as a modulation of the star's apparent position in the sky (astrometry). While the motion is extremely small (0.3 micro-arc-second for an Earth-Sun system at 30 light-years, an angle equivalent to the thickness of a human hair in geostationary orbit), an ultra-stable space-based interferometer or telescope can measure such small angles, as demonstrated by the Space Interferometer Mission (SIM) concept, which has been extensively studied by NASA. The recently launched GAIA mission will identify many giant planets using this technique.

Using chance alignments. While astrometry and radial velocity rely on the ability to measure very small perturbations induced by exoplanets, requiring ultra-high precision measurements of starlight from nearby stars, two other exoplanet detection techniques, microlensing and transits, rely largely on luck.

Microlensing. If an exoplanet is perfectly aligned with a background star, it will act as a gravitational lens amplifying the light from the background star. For a given distant star, the odds that a planet is sufficiently close to the line of sight for this effect to be measurable are extremely small—on the order of a million to one. By monitoring a large number of stars for a long period of time, this technique pays off: dedicated wide-field telescopes have identified about 30 planets by microlensing. More importantly, this technique is the only one able to detect small planets on large orbits, or free-floating planets, as they are both too faint to be imaged and too far from their host stars to perturb their light.

Transits. Exoplanet can occult some of the starlight if they pass directly in front of the star. This, again requires a bit of luck and some patience: first, the planet orbit needs to be aligned with the line of sight (roughly 1 chance out of 100 for an Earth-Sun system), second, the occultation only occurs once per orbital period (once a year for an Earth-Sun system) and at least three transits must be observed to confirm a periodic signal. Dedicated wide field telescopes, equipped with sensitive detectors able to measure precisely and simultaneously the brightness of many stars have been deployed both on the ground and launched in space for this purpose. Deploying networks of small robotic telescopes on the ground is a particularly cost-effective strategy for discovering Jupiter to Neptune size exoplanets with the transit technique. Above the Earth's atmosphere, the brightness of stars can be measured much more accurately, allowing NASA's Kepler satellite to identify planets as small as the Earth.

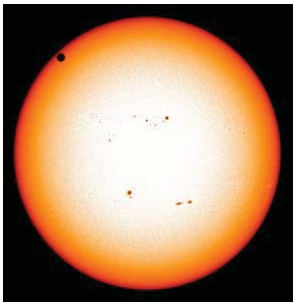

2012 Transit of Venus. Venus is in the upper left part of the image, near the solar limb. During the transit, Venus blocked a small part of the Sun's flux, and solar radiation on Earth decreased by a small but measurable amount. The same measurement can be done on other stars to reveal the presence of exoplanets. (Credit: NASA Solar Dynamics Observatory.)

Direct imaging and life-finding. The planets identified by indirect detection techniques (radial velocity, transit, and microlensing) are very diverse, and can be quite different from our solar system's planets. They include a large population of giant Jupiter-mass planets orbiting close to their host stars (sometimes inwards of Mercury's orbit), dense super-Earths with about 2× our planet's diameter, light puffy planets mostly composed of gas, and free-floating planets that have probably been ejected from their original planetary systems. Most importantly, the exoplanets detected so far include habitable planets: planets with about 1 Earth mass, and orbiting at a distance to their host star that allows liquid water at the planet's surface. According to recent estimates, about one out of ten stars have a habitable planet. This group will be the focus of future generations of instruments aimed at characterizing exoplanets with sufficient sensitivity to remotely detect life, by acquiring to reveal the chemical composition of their atmospheres.

Acquiring high quality spectra of habitable planets requires their light to be physically separated from the much brighter starlight (direct imaging of the exoplanet). This is extremely challenging for Earth analogs, which are approximately 10^{-10} times fainter than a Sun-like star. This extreme contrast, together with the small separation between the planet and its star (typically $1/10^{th}$ of an arc-second, equivalent to the thickness of a penny 3 km away), calls for unusual optical imaging systems optimized for starlight cancellation, named coronagraphs. It also require exquisite control of optical aberrations, which must be continuously measured and controlled. For direct imaging of Earth-like planets around Sun-like stars, the wavefront quality has to be maintained at sub-nanometer level, which can only be done from space.

Ground-based telescopes are currently able to image young giant planets which still have sufficient internal heat (acquired during their formation) to glow at near-infrared wavelengths. Better instruments are being deployed and designed for current 8 meter class telescopes to image a large number of such planets. In the next decade, 30 meter class telescopes will allow light reflected by exoplanets to be detected, and may allow habitable planets to be imaged around nearby stars that are 10× to 100× fainter than the Sun, for which the contrast between the star and the planet is not as extreme as it is for Sun-like stars.

Coronagraph instrument(s) for space telescope(s) are also being developed, and will allow, with the aid of a 4 meter-diameter or larger telescope, spectroscopy of Earth-like planets around Sun-like stars, and potential identification of biomarkers, chemical evidences for the presence of biological activity.

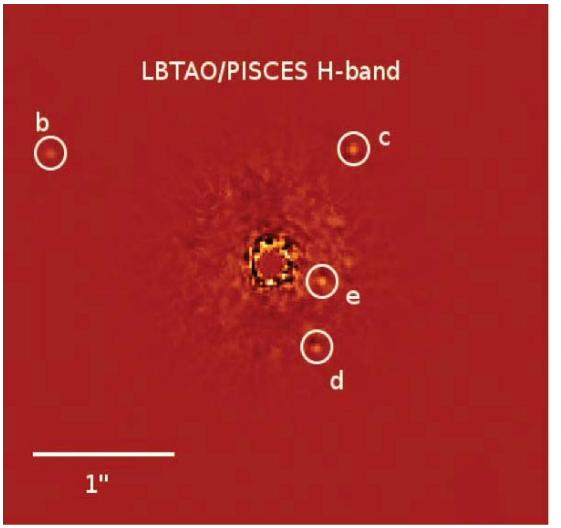

Image of the planetary system around star HR8799, showing four giant planets. The planets have masses between 5 and 10 Jupiter masses, and orbit the central star at distances between 15 and 70 times the Earth-Sun distance. This image was acquired by the ground-based Large Binocular Telescope (LBT) in the near-infrared. The light detected in this image is emitted by the planets' internal heat as they slowly cool down after their formation approximately 30 million years ago. Adaptive optics was used to correct much of the wavefront aberrations due to Earth's atmosphere. Residual uncorrected aberrations can be seen near the center of the image as a cloud of "speckles" preventing the detection of smaller, closer in planets such as habitable planets. (Credit: Andrew Skemer and LBT observatory.)

Assistant Professor of Astronomy and Optical Sciences, Dr. Olivier Guyon splits his time between the Subaru Telescope in Hawaii and the University of Arizona. He attended Ecole Normale Superieure (Paris, France) and did his graduate studies at the University of Paris and the Institut d'Astrophysique de Paris, receiving his PhD in Astronomy in 2002. A 2012 MacArthur Fellow, Dr. Guyon is also the recipient of the 2003 Daniel Guinier Award of the French Society of Physics, and the 2006 Presidential Early Career Award for Scientists and Engineers from the Office of the President of the United States. His research includes coronagraphy, wavefront sensing techniques for Adaptive Optics, and astrometry. Dr. Guyon developed the Phase-Induced Amplitude Apodization (PIAA) coronagraph, a highly efficient optical device that masks the light from a star while preserving the light from planets around it. He is currently leading the Subaru Coronagraphic Extreme Adaptive Optics (SCExAO) group at the Subaru Telescope to use these new techniques for exoplanet detection and characterization. Dr. Guyon's work at the University of Arizona involves developing high contrast imaging techniques for current and future ground and space-based telescopes. Like other amateur astronomers, he is mysteriously driven to dark skies when the moon is not in the way. He spends a good fraction of his time building and using telescopes as an amateur astronomer, doing astronomy just for fun and enjoying the night sky.

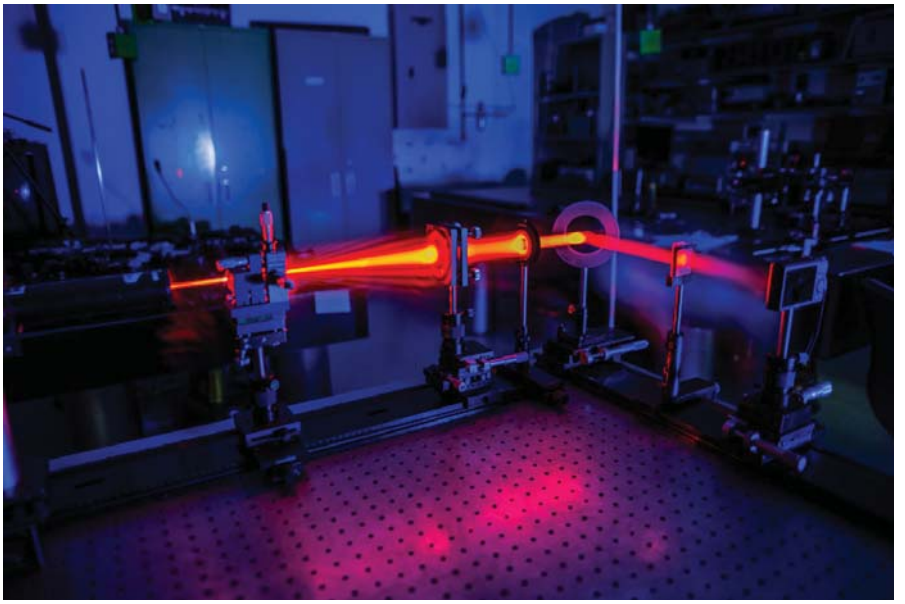

Hands-on Optics. During both the undergraduate and graduate program, students participate in laboratory courses that provide invaluable hands-on experience with optics. A variety of interesting and useful experiments involve many laboratory techniques. The image above illustrates, in a single experiment, a variety of concepts taught in the classroom. This laboratory experiment involved the shear plate interferometer, a device commonly used for testing the collimation of a laser beam. A Helium-Neon laser beam is directed into a microscope objective that is coupled to a 10-μm pinhole. To the immediate right is a singlet lens. These two work together to form a beam expander. The outgoing enlarged beam strikes a thick plate of glass and reflects off of both surfaces. The two reflections are slightly displaced but overlap in the center. This overlap region contains interference fringes that are imaged by a camera and allow the user to determine the accuracy of collimation. In this photograph, the entire path of the laser beam can be observed. The beam begins with a small diameter as it enters the microscope objective. When the beam emerges from the pinhole, it is diffracted into what is commonly known as the Airy pattern. Exiting the lens is an expanded and collimated beam just as one would expect.

Photo Courtesy of Chris Summitt

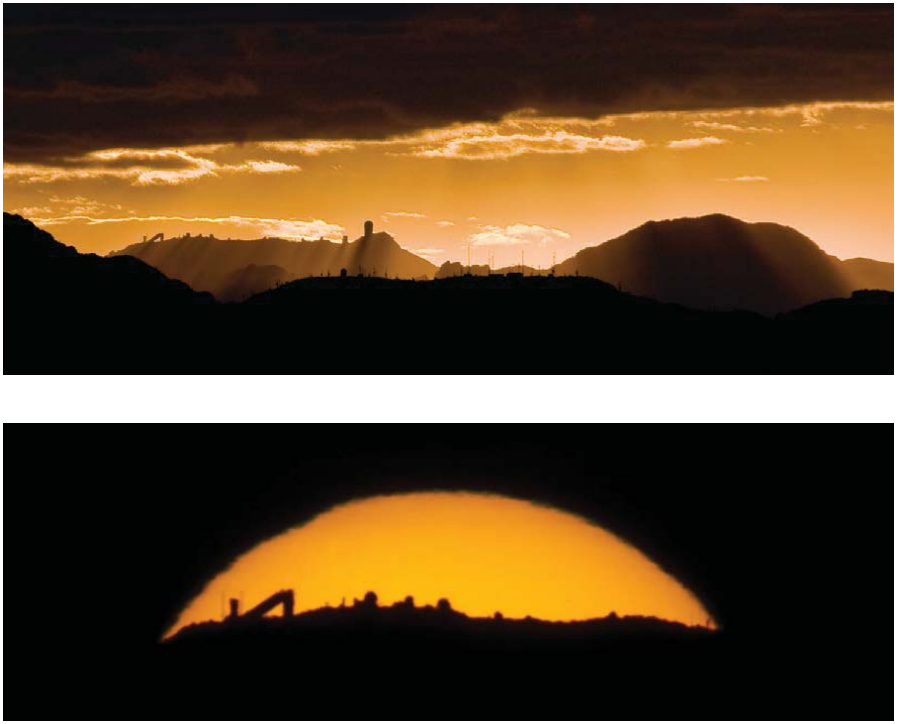

About 60 miles west of Tucson's city center is Kitt Peak. The top of the mountain is home to world-class observatories, including *Kitt Peak National Observatory*, and facilities of the *National Solar Observatory* (NSO), seen in the background of the upper photograph. Below, a sunset photograph taken from east Tucson, shows the sun dropping behind Kitt Peak. The angled silhouette of the McMath-Pierce Solar Telescope of the NSO, appears in the left side of the image.

Photo courtesy of Brian Anderson

The Spin and the Twist: Control and Chaos in the Quantum World

Poul Jessen

Quantum mechanics has been the "theory of everything" for about a century, accounting for the behavior of light and matter at all scales from the microscopic to the macroscopic. It was originally developed to explain the structure of the atom, but quantum mechanics has also been the key to modeling more complex systems such as molecules and solids, and has allowed us to understand phenomena ranging from superconductivity to photosynthesis. As if such tremendous accomplishments were not enough, modern quantum physicists are looking to a new challenge: how do we make quantum systems behave the way we want, rather than having them do what comes naturally to them. This has opened up an entirely new field of "quantum engineering," aimed at developing methods to control individual quantum systems and using them as building blocks for new kinds of devices. In theory such quantum devices have the potential to revolutionize computer, communication and sensor technology.

Quantum optical systems that consist of individual photons and atoms are particularly attractive as test beds with which to explore the basic science of quantum control. This is in part because we can model their intrinsic behavior in exquisite detail, and in part because we can almost completely eliminate perturbations from the outside world which would otherwise mask the quantum effects we seek to manipulate. And among such systems, perhaps none are as amenable to control as quantum mechanical spins, the angular momenta associated with spinning electrons, nuclei, and atoms. Decades of research in nuclear magnetic resonance has given us a powerful toolbox for control of spin ½ particles, which now form the basis of widely used technologies such as magnetic resonance imaging (MRI). Furthermore, because the "spin-up" and "spin-down" states of a spin ½ particle are equivalent to the "0" and "1" states of a quantum bit (qubit), this toolbox has become essential for the effort to build a working quantum computer. Of course there is no reason to stop at spin ½, and experiments have begun to explore the richer physics of larger spins. In the following we will review some of the ways to produce and control exotic quantum states, "image" them by quantum tomography, and use them to probe fundamental aspects of quantum theory.

Quantum and Classical Spins. In classical physics a spin is represented by a vector $\boldsymbol{S}$ that points along the axis of rotation and has a magnitude proportional to the rate of rotation. In quantum physics, the measurable quantities become operators, $\hat{\boldsymbol{S}} = \{\hat{S}_x, \hat{S}_y, \hat{S}_z\}$, and their possible values are *quantized*. Because the three orthogonal components of the spin are not simultaneously knowable, it is often useful to consider quantum states that have well-defined values (i.e., are eigenstates) of $\hat{\boldsymbol{S}}^2$ and one component of $\hat{\boldsymbol{S}}$, say $\hat{S}_z$. Setting the eigenvalue of $\hat{\boldsymbol{S}}^2$ equal to $\hbar^2 s(s+1)$, the possible values of the spin quantum number s are the integer or half-integer numbers greater than or equal to zero. For example, electrons, protons and neutrons have a fixed spin quantum number $s = ½$, while the spin quantum number for composite systems such as atoms or ions can take on additional values. In each case the possible eigenvalues of $\hat{S}_z$ are $\hbar m_z$, where m_z takes on the values $-s, -s+1, \cdots, s-1, s$. Using Dirac notation we write the simultaneous eigenstates of $\hat{\boldsymbol{S}}^2$ and $\hat{S}_z$ as a "ket" $|s, m_z\rangle$.

Even though the behaviors of quantum and classical spins are fundamentally different, a comparison of the two can lead to an appealing visualization of spin quantum states. First let us consider a classical spin with a fixed value of $|\boldsymbol{S}|$. Because such a spin is uniquely determined once we know its direction, all possible (classical) states can be visualized as points on a sphere

of radius $|\boldsymbol{S}|$ (Fig. 1a). Next, consider how we might visualize a spin quantum state on the same sphere. If we prepare the state $|s, m_z = s\rangle$ and measure $\hat{\boldsymbol{S}}$ over and over again in repeated experiments, we will find that the result of measuring $\hat{S}_z$ is always $\hbar s$. The result of measuring $\hat{S}_x$ or $\hat{S}_y$, however, will fluctuate because of the Heisenberg uncertainty relation $\Delta S_x \Delta S_y = \hbar^2 s/2$. Only by taking the average of many measurements (the expectation value) do we get a result similar to a classical spin along the z axis, $\langle s, m_z = s|\hat{\boldsymbol{S}}|s, m_z = s\rangle = \boldsymbol{S}$. This suggests that we think of the state $|s, m_z = s\rangle$ as a probability distribution on the sphere—a "minimum uncertainty patch"—centered on the classical spin $\boldsymbol{S}$. Furthermore, because we are always free to choose our quantization axis along whatever direction we choose, it follows that any quantum state with maximum spin projection along some direction can be represented by a similar uncertainty patch (Fig. 1b). This approach to visualizing spin quantum states can be formalized through the introduction of *quasi-probability distributions*, which can be used to fully describe any arbitrary spin state allowed by quantum mechanics.

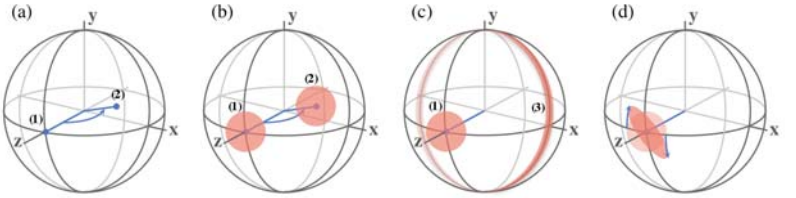

Figure 1. Spin states. (a) A classical spin (blue) is a vector. If its magnitude is fixed it can be represented by a point on the surface of a sphere. A classical spin state (1) can always be transformed into another spin state (2) by a geometric rotation. (b) Quantum states that have maximum projection in some direction, e.g., $|s, m_z = s\rangle$, can be represented by a quasi-probability distribution that forms a minimum uncertainty patch centered on the corresponding classical state. Again, one such "quasi-classical" state (1) can always be transformed into another (2) by a geometric rotation. (c) For spins $s > ½$, there are states that are not spin-up in some direction, for example the state $|s, m_z = 0\rangle$ that has zero projection along z. The quasi-probability distributions for these states have qualitatively different shapes, and it is therefore not possible to transform $|s, m_z = s\rangle$ into $|s, m_z = 0\rangle$ by a geometric rotation. (d) A rotation around the x axis by an angle proportional to S_x transforms the quasi-probability distribution for the $|s, m_z = s\rangle$ state into an ellipse – a *spin-squeezed* state.

Controlling a Quantum Spin. For classical spins, the simplest non-trivial form of control will change the direction of $\boldsymbol{S}$ but not the magnitude. In this scenario any "transformation" of the (classical) spin state is a geometric rotation. The atoms of interest to us have a magnetic moment proportional to their spins, $\boldsymbol{\mu} = -\gamma \boldsymbol{S}$, where γ is the so-called gyromagnetic ratio, and a rotation of the spin can therefore be accomplished by Larmor precession in a magnetic field. This type of control carries over to the quantum case. For spin ½ the analogy is exact: all possible quantum states are spin-up in some direction, and the ability to perform geometric rotations is sufficient to transform any initial state into any final state. Just as for classical spins, this can be done by Larmor precession in a magnetic field. In quantum mechanics Larmor precession is described by the Hamiltonian

$$\hat{\boldsymbol{H}} = -\hat{\boldsymbol{\mu}} \cdot \boldsymbol{B} = \gamma \hat{\boldsymbol{S}} \cdot \boldsymbol{B}. \tag{1}$$

Interestingly, for spin quantum numbers $s > ½$ geometric rotations are no longer sufficient for full control. We can understand this easily by considering the nature of the states $|s, m_z\rangle$. For

an integer spin $s \geq 1$ the allowed values for the quantum number m_z are $0, \pm 1, \cdots, \pm s$. The states $|s, m_z = \pm s\rangle$ are spin up/down along the z axis, and we can transform one into the other by a 180º rotation. However, there are now states, for example $|s, m_z = 0\rangle$, that cannot be transformed into $|s, m_z = \pm s\rangle$ by *any* rotation, as we can easily see from the respective quasi-probability distributions (Fig. 1c). This limitation on control becomes more severe the larger the spin, because as s increases, the vector space of quantum states fragments into a growing number of subspaces that cannot be connected by geometric rotations. Remarkably, if the magnetic field can be time-dependent and we add to the Hamiltonian in Eq. (1) just a single term that is non-linear in the spin degree of freedom, then the system becomes fully controllable for any s. One example is the very simple Hamiltonian

$$\hat{\boldsymbol{H}} = \gamma \hat{\boldsymbol{S}} \cdot \boldsymbol{B}(t) + \beta \hat{S}_x^2. \tag{2}$$

The effect of the new term $\beta \hat{S}_x^2$ is to rotate the spin around the x axis by an amount proportional to S_x. This is known as a *twist*, and as illustrated by the quasi-probability distributions in Fig. 1d, the resulting transformation is qualitatively different from a geometric rotation. Using the mathematical formalism of group theory, we can show that the combined action of this twist and a time-varying magnetic field allows full controllability. In practice, the "control waveform" $\boldsymbol{B}(t)$ required to transform a specific initial quantum state into a desired final quantum state is best found via computer-based numerical optimization. This approach is known as "optimal control" and can be applied to a variety of other control tasks, including the design of unitary transformations which are the most general form of (coherent) control allowed by quantum mechanics.

In a series of experiments beginning in 2004, my research group at the *College of Optical Sciences* has implemented the Hamiltonian of Eq. (2) and explored its use to manipulate individual atoms of Cesium. A Cesium atom in its ground state has a total spin $s = 3$, a non-zero magnetic moment, and an electronic structure that allows the twisting term to be implemented through an interaction with off-resonance laser light. As described in detail in Ref. [1], any desired quantum state-to-state transformation can then be achieved with a computer optimized magnetic field that rotates in the *x-y* plane. As an example, Fig. 2 shows a computer simulation of the gradual transformation of an initial state $|s = 3, m_y = 3\rangle$ (spin-up along *y*) to a superposition state $(|s = 3, m_z = 2\rangle + |s = 3, m_z = -2\rangle)/\sqrt{2}$, visualized in the form of an evolving quasi-probability distribution. This early experiment succeeded in producing a series of additional target states with fidelity (i.e., probability of success) in the 80−90% range, chiefly limited by the decohering effect from spontaneous scattering of laser light.

Imaging a Quantum Spin. So far, our discussion has left out an essential question: how do we verify in an experiment that a given control procedure (a magnetic field $\boldsymbol{B}(t)$ combined with a twist) has successfully taken the system to the desired target state $|\chi\rangle$. One way of accomplishing this is to perform a complete reconstruction of the final state $|\psi\rangle$ that is actually produced by the experiment, and then find the fidelity from the overlap between the desired and actual states, $F = |\langle\chi|\psi\rangle|^2$. Quantum state reconstruction requires a process known as "quantum tomography", in which an "image" of the quasi-probability distribution is computed based on the results of an "informationally complete" set of measurements. As described in detail in Ref. [2], quantum tomography is at least as difficult to perform as quantum control. One reason is that quantum measurements cause disturbance—measure $\hat{S}_x$, and we wipe out the information we could have gained by measuring $\hat{S}_y$ instead. This means that a full tomographic reconstruction requires not

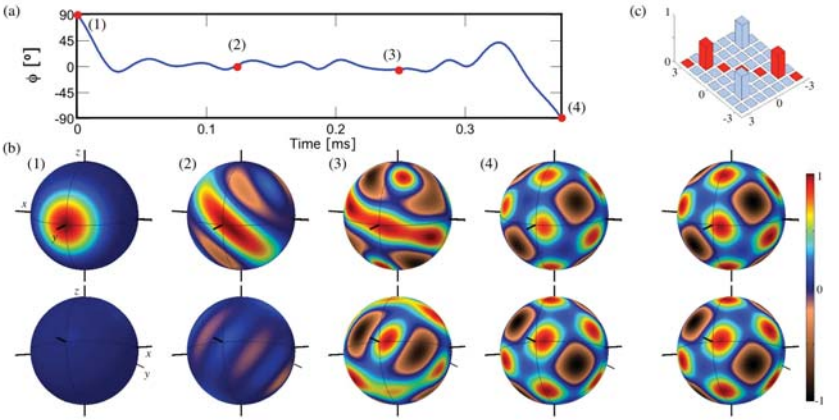

Figure 2. Quantum control of an atomic spin. (a) The control magnetic field $\boldsymbol{B}(t)$. The field rotates in the *x*-*y* plane and is specified by its angle φ with respect to the *x* axis. (b) Quasi-probability distributions for the spin at the times indicated in (a). The initial state (1) is spin-up along the *y* axis, and gradually evolves into the desired final state (4). Top and bottom images show the $y > 0$ and $y < 0$ hemi-spheres, respectively. The quasi-probability function used here is the so-called Wigner function, which is negative-valued in the presence of non-classical quantum interference. (c) Density matrix and Wigner function representations for the target state $(|s = 3, m_z = 2\rangle + |s = 3, m_z = -2\rangle)/\sqrt{2}$.

only the ability to implement many different kinds of measurements, but also the ability to prepare a great number of identical "copies" of the system on which to perform them. Furthermore, we generally rely on the same experimental techniques for control and for tomography, which means that the fidelity with which we can produce a target state $|\chi\rangle$ and the fidelity with which we can reconstruct the actual state $|\psi\rangle$ will usually be comparable. While this makes quantum tomography a blunt instrument for checking the fidelity of a quantum control experiment, the procedure is still an extremely powerful laboratory tool that can be used to great effect when exploring different kinds of quantum physics. As an example of the use of quantum tomography to diagnose quantum control, Fig.3 shows an experimental reconstruction of the quasi-probability distribution for the target state in Fig.2.

From Order to Chaos. At its core, quantum control implements a Hamiltonian and uses it to drive a desired dynamical evolution. From a technology perspective, this is the basis for turning a quantum system into a useful device—our spin system might, for example, be a superior way to encode and process quantum information. Basic science suggests a different perspective: perhaps we can use our highly controllable system with its designer Hamiltonian as a "quantum simulator" and apply it to the study of an interesting physics problem. Most of the current work on quantum simulation is focused on idealized Hamiltonians for many-body systems, which are thought to be responsible for solid state phenomena such as high-temperature superconductivity or quantum magnetism. In the remainder of this article we will discuss a different physics problem that is a particularly good match to our single-spin control and imaging capabilities: the boundary between quantum and classical behavior and the emergence of chaos.

Chaos appears everywhere and at all scales in the natural world, including the energy levels of atoms, electron transport, chemical reactions, neural networks, population dynamics, weather

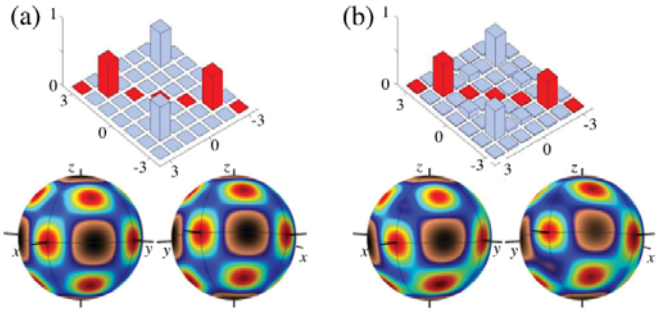

Figure 3. Reconstruction of a quasi-probability distribution (Wigner function) through quantum tomography. (a) Target state for the quantum control sequence shown in Fig. 2. (b) Tomographic reconstruction of the Wigner function for the actual state produced in the experiment. The relative fidelity of the states in (a) and (b) is approximately 85%.

systems, and the motion of planetary bodies. In light of this it is perhaps surprising that physicists are still debating how chaos can emerge from quantum mechanics—which is, after all, believed to be our most complete theory of nature. In classical physics, chaos is characterized by hypersensitivity of the time evolution of a system to initial conditions (the "butterfly effect"). Quantum mechanics does not permit a similar definition, in part because of the uncertainty principle, and in part because the structure of the Schrödinger equation preserves the overlap between quantum states. This fundamental disconnect poses a challenge to our understanding of how classical behavior emerges from the underlying quantum physics, and has motivated a decades long search for quantum signatures of chaos.

One of the popular paradigms for quantum chaos is the so-called quantum kicked top, which can be implemented in a fairly straightforward manner for our Cesium atomic spin. The kicked top is a periodically driven spin that evolves according to the Hamiltonian

$$\hat{\boldsymbol{H}}(t) = p\hat{S}_y \sum_{n=0}^{\infty} \delta(t - n\tau) + \left(\frac{\kappa}{2\hbar s\tau}\right)\hat{S}_x^2. \qquad (3)$$

This corresponds to a periodic sequence of "kick and twist", each made up of a rotation of the spin by a fixed angle p around the y axis (the kick), and a rotation around the x axis proportional to $\hat{S}_x$ (the twist). This is of the same general form as the Hamiltonian in Eq. (2), which we know from our experiments in quantum control that we can implement with great accuracy.

The effect of the kick-and-twist sequence on a classical spin can be illustrated by calculating and plotting its position on a sphere after each individual step of kick-and-twist (Fig. 4). Picking appropriate values for the parameters p and κ, the points traced out by the spin will follow either regular orbits as shown in red, or irregular trajectories as shown in blue, depending on the initial starting point. In the language of chaos theory, the regions of regular orbits are known as "islands of stability", and the regions of irregular trajectories as the "sea of chaos". It can be shown that the motion of a classical spin cannot cross the boundaries between these two regimes of motion, and the simultaneous presence of regular and chaotic regions is referred to as a "mixed phase space".

The "islands in the sea" structure of Fig. 4 suggests a way to explore the similarities and differences between quantum and classical motion: let us prepare the quantum mechanical spin

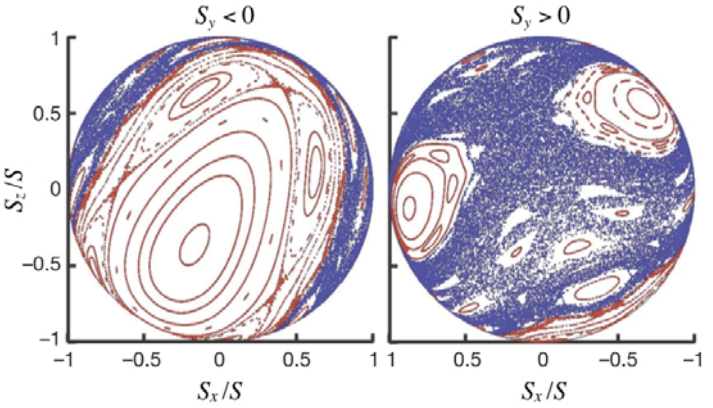

Figure 4. Stroboscopic plot of the motion of a classical kicked top. The position of the spin is marked once following each kick-and-twist sequence. Red points show regular trajectories followed by the spin when the initial (classical) state lies within a regular island; blue points show the chaotic trajectory for an initial state in the sea of chaos.

in a state that forms a minimum uncertainty patch centered on the classical spin we wish to emulate, and then track how the quantum dynamics moves and distorts the quasi-probability distribution. In Ref. [3] we describe an experiment doing exactly that: we prepared a Cesium atom spin in a desired initial state, evolved it for n periods of the kicked-top Hamiltonian, imaged the quasi-probability distribution by quantum tomography, and then repeated many times for different n to build up a stop-motion movie of the resulting evolution. Figure 5 shows two such stop-motion movies made for different initial states. The series of frames in Fig. 5a were acquired for a quantum spin starting on one of the two small islands in the $S_y > 0$ hemisphere, and show that it will not cross into the sea of chaos but instead undergoes *tunneling* to the other island—a unique quantum motion that is forbidden by classical physics. In contrast, the frames in Fig. 5b were acquired for a spin starting in the chaotic sea, where it undergoes irregular motion and distortion without much discernible structure. A better visualization of the dynamics can be achieved by adding all the frames in a stop-motion sequence, which will show the regions explored by the spin when it starts from a particular location. As seen in Fig. 5c, these composite images illustrate the remarkable degree to which the quantum kicked top respects the boundaries of classical motion: if started on an island, the quantum spin remains there or tunnels to another island, while a spin started in the chaotic sea eventually goes everywhere except for the islands. This is more than a little surprising given that the spin of a single atom is a very quantum mechanical object, and may be a result that is peculiar to spin systems. Generally, however, it is exactly the kind of correspondence we expect to see for quantum systems of mesoscopic or macroscopic size.

The Butterfly Effect Gets Entangled[*]**.** One of the most interesting observations to emerge from theoretical studies of quantum chaos is that there appears to be a deep connection between the presence of chaos in classical physics and the generation of *entanglement* in quantum physics.

[*] With thanks to Zeeya Merali, who coined this phrase in *Nature News.*

Quantum entanglement is a property of physical systems that consist of two or more particles, and is responsible for the "spooky" correlations between them that so troubled Albert Einstein. That the intrinsically classical phenomenon of chaos should be correlated with the intrinsically quantum phenomenon of entanglement is extremely surprising and counterintuitive, and has made the study of this effect an important priority for experiments.

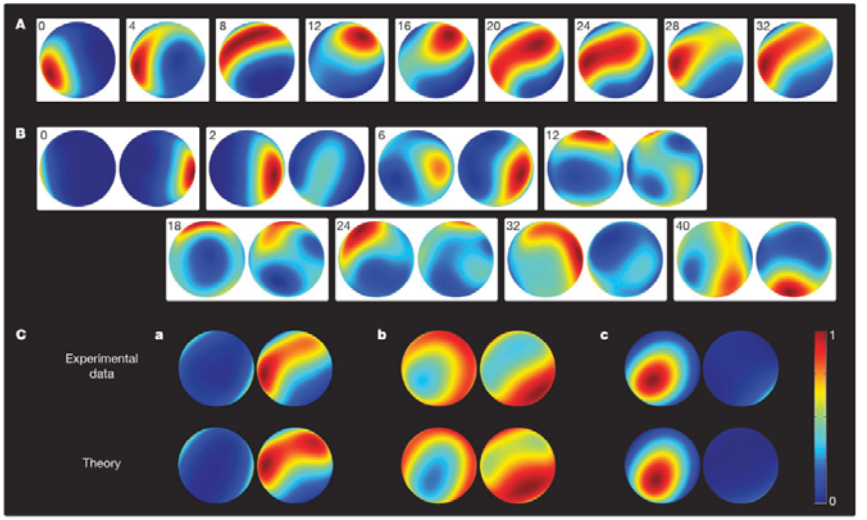

Figure 5. Quasi-probability (Husimi) distributions for a quantum kicked top, showing selected experimental snapshots from the first 40 periods of evolution. The period number *n* is indicated in each frame. The Husimi distribution is used because it is everywhere positive and more easily compared to a classical phase space distribution. (A) Stop-motion movie of a spin initially localized on one of the two islands in the $S_y > 0$ hemisphere, showing quantum tunneling between them. (B) Stop motion movie of a spin initially localized in the sea of chaos. (C) 40-period averages of the evolving quasi-probability distributions, with (a) and (b) corresponding to the movies (A) and (B), and (c) corresponding to an initial state localized on the large island in the $S_y < 0$ hemisphere. Experimental data and theoretical predictions are shown for comparison.

Without going into the formal details of entanglement or how it can be measured and quantified, we note here that the spin of a Cesium atom is actually a composite that results from adding the spin of the electron cloud to the spin of the nucleus—and that the two can be entangled to a variable degree depending on the quantum state of the overall spin. Furthermore, the kind of minimum uncertainty states that we used as starting points in our experiment happen to be minimally entangled, whereas states whose quasi-probability distributions are twisted or broken up become more entangled as they spread across the sphere. Finally, the amount of entanglement present in our experiment is easy to determine because we already did step-by-step quantum state reconstruction when we made the movies in Fig. 5.

To visualize the entangling power of a kicked top in its regular and chaotic regions, we can calculate the average entanglement of the spin state during the first 40 kicks of our experiment, as a function of the starting point for the spin. Figure 6a shows the theoretically predicted amount of entanglement for different starting points, with blue colors indicating those starting points that led to minimal entanglement along the subsequent trajectory, and red colors those

starting points that led to the most. As expected, the blue and red regions overlap nicely with the regular islands and the sea of chaos in Fig. 4. Figure 6b shows the experimentally observed entanglement for a number of starting points distributed along the green line in Fig. 6a, which intersects both regular and chaotic regions. The significant difference in entanglement and its close correlation with the presence of classical chaos served as the first experimental demonstration of entanglement as a quantum signature of chaos.

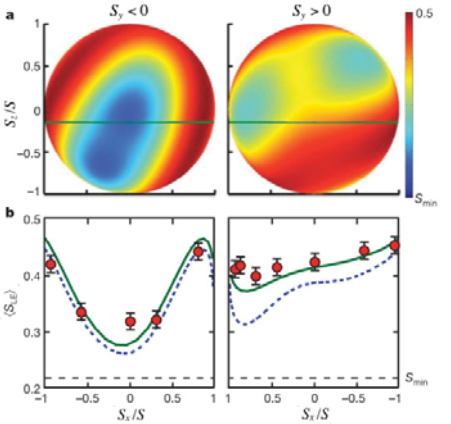

Figure 6. Quantum entanglement as a signature of chaos, quantified by the average of the so-called linear entropy $\langle S_{LE} \rangle$ of the electron spin state over the first 40 periods of the quantum kicked top. The color of each point on the sphere indicates the entanglement generated for an initial spin state centered on that point. (a) Theoretical prediction of the entanglement generated in the experiment. Regions of low and high entanglement generation match the islands and sea of chaos in Fig. 4. (b) Entanglement measured in the experiment for initial states localized on the green line in (a). Also shown are the predictions of a full theoretical model of the experiment (solid line), and the predictions for an ideal kicked top without experimental imperfections (dotted line). A marked contrast can be seen between regular and chaotic regions.

Dr. Poul S. Jessen is a Professor and Chair of Quantum Information and Control in the College of Optical Sciences at the University of Arizona. He received his PhD in Physics from the University of Aarhus in 1993, for research done with Dr. W. D. Phillips at the US National Institute of Standards and Technology. His research interests lie at the intersection of quantum optics and quantum information science, and currently include quantum control and measurement of single and collective atomic spins, quantum control of atoms in optical lattices, and atom-light quantum interfaces based on optical nanofiber traps. Dr. Jessen is a fellow of the American Physical Society.

[1] S. Chaudhury, S. Merkel, T. Herr, A. Silberfarb, I. H. Deutsch, and P. S. Jessen, "Quantum Control of the Hyperfine Spin of a Cs Atom Ensemble," *Phys. Rev. Lett.* **99**, 163002 (2007). DOI: 10.1103/PhysRevLett.99.163002.

[2] G. A. Smith, A. Silberfarb, I. H. Deutsch, and P. S. Jessen, "Efficient Quantum-State Estimation by Continuous Weak Measurement and Dynamical Control," *Phys. Rev. Lett.* **97**, 180403 (2006). DOI: 10.1103/PhysRevLett.97.180403.

[3] S. Chaudhury, A. Smith, B. E. Anderson, S. Ghose, and P. S. Jessen, "Quantum Signatures of Chaos," *Nature* **461**, 768 (2009). DOI: 10.1038/nature08396.

Tucson is surrounded by mountains. The Tucson Mountains, seen here to the west of the city center and the University of Arizona football stadium, are a dry low-elevation range. To the north of the city, the Santa Catalina range rises to over 9000 feet. A road leads to the top, and there are numerous hiking trails throughout the range. To the east of the city lies the Rincon Mountains, a designated wilderness area, and the location of Saguaro National Park's east unit. Like the Santa Catalinas, the upper elevations of the Rincon Mountains are covered with forests and interesting rock formations.

Photo courtesy of Brian Anderson

The Femtosecond Frequency Comb: From Seconds to Attoseconds

R. Jason Jones

From the earliest observations of light-matter interaction by Ibn Sahl to Sir Isaac Newton, light has been used to provide exquisite detail concerning the physical world. In the field of spectroscopy, light has been used to probe the inner structure of atoms and molecules, providing some of the earliest and most stringent tests of the developing quantum theories that governed their configurations. The light emitted from lasers has since enabled experiments based on the *coherent* interaction between light and matter. Using advanced laser sources, light-matter interactions have been studied on very disparate time scales, from highly monochromatic lasers whose pure sinusoidal field can induce and follow atomic oscillations unperturbed for up to several seconds without losing track of its relative phase (i.e., greater than 500,000 billion atomic oscillations), to short bursts of laser light lasting only a few femtoseconds (10^{-15} sec, or a millionth of a billionth of a second!) where it is now possible to observe and even control the motion and rearrangement of atoms and molecules during chemical reactions. As state-of-the-art lasers used for these studies are highly specialized, research groups were often known for their work in either precision spectroscopy or ultrafast science, with each area utilizing different tools and often having little technological or scientific overlap prior to the late 1990s.

A paradigm shift has since occurred with the development of the femtosecond (fs) frequency comb. This powerful tool is nothing more than a highly coherent laser source emitting a periodic train of short pulses. Its development has, however, intimately connected the fields of precision spectroscopy and ultrafast science and coherently linked timescales from seconds to attoseconds (10^{-18}sec). Its impact has ushered in a new era of increasingly accurate time and frequency standards based on optical transitions in atoms and ions (optical atomic clocks), and unveiled the world of attosecond dynamics, where the motion, correlation, and rearrangement of electrons in atoms and molecules can be tracked and even controlled in real time. Such breakthroughs promise not only a deeper understanding of the physical world, such as the implications of our fundamental constants, but also has the potential to significantly advance or even replace technology as significant as our global-positioning system (GPS), the use of laser based radar (LIDAR), the temporal and spatial accuracy by which we can remotely guide unmanned vehicles (e.g., spacecraft, drones, robotic automation), and the precise calibration of astronomical telescopes needed for the detection of extra-solar planets, to name a few.

The frequency comb…simplified. The ideas driving the development of the fs frequency comb originated from the desire to both advance high-resolution spectroscopy by enabling the comparison of different atomic and molecular transitions spanning the ultraviolet, visible, and infrared spectrum, as well as to measure their *absolute* frequencies to develop better atomic clocks based on optical transitions. Although modern electronics can easily count the oscillations of microwave signals, measuring optical frequencies requires establishing a phase coherent link between ~500THz atomic transitions and the 9.192,631,770 GHz frequency of the cesium atomic clock.[1] The basic idea behind the frequency comb and how it can link optical frequencies to microwave or radio frequencies is in fact quite simple, and is the result of the Fourier transform relationship, which relates a signal measured in time to its corresponding frequency distribution. For example, consider the pure sinusoidal oscillation of the electric field from a

[1] The current definition of the second is based on the time it takes for the cesium atom to oscillate 9,192,631,770 times between its hyperfine ground states.

linearly-polarized monochromatic laser as plotted in the left hand side of Fig.1a. For light in the visible portion of the spectrum, a single oscillation of the electric field lasts about 2.1 fs. This sinusoidal waveform corresponds to a single frequency of 474×10^{12} Hz, or a "red" wavelength of 633 nm (right column of Fig.1a). Now consider a single light pulse as shown in Fig.1b. This pulse can be viewed as having the same "carrier" frequency as in Fig.1a, but is strongly amplitude-modulated by a pulse envelope such that the waveform only lasts for $\Delta t \sim 8$ fs, in this example. The corresponding frequency spectrum for this pulse is still centered at 474×10^{12} Hz, but due to the short pulse envelope, the spectrum is very broad. This is also a result of the mathematical properties of the Fourier transform, which tell us that the width of the spectrum is inversely proportional to the pulse duration. Now consider the pair of pulses shown in Fig.1c. In this example the pulses have a time delay T between them that is exactly 13 periods of the laser carrier frequency.[2] Note that the two pulses are identical in this example. In this case we can see

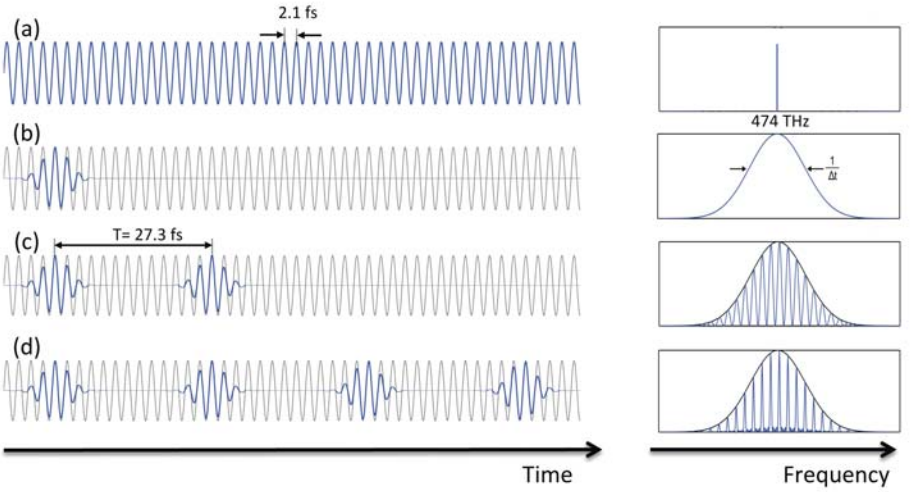

Figure 1. Time (left column) and frequency (right column) relationship of the laser electric field (in blue). Black lines are for reference only. Coherent light emitted from (a) a single frequency cw laser, (b) a single laser pulse, (c) a pair of laser pulses, and (d) 4 laser pulses separated with equal time delays. Note that 1 THz = 10^{12} Hz.

that they are "phase coherent" with the continuous-wave (cw) field of Fig.1a, in the sense that the field nodes and antinodes of the second pulse are still aligned with the original cw carrier frequency. Now consider the spectrum of this two-pulse waveform. Each pulse individually has the same spectral amplitude (as shown in Fig.1b). However, the mathematical property of the Fourier transform tells us that, because one pulse is delayed in time relative to the other, there will be a linear phase shift across the spectrum of the second pulse relative to the first, given by $\Phi(f) = 2\pi T \times f$, where f is frequency. The spectral components from each pulse will constructively interfere only when this relative phase shift is an integer multiple of 2π. Spectral interference peaks therefore occur at $2\pi T \times f = 2\pi n$, or when $f = n/T$, where n is an integer.

[2] This is not a typical example of the pulse period, which is usually on the order of nanoseconds (10^{-9} sec), but is simply used for illustrative purposes.

Now, if instead of a pulse pair we have four pulses, as shown in Fig.1d, or better yet, an *infinite* train of equally spaced pulses, the constructive interference peaks will simply become sharper and sharper until each resembles a narrow frequency similar to that of a cw laser, as in Fig.1a.

The above equation, which determines the location of these peaks, is often written in the following form:

$$f_n = n \times f_{rep}, \tag{1}$$

where f_{rep} is the repetition rate of the laser pulse train and f_n corresponds to one of the lasing frequencies. Modern laser systems are now capable of generating trains of pulses so short that the resulting "comb" of precisely spaced frequencies can span the entire visible spectrum.

The simple expression of Eq.(1) is quite powerful, as it directly relates the individual optical frequencies of the femtosecond comb ($f_n \sim 10^{15}$) to the easily measured microwave/radio frequency of the pulse repetition rate ($f_{rep} \sim 10^7 - 10^9$) by multiples of some large integer n.[3] The absolute frequency of a highly monochromatic cw laser that is used, for example, to excite an atomic or molecular transition, can now be directly measured. One must first compare[4] the frequency of the cw laser with that of a single "tooth" of the femtosecond frequency comb to measure the difference in their frequencies. Then, the frequency of that comb tooth can be determined by simply recording the repetition rate of the pulse train with a standard electronic counter (which can easily be referenced to an atomic clock such as cesium by using, for example, a GPS receiver). In this way one can think of the frequency comb as a set of large gears as found in a bike or clock, which converts the fast oscillations of an optical signal down to a slowly oscillating microwave signal that can be directly counted and/or compared with other transitions. As long as the teeth of these gears do not slip, the measured microwave signal will remain phase coherent with the optical signal.

The phenomenon of spectral interference, the constructive and destructive interference peaks in the frequency spectrum, due to the spacing of the pulses in the time domain, is completely analogous to what is observed in the diffraction of light from a single slit versus a large array of slits (such as a grating). When light illuminates a single slit, the resulting diffraction pattern far away as seen on a screen (known as the "far-field") is related to the slit dimensions by the same Fourier transformation that relates the time and frequency domains. For a single narrow slight (relative to the wavelength of the light), a wide diffraction pattern will appear on a screen in the far-field. For two slits, this diffraction pattern will have a sinusoidal modulation due to the constructive and destructive interference of the light emerging from each individual slit (similar to the spectrum in Fig.1c). If one now has an infinite array of slits such as a grating, the interference peaks in the far-field will become very sharp. The different diffraction peaks correspond to the different diffraction orders of the grating. This is why the *resolving power* of a grating is related to the number of illuminated slits. Since the spatial width of a single diffraction order for a single color of light depends on the number of slits illuminated, the ability to separate or resolve different colors of light that hit the same grating also depends on the number of grating grooves illuminated. The different colors will be diffracted at slightly different angles, but will only be resolved if their separation is greater than the width of their individual diffraction patterns.

[3] Although determining the integer n requires secondary techniques, there is no uncertainty in this quantity. The value of n will be obvious if the frequency to be counted is already known to a precision better than f_{rep}.

[4] This comparison is usually done by mixing the cw laser frequency with the nearest component of the frequency comb on a photodiode and directly measuring their "beat frequency", which is just the small difference of their optical frequencies. This is completely analogous to the tuning of musical instruments by comparing a pure and known tone with the corresponding key of the instrument and audibly detecting any difference from the beating between the two tones.

A closer look at the frequency comb. The concept of the frequency comb may seem simple, but the full realization of this powerful technique took nearly thirty years to develop. Why did this take so long? Many of the basic concepts were explored in early experiments conducted in the 1970s by Theodor Hänsch and colleagues.[5] They were trying to utilize the equally spaced frequencies of a mode-locked dye laser for high-resolution measurements of energy level splitting in sodium atoms (known as fine-structure splitting). This early frequency comb served as a kind of ruler to precisely measure a large frequency interval. However, the laser technology at that time was not sufficiently advanced to answer many lingering questions about the feasibility of expanding the approach, or whether it was possible to measure the *absolute* frequency of optical transitions. In addition, many ultrafast groups focusing on the development of short-pulse laser systems were unaware of the subtle questions raised in this early work due to the minimal overlap of these different research communities. The unresolved question came down to this: "Just what do the pulses coming from the laser *actually* look like?" Laser systems developed to generate a train of ultra-short pulses are usually based on the concept of "mode-locking." The pulse trains from mode-locked lasers in fact do *not* normally look like the pulse train shown in Fig.1d. Another issue was the intrinsic noise of the laser, which could affect each pulse differently, raising the question: "Is each pulse completely independent from the next?" Is it possible that there can exist some stable phase relationship between successive pulses, or between pulses from a mode-locked laser and a cw laser with the same carrier frequency (as illustrated in Fig.1)? Until the late 1990s, ultra-short pulses from mode-locked lasers were generally treated by most experimentalists and theorists as something like that shown in Fig.2a, where the underlying carrier frequency and/or phase is not well defined or even significant. The majority of research considered mainly the short duration of the pulse envelope. With improving laser technology through the 1980s and 90s (e.g. shorter pulse laser systems, reduced technical noise, lower noise pump lasers), researchers once again began to address this question.

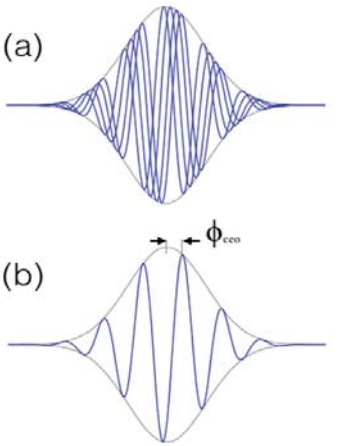

Figure 2. A short pulse with (a) a poorly-defined carrier frequency and phase, and (b) a well-defined carrier-envelope phase.

[5] See, for example, (i) A. I. Ferguson, J. N. Eckstein, and T. W. Hänsch, *J. Appl. Phys.* **49**, 5389 (1978), (ii) A. I. Ferguson, J. N. Eckstein, and T. W. Hänsch, *Appl. Phys.* **18**, 257 (1979), (iii) J. N. Eckstein, *Ph.D. Thesis*, Stanford University, 1978.

The average over multiple pulses from a mode-locked laser may indeed look something like that in Fig.2a. However, it certainly is possible to define, for a *single* short pulse, a phase like that shown in Fig.2b, where the "carrier-envelope offset" (CEO) phase is just the offset of the nearest crest of the electric field to the peak of the pulse envelope. When this pulse is circulating inside a laser cavity, the pulse envelope will travel at its group velocity through the laser gain medium and various optical elements. The carrier frequency, however, travels at its phase velocity. As it turns out, there is no requirement in the general theory of mode-locking that these two velocities must be the same. Therefore, after each round trip, the pulse that is coupled out of the laser through a mirror may in general have a different CEO phase. A more realistic picture of the pulse train is then shown in Fig.3, where the pulses are no longer identical due to this pulse-to-pulse CEO phase shift.

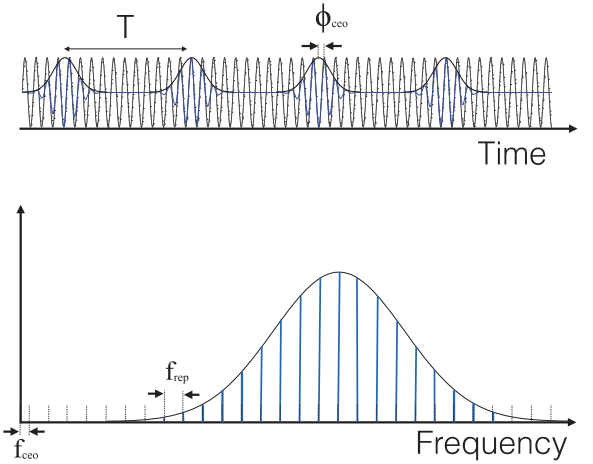

Figure 3. Relationship between the pulse train in the time domain (top) and the corresponding structure of the frequency comb (bottom).

The change of the CEO phases from pulse-to-pulse modifies the simple expression given in Eq.(1). In that expression, we said that the spectrum from successive pulses will only constructively interfere at frequencies where their relative phase shift is an integer multiple of 2π. We must now include in this analysis not only the relative phase shift due to the pulse delay, but also that due to the change in the CEO phase. The relative phase shift of the spectrum between each pulse is therefore given by $\Phi(f) = 2\pi T \times f + \Delta\phi_{CEO}$, where $\Delta\phi_{CEO}$ is the change in the CEO phase from pulse to pulse. Setting this equal to an integer multiple of 2π results in a new expression for the position of the frequency comb teeth, that is,

$$f_n = n \times f_{rep} + f_{CEO}, \tag{2}$$

where $f_{CEO} = \Delta\phi_{CEO}/(2\pi T)$ is known as the carrier-envelope offset frequency. This extra frequency shift of the entire comb (see Fig.3) is just a result of the time changing phase from pulse to pulse.

The final piece to the puzzle. In the 1990s researchers could determine that newly developed and lower noise mode-locked lasers could produce very narrow frequency comb teeth that were

rigorously spaced at exactly the pulse repetition rate and whose spectrum spanned over 100 nm.[6] The individual frequency components of the mode-locked laser could be observed by simply overlapping the beam from a single frequency laser with the mode-locked laser. When this combined beam is sent onto a fast photodiode, the resulting photocurrent will only be sufficiently fast to follow the difference frequency (or beat frequency) between the cw laser and a few of the comb's teeth. These broadband frequency combs were immediately used to measure large frequency intervals between atomic and molecular transitions of interest. However, to determine the absolute optical frequencies of the comb components, one still had to find a way to measure f_{CEO}. Many researchers knew *how* to do it, but the technology still seemed too far away for it to be feasible. The technique would require a laser spectrum that spanned an *optical octave* (i.e., a frequency comb bandwidth so broad that, if the frequency of the lowest comb components were doubled, they would overlap with those at the higher frequencies). If this could be achieved, then when the lower comb frequencies where doubled (this could be done using standard nonlinear crystals), their offset frequency would double as well. When these doubled frequency components are mixed with the higher frequency components from the same comb, their difference frequency (beat frequency) would be exactly equal to f_{CEO}!

Although very short laser pulses could be generated with spectral bandwidths of ~100 nm, this was not yet the needed optical octave. As it turned out, a fortunate development (almost unbelievably so!) in the field of nonlinear optics had just been reported. Researchers at both Bell Laboratories and the University of Bath had developed specialty fibers with unique internal structure capable of broadening the spectrum of laser pulses to over an optical octave, producing a bright and a stunning rainbow of colors. Figure 4 shows one example produced with a Ti:sapphire laser in our lab after sending the light off a prism to be dispersed. The only remaining question was whether this nonlinear generation process preserved the comb-like structure of the original laser. It turned out that under appropriate conditions this "super-continuum" of colors does indeed preserve the original laser coherence. Within weeks of receiving this new "nonlinear" microstructure fiber, groups were able to directly detect f_{CEO}. Now that both f_{CEO} and f_{rep} could be detected, researchers were able to explore techniques for actively stabilizing these frequencies to stable, low-noise microwave references, thus eliminating any significant noise or drift in the optical frequency comb. Due, in part, to their efforts in developing the optical frequency comb, Theodor Hänsch (Munich, Germany) and John Hall (Boulder, Colorado) each received one quarter of the 2005 Nobel Prize in Physics.

Figure 4. Super-continuum of laser light generated from short pulses sent through a nonlinear micro-structured fiber. A zoomed-in look at this spectrum would reveal a discrete frequency comb structure rather than a continuous distribution of frequencies.

Connecting timescales from seconds to attoseconds. With the ability to directly convert optical frequencies to microwave frequencies based on the relationship in Eq.(2), the long envisioned goal of utilizing narrow optical transitions in atoms or ions as atomic clocks now became a reality. The race was soon on to develop superior atomic clocks with this emerging technology.

[6] For comparison, the visible spectrum spans about 300 nm.

Why does this have such potential to improve the stability of atomic clocks? To accurately determine 1.0 second currently requires counting ~9 billion (9×10^9) oscillations of the cesium atom. There will always be some phase error in counting the final cycle of these oscillations, and that will ultimately determine the uncertainty in the measurement of a time interval (or a frequency). For simplicity let us say that we are off by an entire cycle in our count. This would mean our time measurement is off by $1/(9 \times 10^9)$ seconds, or $\sim 10^{-10}$ seconds. However, if one instead uses an *optical* transition frequency to measure (or define) 1.0 second, one will be counting $\sim 10^{15}$ cycles; the one-second interval will then be divided up into much smaller time periods. Assuming the same error in counting the last cycle, the total error will be only 10^{-15} sec (a femtosecond). This potential improvement in precision by five orders of magnitude assumes a number of technical details, such as the stability of the transition itself. However, all else being equal, developing atomic clocks based on significantly higher optical transition frequencies promised to dramatically increase the precision by which one could measure time and frequency.

This has in fact already turned out to be true. Spectacular improvements in atomic clock performance have been demonstrated in laboratories around the world since the development of the frequency comb. The gains are so significant that the cesium atomic clock will almost assuredly be replaced one day by an optical clock as the standard of time. The improvement in stability can impact many areas in science and technology. Most visible may be the precision by which time and navigation can be remotely determined. For example, GPS satellites all carry microwave-based atomic clocks on board as the position of a GPS receiver is based on the precision timing of signals sent from various locations. Improved timing signals can therefore directly impact navigation precision. In addition to benefits in technology, the frequency comb has become an invaluable tool in fundamental science. Atomic clocks are used not only for determining time and improving navigation; they can also be used as precision sensors of anything that might change the atomic resonance frequency. Examples include the study of collisions between ultra-cold atoms, which can shift their oscillation phase during collisions. Atomic transitions sensitive to magnetic fields can be utilized to make sensitive magnetometers. Optically-based clocks are currently capable of mapping out gravitational fields and/or altitude changes due to the effect known as "gravitational red-shifting," which is a prediction of general relativity. If you raise a clock a meter higher, it will "tick" at a slightly different rate due to the difference in the gravitational field! Finally, researchers around the world are comparing measurements of various optical atomic clocks in search of any potential variation of Nature's fundamental constants. Such a possibility is predicted by some physical theories. Since these constants determine the internal structure of atoms and molecules, any variation of certain fundamental constants would result in a change of the atomic/molecular transition frequency and therefore a change in the clock frequency.

We have mentioned how the frequency comb can produce pulse trains that remain phase coherent for time scales up to several seconds. The pulses themselves each consist of optical cycles lasting only a few femtoseconds. Researchers from the precision spectroscopy community who had developed ultra-stable cw lasers for decades quickly worked together with colleagues from the ultrafast community to perfect the frequency comb techniques. This technology, however, not only impacted the field of precision spectroscopy, but also paved the way for the field of attosecond science. In conjunction with Fig.3, it was pointed out that, by producing a well-behaved pulse train, one could generate a useful frequency comb. The reverse is also true. By carefully controlling the optical frequencies, one can precisely control the electric field waveform. As illustrated in Fig.2, without knowledge or control of ϕ_{CEO}, the pulse envelope will

determine the shortest timescales by which one can measure any change in an experiment. By stabilizing and setting f_{CEO} to zero (for example), researchers could now produce trains of *identical* pulses. This opens the door to utilizing a single oscillation of the carrier frequency to measure temporal dynamics.

For example, with extremely short pulses, setting ϕ_{CEO} to zero or π means that the central peak of the electric field will be either positive or negative and can be significantly stronger than subsequent optical cycles. Experiments have since demonstrated that the direction in which an electron is pulled off during ionization of an atom can be controlled by changing ϕ_{CEO} between zero and π. Other experiments use a single cycle of the pulse to produce a strong linear variation of the electric field in time, and use this to determine the exact moment at which an electron is ionized (due to a second pulse, for example). The approach is completely analogous to the use of a streak camera, which also uses a scanning electric field to map out the timing of an event. For example, if an electron is instantly ionized from an atom in the presence of the "streaking field" provided by the short pulse, it would experience a force proportional to the strength of the electric field, which in turn depends on the precise moment it was ionized. This technique enables one to measure when an atom is ionized to within a small fraction of an optical cycle. Since a single optical cycle lasts only a few femtoseconds, the timing resolution in these experiments is on the scale of attoseconds.

A final example is the ability to now generate single pulses of light lasting less than 100 attoseconds through a process known as high harmonic generation. Depending on when the electron is ionized, it is possible that the change in the sign of the electric field after half a cycle can bring the electron *back* to the atom it had just ionized, resulting in a collision. The energy the electron gains while being accelerated by the electric field can be given off as a high-energy photon during the recollision. This recollision happens during a fraction of the optical cycle, resulting in a burst of light on the time scale of attoseconds. By controlling ϕ_{CEO}, researchers can now control this process to generate attosecond pulses of light, which can in turn be used to probe ever-shorter time scales.

The control of ϕ_{CEO} enabled by the frequency comb has enabled new experiments that probe dynamics on attosecond time-scales. It has simultaneously enabled the measurement of atomic transition frequencies by counting their oscillations on time scales of several seconds. From next generation atomic clocks and precision spectroscopy, to attosecond science, the frequency comb has proven to be an invaluable tool that has dramatically impacted and brought together two seemingly unrelated research communities, to the benefit of all.

R. Jason Jones is an associate professor at the College of Optical Sciences at the University of Arizona. He received his PhD from the University of New Mexico in 2001. He continued on as a National Research Council Postdoctoral Award recipient and then senior research associate at JILA (University of Colorado) with Jun Ye and John Hall until July 2006. He joined the College of Optical Sciences as an Assistant Professor in August 2006. His research interests include optical physics, high-resolution and ultrasensitive laser spectroscopy, laser cooling and trapping, optical frequency metrology utilizing femtosecond frequency combs, nonlinear optics, and ultrafast optics. His current research involves the extension of the femtosecond frequency comb into the extreme-ultraviolet using intracavity high harmonic generation. He has over 80 combined journal and conference publications and two patents. He is the recipient of a National Science Foundation CAREER award (2007) and the DARPA Young Faculty Award (2009), as well as a Kavli Fellow of the National Academy of Sciences (Frontiers of Science 2010). He is a member of the American Physical Society and the Optical Society of America.

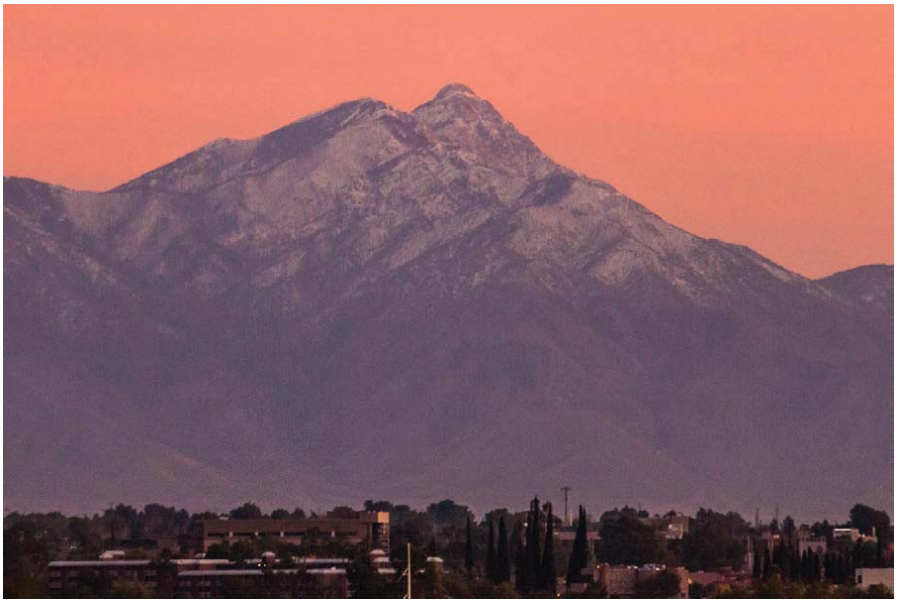

On the southern edge of the Tucson basin is the Santa Rita range, the highest of the mountains in the immediate vicinity. Mount Wrightson, shown here on a winter morning, is over 9400 feet in elevation. The long trail to the top provides one of the most scenic hikes in the area.

Photo courtesy of Brian Anderson

Micro/Nanofabrication Facility

Semiconductor lasers and photonic components have revolutionized a wide range of commercial and defense applications. These miniature components are impacting various areas of science and engineering research including physics, chemistry, biology and medicine. Recent progress in nanotechnology has provided a new vision for the next generation of photonics and bio-photonics components. Miniaturizing photonic structures has revealed unique behaviors in light-matter interaction at the nanoscale, which has in turn enabled the development of novel ultra-compact devices with superior performances. There is, therefore, the promise of development of single-photon sources, threshold-less lasers, ultra-compact wavelength-division multiplexing (WDM) components, and micro-sensors. Nano-photonic devices facilitate the light-matter interaction on subwavelength scales, and have the potential to create new opportunities and applications. Advanced research in micro/nano-photonics requires a state-of-the-art fabrication facility in a highly controlled environment (clean-room). Nanofabrication instruments provide patterning, etching, and contact definition at 10-100 nm size scale.

At the *College of Optical Sciences* we have a unique clean-room facility used for the micro/nanofabrication of various optical, optoelectronic, and photonic components. The 2100 square-foot facility in the central building which consists of class 100, 1000 and 5000 cleanrooms, houses several key instruments including optical and electron-beam lithography, scanning electron microscopy, reactive ion etching (ECR-RIE), electron beam evaporator, rapid thermal annealing, ball-bonding, and fiber pig-tailing. Recently a new cleanroom space was added to expand the micro/nanofabrication capabilities of the College. The second clean-room facility consists of a 600 square-foot class 100 yellow room and a 1200 square-foot class 1000 processing room. The cleanroom facility at the *College of Optical Sciences* is accessible to various researchers and students both inside and outside the College. Some of the key instruments for nano/micro-processing are: contact printing photolithography, electron-beam lithography (EBL), reactive ion-etching with high anisotropy and selectivity, various metal and dielectric deposition chambers, as well as some of the conventional micro-fabrication tools such as rapid thermal annealing, wire-bonding, and auto-align fiber packaging.

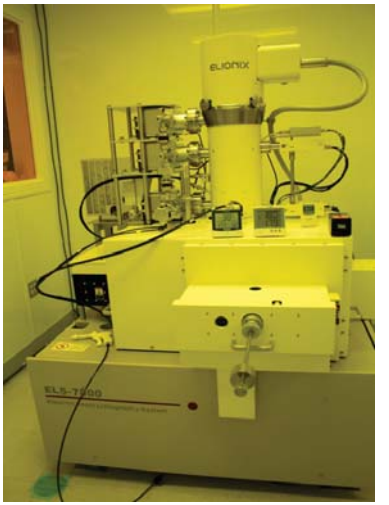

Figure 1. 100 keV Electron beam Lithography system.

Electron Beam Lithography (EBL): An ultra-high-resolution EBL system is an ideal tool for conducting research in advanced nano-structured devices and systems. We have recently acquired an ultra-high precision 100 keV thermal-field-emission ELS-7000 system through a Major Research Instrumentation grant from the National Science Foundation (NSF). The EBL system is available to the University researchers and their collaborators, as well as to other institutions within the State of Arizona. The system enables and originates a wide range of novel opportunities in nano-scale R&D within and outside the University, providing a unique capability especially for our young faculty and students with innovative thinking.

The system has major impact on current/future research projects within the academic and research institutions as well as the companies in the State of Arizona. It also has enriched the educational experiences of science and engineering students at the University. The system provides patterning capability of nanostructures with dimensions as small as 8 nm on various small and large (up to 6") substrates. It allows high-precision fabrication of arbitrary structure (lines, curves, dots) on the nano-scale. A key instrument in the exploration of light-matter interaction in the nano regime, the EBL system boosts research activities in nano-photonics, quantum optics, and quantum computing.

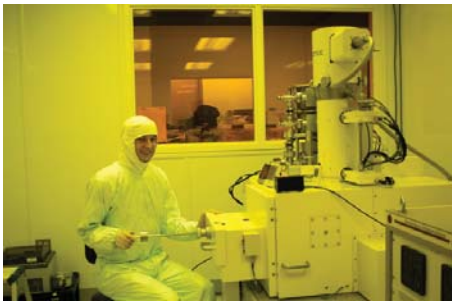

Figure 2. OSC graduate student performing nanofabrication using the EBL system.

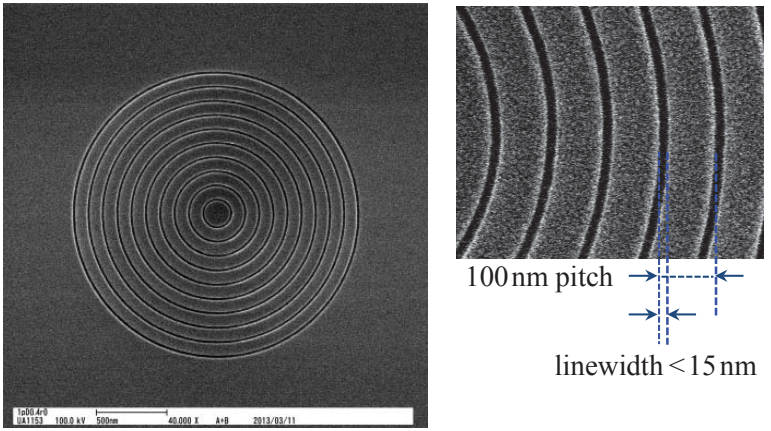

Figure 3. Periodic nanostructure with less than 15 nm linewidth in ZEP on silicon substrate written with our ELS-7000 EBL system.

ECR-RIE with load-lock and six different dry-etching gasses. The system is critical for dry-etching and pattern-transfer into various materials (semiconductor, dielectric, metal) following a lithography process, where low-damage, smooth, and vertical side-walls are desired.

Electron-beam evaporator for metal contact deposition. Active optoelectronic device performance is strongly affected by the quality of metallic contacts, alloy composition, and metal thickness control. Electron beam evaporation is a widely used method for evaporation of various *p*- and *n*-type semiconductor alloys. Due to its directional deposition, the method is suitable for lift-off patterning.

Figure 4. Plasmalab 100 ECR-RIE system

Figure 5. Electron beam Evaporator for metallization.

Figure 6. Ion-beam assisted sputtering system.

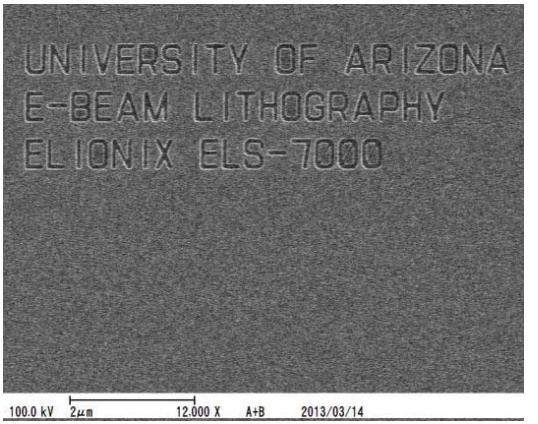

Mahmoud Fallahi received his Ph.D. degree in 1988 from the University of Toulouse and LAAS-CNRS in Toulouse, France. He joined the National Research Council of Canada as a post-doctoral fellow in 1989 and became a member of technical staff as a Research Scientist during 1992-1995. He joined the College of Optical Sciences in 1995 as an Assistant Professor. Dr. Fallahi was promoted to the rank of tenured Associate Professor in 2000 and Professor in 2006. His research interests include high-power semiconductor lasers, micro- and nano-fabrication, photonic integrated circuits, hybrid organic-inorganic heterogeneous integration, and WDM components. Dr. Fallahi is the author or co-author of over 160 journal and conference papers. He has served as Conference Chair and Program Committee member in several international conferences in the field of semiconductor lasers and integrated optics.

Producing Special Colors with Lasers

Yushi Kaneda

Have you ever noticed the difference between the colors of a flashlight and a laser-pointer? Or the difference between the light from an incandescent lamp and a sodium lamp (the kind of orange-colored lamp you might see on the streets in some cities)? In both cases, the latter have "purer" colors. Color, in general, consists of a mixture of light having different wavelengths. If you take a sample of light, break it down to lights of different wavelength, and plot the strength of its various components as a function of the wavelength, you will have what is called a *spectrum*. Several examples of spectra are shown in Fig.1(a). The figure shows the spectra of the sky, sunlight at noon, and Sun at sunset on a clear sunny day.

The wavelengths of the light that the naked eye can see range from about $400nm$ to $700nm$. The short-end at $400nm$ is violet, and, as one moves up to longer wavelengths, the color changes to blue, green, yellow, orange, and red. Shorter wavelengths than violet are called ultraviolet (UV), and longer wavelengths than red are called infrared (IR). So, in Fig.1(a), the components toward the shorter wavelengths (i.e., toward the left of the spectra) are blue/violet and ultraviolet, whereas those toward the right are orange/red and infrared. If the spectrum is broad, spanning the entire visible range, the color is perceived as white. From Fig.1(a) you may infer that the sky is blue, and that the Sun at sunset is redder than it is at noon. Each spectrum has its own pronounced components, which give it its distinct hue. In the comparison mentioned earlier between a flashlight and a laser-pointer, and also between an incandescent lamp and a sodium lamp, the spectra are distinctively different. Lasers and sodium lamps have very narrow spectra compared to flashlights and incandescent lamps, that is, the energy of the light beam is contained in a very narrow region of wavelengths.

Monochromatic light and lasers. Figure 1(b) shows the spectra of sodium lamp and laser-pointers, indicating substantial differences with the spectra depicted in Fig.1(a). These sources are called *monochromatic*, meaning that the light contains essentially only one spectral (wavelength) component. The spectral profiles of monochrome sources are very different than those of natural light, hence they appear "purer" and have "more saturated" colors.

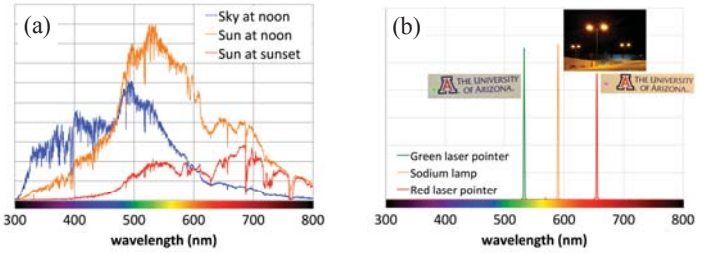

Figure 1. (a) Spectra of the sky during daytime, Sun at noon, and Sun at sunset on a clear day in Tucson. (b) Spectra of red laser pointer ($655\ nm$), sodium lamp ($589\ nm$), and green laser pointer ($532\ nm$).

The wavelength λ of monochromatic light is related to its frequency ν by the identity $\nu = c/\lambda$, where c is the speed of light in vacuum. The energy of a photon is related to its frequency by $\mathcal{E} = h\nu$, where h is Planck's constant. Materials with discrete energy levels emit photons at wavelengths corresponding to the difference in energies of different levels involved in their electronic transitions, that is, $\lambda_{21} = hc/(\mathcal{E}_2 - \mathcal{E}_1)$. This is why the spectrum of light

emitted as a result of electronic transition between distinct energy levels is monochromatic. Lasers take advantage of the existence of materials with discrete energy levels to produce intense, nearly monochromatic light.

In order for the laser material (the so-called *gain medium*) to emit light, atoms or ions in the material need to be excited to higher energy levels; this process is called *pumping*. The material must provide "optical gain," meaning that the excited atoms or ions make a transition to a lower level when "tickled" by a photon whose energy is equal to the energy difference between the upper and lower levels of the atom/ion. The electronic transition from the higher to the lower level results in the emission of a new photon having the same wavelength as the one that "tickled" the atom/ion in the first place. This is the process of *stimulated emission*, which starts with one photon and produces two, so it is an amplification process. If a set of reflectors is placed around such a material, so that light can bounce back and forth passing each time through the gain (i.e., amplifying) medium, at some point the system begins to lase—provided that the gain is sufficiently high and the losses during each round-trip within the cavity are reasonably low. The oscillations could be seeded with fluorescent light, or with the "optical noise" originating within the gain medium itself. The reflectors provide the *feedback* mechanism—much like the howling of a loudspeaker when its microphone picks up its own output. Pumping, Gain, and Feedback thus comprise the three essential elements of a laser. Lasers emit at specific wavelengths depending on their gain medium. Most laser materials emit at a wavelength corresponding to the difference between one pair of their energy levels. In other words, lasers are not capable of emitting arbitrary wavelengths, something that users might have wished for. Some common wavelengths are 488 nm (blue), 515 nm (green), 633 nm (red), and 1064 nm (near IR).

Nonlinear wavelength conversion. If you ever studied for a ham radio license, you have probably heard the term "frequency multiplication." When a sinusoidal wave, which has just one frequency component, say, ω, is injected into an electronic circuit, sometimes the resulting waveform gets distorted, so it is no longer a pure sinusoid. Those distorting components of the signal have frequencies that are integer-multiples of the original frequency, so that the periodic nature of the signal is maintained: the waveform repeats itself with a period of $2\pi/\omega$. The signal now contains frequency components at $2\omega, 3\omega, \cdots$; this is frequency multiplication. The same effect can occur in the optical frequency regime. When a dielectric polarization induced in the material by the electric field of the incident light has a "distorted" profile, that distortion represents optical frequency components that are integer-multiples of the incident optical frequency. If the frequency of the distorted component happens to be twice that of the incident light, we speak of second-harmonic generation (SHG). As a result of SHG, the wavelength of the newly-generated light is reduced by a factor of 2 relative to that of the incident beam. When certain conditions are met in the optical material, including what is called *phase-matching*, the 2ω component grows as the light propagates through the material. Therefore, this phenomenon can convert, for example, near infrared light, which has a relatively long wavelength, to visible light having a shorter wavelength. The most frequently encountered example of SHG is a green laser-pointer, which is fairly common these days. It uses a "fundamental" laser emitting at $\lambda = 1064\ nm$ in the near infrared (invisible), and the SHG process within the nonlinear material of the laser-pointer converts the energy of the 1064 nm light into another beam having twice the fundamental frequency, or half the wavelength ($\lambda = 532\ nm$), which is the emitted green light.

The existence of the physical phenomenon of SHG implies that, if one has a laser that emits at a wavelength λ_0, one may be able to convert its energy to another light beam having $\lambda = \lambda_0/2$ (but not always). However, one still needs a laser source having the wavelength that is twice as

long as the desired wavelength. The process of second harmonic generation substantially broadens the accessible range of laser wavelengths.

Semiconductor lasers. The lasers most often encountered in daily life are diode lasers, which belong to the class of semiconductor lasers. These lasers are used in optical disc drives (i.e., CD/DVD/Blu-Ray players and recorders). You also see these semiconductor diode lasers at the checkout counters of supermarkets—although, in some places helium-neon (He-Ne) lasers, which are fairly common gas lasers, may still be in use. Diode lasers take an injected electric current as the source of their energy, just as other optoelectronic components such as light emitting diodes (LEDs) do. The operation of laser diodes relies on the transition of electrons between different energy levels of their quantum wells, which are small structures fabricated in semiconductor materials. Unlike other laser materials, which use transitions of their natural energy levels, semiconductor materials are grown to have artificial energy levels, so that transitions occur at engineered wavelengths, albeit within the extent of energy levels that the semiconductor material can handle.

Conventional semiconductor lasers cannot produce very high powers; as such, they are not suitable for wavelength conversion via SHG. A fairly new class of lasers, optically-pumped semiconductor lasers (OPSLs), also known as vertical external cavity surface-emitting lasers (VECSELs), can provide high power in output beams of good quality, which is suitable for wavelength conversion. The OPSLs greatly broaden the range of accessible wavelengths by filling in the gaps, so that almost any wavelength, covering the entire visible spectrum for instance, can be generated. Figure 2 shows the reported demonstration of OPSLs, covering a wide range in the infrared and much of the visible by means of SHG. Two consecutive SHG stages give rise to fourth harmonic generation (4HG), which extends the range of available wavelengths into deep UV.

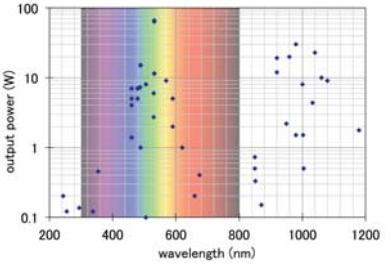

Figure 2. Reported output powers of optically-pumped semiconductor lasers (OPSLs) as a function of the emitted wavelength.

Why the need for specific colors? Can a green laser do something an infrared laser cannot, or the other way around? This is indeed the case; for a job you are trying to accomplish, the color (i.e., the wavelength) does matter. In a simplest example, suppose you are trying to drill a hole into something that looks green, say, a printed circuit board (PCB). In this case, a green laser may not do a good job; the fact that the object looks green means that most of the green light is reflected, while other colors are absorbed. That is why either infrared lasers or ultraviolet lasers are used in PCB drilling applications. This is one example of the difference in usability of different colors of lasers. However, there are applications requiring much tighter control of colors. One example is what is called a *guide star*.

The United States launched the Hubble Space Telescope (HST) into Earth's orbit at an altitude of $559\ km$, so that the telescope could look into the deep space without disturbance from

atmospheric turbulence. While HST takes wonderful pictures of various stars and galaxies in our universe, a much larger ground-based telescope can be built to image faint astronomical light sources. These ground-based telescopes need what is called *adaptive optics*, something that corrects atmospheric disturbances so that clear images of heavens can be constructed. In order to compensate for the image distortion, a telescope needs a reference, for example, a point of light at a known location in space, near the direction the telescope is looking at. Such a "light point," called an artificial star, can be created by sodium atoms in the mesosphere (the layer of atmosphere above stratosphere). When these sodium atoms are excited, they fluoresce, that is, they emit light of a somewhat longer wavelength. The mesospheric sodium atoms can be excited by laser light at a specific wavelength corresponding to the difference between their energy levels. Therefore, such an excitation laser must operate precisely at a particular wavelength, $\lambda = 589\ nm$, which is the color of the sodium lamp shown in the inset of Fig.1(b).

Another example of applications needing precise control of the wavelength is atomic physics experiments. Atoms are cooled when illuminated by light of a specific wavelength, corresponding to one of their transitions; a process commonly referred to as *laser cooling*. A cold atom does not vibrate as much as it would at higher temperatures, so its intrinsic nature can be investigated. One such natural property of atoms is their precise transition frequency. By measuring the transition frequency of cold atoms, one can build accurate clocks to act as time standards—that is, clocks that provide a precise definition for *one second*. Scientists around the globe are working hard to realize an atomic clock that is accurate to 18 digits.

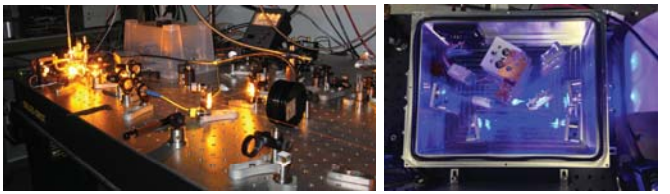

Figure 3. Examples of laser experiments at the *College of Optical Sciences*.

What we do at the University of Arizona. At the *College of Optical Sciences* we are working on different types of novel lasers (one example is OPSL), studying various mechanisms of wavelength conversion. An OPSL was made to work at $\lambda = 1178\ nm$ using high-indium-content $InGaAs$ quantum wells, and light at $\lambda = 589\ nm$ was subsequently generated by SHG; see Fig.3. An OPSL operating in IR was also converted to deep UV to probe the atomic transitions of mercury and other atoms with potential applications in atomic clocks. Many of the lasers built in our laboratory are unique, helping to propel various science projects forward.

Yushi Kaneda is a research professor at the *College of Optical Sciences* of the University of Arizona, where he has been a faculty member since 2004. He received his B.E. from University of Tokyo (1988), M.S. from Stanford University (1993), and Ph.D. from University of Tokyo (1998), all in Applied Physics. Prior to joining the University of Arizona, he worked for Sony Corporation in Tokyo (1988-2000), where he was a Senior Research Scientist, and for NP Photonics in Tucson (2000-2004), where he was the Chief Laser Scientist. Throughout his career, Dr. Kaneda has worked on various types of lasers and nonlinear frequency conversion techniques. His current areas of research interest are optically-pumped semiconductor lasers and nonlinear frequency conversion in the ultraviolet region. Dr. Kaneda is a senior member of the Optical Society of America (OSA).

At the top of the Santa Catalina range, at 9159 feet, Mount Lemmon is a jumping off point for short and long hikes into the 56,933-acre Pusch Wilderness. Lookout points at the top of the mountain, and along the road leading to the peak, open up grand vistas to Tucson and the deserts and mountain ranges of Southern Arizona. Once in the forest and among the rock formations, springs, creeks, and trees, the sense of being only an hour's drive or a day's hike from a major city evaporates.

Photo Courtesy of Brian Anderson

Compact Femtosecond Fiber Lasers and Applications

Khanh Kieu

Lasers have found many important applications in scientific research as well as in industrial manufacturing facilities. The internet is running in part due to the work of millions of lasers. Most people have used CDs, DVDs, or printers, where a laser plays a crucial role. Lasers' magical power has also been popularized by the great imagination of writers and movie-producers who have come up with the laser sword as in "Star Trek," for example. The underlying physics of the lasers (stimulated emission) was proposed by Einstein in the early 20th century but the first laser was demonstrated by Theodore Maiman of the Hughes Research Laboratories only about fifty years later. The laser is now a little over fifty years old; it has seen tremendous triumphs and, despite its age, it is still going strong. Its best days are probably still ahead.

In general, a laser consists of three main components: (i) a gain medium in the form of a doped crystal, a semiconductor structure, or a doped optical fiber; (ii) a pump source, which supplies energy for the laser to run (lasers are not perpetual motion machines, unfortunately); and (iii) a cavity, which is typically formed by a pair of highly reflective optical mirrors—the use of a ring cavity is also widespread, where the laser beam travels around a closed loop. The laser cavity supports only a set of discrete optical frequencies. These are the frequencies (or wavelengths) that will oscillate inside the cavity when the laser operates. The pump source, which can be another laser, a flash-lamp, or just an electrical current, provides energy to the gain medium and moves its atoms to the excited state. There is typically a fast non-radiative decay from the initial excited state down to a metastable state (where the electron can stay for a relatively long time; this could be a few nanoseconds up to milliseconds). When the number of atoms in the metastable state exceeds the number in the ground state, which is the condition for the so-called "population inversion," a laser beam of the right wavelength can be amplified upon propagating through this gain medium.

A laser can operate in three main regimes: continuous wave (CW), *Q*-switched, and mode-locked. As the name suggests, the laser emits a continuous stream of light in the CW regime; here the peak power is equal to the average power. To increase the peak power of the laser beam, which is useful for many applications in nonlinear optics or material processing, the continuous stream of light is squeezed into very short and energetic optical pulses using *Q*-switching or mode-locking techniques. The quality-factor (or *Q*-factor) of the laser cavity is rapidly modulated in a *Q*-switched laser. The energy from the pump is first stored in the gain medium in the form of a large population inversion, and then quickly released to form short, giant optical pulses at the output facet of the laser, carrying all the stored energy. The duration of the pulses from a *Q*-switched laser is on the order of a few nanoseconds to a couple of hundred nanoseconds, while typical pulse energies are on the order of micro-Joules to milli-Joules. So the peak power can reach hundreds of kiloWatts, even though the average output power is many orders of magnitudes smaller.

To reach shorter pulse-durations or higher peak-powers, mode-locking is required. Mode-locking in lasers is a striking phenomenon provided by the generosity of Nature! It turns out that it is possible to design a laser so that all the allowed oscillating frequencies or wavelengths (longitudinal modes) are locked in phase. The number of locked frequencies could be in the hundreds of thousands to about a million. The optical fields from all these laser modes add up coherently within the cavity, and an ultra-short optical pulse is formed at the laser output. The pulse circulates around the cavity, and a fraction of it exits the output facet during each cavity

roundtrip. The laser thus emits a train of very short optical pulses, with the distance between adjacent pulses matching the cavity roundtrip time. The duration of each pulse is typically on the order of a few picoseconds (10^{-12}sec) or tens of femtoseconds ($1fs = 10^{-15}$sec). One femtosecond is an extremely short time. To get a sense of how short it is, imagine it as being extended to one second; then one second would extend to about 32 million years!

Why should one care about such short time intervals? The quick answer is that we can do a lot of things with ultra-short pulses. For instance, if we made a single bit of information $1fs$ long, then the speed of the internet would become three to four orders of magnitude faster than it is today. The timescale over which atoms move within a molecule is in the picosecond or femtosecond range, so we can use femtosecond optical pulses to follow (or "see") the movement of atoms and molecules in real time. This is similar to high-speed photography. You may have seen a slow-motion movie of a flying bullet; the key to capturing the motion of the bullet is the use of a strobe-lamp, which emits short bursts of light; so short in fact that the bullet appears stationary within the duration of each burst.

Mode-locked lasers are useful for many other important applications. It has been shown that they can form the basis of extremely precise clocks, with only one second of error in 30 million years. Femtosecond lasers have also found applications in medicine: In the technology known as *Lasik*, vision correction is currently done with femtosecond lasers. The peak power of the laser beam is so high that, when focused onto any material, the electrons are torn apart from the atoms under the influence of the strong optical field. Ablation (i.e., removal of material) thus occurs with minimal thermal effects, enabling high-precision, clean cuts. All of the above interesting applications are made possible with ultra-short optical pulses generated by mode-locked lasers. These lasers have unique properties that no other source of concentrated energy can provide. For example, they generate the highest peak-power among all available lasers; mode-locked lasers produce one of the shortest events in nature, and are one of the best frequency rulers ever made; they also exhibit very low timing-jitter compared with most electronic devices. At the same time, mode-locked lasers do not do any "work" for 99.9999% of the time! This is because each pulse is so much shorter than the interval between adjacent pulses.

In what follows I will focus on my group's areas of research at the *College of Optical Sciences*. Broadly speaking, we do research in the fields of quantum electronics, ultra-fast lasers, nonlinear optics, and optical communication. We are particularly interested in areas involving optical fiber technologies such as fiber lasers, fiber-optical sensors, and nonlinear effects/devices involving waveguiding structures. Our goal is to develop advanced and novel components and instruments that enable new discoveries and enhance education. Our research program has two main directions: laser source development and exploration of new applications enabled by these sources. Research in this area has not only extended our understanding of Nature, but also has improved our lives significantly. Generation of ultra-short pulses via mode-locking has had tremendous impact in several other fields. The rapidly-advancing techniques for producing shorter pulses and higher pulse energies have enabled many breakthroughs in science and technology. Two recent Nobel Prizes (the femto-chemistry award to Ahmed Zewail in 1999, and the frequency metrology award to John Hall and Theodor Hänsch in 2005) were awarded for contributions to this field.

The goal of laser development is to create the next generation of light sources for telecommunications, bio-imaging, and other applications. Recently, fiber lasers have been the subject of intense research and development. In a relatively short period of time the performance of lasers based on fiber technology has surpassed the levels offered by traditional solid-state

lasers. The advantages of fiber format include low cost, passive cooling, alignment-free operation, and minimal maintenance. To get a laser to mode-lock, a saturable absorber (SA) must be inserted into the cavity. The SA is the device responsible for locking the phases of the cavity modes, thus enabling the formation of ultra-short optical pulses. In general, a SA is any device that transmits more light at high intensities than at low intensities. In ultra-fast fiber lasers, typically two types of SA are used: semiconductor saturable absorber mirrors (SESAM), and an artificial SA based on nonlinear polarization evolution (NPE). Nanoscale carbon-based materials have many interesting properties and, it turns out, one of their surprising applications is in ultra-short optical pulse generation. Single-walled carbon nanotubes (CNTs) possess an ultra-fast (less than 1 ps) recovery lifetime, which is a desirable feature for a SA. After a few years of research and development (by us and others), it is now clear that this new SA material has real advantages compared to traditional SESAM and NPE. These advantages include fabrication simplicity, low cost, and feasibility of broadband operation.

There exist several methods of incorporating CNTs into a laser cavity. The simplest way is to deposit a thin film of CNTs on one of the cavity mirrors. This thin film configuration, however, suffers from low damage threshold, which is also a drawback in SESAMs. To solve this problem, we developed a new type of arrangement where the interaction with the CNTs is done through the evanescent field of a thin fiber taper; see Fig.1. This configuration increases the damage threshold of the SA significantly, since the absorption is now distributed along the fiber taper (a few cm in length) instead of being concentrated in a very thin layer (less than 1 μm). Furthermore, the device is now compatible with fiber format and adding the SA into the cavity is as simple as adding a fused fiber-coupler.

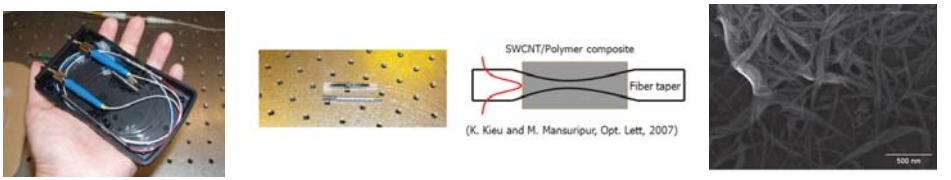

Fig.1. (Left) Photograph of a compact handheld mode-locked fiber laser with a carbon-nanotube saturable absorber. (Middle) Fiber-taper surrounded by a carbon-nanotube saturable absorber; (Right) Scanning electron microscope (SEM) image of carbon nanotube bundles.

We have demonstrated different laser designs featuring both record-breaking performance and new physical insights. Our current effort is focused on creating a universal ultra-fast laser platform suitable for all applications. To achieve this, we developed an extremely compact, mode-locked fiber-laser oscillator operating in the telecommunication window (around 1550 nm) as the starting point. New functionalities of the laser system will then be created by introducing additional components. The laser wavelength can be shifted to different regions of the spectrum using nonlinear optics (e.g., self-phase modulation, Raman scattering, four-wave-mixing). The laser spectral bandwidth and wavelength tunability can be achieved by using appropriate tunable bandpass filters. The strategy is to first create a very short pulse with broad spectral bandwidth. A wide range of pulse durations is then accessible through spectral filtering. Thus, a tunable bandpass filter with adjustable bandwidth is a good candidate to control not only the center wavelength and output spectral bandwidth, but also the pulse duration. Power scaling should be done using well-developed existing fiber amplifiers. (Er-doped amplifiers are suitable for $\lambda\sim1550\ nm$, whereas Yb-doped amplifiers are good for $\lambda\sim1000\ nm$. Future development of

new materials for fiber amplifiers may provide access to other useful operating windows; the Thulium-doped fiber working around $2\mu m$ is a good example.) This approach should allow the construction of extremely complex laser systems for a range of current and new applications.

Figure 2 shows an example of the laser systems we have demonstrated, where pulses as short as $10fs$ were generated. The laser could be put inside a small handheld box as shown. To create the large spectral bandwidth, we used super-continuum generation in a high nonlinear optical fiber (HNLF) pumped by one of our compact femtosecond fiber lasers. The spectrum of the pulses broadened as they propagated along the HNLF due to various nonlinear processes including self-phase modulation, four-wave-mixing, and Raman generation. The starting pulse duration was around $500fs$ but, at the end, we could compress the pulses down to about $10fs$.

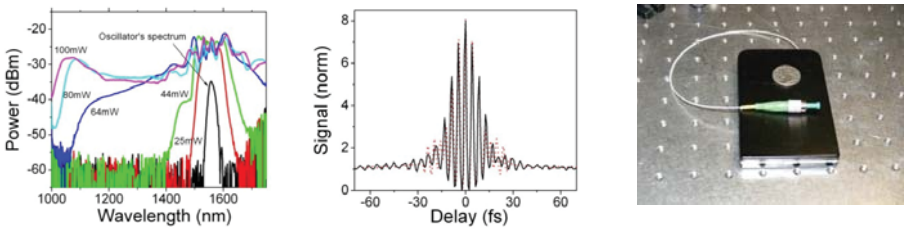

Fig. 2. (Left) Dramatic spectral broadening of a femtosecond laser pulse in a HNLF. (Middle) An autocorrelation trace of the pulses at the output of the HNLF showing about $10fs$ FWHM pulse duration. Note that there are only about three optical cycles underneath the pulse. (Right) The entire laser system is packaged into a handheld box.

There are many applications for femtosecond fiber lasers. Here I will describe our new research effort in multi-photon (MP) imaging—a powerful technique that allows three dimensional mapping of samples that have a measurable nonlinear optical response such as second or third harmonic generation (SHG or THG), or fluorescence induced by MP absorption. This provides us with a way to see the nonlinear microscopic world in 3D with high resolution. After about two decades of intensive development, multi-photon imaging (MPI) has found important applications in biological research and in diagnosing medical conditions. Among the main remaining barriers to making MPI a widespread diagnostic and research tool are the size and cost of the MP microscope—presently only major research institutions can afford to purchase, house, and maintain such an instrument. We seek to address this challenge by developing compact and affordable MPI microscope systems in order to make them available to a greater number of researchers and, ultimately, to hasten their adoption in medical testing. New applications, ideas, and discoveries are certain to emerge from the high throughput and reliability of these unique instruments.

The laser source normally comprises a major fraction of the total cost of a typical MP microscope. So a clear approach to solving the aforementioned problems is to create new, robust and low-cost ultrafast laser sources suitable for MPI. Ultrafast lasers based on Ti:sapphire (Ti:sa) crystals which played an important role in the early stages of MPI development continue to be the work-horse of the field due to their versatility and good performance. However, there is a consensus in the research and applications communities that these lasers are not currently suitable for applications outside of the research laboratory environment. In contrast, fiber lasers are quite attractive owing to their compactness, freedom from alignment issues, and potentially much lower cost. Recently, there has been a strong push to develop low-cost fiber lasers for MPI.

Promising results have been published, but it is not yet clear if fiber lasers will be able to fully replace the standard Ti:sa laser for this application. In recent months, we have demonstrated label-free MPI of biological samples using a compact Er^{3+}-doped femtosecond fiber laser mode-locked by single-walled carbon nanotubes (CNTs). These compact and low-cost lasers have been developed by various groups, but they have not been exploited for MP microscopy. As will be seen below, various MPI modalities such as SHG, THG, and two- and three-photon excitation fluorescence (TPEF and 3PEF), can be effectively performed on various biological samples using a compact handheld CNT mode-locked femtosecond fiber laser operating in the telecommunication window near $1560\ nm$.

The schematic diagram of our MP microscope is shown in Fig. 3 (left). The excitation laser is an all-fiber femtosecond laser based on Er^{3+}-doped gain fiber. The laser oscillator is amplified using a core-pumped Er^{3+}-doped amplifier to about $60\ mW$ average output power (limited by the available $980\ nm$ pump power). The laser system is designed so that the pulses coming out of the end-face of the output fiber achieve nearly their shortest duration just before entering the microscope. This system has been built with all-fiber components, avoiding the need for difficult free-space alignment. As a result, the entire system including pump laser and electronics can be packaged in a handheld box with dimensions of only $20 \times 12 \times 5\ cm^3$; see Fig. 3 (right).

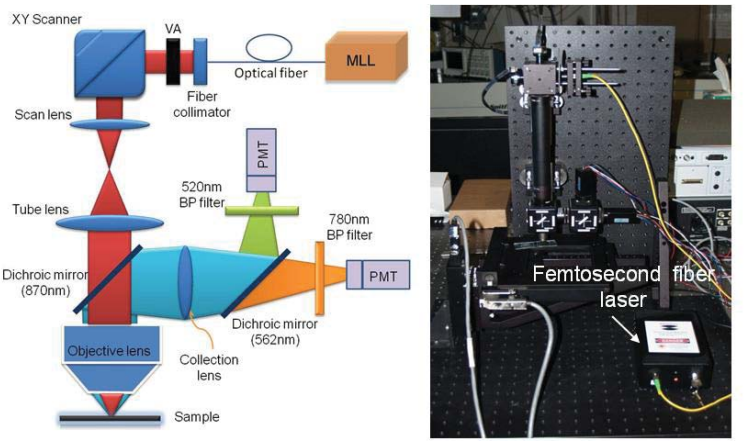

Fig. 3. (Left) Schematic diagram of the multi-photon microscope; MLL: mode-locked fiber laser with carbon nanotube saturable absorber; VA: variable attenuator. (Right) Photograph of the actual microscope, the handheld femtosecond fiber laser is indicated.

The laser output is collimated using a fiber collimator (Thorlabs, F280APC-1550), and the collimated beam is scanned in the *xy*-plane with a 2D galvo-scanner (Thorlabs, GVSM002). The beam is then relayed and expanded using a telescopic system formed by two achromatic doublets. The dimensions of the system are set such that the first galvo-mirror is imaged onto the back aperture of the focusing objective to avoid signal variation during scanning. The objective lens used for imaging is a $0.5NA$ aspheric lens, which is anti-reflection coated for $1550\ nm$ wavelength (New Focus, 5723-H-C). The lateral and axial resolution achievable with the aspheric lens for THG imaging was measured at $\sim 1.1\ \mu m$ and $7.3\ \mu m$, respectively, using a nano-waveguide silicon chip as the sample. The lateral resolution is better than the diffraction-

limited spot size ($\sim 1.8\ \mu m$) due to the nonlinear response nature of the THG signal. We use the non-de-scanned detection scheme to detect the generated nonlinear signals. The excitation laser and the generated signals are separated using a dichroic filter with its cutoff wavelength at $\sim 870\ nm$ (Semrock). A second dichroic filter with cutoff at $562\ nm$ is used to split the signal into two channels for simultaneous recording. Two identical photomultiplier tubes (PMTs) (Hamamatsu, H10721-20) are used in the two channels for detection. The short-wavelength channel is used for THG imaging, where a band-pass filter at $520\ nm$ ($20\ nm$ pass-band, Semrock) is used before the PMT. The second channel can be used for 3PEF, TPEF or SHG imaging (depending on the band-pass filter used in front of the PMT). The signals from the PMTs are amplified using low-noise current amplifiers (Stanford system, SR570) before being digitized with a PCI data acquisition card (NI, PCI-6115).

Figure 4 shows an example of MPI of a fresh leaf from an indoor plant. Without any special contrast agents, we were able to detect strong THG signal from lipid cell layers within the leaf. Interestingly, we also detected 3PEF emission in the $650 - 750\ nm$ range (Fig. 4), which we attribute to chlorophyll species, since these molecules are known to have strong fluorescence emission in this spectral range. To explore further, we also recorded an image of a small fresh mesquite leaf (mesquite is a desert plant native to Arizona). The leaf was small enough that we could record the image of the entire structure using the tiling technique (Fig. 4, right). It is apparent that the lipid cell layers (which generate the THG signal) in the mesquite leaf are fewer in number than those in the indoor plant. Our approach may provide a new tool for the study of photosynthesis, where the 3D distribution of chlorophyll can be obtained with high resolution.

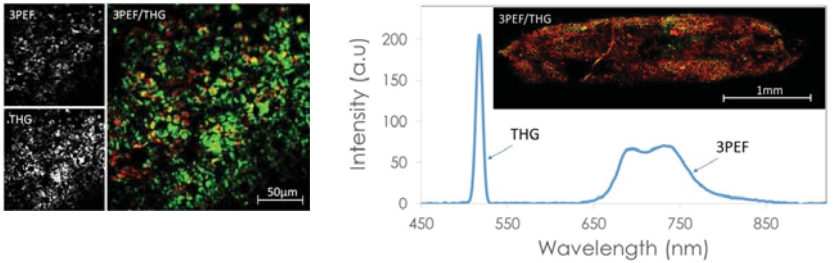

Fig. 4. (Left) Multi-photon image of a fresh leaf from an indoor plant. We observed a strong THG signal (green) from lipid cell layers and a 3PEF signal (red) from chlorophyll. (Right) Optical spectrum of the generated light due to the femtosecond laser excitation. Inset: Multi-photon image of a whole mesquite leaf. The image was composed by tiling 56 frames; the frame rate was ~3s/frame.

As with the fresh leaves, a strong THG signal was also produced by lipid cell layers inside the chloroplasts and 3PEF was emitted from chlorophyll of living centric diatoms *Coscinodiscus wailesii* (Fig. 5, left); this is probably the first time that living diatoms have been imaged with an MP microscope. Furthermore, strong MP signals were also observed for the non-centric diatoms *Pyrocystis fusiformis* (Fig. 5, right). We mapped out the spatial distribution of the chloroplasts inside the diatoms with $\sim 1\ \mu m$ resolution; the resolution can be pushed to $\sim 0.5 \mu m$ using a higher-NA lens. This may allow us to explore the efficient photosynthesis machinery of diatoms, which are little understood. Interestingly, we can image living organisms in an underwater environment ($\sim 200\ \mu m$ from the water surface) using a $1560\ nm$ femtosecond laser, even though this laser wavelength has been avoided in the past due to water absorption concerns. In

addition, we were able to image the centric diatoms continuously for days without damaging them with the laser radiation; clearly, our exploitation of telecommunications wavelengths and lasers shows that this region is an untapped landscape for MP microscopy.

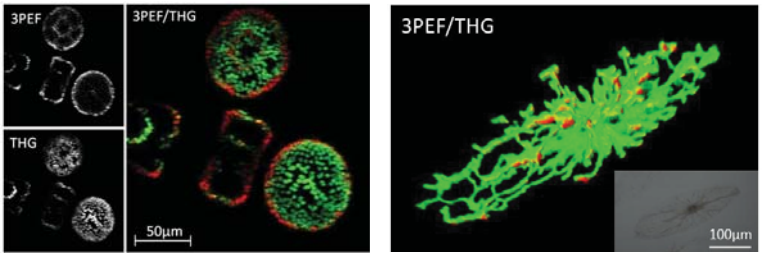

Fig. 5. (Left) Multi-photon image of living centric diatoms *Coscinodiscus wailesii*. As with the fresh leaf, we observed strong THG signal (green) from lipid cell layers inside the chloroplasts and 3PEF signal (red) from chlorophyll. (Right) 3D view of a 3PEF and THG image of a living non-centric diatom *Pyrocystis fusiformis*. Inset: Optical image of the non-centric *Pyrocystis fusiformis* diatom.

To explore further, we imaged different fixed biological samples such as mosquitos, drosophila, mouse organs, etc. It turns out that most samples we examined had strong SHG and THG response, which can be used to perform label-free MPI. Figure 6 shows representative images of a thin section of a mouse kidney and heart tissue. Most cell membranes generated the THG signal, whereas connective tissues and blood vessels with fibrosis provided the SHG signal.

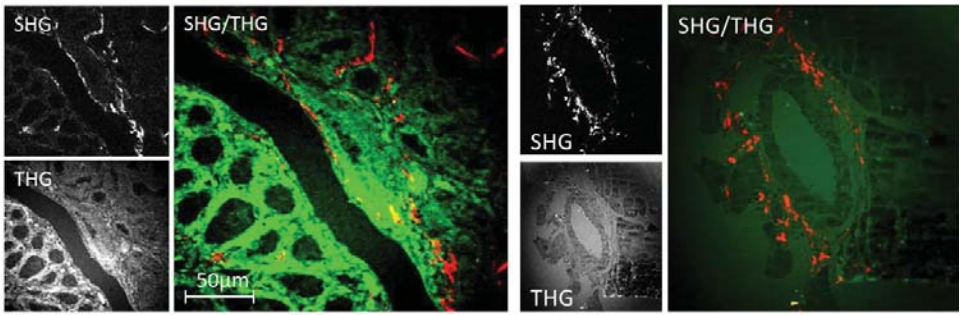

Fig. 6. SHG (red) and THG (green) image of a thin section of a mouse kidney and a thin section of a mouse heart with fibrosis.

Three-dimensional brain imaging is another of our active research areas. Interactions between neurons in anatomically-distant regions of the brain are at the core of the capacity to learn and act. Yet our ability to understand these brain-wide networks has been severely limited because we cannot rapidly image the whole brain with single-cell resolution. MPI using compact femtosecond fiber lasers may be the right tool to unlock many secrets of the brain. Figure 7 shows an example of a cross-section of a full mouse brain imaged with our MP microscope. The femtosecond laser used here is based on Yb-doped fiber operating at $1030\ nm$. The high peak-power of the pulses enables excitation of the yellow fluorescence proteins (YFP) which some neurons produce as the result of gene modification.

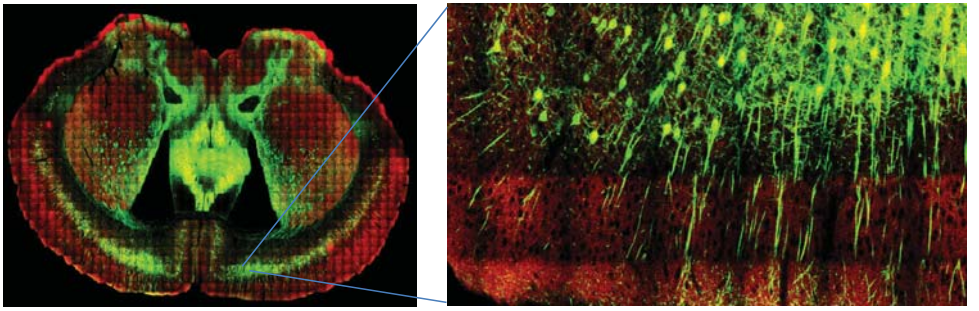

Fig.7. Multi-photon image of a mouse brain. The green channel is from YFP and the red channel is from some intrinsic fluorescent proteins that the brain produces. The laser excitation wavelength is around 1030 nm and the laser pulse duration is ~$100fs$. Peak power at the sample is a few kWs.

In summary, compact femtosecond fiber lasers are interesting tools in modern science and technology. The development of a compact, easy-to-use, and low-cost ultrafast fiber laser platform suitable for MPI and other important applications will give more researchers access to this useful instrument. This, in turn, may trigger new scientific discoveries that widen our understanding of biological processes behind major diseases such as fibrosis and cancer.

Dr. Khanh Kieu is an Assistant Professor at the *College of Optical Sciences*. He received his B.S. in Applied Physics (2002) and M.S. in Laser Technologies (2004) from the St. Petersburg State University of Information Technologies, Mechanics, and Optics (Russia). His research was focused on laser material processing and laser-matter interactions. He received his Ph.D. in Optical Sciences from the University of Arizona in 2007, where he developed novel devices for fiber-laser applications. Dr. Kieu joined Prof. Frank Wise's group at Cornell University in 2007 to conduct research in ultrafast fiber lasers. He returned to the *College of Optical Sciences* in 2009 as a Research Assistant Professor, and was promoted to the rank of Assistant Professor in 2012. Dr. Kieu is also the founder and president of *Kphotonics, LLC*, a Tucson-based supplier of fiber lasers and accessories.

Kphotonics, LLC

Khanh Kieu

Kphotonics is a spin-off company from the *College of Optical Sciences*. *"K"* in the company's name stands for kitchen, since we started the company out of our kitchen, where we could mix carbon nanotubes with a polymer matrix in the sink. (We have recently moved to a garage and added a new room.) *Kphotonics* develops experimental kits for educational purposes in the area of ultrafast laser physics and applications. We also provide affordable ultrafast lasers for research laboratories and for the industry. Our company's key technology is based on a fiber-format saturable absorber (SA), which I developed at the *College of Optical Sciences* as part of my Ph.D. dissertation during the period 2006-2007. This SA allows us to construct compact and low-cost femtosecond fiber lasers, which can be used in many important applications. *Kphotonics* was founded in 2010 with two people on board: my wife and myself. We have now delivered our lasers to four different continents (America, Europe, Australia, and Asia). Perhaps more importantly, our femtosecond lasers are being used for teaching and research purposes in many universities including Caltech, Harvard, MIT, and of course, The University of Arizona. Our goal is to make these laser sources available to every classroom where there is a need.

Kphotonics compact femtosecond fiber lasers

Our main line of laser products includes an educational femtosecond fiber laser kit (which is the first of its kind in the market), a battery-powered femtosecond fiber laser oscillator, also the first in the market, which runs on a small $9V$ battery, and an amplified laser system, which provides about $100fs$ pulse duration at about $10kW$ peak power directly from a handheld box. We are particularly proud of our educational laser kit, which allows students to learn the fundamental principles of laser physics as well as its scientific and technological applications. Our lasers have been based on Er-doped fiber technology working around $\lambda = 1.55\ \mu m$, but there are new products currently being developed for $1\ \mu m$ and $2\ \mu m$ wavelength region.

We are in the first phase of our company's development, where we create new laser systems and test their robustness and long-term reliability through our expanding customer base. Our plan is to expand the company significantly in the next phase in order to serve the growing need from the industry, academia, and research institutions. We see a bright future where our lasers will work in classrooms, research laboratories, hospitals, and manufacturing facilities around the globe, enabling new discoveries and new technologies, and, in some instances, even saving lives.

The mountains surrounding Tucson offer numerous areas and parks for year-round hiking, biking, wildlife viewing, and other outdoor activities. *Sabino Canyon Recreation Area*, at the foot of the Santa Catalina mountain range in the northeast portion of the Tucson basin, is one of these special areas. The canyon holds a lush riparian area, a perfect spot for enjoying the outdoors during hot weather. From the parking lot and visitor center, multiple trails lead off into the wilderness, up ridges, into canyons, past waterfalls, and towards stunning vistas.

Photo Courtesy of Brian Anderson

Optical Filamentation

Miroslav Kolesik, Jerome V. Moloney, and Ewan M. Wright

The goal of this article is to provide the reader with a physical understanding of the nonlinear phenomenon of optical filamentation in which a high power laser beam propagating in a bulk medium, such as air or glass, can resist spreading and produce a spatially localized optical filament that persists over long distances. This is counter to the familiar notion that waves must spread as they propagate, an everyday example being the spreading of the cylindrical water wave excited by dropping a stone in a pond.

We start our explanatory journey by first considering light propagation in linear media whose optical properties are independent of the incident field strength, the optical properties consisting of the absorption and refractive index of the media evaluated at the incident light frequency. More specifically we consider transparent dielectric media for which absorption may be safely neglected over the lengths scales of interest. For example, on most days in Tucson one can see the Catalina Mountains at ten miles distance from the College of Optics, so that air is a transparent dielectric medium to a good degree in the visible. Transparent dielectric media are therefore characterized by their refractive index, the speed of light in the media being given by the speed of light in vacuum divided by the refractive index. Likewise the wavelength of light in a medium is reduced by the refractive index with respect to the value in vacuum. Denser dielectric media tend to have higher refractive indices, so that, for example, light travels faster in air than in glass.

To proceed we consider how light propagation is modified at the planar interface between two media. We shall use air and glass as examples of gaseous and condensed media with lower and higher refractive indices, respectively. Figure 1 shows an interface between air and glass (shaded region), the vertical line showing the normal to the interface. A train of planar wavefronts spaced by the wavelength in air is shown impinging onto the air-glass interface at an angle θ with respect to the normal. The leftmost portion of the wavefront train enters the glass first and suffers a reduction in wavelength, with concomitant reduction in the spacing between the wavefronts, and this causes the wavefront train in the glass to travel at an angle $\varphi<\theta$ bent towards the normal, see Figure 1. This provides an intuitive physical picture of how light is refracted at a dielectric interface as described mathematically by Snell's law of refraction. But there is a second case involving light incident from glass onto a glass-air interface. By adapting the previous argumentation to this case, and for small incident angles θ, light incident from glass and refracted at the glass-air interface will be bent away from the normal and towards the plane of the interface. However, for a critical value of the incident angle θ_{cr} the refracted wave propagates along the interface, and for incident angles greater than the critical value the incident wave is totally reflected and no field propagates into the air from the glass. This is the phenomenon of total internal reflection (TIR) and the transition from partial transmission into air to total reflection as the incident angle is varied is illustrated in Figure 2.

Total internal reflection is the basis for fiber optics as illustrated in Figure 3. The fiber basically consists of a silica glass core (shaded region) surrounded by a cladding medium of lower refractive index. Then TIR at the fiber surfaces can confine light to the fiber core for incident angles such that the light grazes the core-cladding interfaces beyond the critical angle. The ability of optical fibers to guide light in the core region via TIR means that light incident onto a fiber end can be guided over very large distances without spreading, and this underlies the use of optical fibers for trans-Atlantic communications using pulses as bits of information. We

note that the light guiding properties of optical fibers is reminiscent of the non-spreading property of optical filamentation that we wish to explain. The distinction is that optical fibers require a layered structure involving media of different linear refractive index (see Figure 3), whereas optical filamentation occurs in a bulk medium whose linear refractive index does not vary throughout space.

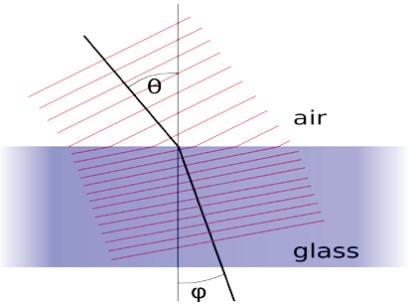

Figure 1. Illustration of Snell's law of refraction for a plane-wave incident on an air-glass interface. Rays are bent towards the normal.

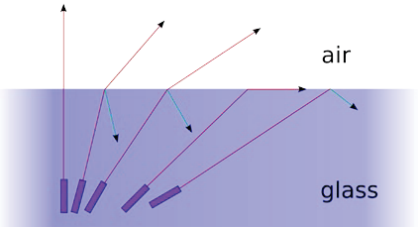

Figure 2. Illustration of TIR for a plane-wave incident from glass onto air. The red lines indicate refraction of the incident wave, the green lines the reflected waves. Above the critical angle the wave is totally reflected.

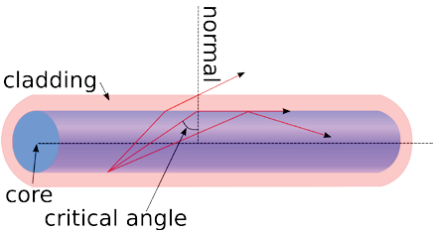

Figure 3. Illustration of TIR as the basis for guiding in optical fibers. Rays that are incident at an angle shallower than the critical angle can be guided by the fiber.

Key to understanding optical filamentation is that it is a nonlinear optical phenomenon in which the optical properties of a medium become dependent on the strength of the incident laser field. For transparent dielectric media there are two dominant sources of this optical nonlinearity, namely the nonlinear optical Kerr effect, or simply Kerr effect, and plasma defocusing. The Kerr

effect describes the fact that the refractive-index of a transparent dielectric medium is actually the linear value plus a small *positive* contribution proportional to the intensity of the incident field, this being named after the 19th century Scottish physicist John Kerr who looked at the modification of the refractive-index due to applied static electric fields. (The nonlinear optical Kerr effect is also referred to as a self-focusing nonlinearity for reasons to be discussed later.) The intensity of a light field provides a measure of the power per unit area carried by the field (units of Watts per meter squared or W/m^2) and is proportional to the square of the electric field strength (units of volts per meter or V/m). As a rule of thumb nonlinear optics comes into play for incident electric field strengths that approach the Coulomb fields that bind electrons to their nuclei in the constituent atoms, which are on the order of 10^{11} V/m or 10^{19} W/m^2 expressed as an intensity. In transparent dielectric media essentially all of the electrons are bound to their parent nuclei in the absence of any applied fields. For field strengths well below the Coulomb binding field the Kerr effect is the dominant optical nonlinearity. However, the electric field strengths in optical filaments can approach the Coulomb binding field so that some of the constituent atoms are ionized leading to a weak plasma, a strong plasma being a state of matter in which all of the electrons are separated from their parent nuclei. In general as the applied electric field strength approaches the Coulomb binding field a larger fraction of atoms will be ionized, and the density of the generated plasma will increase. This weak plasma gives rise to a second source of optical nonlinearity that yields a small *negative* contribution to the medium refractive index that is proportional to the density of the generated plasma, the plasma density being the number of electrons per unit volume. This negative contribution to the refractive index is termed plasma defocusing. To summarize, for field strengths well below the Coulomb binding field the Kerr effect is the dominant optical nonlinearity and causes an *increase* in refractive index proportional to the field intensity. However, for applied electric fields that approach and become larger than the Coulomb binding field plasma defocusing causes a *reduction* in the refractive index proportional to the generated plasma density. Plasma defocusing therefore limits the maximum nonlinear refractive-index change that can be induced in the medium.

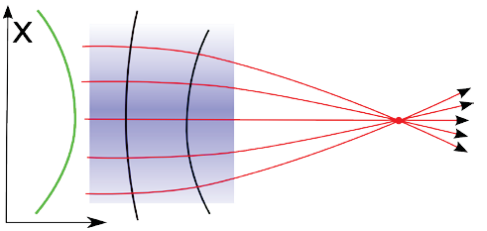

Figure 4. Illustration of Kerr lensing, or external self-focusing, of a bell shaped beam, shown on the left in green, incident on a thin nonlinear medium. The Kerr lensing effect causes incident rays, shown in red, to focus in the region past the medium.

At first sight the nonlinear change in refractive index due to the Kerr effect seems rather benign particularly since the induced change is small compared to the linear refractive index. To appreciate why the Kerr effect can have a profound effect upon laser beam propagation we consider propagation of a bell-shaped laser beam through a thin slab of the nonlinear medium as shown in Figure 4. The key is that the laser beam has its peak intensity at the beam center that falls off towards the wings, and this induces a refractive-index profile in the medium due to the Kerr effect that is peaked in the center and also falls off towards the wings. This in turn means

that the speed of light will be smaller at the center of the beam compared to the wings. The net effect of this is that if the laser field has a planar wavefront to the left of the medium it will develop a concave curvature to the right of the medium. This nonlinearly induced curvature is akin to the action of a thin focusing lens and is termed Kerr lensing. For sufficiently high peak input intensity the Kerr lensing can cause the laser beam to focus as it propagates into the free-space region past the medium, and this is called external self-focusing, whereas for low intensities the laser beam will spread as expected on the basis of linear optics.

We can extend the above idea of Kerr lensing to intuit what happens during propagation in an extended nonlinear medium by considering it as a sequence of thin slabs. Then for an input laser beam of sufficiently high peak input intensity a Kerr lens is induced in the first slab that will cause the beam to contract slightly in width thereby slightly increasing the peak intensity. This contracted field will act as the input to the second slab, and since the peak intensity is increased a slightly stronger Kerr lens will be induced in the second slab leading to even more contraction of the beam width and further increase in the peak intensity. One can continue this argument to more slabs to see that the laser beam can continue to contract and increase its peak intensity under propagation in the medium, a phenomenon called nonlinear self-focusing. Whether or not a bell-shaped laser beam will be subject to self-focusing can be assessed based on the critical power for self-focusing (units of Watts) for the medium of interest. As a guide the critical power is around Gigawatts in air and Megawatts in glass. Then if the laser beam power is less than the critical power the laser beam may experience some initial Kerr lensing but it will ultimately spread as it propagates in the medium. In contrast, for input powers larger than the critical power the laser beam will continue to self-focus as it propagates and can in principle collapse to a point or singularity in a finite medium length! This process, which is analogous to the collapse of stars to form black holes, is called self-focusing collapse and is a spectacular consequence of the Kerr effect. Given that beam expansion follows for input powers less than the critical power and beam contraction results for input powers larger than the critical power, it is a reasonable to posit that the beam will propagate with unchanging beam width for an input power equal to the critical power. The situation with the input power equal to the critical power is called nonlinear self-trapping or self-guiding and clearly bears a resemblance to light propagation in a fiber where beam spreading is negated. The key is that for self-trapping the light field induces its own fiber structure via the nonlinearly induced refractive-index profile that results from the Kerr effect, that is, the bell shaped laser beam can induce a nonlinear refractive-index profile that self-consistently guides it.

We are now in a position to elucidate some of the properties of optical filamentation. It is a high power nonlinear phenomenon that has its origin in the self-focusing and self-trapping properties associated with the Kerr effect. There is one more key ingredient, however, since self-trapping in a medium with just the Kerr effect is unstable. This follows since if the power is just less than the critical power the beam will ultimately expand, whereas if it is just greater it will collapse. Optical filamentation requires an input power a bit bigger than the critical power and what stabilizes the propagation is that as the collapse advances the field strength approaches the Coulomb field strength that generates a plasma and concomitant negative contribution to the refractive-index change. Recalling that plasma generation limits the maximum possible change in refractive index, plasma defocusing subsequently softens and tames the self-focusing collapse and allows for a stable self-trapped filament. The precise dynamics of the optical filamentation process depends on the temporal duration of the input pulse. For longer pulses, say nanoseconds or longer, a strong plasma is produced by the collapse which absorbs the field energy, thereby

terminating the propagation, and this can produce significant collateral damage in crystals, termed optical damage, as the generated electrons recombine with their parent nuclei and deposit their energy to the crystalline lattice. In contrast a pulse of a picosecond or less duration has a sufficiently low energy that only a weak plasma is generated and optical filamentation can arise.

Summarizing, we see that optical filamentation arises for sub-picosecond pulses with peak powers a few times the critical power, and results from the fact that the input pulse can create its own nonlinearly induced optical fiber, and this in turn allows the optical filament to propagate over large distances without significant spreading. In practice limits to the filament length come from a number of sources including linear absorption and medium scattering, energy loss due to the generation of the weak plasma, and medium dispersion that causes the input pulse to spread temporally. We remark that the simulation of optical filamentation poses a formidable theoretical and computational task that our group has spearheaded for two decades. In particular, a comprehensive computational model requires microscopic models of the detailed nonlinear light-matter interactions, high-resolution macroscopic field propagation algorithms that can capture the space-time dynamics of the optical filamentation process, and the computational capability and resources to dovetail the microscopic and macroscopic aspects of the problem. This problem remains at the forefront of computational nonlinear optics.

Figure 5. Laboratory experiment showing the ability of an optical filament to guide an electrical discharge in air. The optical filament is present in the example of the right and is seen to straighten the electrical discharge.

Optical filamentation has now been observed in a variety of media for wavelengths spanning the infrared to ultraviolet, and pulse durations ranging from picoseconds to femtoseconds. Much interest has focused on atomic and molecular gases with air being of particular interest due to applications involving atmospheric propagation. Indeed experiments using femtosecond pulses in air have demonstrated that optical filaments can persist for tens of meters to kilometers. The ability to deliver an intense focused laser beam to a remote target at kilometers range is of great interest for remote sensing applications in which backscattered light from the target illuminated by the filament is used to obtain information about the target. Current proposals include measuring ozone in the atmosphere, pollution monitoring, and remote detection of biological and chemical agents. In this respect the fact that optical filaments use femtosecond pulses means that they are spectrally broad which makes them ideal for spectroscopic identification of the target. Another application is lightning diversion in which the weak plasma left in the wake of an optical filament propagating in the atmosphere is used as a modern day version of Benjamin Franklin's kite. In particular, the hope is that being electrically charged the filament-induced plasmas can be used to divert lightning strikes to locations away from sensitive areas such as power stations. A laboratory experiment showing the guiding ability of a filament is given in Figure 5 that shows an electrical discharge without (left) and with (right) the filament present.

Optical filamentation has also been explored in condensed media such as glasses and water. In this case the filaments are typically millimeters to centimeters in length but still significant. In particular, in glasses the high field strengths in the filaments can cause structural and photo-chemical changes in the glass matrix, which modifies the refractive index in the vicinity of the filament that survives after the filament is turned off. This has provided a new way to write very clean waveguiding structures into glass media without the need for fabrication and has great potential.

In summary, we hope to have conveyed the underlying physics of optical filamentation to the reader along with an appreciation of the wide range of theoretical, experimental, and applied challenges it presents. Forefront research on optical filamentation has been underway for around 20 years with no signs of slowing down as new ideas emerge. For example, it has recently been realized that the high intensities in optical filaments can create conditions approaching astro-physical conditions. This has lead to an exploration of nonlinear optical analogs for black hole physics and Hawking radiation in optical filaments that are normally considered the domain of quantum cosmology. Such developments keep optical filamentation vibrant and at the forefront of contemporary optical physics research.

Miroslav Kolesik received his MS and PhD in Physics from the Charles University in Prague, and the Slovak Academy of Sciences, respectively. He is an Associate Professor at the College of Optical Sciences of the University of Arizona. Professor Kolesik's research interests are in the general area of computational physics, and span statistical mechanics, Monte Carlo simulations, critical phenomena, non-equilibrium and driven systems, semiconductor laser simulation, and nonlinear optics. His current research concentrates on computational optics, and especially on modeling of light-matter interactions in extremely nonlinear regimes.

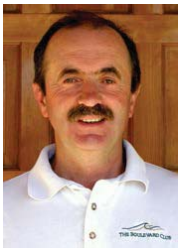

The Theoretical-Computational Optical Physics and Applied Mathematics Group of Prof. Jerome Moloney is focused on the study of ultra-short laser pulse interaction with gases and condensed media under extreme conditions. Extreme intensities acting over tens to hundreds of femto-seconds (10^{-15} s) strip and accelerate electrons from the nucleus creating anisotropic distributions of electrons and ions that eventually equilibrate to form a plasma channel. This channel acts like an extended conducting wire and can direct high-voltage charges and potentially lightning strikes. Accompanying this explosive event is the creation of a white light super-continuum source that can be used to do remote spectroscopy and detect atmospheric molecules and pollutants at multi-kilometer ranges. In another activity, the group is engaged in designing new classes of high power ultra-short pulsed semiconductor disk lasers using first-principles quantum many-body theory, processing these into laser devices and demonstrating them in the laboratory.

Prof. Ewan Wright conducts theoretical research across a broad range of areas including nonlinear optics, the physics of ultra-cold gases, and exploration of novel laser beams. Key theoretical contributions include elucidation of the physics underlying light string propagation in media such as air, early treatment of the field of nonlinear atom optics, and optical binding of nano-particles.

Beyond Tucson, southern Arizona contains numerous other mountain ranges, each with its own character, trails, and unique scenic areas. The Cochese Stronghold area, shown here, is in the Dragoon Mountains, about an hour's drive east of Tucson. A hiking trail provides easy access to this beautiful area with fantastic rock formations.

Photo courtesy of Brian Anderson

Image Science

Matthew A. Kupinski

In science and medicine, images are routinely analyzed, either visually or computationally, to yield experimental results. For example, radiologists inspect images looking for signs of abnormality and disease. In addition, scientists routinely extract information from images to help draw their conclusions. Thus, considerable research effort is being spent to produce better imaging systems and image-analysis tools. Of fundamental importance to this research is the definition of image quality.

In consumer electronics, the quality of imaging systems is determined by, for example, resolution, number of pixels, contrast, brightness, and detector size. These metrics, while quantitative, are not suitable for medical and scientific imaging since they do relate to how well the desired information about the scene can be extracted from the imaging measurements. In addition, a subjective claim is often made that, for example, the images produced from imaging system A are better than those of system B. The images and the subjective statements about the images become the results of the study, ignoring the fact that modern imaging science is quantitative and objective.

Scientific images are obtained so that specific tasks can be performed. These tasks include signal detection, parameter estimation, and combinations of the two. Observers, either human or computer, perform these tasks. Thus, there is a tight connection between imaging, tasks and observer performance. A consensus of opinion has been forming around the idea that image quality should be assessed using observer performance as the metric instead of subjective measures or quantitative measures that ignore the reason the images were acquired—the task. Through the use of objective, task-based measures of image quality, statements about the merits of imaging systems and image-analysis methods can be backed up by quantitative metrics instead of pictures and subjective claims.

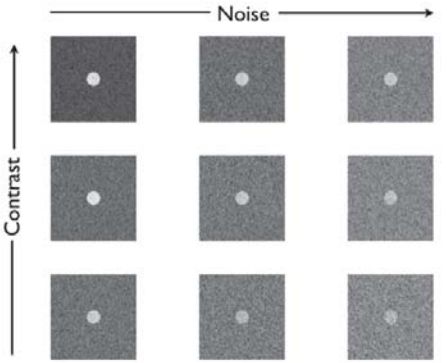

Fig. 1. The task is to detect signals in a noisy background. It appears that the signal is easier to detect when the contrast is high and the noise level is low.

To illustrate the need for objective measures of image quality, we consider the example of imaging to detect the presence of a circular signal in a uniform, noisy background. This example is extremely simple and stylized, but drives home the point that conventional metrics are not suitable for quantitative imaging. In Figure 1 we see a signal of varying contrasts (across rows)

embedded in noise of varying strength (across columns). This figure indicates that the signal is easiest to detect when the contrast is high and the noise level is low. On the surface, a contrast-to-noise ratio (CNR) seems like a reasonable figure of merit. While CNR is a quantitative metric, it does not measure observer performance. This point is illustrated in Figure 2a, in which signals of equal contrast are embedded in the same noisy background (first row); however, the size of the signal varies (shown in second row). Clearly, our ability to detect this signal depends on much more than just a measure of contrast and noise. This is further illustrated in Figure 2b, in which the equal-contrast signals are embedded into noisy images with different pixel sizes. The signal is visually easier to see with smaller pixels than it is with larger pixels. The goal is thus to assess image quality based on how well, for example, signals can be detected, and not rely on surrogates such as contrast, noise level, resolution, etc.

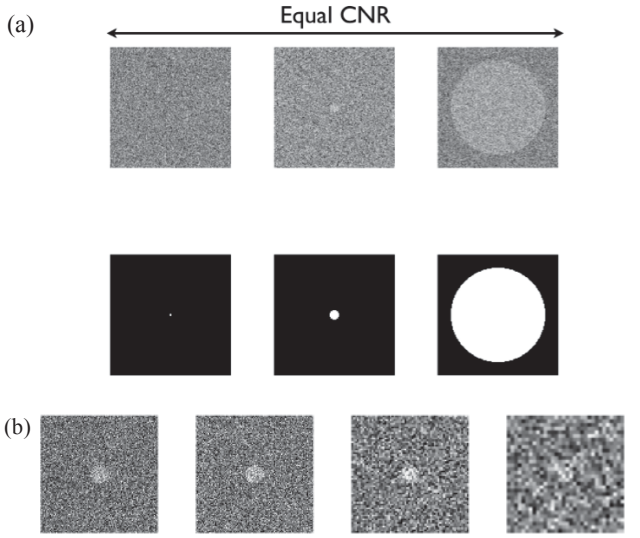

Fig. 2. Our ability to detect signals depends on much more than just signal contrast and noise. In (a) we see that signal size plays a role in detectability and in (b) we see that pixel size also plays a role.

The ability of an observer to perform a relevant task is limited by the noise sources in the imaging chain and by the normal "background" present in most images. Not only are image quality and observer performance tied together, but image quality is an inherently statistical concept. The statistics and physics governing the image formation and the statistics characterizing the object being imaged all contribute to the ability, or inability, of an observer to perform tasks and, hence, image quality. In addition, when humans or human models are used as observers, the characteristics of the human visual system must be taken into account.

The Image Science Laboratory in the *College of Optical Sciences* works to design novel imaging systems and image-analysis methods that incorporate task-based information as the end figure of merit. We have worked on diverse imaging problems including nuclear-medicine imaging [1, 2], homeland security, computed tomography [3], optical coherence tomography [4], and fluorescence-enhanced optical imaging [5]. To illustrate the methodologies discussed above, consider our work in diffuse-optical imaging [6-9].

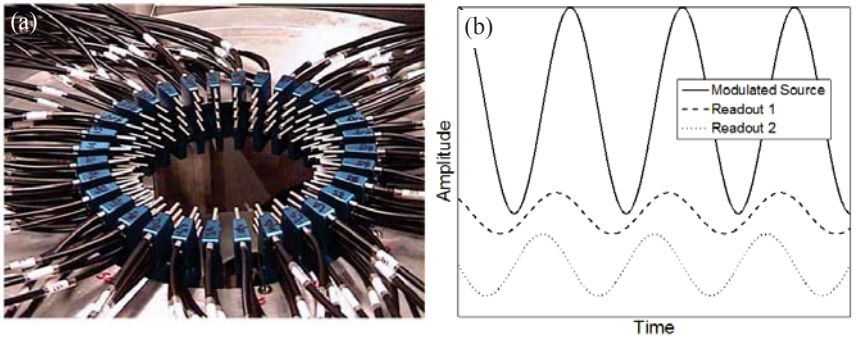

Fig.3. (a) An example of a DOT imaging system. This system developed by the University of Florida is used as a breast imager. Each fiber probe can act as a source and/or a readout fiber [11]. (b) A schematic of frequency-domain imaging in which the source is modulated and modulated signals are read out. The amplitude, level, and phase of the readout signal provide information regarding the absorption and scattering properties of the probed tissue.

In diffuse optical imaging, optical properties of tissue are derived based on measurements of near-infrared light on the surface of the object. In a typical setup, various fiber optics are attached to the tissue to both administer the near-infrared light into the tissue and to read out the light on the surface of the object (see Figure 3a). By taking many measurements using each fiber as the source, one can estimate the absorption and scattering properties of the tissue in three dimensions. Near-infrared light is chosen because the absorption properties of tissue are typically low for this wavelength; however, the scattering properties are very high. Thus, each readout fiber measures a weak, diffuse signal. Diffuse optical imaging has received a lot of attention because it has the potential to provide functional images using non-ionizing radiation [10]. In other words, the absorption and scattering properties of tissue have been shown to be extremely useful for patient diagnosis and, especially, for early cancer detection.

Frequency domain techniques are common in diffuse optical imaging in which the source intensity is modulated at a known frequency and each readout fiber measures a modulated signal (see Figure 3b). The amplitudes, levels, and phases of the readout signals provide information regarding the absorption and scattering properties of the tissue. When building frequency-domain diffuse optical imaging systems, one of the primary design choices to make is the modulation frequency. It has typically been thought that the higher the modulation frequency, the better the system performance. Unfortunately, operating at high frequencies (>500 MHz) substantially raises the cost of the equipment and makes the measurement process difficult. This line of reasoning regarding the modulation frequency is derived based on considering the contrast-to-noise of the phase measurement alone. In Figure 4a we see that when the CNR of the phase is considered, the "optimal" frequency can reach 650 MHz depending on the type of signal to be detected. (For a complete description of this figure, please see reference [7].)

We took a slightly different approach to system design. Instead of looking only at the phase signal, we used all the measurements (i.e., the amplitude, phase, and level) and employed an observer model to compute the ability of the observer to detect weak, cancerous signals embedded in the tissue. The observer model we chose to use is called the Bayesian ideal observer; this observer makes optimal use of all the information to detect signals. Typically, this observer model is impossible to compute but for tasks where the signal location and optical

properties are fixed, we can approximate this observer model to high accuracy. The results of our analysis are shown in Figure 4b where observer performance has been converted into a quantity that can be directly compared to CNR. Our results indicate that not only is our performance far greater than what is observed using phase alone, but the optimal modulation frequency remains below 400 MHz for even the most extreme situations. Thus, we have shown that we can achieve better performance, as measured by our ability to detect weak, cancerous signals, at lower modulation frequency.

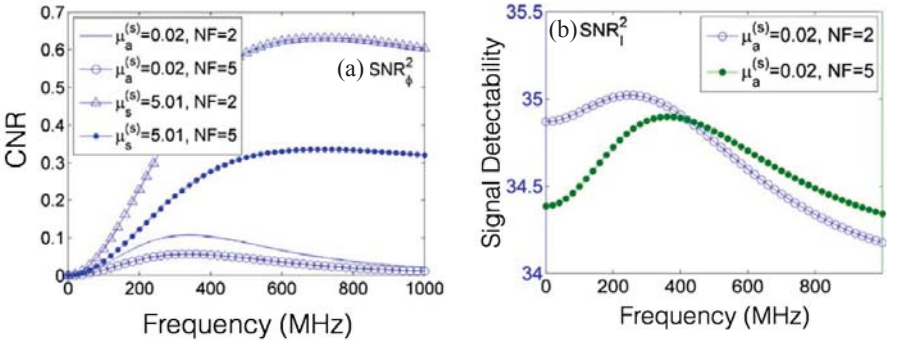

Fig. 4. (a) The contrast-to-noise ratio of the phase signal alone. When considering only phase, the optimal modulation frequency approaches 1 GHz. (b) The signal detectability using all measurements (i.e., phase, amplitude, and level). Not only does performance greatly improve, the optimal modulation frequency drops to around 200 MHz, which dramatically reduces the equipment cost and eases the measurement process. The signal detectability has been converted into a number that can be compared to CNR.

Our overall goal is to design imaging systems that enable better quantitation of scientific information and/or better patient diagnosis. To achieve this goal, we have adopted a framework in which image quality is defined directly by how well these tasks can be performed. The task must be relevant and well defined and an observer or observer model must be chosen to perform the task. In addition, the characteristics of the objects being imaged must be well defined. Using task-based assessment of image quality, we are able to better design imaging systems for their intended purposes. Quantities such as resolution, contrast, and noise, become of secondary importance. We have presented a single example in which design decisions were incorrectly made because the task in question was not properly considered. Numerous other examples exist and can be found by perusing the references cited at the end of this paper.

1. Chih-Jie Lee, Matthew A. Kupinski, and Lana Volokh, *Assessment of cardiac single-photon emission computed tomography performance using a scanning linear observer*, Medical physics **40** (2012), no. 1, 011906.
2. Eric Clarkson, Matthew A. Kupinski, Harrison H. Barrett, and Lars Furenlid, *A task-based approach to adaptive and multimodality imaging*, Proceedings of the IEEE **96** (2008), no. 3.
3. Jiahua Fan, Hsin-Wu Tseng, Matthew Kupinski, Guangzhi Cao, Paavana Sainath, and Jiang Hsieh, *Study of the radiation dose reduction capability of a CT reconstruction algorithm: LCD performance assessment using mathematical model observers*, SPIE Medical Imaging, International Society for Optics and Photonics, 2013, pp. 86731Q–86731Q.

4. Jinxin Huang, Kye-sung Lee, Eric Clarkson, Matthew Kupinski, Kara L. Maki, David S. Ross, James V. Aquavella, and Jannick P. Rolland, *Phantom study of tear film dynamics with optical coherence tomography and maximum-likelihood estimation*, Optics letters **38** (2013), no. 10, 1721–1723.
5. Amit K. Sahu, Amit Joshi, Matthew A. Kupinski, and Eva M. Sevick-Muraca, *Assessment of a fluorescence-enhanced optical imaging system using the Hotelling observer*, Optics Express **14** (2006), no. 17, 7642–7660.
6. Abhinav K. Jha, Eric Clarkson, and Matthew A. Kupinski, *An ideal-observer framework to investigate signal detectability in diffuse optical imaging*, Biomedical optics express **4** (2013), no. 10, 2107–2123.
7. Dongyel Kang and Matthew A. Kupinski, *Noise characteristics of heterodyne/ homodyne frequency-domain measurements*, Journal of biomedical optics **17** (2012), no. 1, 0150021–01500211.
8. Dongyel Kang and Matthew A. Kupinski, *Effect of noise on modulation amplitude and phase in frequency-domain diffusive imaging*, Journal of biomedical optics **17** (2012), no.1, 0160101–01601010.
9. Dongyel Kang and Matthew A. Kupinski, *Figure of merit for task-based assessment of frequency-domain diffusive imaging*, Optics letters **38** (2013), no. 2, 235–237.
10. David A. Boas, Dana H. Brooks, Eric L. Miller, Charles A. DiMarzio, Misha Kilmer, Richard J. Gaudette, and Quan Zhang, *Imaging the body with diffuse optical tomography*, Signal Processing Magazine, IEEE **18** (2001), no. 6, 57–75.
11. Mohammad Reza Hajihashemi, Stephen R. Grobmyer, Samer Z. Al-Quran, and Huabei Jiang, *Noninvasive evaluation of nuclear morphometry in breast lesions using multispectral diffuse optical tomography*, PloS one **7** (2012), no. 9, e45714.

MATTHEW KUPINSKI is a professor at The University of Arizona with appointments in the *College of Optical Sciences*, the Department of Medical Imaging, and the program in Applied Mathematics. He performs theoretical research in the field of image science. His recent research emphasis is on quantifying the quality of multimodality and adaptive medical imaging systems using objective, task-based measures of image quality. He has a B.S. in physics from Trinity University in San Antonio, Texas, and received his Ph.D. in 2000 from the University of Chicago. He is the recipient of the 2007 Mark Tetalman Award given out by the Society of Nuclear Medicine, and is a member of the OSA and SPIE.

Graduate students Genevieve Allouche and Victoria Chan with Senator Steve Farley (D). *Women in Optics* (WiO) Congressional Visit Day in Phoenix, Arizona.

One of the more interesting hiking trails in the Santa Catalina Mountains starts at the base of the mountains at the edge of Tucson, and leads up to the Window, a huge natural arch at the top of a ridge. From the arch, one can gaze far down to the desert floor. In the wide view shown here, the University of Arizona and downtown Tucson are shown, but are so far away that they can barely be resolved. They are more readily seen by magnifying the relevant portion of the image.

Photos courtesy of Brian Anderson

Mechanical Properties of Light

Masud Mansuripur

Linear momentum of the electromagnetic field. It is well known that electromagnetic (EM) fields carry momentum as well as energy. Johannes Kepler (1571-1630) appears to have been the first to notice that a comet's tail always points away from the Sun, a phenomenon he attributed to the pressure of the sunlight on particles that evaporate from the comet's surface; see Fig. 1.

Fig. 1. Johannes Kepler suggested that the comet tails always point away from the Sun because of the pressure exerted by the sunlight on particles that evaporate from the comet.

Perhaps the simplest way to deduce the magnitude of the EM field momentum from first principles is by means of the Einstein box thought experiment. Shown in Fig. 2 is an empty box of length L and mass M, placed on a frictionless rail, and free to move forward or backward. At some point in time, a blob of material attached to the left wall emits a short EM pulse of energy $\mathcal{E}$ and momentum $\boldsymbol{p}$, which remains collimated as it travels the length of the box and gets absorbed by another blob attached to the right-hand wall. The recoil velocity of the box is thus $-\boldsymbol{p}/M$, the time of flight is L/c, and the box displacement along the rail is $-(p/M)(L/c)$.

Associating a mass $m = \mathcal{E}/c^2$ with the EM pulse and assuming that $M \gg m$, it is easy to see that the displacement of the center-of-mass of the system must be proportional to $(\mathcal{E}/c^2)L - M(p/M)(L/c)$. In the absence of external forces acting on the box, however, its center-of-mass is not expected to move. Setting the net displacement in the above expression equal to zero, we find that $p = \mathcal{E}/c$. Thus, in free space, a light pulse of energy $\mathcal{E}$ carries a momentum $p = \mathcal{E}/c$ along its direction of propagation. This result, which is independent of the particular shape of the pulse as a function of time, is accurate provided that the amplitude and phase profiles of the EM wave are smooth and uniform over a large cross-sectional area, thus ensuring that the pulse remains collimated as it traverses the length of the box.

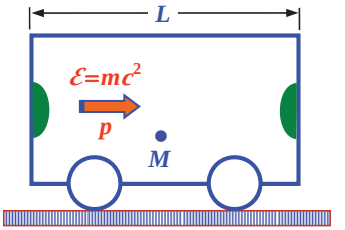

Fig. 2. Einstein box gedanken experiment.

Electromagnetic fields in free space are defined by their electric field $\boldsymbol{E}(\boldsymbol{r}, t)$ and magnetic field $\boldsymbol{H}(\boldsymbol{r}, t)$, where $(\boldsymbol{r}, t)$ represents the space-time coordinates. The rate of flow of energy (per unit area per unit time) is then given by the Poynting vector $\boldsymbol{S} = \boldsymbol{E} \times \boldsymbol{H}$. In terms of the Poynting vector, one can readily show that the momentum-density of the EM fields in the Einstein box thought experiment is given by $\boldsymbol{S}(\boldsymbol{r}, t)/c^2$. To see this, assume a cross-sectional area A for the pulse, and note that the entire pulse moves at constant velocity c from left to right. Choose an arbitrary cross-section of the pulse (perpendicular to its propagation direction), and observe that the EM energy passing through this cross-section during a short time interval Δt is given by $\Delta\mathcal{E} = S(\boldsymbol{r}, t)A\Delta t$. This energy, which proceeds to occupy the infinitesimal volume $\Delta v = Ac\Delta t$ to the right of the chosen cross-section, yields an energy density $\Delta\mathcal{E}/\Delta v = S(\boldsymbol{r}, t)/c$ at point $\boldsymbol{r}$ at time t and, consequently, a momentum density $\Delta\boldsymbol{p}/\Delta v = \boldsymbol{S}(\boldsymbol{r}, t)/c^2$ at that location.

A straightforward application of radiation pressure is found in the concept of solar sails; see Fig. 3. At 1.0 astronomical unit (i.e., the Sun-Earth distance), sunlight provides $\sim 1.4\ \mathrm{kw/m^2}$ of EM power density. Dividing this by the speed of light c and multiplying by 2 (to account for momentum reversal upon reflection from the sail) yields a pressure of $\sim 9.4\ \mu\mathrm{N/m^2}$. Over a sufficiently long period of time, the continuous force of sunlight exerted on a large-area solar sail can propel a small spacecraft to speeds comparable to or greater than those achievable by conventional rockets.

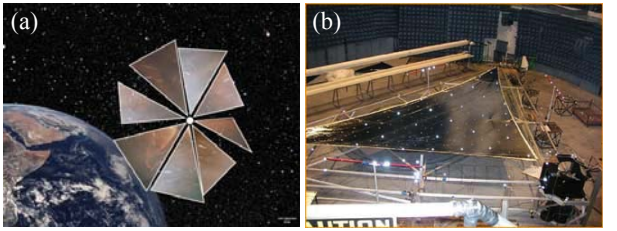

Fig. 3. (a) Artist's conception of a small solar-sail-driven spacecraft traveling away from the sun outside the Earth's atmosphere. (b) A 10-meter solar sail sits fully deployed in a vacuum chamber at NASA's Langley Research Center.

Optical tweezers. The first optical traps were built by Arthur Ashkin at AT&T Bell laboratories in the 1970s. "Levitation traps" used the upward-pointing radiation pressure to balance the downward pull of gravity, whereas "two-beam traps" relied on counter-propagating beams to trap particles. Then, in 1986, Ashkin and colleagues realized that the gradient force alone would be sufficient to trap small particles. They used a single, tightly-focused laser beam to trap a transparent particle in three dimensions. The principle of single-beam trapping is shown in Fig. 4. A small spherical dielectric bead of refractive index n_{bead} is immersed in some liquid of refractive index n_{liquid}. A laser beam is focused from above into the glass bead, with the focal point placed slightly above the center of the sphere. (Only two of the incident rays are shown, but the remaining rays behave essentially in the same way.) The bending of the rays by the glass bead causes them to exit with a smaller deviation from the optical axis. The projection of the exiting rays' momenta on the optical axis is thus greater than that of the incident rays. Stated differently, optical momentum along the z-axis increases upon transmission through the bead. In the process, this change of optical momentum is transferred as a lift force to the glass bead, helping to support it against the downward pull of gravity. Additionally, it is not difficult to show that, if the bead is laterally displaced from equilibrium, the resulting gradient force will return it to its original position; in other words, the equilibrium is a stable one.

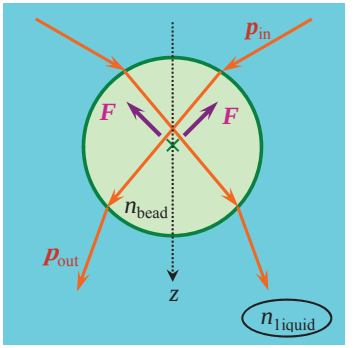

Fig. 4. Single-beam optical trap.

Electromagnetic spin and orbital angular momenta. It was mentioned earlier that the linear momentum-density (i.e., momentum per unit volume) of an EM field is $\boldsymbol{p}(\boldsymbol{r},t) = \boldsymbol{S}(\boldsymbol{r},t)/c^2$, where $\boldsymbol{S}$ is the Poynting vector and c is the speed of light in vacuum. The angular momentum density with respect to the origin of coordinates is thus given by $\boldsymbol{j}(\boldsymbol{r},t) = \boldsymbol{r} \times \boldsymbol{S}(\boldsymbol{r},t)/c^2$. A bullet of light having a finite duration and occupying a finite volume of space will carry, at any given time, a certain amount of linear and angular momenta, which amounts can be determined by integrating the corresponding momentum densities over the region of space occupied by the light bullet at any given instant of time. In the absence of interactions with material media (i.e.,

when the light bullet resides in free space), one can show, using Maxwell's equations, that the total linear momentum and also the total angular momentum of a given bullet remain constant in time, that is, the linear and angular momenta of the bullet are conserved. If the light enters a region of space where material media reside, it will exert forces and torques on various parts of these media in accordance with the Lorentz force law. Such exchanges between fields and material media cause the EM momenta (linear as well as angular) to vary in time. These variations, however, are always accompanied by corresponding variations in the linear and angular momenta of the material media (i.e., mechanical momenta), in such a way as to conserve the total momentum of the system of fields-plus-media, be it linear or angular, at all times.

The angular momentum of a light pulse (or bullet) in free space could arise as a trivial consequence of its center-of-mass trajectory (i.e., a straight-line along the linear momentum of the pulse) not going through the chosen reference point. Selecting a reference point on the center-of-mass trajectory then eliminates this trivial (extrinsic) contribution. The remaining contributions to angular momentum can be divided into two categories: *spin* and *orbital* angular momenta. In general, spin has to do with the degree of circular polarization of the light pulse, whereas orbital angular momentum arises from spatial non-uniformities of amplitude and phase that render the beam asymmetric around its propagation axis. Vorticity, which is associated with a continuous increase or decrease of phase around closed loops in the beam's cross-sectional plane, is a particularly interesting (and useful) source of orbital angular momentum.

A circularly-polarized light pulse of energy $\mathcal{E}$ propagating along the *z*-axis carries a spin angular momentum $\boldsymbol{S} = \pm(\mathcal{E}/\omega)\hat{\boldsymbol{z}}$. The ± signs indicate the dependence of the direction of $\boldsymbol{S}$ on the handedness of circular polarization (i.e., right or left). Such a light pulse, upon passing through a half-wave plate, will have its sense of polarization and, consequently, its direction of spin angular momentum (SAM) reversed. Conservation of angular momentum then requires the transfer of $2\boldsymbol{S}$ units of angular momentum to the half-wave plate, as shown in Fig. 5. The passage of the light pulse thus sets the wave-plate spinning around the *z*-axis, a phenomenon that has been exploited in optically-driven micro-machines.

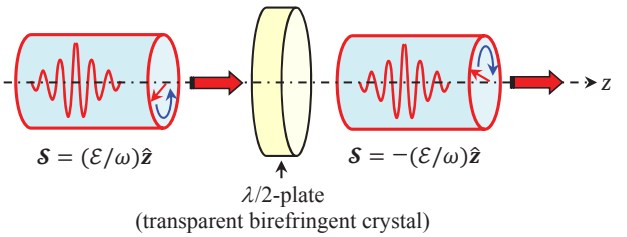

Fig. 5. A circularly-polarized light pulse of energy $\mathcal{E}$ and frequency ω carries a spin angular momentum $\boldsymbol{S} = \pm(\mathcal{E}/\omega)\hat{\boldsymbol{z}}$. Upon transmission through a half-wave plate, the change in the optical angular momentum ($2\boldsymbol{S}$) is transferred to the wave-plate, thereby setting the plate spinning around the z-axis.

When a collimated beam of light passes through a transparent spiral ramp, as depicted in Fig. 6, the emergent beam acquires optical vorticity, which carries orbital angular momentum (OAM). Once again, conservation of angular momentum requires the transfer of an equal but opposite angular momentum to the spiral ramp. Both SAM and OAM may be used to drive micro-machines. While the SAM associated with a single photon ($\mathcal{E} = \hbar\omega$) can only have a magnitude of $\pm\hbar$ (i.e., the reduced Planck's constant), the magnitude of OAM could be any integer multiple of $\hbar$.

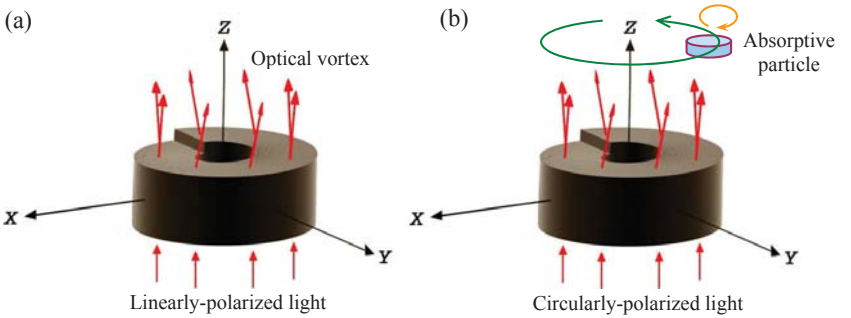

Fig. 6. (a) A transparent spiral ramp endows an incident beam with phase vorticity, which carries a certain amount of orbital angular momentum. (b) When the beam incident on the spiral ramp happens to be circularly polarized, the transmitted beam, a circularly-polarized optical vortex, carries both spin and orbital angular momenta. A small absorbing particle, placed in the path of such a beam, will spin on its own axis while, at the same time, travelling in a circle around the axis z of the spiral ramp.

The Balazs thought experiment. The arguments of the preceding sections do not shed any light on the momentum of EM waves inside material media. However, a different thought experiment, due to N. L. Balazs and dating back to 1953, reveals that the EM momentum-density within a transparent material must also be $\boldsymbol{p}(\boldsymbol{r},t) = \boldsymbol{S}(\boldsymbol{r},t)/c^2 = \boldsymbol{E}(\boldsymbol{r},t) \times \boldsymbol{H}(\boldsymbol{r},t)/c^2$. This particular expression is known as the Abraham momentum-density of EM waves inside material media.

With reference to Fig. 7, consider a transparent dielectric (e.g., glass) rod of length L, refractive index n, and large mass M. Let a short light pulse enter the rod from the left and exit from the right, without losses due to absorption, scattering, or reflections at the entrance and exit facets. Balazs suggested three different schemes for avoiding reflection at the facet, but, for our purposes, it suffices to assume the existence of perfect anti-reflection coatings on these facets.

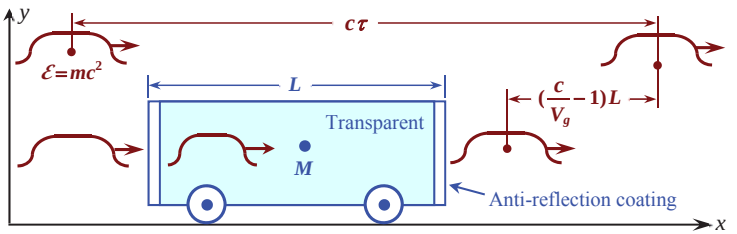

Fig. 7. The thought experiment of Balazs involves the propagation of a light pulse of energy $\mathcal{E}$ through a transparent rod of length L and mass M. The rod can move on a frictionless rail along the x-axis. Since the group velocity $V_g = c/n_g$ of the pulse inside the rod is less than c, the emergent pulse is somewhat behind the location it would have reached had it travelled in vacuum all along.

When the pulse emerges from the rod it will be delayed by the reduced speed of light within the glass. In other words, had the pulse travelled parallel to its current path but outside the rod, it would have been ahead a distance of $(n-1)L$ compared to where it will be upon emerging from the rod. Since there are no external forces acting on the system of rod plus the light pulse, the center-of-mass of the system should be in the same location irrespective of whether the pulse went through the rod or followed a parallel path outside the rod. Let the energy of the light pulse in vacuum be $\mathcal{E}$, which corresponds to a mass of $\mathcal{E}/c^2$. The delay has caused a leftward shift of

the product of mass and displacement by $(n-1)L\mathcal{E}/c^2$. This must be compensated by a rightward shift of the rod itself. Let the light pulse have EM momentum p while inside the rod. Considering that the momentum of the pulse before entering the rod is $\mathcal{E}/c$, the rod must have acquired a net momentum of $(\mathcal{E}/c)-p$ while the pulse travelled inside. Its net mass times forward displacement, therefore, must be $[(\mathcal{E}/c)-p]nL/c$. Equating the rightward and leftward mass × displacement yields $p=\mathcal{E}/(nc)$ for the EM momentum of the pulse inside the rod. In particular, the EM momentum of a single photon inside a transparent dielectric is $p=\hbar\omega/(nc)$. This argument not only assigns the Abraham value to the EM momentum of the light pulse, but also indicates that the refractive index appearing in the Abraham expression for photon momentum is the group index (as opposed to the phase index) of the transparent medium.

Photon momentum deduced from the Fresnel reflection coefficient. A simple argument yields a formula for the *total* photon momentum (i.e., electromagnetic plus mechanical) inside a transparent dielectric. Consider a glass slab of refractive index $n=1.5$ surrounded by vacuum, as shown in Fig. 8. The Fresnel reflection coefficient at the entrance facet of the slab being $r=(1-n)/(1+n)=-0.2$, a total of $|r|^2=4\%$ of all incident photons bounce back from the interface. Momentum conservation dictates that a reflected photon must transfer a momentum of $2\hbar\omega/c$ to the slab, while a transmitted photon must maintain its vacuum momentum of $\hbar\omega/c$. Assuming the incident light pulse contains a total of 100 photons, the total momentum of the photons entering the slab plus that of the slab itself must be $(96+4\times 2)\hbar\omega/c=104\hbar\omega/c$. The momentum associated with individual photons that have entered the slab is then given by $(104/96)\hbar\omega/c=1.0833\hbar\omega/c=½(n+n^{-1})\hbar\omega/c$. (This argument holds for any value of n and any number of photons contained in the incident light pulse, provided, of course, that the number of incident photons is sufficiently large to justify statistical averaging.) Recalling that the Balazs thought experiment associates the Abraham momentum $p=\hbar\omega/(nc)$ with the EM component of the photon momentum, the additional contribution to photon momentum in the preceding expression must be mechanical. (A similar argument applied to the angular momentum of circularly-polarized photons reveals the angular momentum of individual photons inside the dielectric to be the same as that in vacuum, i.e., $\hbar$, simply because reflected photons do *not* transfer any angular momentum to the glass slab upon reflection from its front facet.)

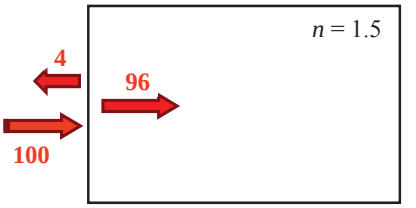

Fig. 8. Light pulse containing 100 photons arrives from free space at the entrance facet of a glass slab of refractive index $n=1.5$.

Masud Mansuripur (PhD 1981, Stanford University) is Professor and Chair of Optical Data Storage at the *College of Optical Sciences*. He is the author of *Introduction to Information Theory* (Prentice-Hall, 1987), *The Physical Principles of Magneto-Optical Recording* (Cambridge University Press, 1995), *Classical Optics and Its Applications* (Cambridge University Press, 2002, Japanese expanded edition 2006, 2nd English edition 2009), and *Field, Force, Energy and Momentum in Classical Electrodynamics* (Bentham Science Publishers, 2011). His areas of research interest include optical/magnetic/macromolecular data storage, thin-film optics, magnetism and magnetic materials, magneto-optics, theory of diffraction, and theory of the mechanical effects of light. A Fellow of the Optical Society of America (OSA) and the International Society for Optics and Photonics (SPIE), Professor Mansuripur is the author or co-author of over 250 papers in various peer-reviewed journals.

MM Research, Inc.

MM Research, Inc., a Tucson-based company founded by Professor Mansuripur has been providing simulation software and consulting services to the Optics industry since 1992. The company specializes in analytical and numerical analysis of physical optics problems including:

- Propagation of laser beams in free space and through homogeneous media
- Interaction of light with isotropic, birefringent, and optically active materials
- Scalar and vector diffraction
- Reflection, absorption, and transmission of coherent beams from multilayer structures
- Diffraction of light from gratings and other patterned surfaces
- Ellipsometry and polarimetry
- Optics of uniaxial and biaxial crystals
- Optics of high-numerical-aperture systems
- Coherent and incoherent imaging systems
- Electro-optical and magneto-optical effects and sensors
- Optical microscopy (phase-contrast, polarized-light, Nomarsky, scanning)
- Electron microscopy (Fresnel, Foucault, differential phase-contrast)
- Polarization-sensing in optical systems
- Wavefront analysis and interferometry
- Optical disk data storage (compact disk, digital video disk, CD-Recordable, write-once-read-many, magneto-optical, phase-change erasable)
- Thermal aspects of laser beam interaction with matter
- Photodetection and noise analysis (shot noise, thermal noise, avalanche noise)

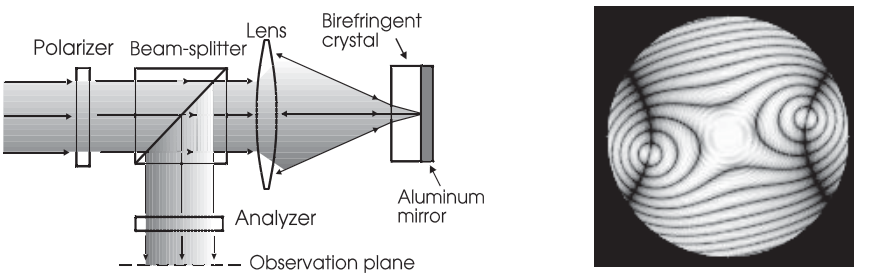

(Left) Diagram of a simulated optical system. Double passage of the focused beam through the birefringent crystal slab causes variation of the polarization rotation angle over the beam's cross-section. Crossed polarizers convert polarization rotation into intensity variation. (Right) Logarithm of the intensity distribution at the observation plane.

MM Research, Inc. strives to bring the latest developments in the fields of physical optics and numerical analysis to bear on the work of engineers/scientists involved in industrial/academic research and development. Software packages developed by the company have helped many students of optics and designers of optical systems to understand, analyze, and optimize diverse optical systems.

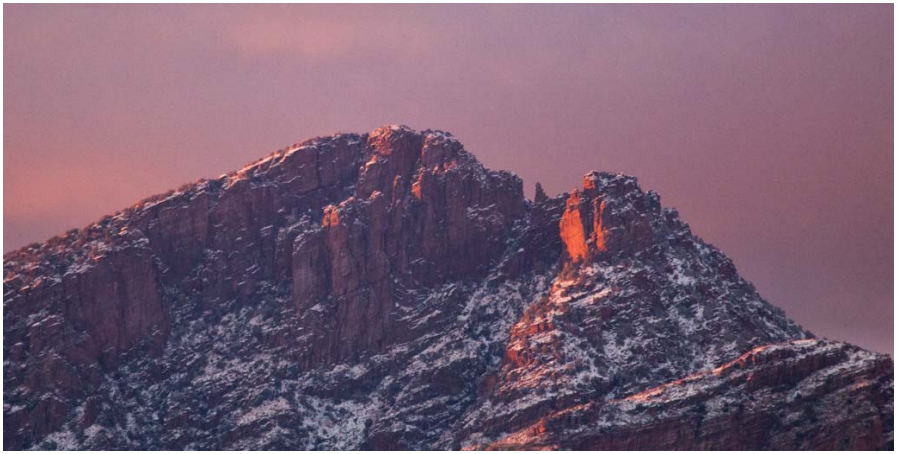

Finger Rock, shown here during a winter sunset, is one of the most recognizable formations on the ridge of the front range of the Santa Catalina Mountains.

Thanks to the usually clear dry weather, and relatively dark skies for a city of this size, the skies around Tucson are fantastic for stargazing and watching meteor showers and other sky phenomena. The left photograph shows the May 20, 2012, solar eclipse. The right photograph was taken from the outskirts of Tucson during the Leonids meteor shower of 2001.

Photos courtesy of Brian Anderson

Computer Assisted Optical Design

Kenneth E. Moore

In the year 1608, the Dutch spectacle maker Hans Lippershey invented the telescope. Although simple magnifiers and spectacles had been used for centuries, this was one of the earliest types of optical systems that employed two lenses used together. The famous Italian scientist Galileo heard of the invention, and began to make improved versions. Galileo had no design tools, and created telescopes by grinding lenses from glass and combing them at random until he found pairs of lenses that gave good results - a clear image with modest magnification. Yet Galileo achieved remarkable results for the day, discovering the moons of Jupiter in early 1610. Galileo could see the moons of Jupiter, which are invisible to the naked eye, were orbiting Jupiter and not the Earth. This was a stunning and controversial discovery at the time. The telescope Galileo built created the entire science of observational astronomy and the age of optical design for scientific instruments had begun.

Figure 1. Galileo and his early telescope. Image by Hulton Archive/Getty Images.

The goal of optical design is to determine the minimum number of lenses, and the shapes and positions of each those lenses, to provide the desired performance. The desired properties for optical designs include clarity of the image (sharp rather than blurry), how wide the field of view is (how much can you see at once) and the magnification (how well can you see things that are far away or things that are very small).

Around 1670, about 50 years after Galileo made his first telescope, the mathematical description of how light travels through lenses and mirrors was developed by Isaac Newton. A brilliant scientist, Newton not only worked out the mathematics for optical design that we still use today, but also developed the laws of motion and gravity, and invented calculus as well!

However, in practice, the equations Newton discovered cannot be solved when there are more than two lenses involved. Each added lens adds an ever more complicated set of equations to the mathematical description, and the problem quickly becomes too difficult. For this reason, optical designers had to use a set of simple, approximate mathematical models of lenses. This approach works only for limited cases, and with results well below the true potential of the design. For nearly 300 more years, optical design progressed fairly slowly.

Starting around 1950, computers were used to aid in the design of optical systems. The software used to design optical systems is based upon the idea of a ray of light. The ray of light is mathematically propagated from one lens to the next using a series of simple equations called tracing. If many rays are traced, the system performance can be predicted.

Here is a computer model of a single lens forming an image. The model allows engineers to predict the performance of the lens, and simulate the images the lens can form if used for example in a camera in a cell phone. The lens is drawn on the left. The Blue, Green, and Red lines are the rays tracing through lens and coming to the image surface on the right. The primary goal of optical design is to get all rays to come to a focus, which yields the highest image quality.

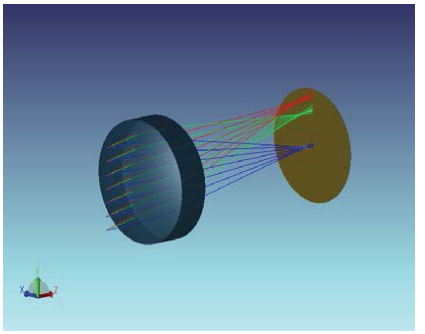

Figure 2. A computer model of a single lens.

If many rays are traced, the software can predict the appearance of images the lens will form. The single lens above for example forms an image that might look like that shown in Figure 3.

Figure 3. A simulated image. Note the blurry quality, especially near the edges of the image.

The software provides diagnostic and analysis tools which help the engineer understand the behavior of the optical design and how to improve it. These tools guide the engineer to consider different types of glass, the number of lenses, and the shapes and positions of those lenses.

Modern optical design software does much more than just predict image quality. Instead of just tracing rays, the software can be used to make small adjustments to the design itself - changing the shape of the lenses, the positions, or even the type of glass the lens were made of. The computers are so fast at ray tracing that many potential designs can be automatically studied, and the software continually modifies the design until the best performance is achieved. This process, called Optimization, is a critical part of modern optical design. Shown in Figure 5 is an optimized version of the previous example, using three lenses instead of one.

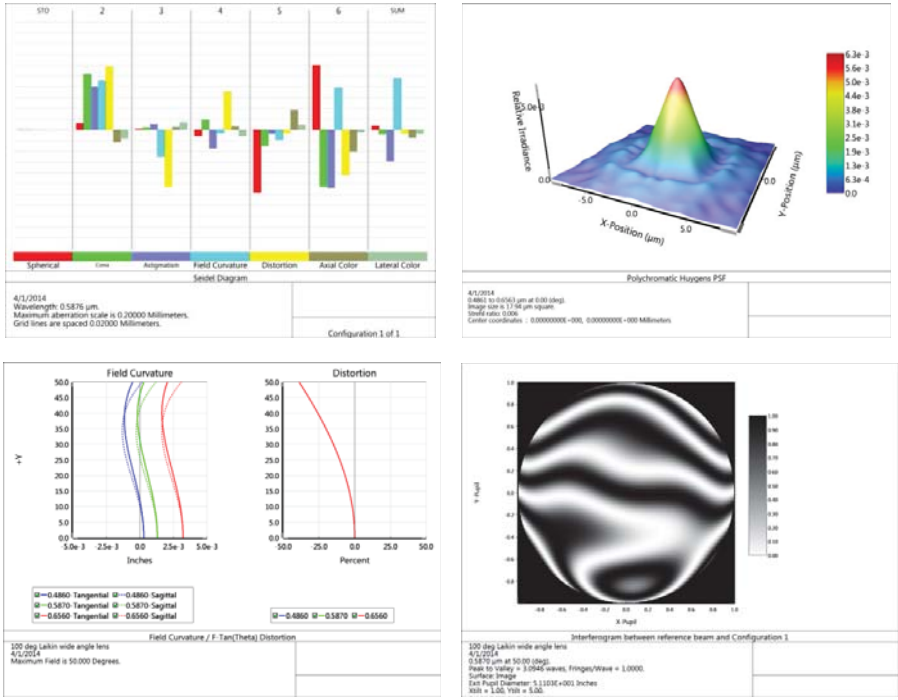

Figure 4. Some sample analysis features used by optical engineers to improve the design.

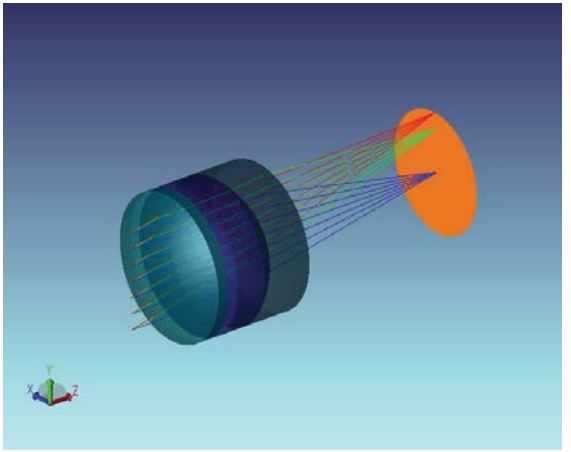

Figure 5. A computer model of an optimized lens.

The image is dramatically sharper, with less distortion and better color performance, as shown in Figure 6.

Figure 6. A simulation of an image formed by an optimized lens

Modern camera lenses, used in photography may have dozens of individual lens elements, such as the wide angle lens shown in Figure 7.

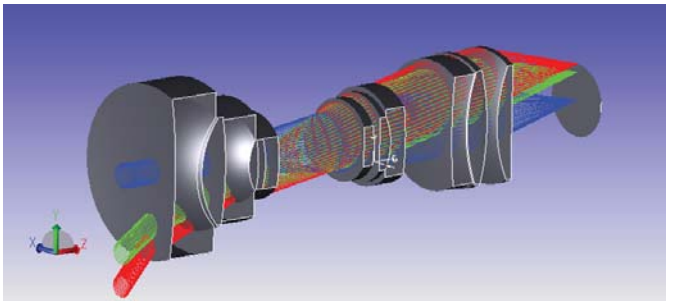

Figure 7. A modern wide angle lens for photography. Lens design by Milt Laikin.

Improvements in optical engineering and software design tools are still going on today. In additional to just optical design using glass lenses or mirrors, modern software can model more exotic optical components such as holograms, gratings, thin film coatings, optical fibers, and crystals. Computer aided lens design software can also model many complex phenomenon, such as temperature changes and fabrication errors. Software is also used to describe the optical components to specialized machines that create the lenses automatically. Virtually all optical design today is done entirely on a computer, from concept to fabrication.

The role of the modern optical designer is to understand the system requirements, such as size, weight, cost, field of view, magnification, image quality, and other parameters. The engineer then comes up with a concept design that provides approximately the desired performance. The design is created on a computer and analyzed. The software does most of the tedious work; tracing rays and providing a myriad of performance analysis functions. The engineer and the software work together to optimize the design to provide the best possible system design.

This type of engineering requires advanced education in the optical sciences. The demand for highly trained optical designers has never been greater. Optical system designers are still needed for traditional applications such as camera lenses, telescopes, and microscopes. However, the application of optics into more and more fields of engineering is driving ever greater demand for designers. Optics are now widely used in consumer products, medical devices, environmental and industrial monitoring, aerospace, telecommunications, and lighting, to name just a few. A career in optical design offers excellent employment prospects and interesting work in a wide variety of fields.

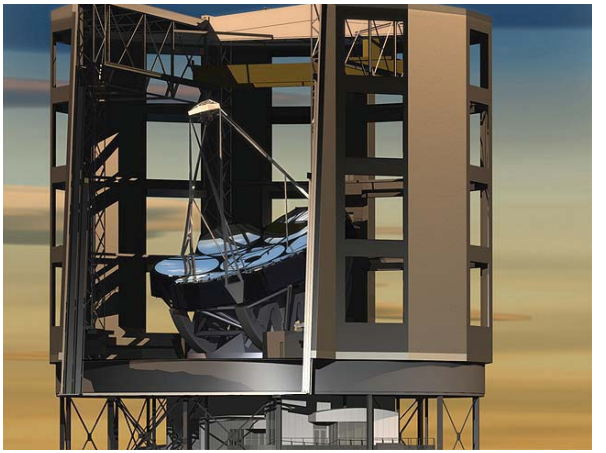

Figure 8. The Giant Magellan Telescope. Image by GMTO Corporation.

Optical design has come a long way since the days of Galileo. The current state-of-the-art in telescope design is well represented by the Giant Magellan Telescope, with a main mirror array 80 feet in diameter. These giant mirrors are being made at the University of Arizona's Steward Observatory Mirror Lab. The Giant Magellan Telescope is roughly one million times as powerful as the very first telescopes. Galileo would surely be amazed!

Dr. Kenneth E. Moore is the founder of Zemax Development Corporation and the original author of the Zemax OpticStudio software program. He currently is the Chief Technology Officer at Radiant Zemax in Redmond, Washington. Dr. Moore received his Ph.D. In Optical Sciences from the University of Arizona in 1991. He is a Fellow of both the Optical Society of America (OSA) and the International Society for Optics and Photonics (SPIE).

Zemax, LLC

Kenneth E. Moore

In 1988, I started graduate school at what is now the *College of Optical Sciences* at the University of Arizona. There were many fascinating research opportunities, but I was immediately drawn to optical modeling. The field of optical modeling encompasses the computer based modeling and design of lenses, illumination systems, fiber optics, lasers, or any interaction of light and matter. My research interests were in the area of physical optics modeling and optimization of the performance of physical optics systems using computers.

While I was still a student, it was clear to me that there were applications for the technology I was developing in the field of lens design. I decided to write my own lens design code, initially for fun, that would test these new ideas for optimization of camera lenses and telescopes. I found the work fascinating and realized that indeed the technology was applicable, and there was likely a commercial market for software based upon the algorithms and methods I had developed.

When I graduated with a Ph.D. in 1991, I turned my attention to developing the software with the intent of selling the program commercially. I named the program Zemax, after my pet Samoyed whose name was Max. Max always laid at my feet when I was at my desk working on the program, so it seemed fitting to name the software after him, and the truth is I didn't have any better ideas for a name anyway.

Many fellow students heard I had a little program, and asked to use it. Those students gave me valuable feedback about what to add or improve in the program. I had no idea then that most of my professional life over the subsequent 24 years would be listening to that steady stream of advice from customers, and that constantly improving the software would be my career.

My wife and I placed our first ad for Zemax in *Laser Focus World* in 1992. This was in the early days of the Internet, and the most effective way of reaching customers back in the pre-Google days was advertising in trade magazines. We sold two copies of the software from the ad - enough to pay for the first ad and buy another one. That was exactly the minimum we needed to get started, and no more! Every month we bought new ads, and rolled over virtually of the proceeds into more ads. Within a year, we started getting a lot of word of mouth sales, and Zemax took off like a rocket.

We hired our first full time employee in 1994, and soon hired several more. We grew our business by developing our technological expertise and reputation steadily, and for more than 20 years Zemax has steadily grown into the most widely used optical design software in the world.

As the company grew, I eventually realized that the best future for Zemax was one without me as the owner and President. There were too many types of expertise required for me to manage on my own. So in 2011, the company was sold to a group of private investors. My long run of 80+ hour work weeks had thankfully come to an end! I remain active with the company today as a technical consultant.

The education provided by the University of Arizona College of Optical Sciences unquestionably made the existence and subsequent success of the Zemax software, and of the Zemax company, possible. Not only was I educated there, but many of our key employees over the years have studied there as well. Many of the Professors, Researchers, and Students use Zemax, and they have been providing valuable feedback on the software as they work on the latest technological problems. As the founder of Zemax, I am particularly proud that Zemax is one of the spin-off success stories to come out of the *College of Optical Sciences.*

Tucson's *All Souls Procession* is a public event held at the beginning of November to celebrate and honor the lives of friends, family, and loved ones who have passed away. The two-mile-long procession through downtown Tucson draws tens of thousands of participants.

Photo courtesy of Brian Anderson

Organic Photonics: Performance Meets Practicality

Robert A. Norwood

Over the past few years, organic photonic materials have become firmly established alongside their classic counterparts, such as glass, inorganic semiconductors and metal oxides, in applications ranging from data center interconnects to materials for flat panel displays and smart phones. Because of their innate flexibility, organic compounds can be customized for specific applications, including materials for optics and photonics. Synthetic chemists, physicists, and engineers have shed light on the secondary structural properties that control stability in organic materials, providing more options than ever for the use of polymers, organic crystals and novel forms of carbon in photonics.

The scope of organic and polymeric photonics research is vast. The College of Optical Sciences at the University of Arizona and our collaborators have made great strides in developing electro-optic polymers for high-bandwidth demands, organic and inorganic nanocomposites for designer optical materials, integrated liquid core optical fibers for nonlinear organic photonics, organic photovoltaics for renewable energy applications, graphene model-locked fiber lasers, and sulfur-based polymers for infrared optics including thermal imaging. Exciting discoveries in these areas are poised to improve materials technology, exploit existing optical systems, and create entirely new markets for optical technology.

Driving the big data engine. Recently, we have all witnessed the increased pervasiveness of information technologies and the explosion of wireless device, streaming technology and cloud computing. It is easy to forget that Internet networks and large data centers (Figure 1) must continually increase capacity to keep up with our growing demand for data. Last year, the Internet carried on the order of 60 exabytes (10^{18} bytes) of information per month. To put that into perspective, consider that the total text, audio and video output of humanity up to the year 2000 is estimated to have been about 12 exabytes—and a single exabyte is roughly 100,000 times the textual information stored in the U.S. Library of Congress! Of course, video is primarily driving this growth owing to the tremendous bandwidth required for even a single high resolution picture.

Figure 1. A Google data center; such data centers can hold up to 1,000,000 high performance servers.

Many scientists and engineers believe that the only way to keep up with our increasing need for data is to adopt a multi-pronged technology development program that continues to ride the success of microprocessor technology (Moore's Law—smaller and faster), while using photonics technology to provide both transmission and limited processing functionalities. Optical computing per se is not the answer; there are certain things that electrons do extremely well

(switching, data storage) and other things that photons do very well (transmission, multiplexing); the answer for the future is to get photons and electrons to work together as well as possible.

Recent advances in organic photonics can help us keep ahead of the data explosion—an example is commercialized electro-optic (EO) polymers with high thermal- and photo-stability. Soluxra, LLC, a University of Washington spinoff, has introduced a series of EO polymers with exceptionally high EO coefficients. The EO effect was originally observed by Pockels in the 19th century and involves the ability to change the refractive indices of certain materials by applying an electric field to them. Through integrated optics it is possible to fashion an optical interferometer on a chip; by making the interferometer electro-optic, one can make an optical modulator (turning light on an off) or an optical switch. In EO polymers, the EO effect is extremely fast since it involves only the motion of electrons, so that the fundamental bandwidth is on the order of 1 terabit/second. With high EO coefficients, it is feasible to design and fabricate ultracompact modulators that can be easily integrated with silicon photonics. Silicon is an increasingly important photonics platform poised to revolutionize data center and computer interconnections the way that sophisticated bulk optical components such as amplifiers, dense wavelength division multiplexing filters, and wavelength-selective switches have transformed the fiber-optic core of the Internet. In Figure 2 we show the silicon photonic foundation for an EO polymer-based wavelength selective switch that is currently under development in our group. The rings in this picture are only about 100 μm in diameter, about the width of a human hair.

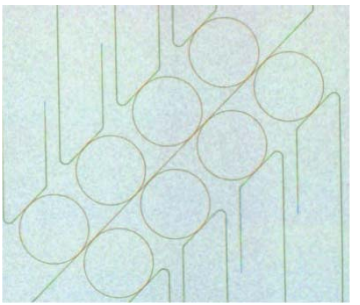

Figure 2. Silicon photonics backbone of a 4 channel EO polymer/silicon reconfigurable optical add drop multiplexer; the rings are about 100 microns in diameter.

Nanocomposites: At the organic inorganic interface. Nanomaterial technology has exploded over the last decade, particularly nanocarbon species such as fullerenes, carbon nanotubes, graphene and nanodiamond, as well as metal oxide and semiconductor nanoparticle technologies. At the same time, passive optical polymer technology has reached a level of maturity and availability that has led to the development of optical polymer nanocomposites, materials that combine the processability and low-cost of polymer technology with specific performance features of inorganic nanoparticles. These developments allow us to create designer optical materials with a unique combination of properties, including organic polymer processability with inorganic crystal technology.

When making a nanocomposite, basic considerations regarding mixing materials come into play; we all know that alcohol mixes easily with water, while oil does not. Our approach to this problem is to promote specific material interactions between the nanoparticle and the polymer as well as to maximize entropy. We have used this principle to develop new optical polymer nanocomposite magneto-optic materials with properties that are practically equivalent to those of

the fragile inorganic crystals that have been used for decades to make a critical optical component used in optical networks, namely optical isolators, the optical equivalent of an electrical diode.

Our nanoparticle composite consists of 15-20 nm cobalt ferrite nanoparticles with a coating of polybenzylmethacrylate (PBMA) embedded in a PBMA matrix (Fig. 3a). The optical quality of the material is excellent: One can easily view a distant object through a 100 μm-thick film of the composite (Figure 3b). The Verdet constant of our composite at 1550 nm wavelength is -1.5×10^4 °/T-m, which is larger than that of the commercial material terbium gallium garnet and approximately equal to that of yttrium iron garnet, widely used in optical isolators. These new optical polymer nanocomposites have a broad range of potential applications, including optical isolators and circulators that are directly integrated with silicon photonics and other photonic platforms, as well as ultrasensitive magnetic field sensors with potential use in non-intrusive brain imaging.

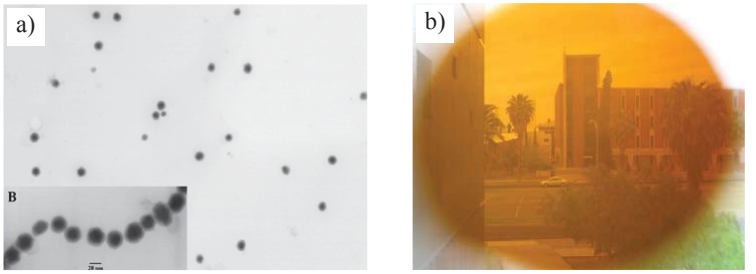

Figure 3. a) Transmission electron micrograph of polymer-coated cobalt ferrite nano-particles. The insert clearly shows the polymer shell (light grey) enveloping the particle; b) the cobalt ferrite nanoparticle polymer composite has excellent optical clarity.

Organic PVs with nanostructures and plasmonics. Recently, researchers have devoted extensive effort to exploring organic photovoltaics (OPV) as low-cost, lightweight renewable energy resources; the ultimate goal is to make these devices by conventional polymer film processing techniques such as roll-to-roll printing. Thus far to achieve high efficiencies (now approaching 12 percent), one must either make tandem cells (which involves growing two or more photovoltaic cells on top of one another) or use evaporated organic crystalline materials. Both approaches partially squander the cost advantages of using organic materials. A new alternative is to rely on wet-coatable polymer materials and compensate for their lower intrinsic efficiencies through the use of nanostructuring and plasmonic nanoparticles. Plasmonic nanoparticles such as gold, silver and aluminum create regions of greatly enhanced electric field within 10-20 nm of their surfaces, such that active absorbing materials in this region will exhibit enhanced absorption of incoming solar radiation. We have created a plasmonically enhanced OPV in which gold nanoparticles are embedded in the PEDOT:PSS layer (Figure 4a); this structure was chosen so that the field enhancement effects of the plasmonic nanoparticles would not be confounded with their effects on charge transport and exciton dissociation. We modeled and measured the absorption spectrum of fabricated cells and observed the anticipated increase in absorption, resulting in a 30 percent increase in traditional OPV efficiency (Figure 4a). Note that while gold nanoparticles are quite costly, similar improvements could be achieved with aluminum nanoparticles.

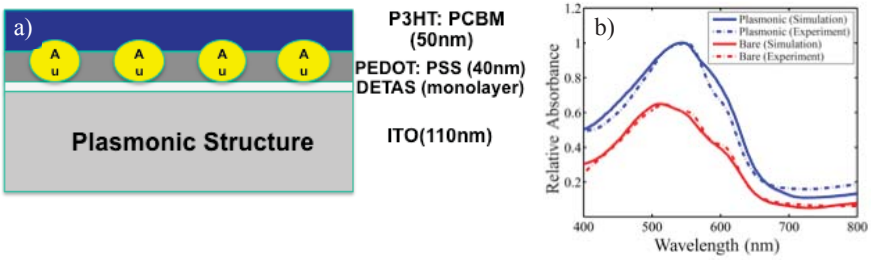

Figure 4. a) Design of plasmonically enhanced organic photovoltaic. The gold nanoparticles are positioned at the interface between the PEDOT:PSS polyelectrolyte layer and the P3HT:PCBM active layer; b) relative absorbance of plasmonic and non-plasmonic (bare) regions of the OPV showing excellent agreement between simulation and experiment.

The past decade has seen the widespread adoption of organic photonics technology for applications ranging from light emitting diodes to short range interconnects for computing applications. In this article, I have highlighted some emerging areas of organic photonic technology in our group, many of which rely on combining organic materials with their benchmark inorganic counterparts in both materials and devices. As these technologies come into their own, the chemists, engineers and physicists who have achieved many initial successes in this highly interdisciplinary field stand poised to commercialize the next generation of organic photonics technology.

Robert A. Norwood is a Professor in the *College of Optical Sciences*, where he performs research on photonic materials and devices, principally involving organic materials. He holds the Ph.D. degree in physics from the University of Pennsylvania, and the B.S. degree in physics and mathematics from MIT. Prior to his current position, Dr. Norwood spent 15 years in R&D leadership positions in industry at both Fortune 100 corporations (Hoechst Celanese and AlliedSignal) and venture-capital backed startups (VP and CTO of Photon-X). He is a world expert in polymer integrated optics and optical materials, with more than 100 refereed publications, 7 book chapters, 30 issued US patents, and 65 invited talks. Dr. Norwood has served as a conference chair or co-chair for OTF (OSA) and *Linear and Nonlinear Optics in Organic Materials* (SPIE), and has served on the program committee for OFC and CLEO, among others. He has served as an Associate Editor for *Optical Materials Express* and *IEEE Photonics Technology Letters*. Dr. Norwood is both an OSA Fellow and an SPIE Fellow, as well as a member of APS and IEEE.

The 8th floor of the College of Optical Sciences is fortunate to have great views to the north, towards the Santa Catalina mountain range.

Photo courtesy of Brian Anderson

Fluorescence Microscopy in Biomedicine

Leilei Peng

Fluorescence is one of the processes that use optical energy to produce light. Fluorescent substances such as minerals, plants and animals are readily found in nature (Figure 1). Fluorescence is also widely used in daily life. Fluorescent highlighters are one of the most commonly used fluorescent substances. Fluorescent light bulbs are coated with fluorescent chemicals on their inner surfaces; the emission from these light bulbs is actually fluorescence excited by ultraviolet light. Fluorescent paints are increasingly used to mark road signs, emergency service personnel, and others (such as runners and cyclists) to ensure safety in sharing the road.

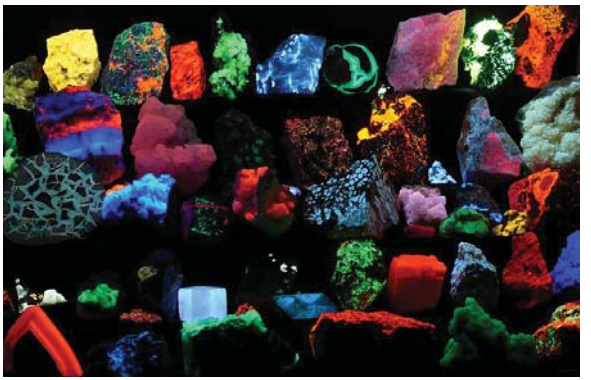

Figure 1. Minerals exhibiting fluorescence when illuminated with ultraviolet light.

When a fluorescent molecule absorbs a photon, an electron of the molecule is promoted to an excited state. As the excited electron returns to the ground state, a photon at a red-shifted wavelength is emitted. This quantum picture of the fluorescence process is illustrated by the simple Jablonski diagram shown in Figure 2. The cycle of excitation and emission of a fluorescent molecule may repeat many times before being stopped by permanent damage to the molecule (photo-bleaching).

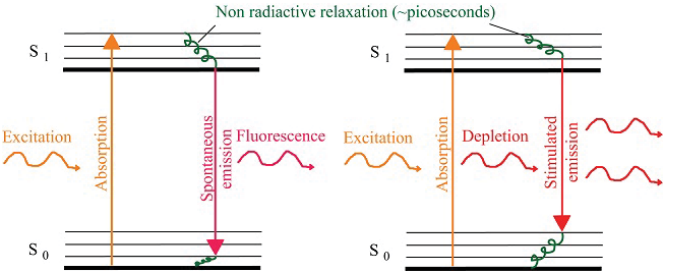

Figure 2. (a) Principle of fluorescence. (b) Principle of the Stimulated Emission Depletion (STED) process.

Although many naturally existing compounds exhibit fluorescence, their fluorescent properties such as brightness, the required excitation wavelength, chemical stability, and bio-compatibility are seldom optimal for applications in daily life or for research purposes. Fueled by the demand in biomedical research, many different kinds of fluorescent compounds have been developed during the last few decades. These compounds are called fluorophores or fluorescent dyes. Nowadays, there exists a massive selection of fluorophores whose fluorescent emission colors cover the entire visible spectrum while exhibiting superior brightness, enhanced stability, and reduced photo-bleaching. In biomedical research, man-made organic fluorophores are widely used to stain tissues and cells for the purpose of illustrating microscopic features and structures. Figure 3 is a mouse kidney slice stained by three different fluorescent dyes. The red color is Alexa 568 stained cytoskeleton; the green color is Alexa 488 labeled proximal tubules of kidney; and the blue color is DAPI labeled nucleus.

If the use of organic fluorophores has provided an unprecedented tool to visualize cellular and tissue structures, the discovery and continuous development of fluorescent proteins have truly revolutionized modern biomedical research. The isolation of the first such protein, the Green Fluorescent Protein (GFP), which eventually lead to the 2008 Nobel Prize in chemistry, has made it possible to label a specific protein of interest with a fluorescent tag through genetic manipulation. Instead of observing dead and fixed samples with organic fluorophore staining, dynamic biological processes in live cells and in animals are now open to human investigation in real time (Figure 4). Further fueled by advances in optical, biological, and electronic techniques, fluorescence microscopy nowadays is an irreplaceable tool that will continue to advance life sciences in an unparalleled fashion.

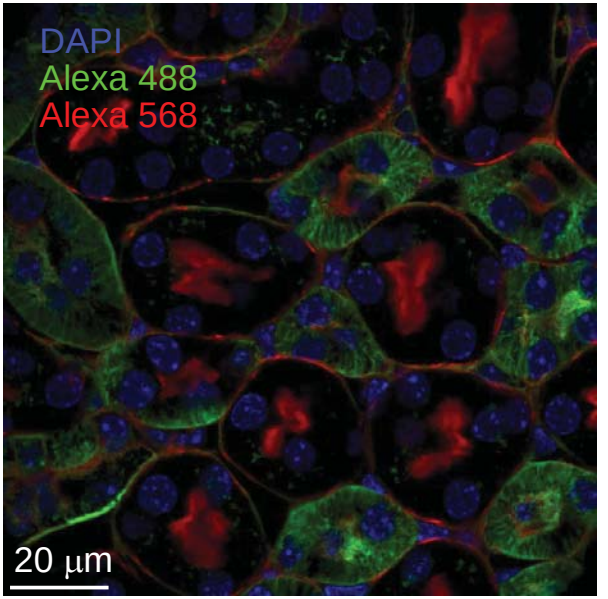

Figure 3. Image of triple fluorescently labeled mouse kidney slice.
(Peng laboratory, College of Optical Sciences)

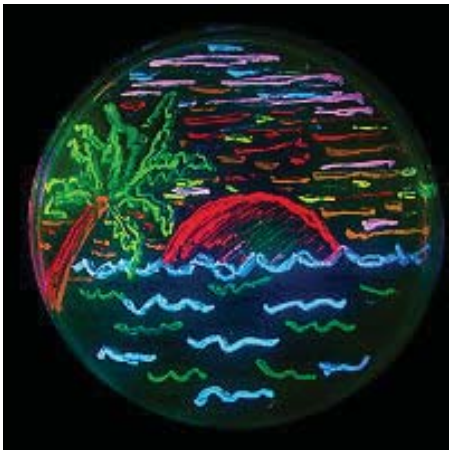

Figure 4. A San Diego beach drawing which is actually composed of living bacteria. These bacteria were genetically manipulated to express eight different fluorescent proteins. (Courtesy of the UCSD group of Roger Tsien, the 2008 Nobel laureate in Chemistry).

A fluorescence microscope utilizes fluorescence, in addition to reflection and absorption, to study specimens of interest. The microscope needs to illuminate the sample with specific wavelength(s) of light, and then separate and collect emitted fluorescent light, which is usually much weaker compared to the excitation light. This is achieved by a combination of several optical elements, as demonstrated in Figure 5. The elements include an excitation filter to select the appropriate wavelength, a dichroic mirror (or beam-splitter) to reflect the excitation light into the sample while passing the fluorescent light collected by the objective lens, and an emission filter to further block any excitation light that might reach the detectors.

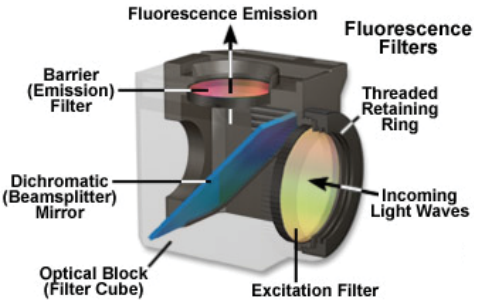

Figure 5. A typical filter tube in a modern fluorescence microscope.

The resolution limit of conventional optical microscopy is governed by the diffraction of light (first described by Ernst Abbe in 1873), as follows:

$$d = \frac{\lambda}{2NA}.$$

Here λ is the wavelength of the light and NA is the numerical aperture of the objective lens. The numerical aperture is defined as:

$$NA = n \sin \theta,$$

where n is the refractive index of the medium while θ is the half-angle of the light cone produced by the objective lens. Increasing the numerical aperture will lead to higher resolution. Research microscopes often use immersion oil having a high refractive-index to increase NA. Given that a typical immersion oil has a refractive index of 1.52 and that the half-angle θ is generally smaller than 90°, the NA of a commonly used objective lens is typically below 1.5. Hence the resolution limit of conventional optical microscopy in the visible spectrum is about 150 to 250nm .

In recent years, a wide array of novel microscopy methodologies has been developed with the ambitious goal of breaking the aforementioned resolution limit. These methods are collectively referred to as super-resolution microscopy. Super-resolution optical microscopy has achieved lateral and axial resolutions in the range of tens of nanometers. Figure 6 shows a diffraction-limited image and a super-resolution image of the same fluorescent beads affixed to a glass coverslip. Each individual bead is clearly discernable in the super-resolution image but not in the regular diffraction-limited image.

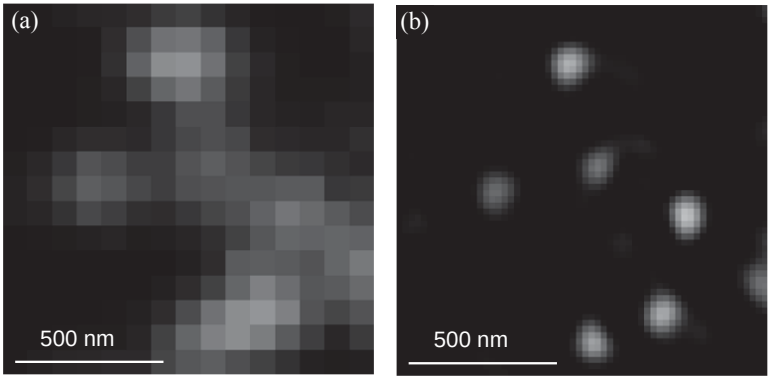

Figure 6. (a) A diffraction-limited image. (b) Super-resolution image of the same fluorescent beads immobilized on a cover-slip, taken by the Peng group in OSC.

One group of super-resolution methodologies is based on single-molecule localization, which includes photo-activated localization microscopy (PALM), stochastic optical reconstruction microscopy (STORM), and fluorescent photo-activation localization microscopy (FPALM). The fundamental principle underlying all these techniques is that the coordinates of individual molecules can be locally determined with an accuracy of a few nanometers provided that the molecules are sparse enough that inter-molecule distances are greater than the resolution limit. These localization-based techniques require photo-switchable fluorescent probes. Through random photo-switching, a subset of fluorophores are lighted up in the same image frame. Tens and even hundreds of frames will have to be collected and merged in order to produce a final super-resolution image (Figure 7).

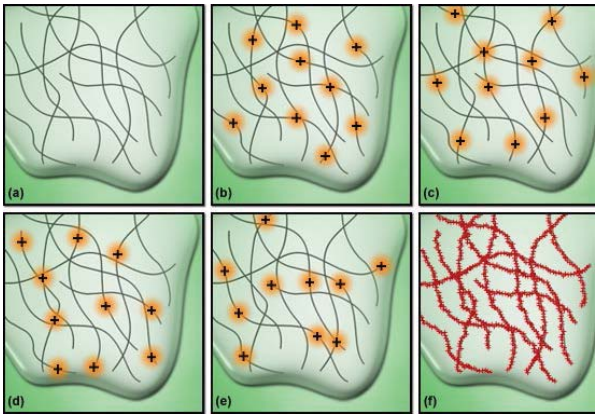

Figure 7. Principle of PALM/STORM super-resolution optical microscopy.

Another category of super-resolution microscopy techniques is based on focal volume engineering, which is represented by stimulated emission depletion (STED) microscopy. STED microscopy is built around a confocal laser scanning microscope. A conventional confocal laser scanning fluorescence microscope scans a focused excitation laser beam across the sample, and collects the fluorescent image pixel by pixel. The focal size of the excitation laser cannot be narrower than the diffraction resolution limit. Therefore, the resolution of a confocal microscope cannot be better than 150-250nm. When an excited fluorophore is exposed to a STED beam, the STED beam may impose a "resonant" effect on fluorescence emission, and the wavelength of this fluorescent emission may be "tuned" to be the same as that of the STED beam; see Figure 2(b). The wavelength of the photons emitted through the STED effect can substantially differ from that of the naturally-occurring spontaneous fluorescent emission, and can therefore be easily filtered out. In effect, the STED beam can turn off spontaneous fluorescent emission. By employing a donut-shaped STED beam whose center overlaps with the excitation beam, spontaneous emission at the edges of the focal spot are depleted, and the focal spot can be narrowed down to 20～50nm range, as shown in Figure 8, resulting in significant improvement in optical resolution.

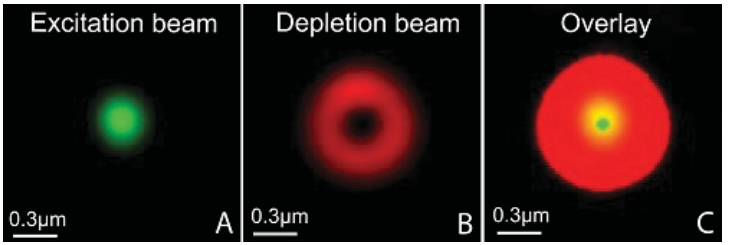

Figure 8. Focal spot of (a) a typical excitation beam, (b) a donut-shape STED beam, and (c) the overlay of the two beams.

The third category of super-resolution microscopy techniques is structured illumination microscopy (SIM). The basic concept of resolution enhancement in this technique can be

explained in terms of the well-known moiré effect, namely, when a sample is illuminated with an excitation pattern, the final image observed is the product of the illumination pattern and the unknown pattern of fluorescent probes, resulting in a beat pattern or moiré fringes. The features of the final moiré fringes can be much coarser than either of the original patterns and, therefore, readily observable through an optical microscope, even when one or both of the initial patterns are too fine to be resolved; this is shown schematically in Figure 9. SIM can be performed on a large field of view and is very compatible to live cell imaging, although it provides relatively moderate resolution enhancement compared to other super-resolution techniques.

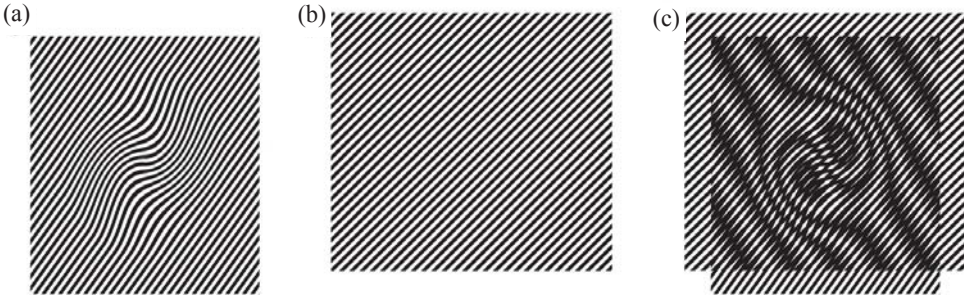

Figure 9. Basic principle of structured illumination microscopy (SIM). When an unknown sample pattern (a) is multiplied by a known illumination pattern (b), a beat pattern (moiré fringes) will appear (c). The moiré fringes occur at the spatial difference frequencies between the frequencies of the two patterns. The moiré fringes can be coarse enough to be observed through an optical microscope even when the original (unknown) pattern is unresolvable.

Most fundamental biological processes occur at the macromolecular level, corresponding to physical dimensions ranging from tens to hundreds of nanometers. Super-resolution microscopy greatly advances our knowledge of molecular interactions and dynamic processes in living systems. Rapid technical developments in this field will allow the biomedical research community to understand biological processes and structures with previously unresolvable detail.

1. E. Betzig, G. H. Patterson, R. Sougrat, O. W. Lindwasser, S. Olenych, J. S. Bonifacino, M. W. Davidson, J. Lippincott-Schwartz and H. F. Hess, *Science* **313** (5793): 1642–1645 (2006).
2. S. W. Hell and J. Wichmann , *Optics Letters* **19** (11): 780-782 (1994).
3. M. G. Gustafsson, *Journal of Microscopy* **198** (2): 82-87 (2000).

Leilei Peng is Assistant Professor of Optical Sciences and Assistant Professor of Molecular and Cellular Biology at the University of Arizona. She received her BS and MS degrees from the University of Science and Technology of China in 1997 and 2000, respectively. Her PhD is from Purdue University in 2005. From 2005 to 2008, Dr. Peng was a Research Fellow at the Harvard Medical School, Wellman Center of Photomedicine. Her research interests include Fourier transform fluorescence spectroscopy, fluorescence lifetime and hyperspectral imaging, optical tomography, and single-molecule and super-resolution optical imaging.

Summer storm at sunset, with Baboquivari Peak in the background.

Photo Courtesy of Brian Anderson

The Art of Lens Design

José Sasián

Lens design is at the heart of optical engineering and is one of the oldest and still most exciting fields in Optics. Lens design requires that an optical engineer/scientist understand the physical mechanisms of image-formation, which ultimately make the difference between sharp, high-resolution images and aberration-degraded, low-quality ones. Designing a lens from the scratch in order to achieve images with desirable characteristics is an enabling and rewarding activity. The understanding of the various attributes of image-forming systems in an attempt to enhance image quality and system performance is interesting and intellectually fulfilling. Great scientists such as Galileo, Newton, and Gauss have delved into lens design. Today, in a most exciting era in the use and manipulation of light, competent engineers and scientists routinely rely on the science and art of lens design.

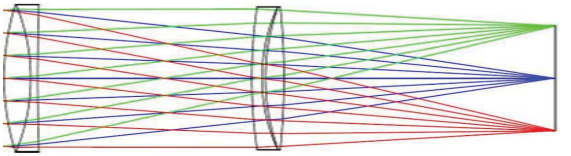

Petzval portrait objective lens with ray trace for three field points.

Lens design can be defined as the art and science of arranging optical elements such as lenses, mirrors, and prisms to manipulate light in order to form an image or to create a particularly desirable light distribution. With the invention and disclosure of the photographic process by Louis Daguerre in 1839 there was the need for an optically fast lens that could take pictures in just a few seconds. The first lens thus used was a simple achromatic doublet operating at $F/16$ which could expose the film in about 40 minutes. It was a young and brilliant scientist, Joseph M. Petzval, who designed the first calculated photographic objective lens operating at a speed of $F/3.6$ and made photography a practical reality. Photography and microscopy played a major role in developing the art of lens design in the second half of the 19th century. The accurate determination of indices of refraction, development of efficient ray-tracing algorithms, improvement in optical glass fabrication, and advances in the theory of aberration also helped the development of the art of lens design. Lenses like the Planar lens by Paul Rudolph of Zeiss, and the famous Cooke triplet by Dennis Taylor, were designed and fabricated during that period.

Progress in lens design continued in the early part of the 20th century. Much attention was given to establishing efficient methods for calculating lenses. A classic book in lens design is A. E. Conrady's *Applied Optics and Optical Design*, which provided an in-depth study and methodology about the design of lens systems. A major problem was the tedious process of ray-tracing, which was somewhat simplified from trigonometric ray-tracing to an efficient algorithm using tables of logarithms. Nevertheless, calculations were made by hand, and only a few patient and talented people had sufficient expertise in optics and training in specialized calculations to attempt a lens design. The need for better lenses was great, and master lens-designers were sought after and well paid, but the job required a high level of skill and ingenuity. Progress in lens design during this period was further spurred by cinematographic lenses including zoom lenses, telescopes, and lenses for aerial photography.

The advent of mechanical calculators significantly helped lens designers in their arduous ray-tracing calculations. In the early 1950s electronic computers appeared on the scene and were immediately applied to ray-tracing and lens optimization tasks. This relieved the lens-designer from the tedious burden of rote calculations, and further enhanced the art by allowing the programming of a variety of complex functions including automatic lens optimization. The design and performance optimization of intricate optical systems with the aid of electronic computers can be said to have started the modern era of lens design.

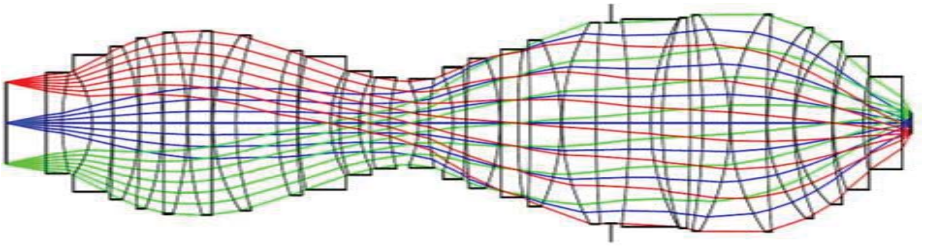

Layout of a complex projection lens for photolithography.

The development of lens-design software in industrial corporations, followed by the advent of commercial lens-design software, such as ACCOS, CodeV, Genii, OSLO and Synopsys, heralded much further progress in the art as it placed design/analysis capabilities within the reach of any engineer who was willing and able to take advantage of the speed and automation now available through these software packages. Lens design courses (offered at the *Institute of Optics* of the University of Rochester by Rudolph Kingslake, at the *Optical Sciences Center* of the University of Arizona by Robert R. Shannon, and, somewhat later, by the professional engineers at various software companies) took the art of lens design from the exclusive domain of large corporations and a few well-trained individuals, into open territory and to a large number of practitioners.

At the core of lens design is one of the most exciting activities of the human mind, entailing original and significant creativity. The lens-designer or optical engineer participates in producing the specification list—that often elusive list which defines a successful new product. Once the performance requirements are set, the engineer has several options to start the design process in order to come up with an optimal yet practical solution. These activities may encompass a routine literature search, embarking on a design from the scratch using first principles, or using, say, genetic algorithms within a lens-design program to automatically develop promising solutions. Most often, successful lenses are produced by clever and experienced designers who not only understand the needs of a given field but also manage to navigate their way through the complex design process to materializing a lens prescription out of theoretical concepts augmented by shear imagination. The lens-designer has at his/her disposal the geometrical arrangement of the various optical elements along with the option of using spherical, aspherical and freeform surfaces, in addition to a vast arsenal of glasses and other optical materials, which he/she can employ to satisfy the performance criteria in accordance with the lens specification.

The image simulation capability of commercial lens-design software is a powerful tool that enables the designer to assess the achievable image quality prior to lens fabrication. For example, the effects of field curvature aberration can be readily modeled and appreciated in the object and its aberrated image in the simulations depicted below.

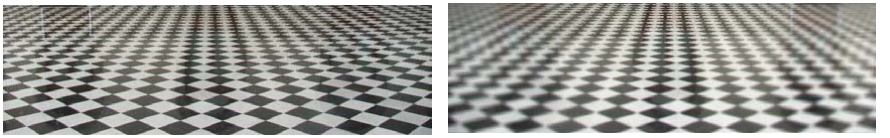

Field curvature aberration produces increasing defocus and loss of contrast away from the field center. (Left) original scene. (Right) simulated image in the presence of field curvature aberration.

Some of the most complex state-of-the art lens systems are designed for photo-lithography, which requires an illumination lens and a projection lens. These lenses are used to fabricate the nanometer-scale elements in electronic integrated circuits. It is quite remarkable that, through the rather mundane process of tracing geometric-optical rays, the designer can predict, in excruciating detail, the performance of such complex lenses which, when built, perform precisely as specified and as expected.

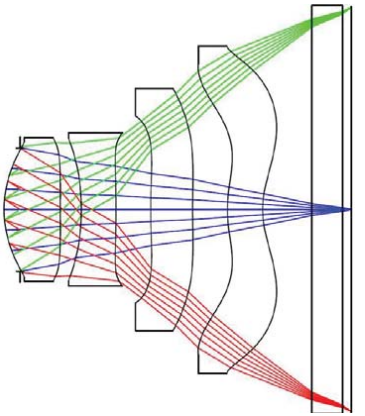

Miniature lens for a mobile phone. Note the highly aspheric lenses for field aberration correction.

An intriguing recent development in the field is the design and construction of powerful compact lenses for use in mobile phones. These lenses incorporate new forms made possible by the advanced field-correction techniques that employ highly aspheric surfaces. Of course, no one can claim that all possible lens shapes and forms have already been designed. New technological needs, harder-to-meet specifications, new optical materials, and novel imaging concepts continuously drive innovations in the fields of lens-design and optical engineering.

Applications that do not require classical image formation but rather require a desirable illumination pattern are equally in great demand. Headlights in cars, LED reflectors, and solar energy concentrators are some of the more frequently encountered examples of such applications. Lenses for imaging and non-imaging applications make optical design a rich and exciting field.

One of the best and most comprehensive curricula in optical design is currently being offered at the *College of Optical Sciences* of the University of Arizona. Courses in basic geometrical optics, introductory and advanced lens design, illumination optics, and applications

of lens-design to a variety of fields are an important part of the curriculum. Students learn optical design using modern software provided by the leading optical design software companies.

The field of optical design is old and new at the same time. What makes it new, in addition to the availability of superb software packages for modeling highly complex optical systems, is the explosive growth and incessant demand arising from novel and demanding applications. In today's high-technology workplace, there exist numerous job opportunities for optical designers as their expertise are sought by small and large companies alike. Optical design as an exciting and rewarding field of human endeavor is indeed alive and prosperous.

Further Reading

1. R. Kingslake and R. Barry Johnson, *Lens Design Fundamentals*, Elsevier, Academic Press, SPIE Press, 2010.
2. R. R. Shannon, *The Art and Science of Optical Design*, Cambridge University Press, 1997.

José Sasián is a professor at the College of Optical Sciences of the University of Arizona. His research interests are in the areas of lens design, novel methods for aberration correction, illumination optics, aspheric surfaces, optical testing methods and modeling, optics for lithography, microscope design, visual optics, light in gemstones, art in optics and optics in art, and modeling of light propagation in optical systems. Dr. Sasián obtained a B.Sc. From the University of Mexico (UNAM) in 1982, and a Ph.D. degree from the University of Arizona in 1988. He is a Fellow of the Optical Society of America (OSA), and of the International Society for Optical Engineering (SPIE). He is also a lifetime member of the Optical Society of India. Professor Sasián has published over 100 technical papers and is the author of the book "*Introduction to Aberrations in Optical Imaging Systems*," published by Cambridge University Press in 2013.

Baboquivari Peak is one of the most conspicuous mountains near Tucson. The 7730-foot-high summit can be reached by a multi-pitch technical climb. This is one of the few technical climbs of a major peak in Southern Arizona.

Photo Courtesy of Brian Anderson

Space Missions and the Optical Sciences Center

Peter H. Smith

The sixties represented the beginning of the Space Era and the Optical Sciences Center (OSC) was part of this exciting time in close collaboration with the Lunar and Planetary Laboratory (LPL) directly across the Mall. Personally, I had just arrived in January 1975 anxious to continue my involvement in Space Optics. Coming from five years at the University of Hawaii's Institute for Astronomy where we designed, built and operated a UV spectrometer that was launched into space on a sounding rocket from White Sands, NM to observe solar prominences. This small program had all the elements of much larger space projects and served as an excellent apprenticeship for a young scientist.

Pioneer 10/11 Jupiter Encounters. The Pioneer project had just experiencing a second flyby of Jupiter when I arrived in Tucson. Dr. William Swindell led the OSC team that was tasked with creating images from the Imaging PhotoPolarimeter (IPP) data tapes (7 track!). Pioneer had successfully imaged the planet and its environment for approximately six weeks from first approach through the closest approach and during the departure. Both Pioneers returned large volume of data and the team was quite busy making hard copies. As a member of Swindell's group, my task was to apply image-processing techniques to the data to bring out the subtle features.

The IPP had begun many years before under the guidance of Dr. Tom Gehrels, a professor in the Lunar and Planetary Laboratory, who became the Principal Investigator (PI). He had been studying the polarization of light reflected from solar system objects and wanted a platform outside of the atmosphere. Partnering with Dr. Samuel Pellecori, a graduate of OSC, they designed the IPP and proposed it for the Pioneer mission; it was selected for flight from among 150 instrument proposals in 1970. The Pioneer 10 was launched from Cape Canaveral on March 3, 1972 and closest approach to Jupiter was on December 4, 1973. This became the first spacecraft to successfully traverse the asteroid belt and enter the Jovian environment. Pioneer 11 shortly followed on April 6, 1973 and reached Jupiter on December 2, 1974.

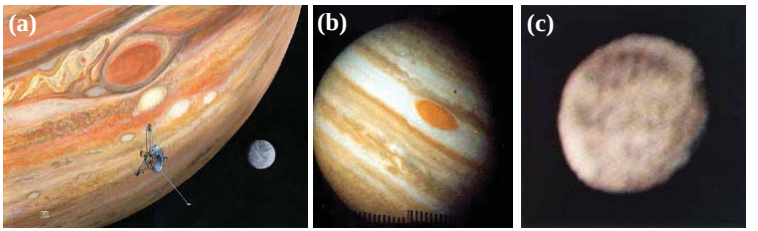

Fig.1. (a) Artist's drawing showing the Pioneer spacecraft during its closest approach to Jupiter. Note the Great Red Spot. (b) Pioneer image of Jupiter showing the bands and rings. Io can be seen with its shadow. (c) Pioneer image of Ganymede not quite able to distinguish the surface features.

During the flybys, objects were imaged through a 25-mm-diameter lens onto a small aperture and then divided into S and P polarization components through a Wollaston prism before being finally split apart through dichroic filters into two wavelength bands red (640 nm) and blue (440 nm). Thus, four detectors were needed to capture the data sets, each one was essentially a one-pixel camera. An image was created using a spin-scan technique taking

advantage of the spacecraft's spin stabilization and adjusting the clock angle (the angle between the lens optical axis and the spacecraft spin axis) for pointing. It was naturally important to limit the data-taking period to the proper portion of the spin cycle. Sometimes the clock angle was stepped to create an image, other occasions would allow the relative motions of the spacecraft and object to scan the image.

Unlike a normal framing camera every pixel is exposed at a different time, being on a moving platform the geometry of the images was often severely distorted especially during the high-speed, close flybys. We called the images banana plots and developed methods for proper geometric reconstruction. However, there is a great advantage for imaging with a single pixel—all parts of the image have the same radiometric properties, there are no bad pixels or flat fielding effects. Furthermore, once the data is returned to Earth, images are created by reversing the process. Photographic film or paper attached to a drum is slowly rotated while a light source modulated by the pixel intensity is scanned along its length. The small group who were tasked with converting digital tapes containing the image data to hardcopy consisted of Ed Beshore, Joe Gotobed, Rob Kingston, and Rod Norden. The photographic processing went though Gil McLaughlin's photographic studio and keeping us all on budget was Charlie Blenman.

The photometry and polarimetry was analyzed across the street at the Lunar and Planetary Lab by Tom Gehrels' team. The primary scientist was Martin Tomasko along with Lyn Doose and supported by co-investigator Charles Kenknight, Del Castillo, and Lonnie Baker. The high phase angle observations not possible from Earth gave important clues to the structure of the Jovian atmosphere.

Several degrees were earned by using the Pioneer Jupiter data. I published a paper in Icarus measuring the diameters of the four Galilean Satellites with an accuracy of about 0.1 pixels. This paper was later accepted as a masters thesis. Lyn Doose wrote his doctoral dissertation on the observations of Jupiter's famous great red spot. Cliff Stoll also did a thesis on the photometry of the belts and zones that make up the banded appearance of Jupiter. Robert West, now at JPL, also used some of the Pioneer data in his dissertation.

Pioneer 11: Saturn Encounter. By adjusting the trajectory of the Jovian encounter, Pioneer 11 was sling shot, using the immense Jovian gravity and orbital speed, into an orbit toward Saturn reaching it on September 1, 1979. It took nearly five years to get from Jupiter to Saturn because the planets were in nearly opposite positions in their orbits around the Sun.

The mission was operated from a building at the Ames Research Center in Mountain View, CA. An invaluable aid in operating the IPP was a display system designed and built by Ralph Baker of OSC. He called it the Pioneer Image Converter System, or PICS, and it was used to convert the digital images to analog and then speed up the data rate so that the images could be displayed in real time on a TV monitor. In order to give the impression of true color, a green channel was synthesized from the blue and red data sets.

The IPP team from the UA led by Tom Gehrels encamped near Ames for 6 weeks. The one-way light time to Saturn was approximately 1.5 hours and commands were processed on arrival at the spacecraft and the data immediately returned. Therefore, the uplink group sending commands according to the master list were sitting next to the downlink group who were receiving data and looking for any errors—close in space but separated by 3 hours in time. Once the data were received and verified they were displayed on the PICS video screens. We worked three shifts during the closest approach so as not to lose any opportunities for important views from angles unachievable from Earth.

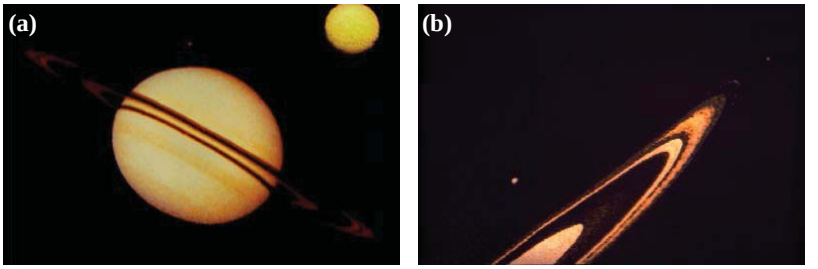

Fig.2. (a) A backlit view of Saturn from the Pioneer flyby. The gaps in the rings appear bright unlike our normal Earth view that show the rings as bright and the gaps dark. Titan has been added to this frame. (b) The F-ring discovery image. Starting from the upper right, the faint dot is Epimetheus, then comes a very faint, broken F-ring before the outer edge of the A-ring. The bright area at the bottom of the frame is the edge of the B-ring.

Observing the ring system while backlit gave an inverse image of the rings with bright gaps and dark bands. But the most exciting parts of the encounter were the closest views of the rings. As the images began to appear on the screen, a bright dot was seen, then the beginning of the ring system. However, it was not the edge of the A-ring that we were expecting to see; it was a brand new ring that had never been seen before. We called it the F-ring. Searching our catalog of Saturnian satellites none could be found that would explain the dot, it was a new object dubbed Epimetheus. Later it turned out to have been seen from the ground, but not part of our catalog. This object is not alone as a second satellite, named Janus, shares its orbital parameters.

Pioneer Venus: The Large Probe. On December 9, 1978, the Pioneer Venus Large Probe entered the atmosphere of Venus. First it decelerated using its aeroshell, thereupon, it deployed a parachute and slowly descended through the thick atmosphere to the superheated surface. On board was an experiment named the Large Probe Solar Flux Radiometer (LSFR), an experiment developed at the UA jointly between the Lunar and Planetary Lab with Dr. Martin Tomasko as the PI and the Optical Sciences Center, where co-investigator Dr. William Wolfe contributed to the optical design and the calibration strategy.

Fig.3. The Pioneer Venus Multi-probe delivery spacecraft. The large cone-shape in the middle is the large probe that carried the Solar Flux Radiometer to the surface of Venus.

The scientific goals of the instrument were to determine where in the deep atmosphere solar energy was being absorbed in order to explain the high temperatures that had been measured by Russian probes. To accomplish this goal, three upward-looking channels were spaced at convenient angles so that the downward solar flux could be integrated. Two downward-looking channels were used to retrieve the upward flux. The difference between the up and down fluxes, or the net flux, was a measure of the total heating below the altitude of the measurement. The slope of the net flux therefore constrained the altitudes where heating occurred. Balancing the heating with the thermal radiative cooling was an additional calculation that explained the temperature profile and could constrain the mixing ratio of water in the atmosphere.

The amazing result of the experiment is that globally only about 2.5% of the incident sunlight is absorbed in the ground. Even so, the opacity of the atmosphere in the infra-red caused by CO_2 plus a small amount of water combined with the thick clouds traps this heat and raises the temperature near the surface to 462°C (863°F).

Early in the development cycle in 1973-4, James Palmer filled the role of chief engineer working with the science team to finalize the opto-mechanical design. This was no easy task given the extreme environmental conditions that Venus provides. His work on the design and calibration of the LSFR under the guidance of Dr. Wolfe led to his dissertation that was completed in 1978.

Others who contributed to the design and construction of the instrument were Dr. Arthur Clements, Arthur G. Bell, Charles Blenman, Lang Brod, Alan Holmes, Roger Kinnard and Even Rosen. Supporting Dr. Tomasko were Dr. Lyn Doose and myself (now an employee of LPL). One of the major challenges facing the team was the design and construction of the five light pipes that transferred the light deep within the instrument where the detector array was cooled by a phase-change material. These tiny glass tubes with field stops deposited on their ends were made in the OSC optics shop.

Other Space Missions. In the late eighties, Martin Tomasko and William Wolfe began work that led to proposing a Descent Imager/Spectral Radiometer (DISR) for the Huygens Probe destined to enter Titan's atmosphere and parachute to the surface in January 2005. The probe, built in Europe by the European Space Agency, was carried to the Saturnian system aboard the CASSINI spacecraft and the spacecraft both released the probe on target for the Titan encounter and acted as the communications relay as it flew by the satellite. This long-term project required an extremely complex opto-mechanical and electrical design and Tomasko sought the help of Lockheed Martin in Denver to take responsibility for the design and construction of the instrument.

The sensors for the instrument were provided by European colleagues in Germany (CCD focal plane array) and France (IR senor package). These partnership proved very valuable and helped in proposing future missions. In fact, the German CCD sensor and some of the optical designs became the basis for a Mars Pathfinder camera called IMP and led by myself as PI. The proposal was accepted in 1993 and the mission returned data from the surface of Mars starting on July 4, 1997. The public found this mission very exciting as a small rover called Sojourner was driven from rock to rock exploring the alien landscape.

I was fortunate to lead a series of instrument development projects on missions to Mars, but there was little OSC participation. One student, Brent Bos, received his PhD in Optical Sciences by analyzing the performance of a Robotic Arm Camera (RAC) that became the basis for his long career working with the James Webb Space Telescope at Goddard Space flight Center.

Fig.4. A frontal view of the Descent Imager on the Huygens Probe that landed on Titan in January 2005. There are 13 different optical instrument crammed into this small space along with a calibration system.

Recently, after two failed proposal attempts, LPL, first led by Michael Drake and now led by Dante Lauretta after Drake's passing, won a New Frontiers mission to return a sample from an asteroid. The mission, named OSIRIS-REx, is set to launch in 2016 and approach asteroid Bennu in 2019, grabbing a small sample and returning it safely to Earth in 2023. The UA proposed to build the camera system (OCAMS) with the largest element an 8″ telescope being designed and built at OSC. Early in the partnership, Jim Burge and Marty Valente led the OSC effort, now Rongguang Liang is taking over as science lead. As of this writing, the telescope, called PolyCam, is being tested as an engineering model. Soon the flight model design will be released for construction and testing before delivery in the summer of 2015.

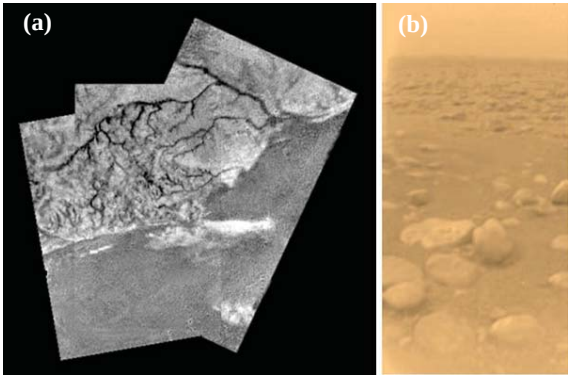

Fig.5. (a) An intriguing view of a hillside on the surface of Titan with a dark-toned river system that probably flows with methane during its rainy season. There appears to be a lakebed that accepts the flow from the streams. (b) Huygens landed inside the lakebed and took this frame from the surface. Notice the rounded river rock that is likely composed of water ice that would be rock hard at the freezing surface temperatures.

Thus, OSC (now the College of Optical Sciences) has been a major player in many space instruments from the beginning of the Space Era. The College is continuing in this tradition even today, and has now formed a logical partnership with the Steward Observatory as well as the LPL space group. Together we provide the talent that previously was found only in large aerospace companies.

Fig.6. An image of Yogi Rock with the Sojourner Rover measuring its composition. The two-toned appearance is caused by the reddish sky illuminating one side and the bright Sun the other.

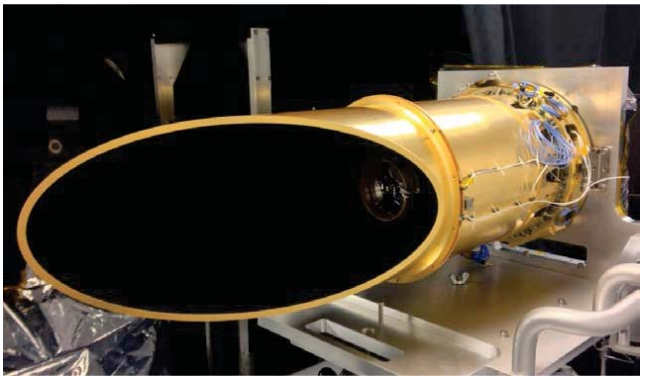

Fig.7. The PolyCam designed and built at the College of Optical Sciences as part of the OSIRIS-REx Mission to return samples from asteroid Bennu in about a decade.

Dr. Peter Smith is a Professor Emeritus of Planetary Sciences at the University of Arizona and held the Thomas R. Brown Distinguished Chair of Integrated Science. His career spans four decades during which he has participated in many space missions to various planets in the solar system. Combining a background in optical sciences with a deep interest in geology and planetary atmospheres, Smith has contributed to cameras that have flown to Venus, Mars, Jupiter, and Titan. In 1997 his camera on board the Mars Pathfinder lander returned exquisite pictures of the dry, rocky plains in Chryse Planitia. The world watched as the team drove a small rover around the spacecraft studying the composition of the local rocks and soils. In preparing for his missions Smith has spent summers in the Dry Valleys of Antarctica, lived in a simulated Mars environment on Devon Island, sampled glaciers, explored Icelandic flood plains, and camped in Death Valley. In 2008, Dr. Smith was the Principal Investigator, or leader, of the Phoenix mission to the icy northern plains of Mars. This mission was operated from its science center in Tucson for five months and found that the ice of the northern plains is a potential habitable zone on Mars. He has won numerous awards including the prestigious NASA Exceptional Scientific Achievement Medal. He is an imaging scientist on the OSIRIS-REx mission to return samples from a nearby asteroid. Recently, Dr. Smith started his own company to produce space-qualified cameras.

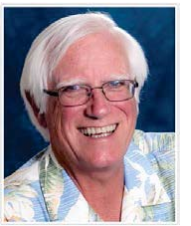

After sunset, twilight provides an intense glowing backdrop to Baboquivari Peak and the mountains west of Tucson.

Photo courtesy of Brian Anderson

Breault Research Organization

Robert Breault

In 1954, at the age of 13, I planned out my life as I sat in contemplation one Saturday morning in my bedroom. It was on that weekend that I decided to go to college to get a BS in mathematics, but not become a "mathematician." I was interested in space because it was an age when many young boys around the world "played" with rockets, rocket engines, and explosive fuels. According to my plan, after graduation with my BS in Math, I would join the Air Force as a fighter pilot, be awarded a PhD in astronomy from the University of Arizona at age 36, and I would design space-based satellites and then become an astronaut. With the launch of Sputnik in 1957, this track became something I just had to do.

While stationed at Nellis Air Force Base in Las Vegas in 1969, I applied to the Department of Astronomy's Steward Observatory. Shortly thereafter I received a call from them saying that their September class was full so they took the liberty of passing my application to a newly-formed *Optical Sciences Center*, and the good news was that the OSC would accept me. I could major in Optics and minor in Astronomy and, come January, I could reverse the major and minor. I thought about it and decided that if I could design telescopes I probably would know enough to use them and I surmised that as a designer I would command a higher salary. Optical Sciences here I come and I had no intention of switching my major come January.

When we arrived in Tucson in August 1969, my wife Judi and I drove by the location of the OSC. They were digging the hole for the first building. I had a sickening feeling. Soon after we arrived Judi landed a job at Burr-Brown as their one and only Information Technology (IT) person. She did the payroll and other studies. Her pay was decent but I also got money from the GI Bill as a Veteran. For the first three years this money was more than enough as we had no kids yet.

Tom Brown, of Burr Brown, was an innovative pioneer in the semiconductor industry. Running a business was never part of my plan until an evening at a Burr-Brown's Christmas Eve party in 1969. Tom was giving his employees a "Thank You" type Christmas address. For some reason I was standing right next to Tom as he spoke. Tom had started his business in his home. He made parts in his sink and in his garage. While Tom was giving his talk I mentally said to myself "If Tom could do this in the semiconductor industry, I could do it in optics." Why I ever thought that, I have no idea. There was no rational reason to think that I could do such a thing. I was there to get my PhD and become an astronaut.

Two years later, Judi was pregnant and was going to have to quit her job. One crisis after another was coming down on us. A few months after my arrival, I was required to take the PhD entrance exam. I failed it twice. So the OSC sadly told me that I was being dropped as a PhD candidate but if I wished I could stay and get a Master's degree. I decided to stay and get the education. I did well in the program, got my Master's degree, and the OSC committee decided to reinstate me into the PhD program. Shortly afterward, in January 1972, on the sidewalk in front of OSC, Prof. Roland Shack stopped me and the gist of the following conversation took place:

"Bob, I heard that you were back in the PhD program and that your wife is pregnant, and I thought that I might be able to help you get a research job here at the Center. I wrote a proposal to NASA urging them to do a stray-light analysis of the Large Space Telescope (now called the Hubble Telescope). The contract has been awarded to us. I was hoping you would accept the position. I have worked it out with the university and the position would be a Research Associate appointment. It will pay $9,100 a year for 20 hours of work a week. A Research Associate is a non-voting faculty position, so your tuition and fees will then only cost you $5 a year, and the position comes with medical coverage for you and your wife. Would you take the appointment?" "Yes sir! I accept." So it went. The work became my dissertation, my company, and my career. For all I have been fortunate to participate in, I thank Prof. Shack.

I was successful at helping in the redesign of the Hubble and in creating a deterministic stray-light analysis program called APART. At the time computers were slow in doing Monte Carlo ray-based analyses, so APART was faster. Both for OSC, and as a private consultant, I took on contracts to do stray-light analyses. I had no competition save for people locked up with Honeywell and ITEK, who were not

allowed to consult. By 1975 I generated many contracts, so the OSC hired two great student assistants for me, Al Greynolds and Steve Lange. By the time I graduated I had a customer base of 120 people. Upon graduating I created the *Breault Research Organization, Inc.* and in short order hired both Al and Steve.

What was obvious to me from my years at the OSC was that Optics and Photonics were Emerging, Enabling, and Enhancing (E^3) disciplines. They had and still have a great future. Just as Optics is enabling and enhancing, I can honestly say that about OSC with regard to my own career. It has enabled and enhanced so many wonderful things in my personal and professional life. The OSC professors are pioneers in their fields and are very good at embedding not only technical knowhow but also innovation into their graduate students. To dramatically prove this, here is a list of distinguished past students from the OSC that BRO has been honored to hire (I apologize for any that I may have missed): Al Greynolds, Dr. Steve Lange, Dr. Phil Stahl, Dr. Kevin Garcia, Dr. Mary Turner, Kristi Helmrich, Paul McClellan, Patricio Durazo, Dr. Steve Johnson, Dr. Marie Cote, Stacy Munger, Robert Crawford, Dr. Bill Kuhn, Dr. Matt Dubin, Dr. Mike Monahan, Dr. Andrew Cheng, Chris Campio, Terry Ferguson, Dr. John Koshel, Dr. Kit Cheong, Dr. Gary Peterson, Michael Stevenson, Joe Shiefman, Joe Barcelo, Jeremie Jackson, Mark Fink, Bill Fogarty, Dr. Michael J. Nofziger, and Dr. Tony Gleckler.

In the 1980s BRO performed many studies for the Strategic Defense Initiative (SDI). When the Cold War was ending, a couple of things became apparent to me. Computers were getting much faster, so Monte Carlo techniques could out-perform APART. Al Greynolds was the brains behind the ASAP program that replaced APART and took BRO safely into the 1990s.

Products. BRO is known as a software and optical engineering company. Nevertheless it has pioneered some significant hardware products: scatterometers, interferometers, parts of some of Raytheon Missile Company's advanced missiles, and unique optical telescopes. After hiring Dr. Phil Stahl in 1985, BRO introduced the first commercial IR phase-shifting interferometer. BRO stayed in the interferometer business until 1988, when I decided to leave the field to WYKO, Phase Shift, and ZYGO, as the cold war was ending and most of our customers were government funded. I decided to go into the commercial illumination software business for which there was no competition. I believed that the market was large.

Software. BRO has been known as the stray light software and analysis house. We developed the software packages APART, ASAP, APEX, REFCAD, GALLOP that calculate the propagation of photons either away from detectors (stray light) or to places (illumination).

Training. For nearly 40 years, BRO has trained hundreds of engineers in stray-light concepts and processes (I have trained over 300 myself), and Dr. Mary Turner has incorporated optical design into our training. She has trained over 4,000 people in optical design.

Dr. Robert Breault is a pioneer in the field of computerized stray-light analysis. He founded *Breault Research Organization* in 1979, an optical engineering software developer and optical engineering consulting company. He has participated in the stray-light analysis of the Hubble Telescope, IRAS, DIRBE, IBSS, ISO, GALILEO, CASSINI, MERIS, CRISTI, XMM, and many military optical sensors. As chairman of the Arizona Optics Cluster since 1992 (also known as the Arizona Optics Industry Association – AOIA), he has demonstrated an ability to bring corporate leaders together for common causes. Internationally he has endeavored to create good will between regions with their national political leaders. He has played a role in exporting the concept of regional Clusters—a partnership of regional government agencies, the educational system at all levels, and businesses—in 18 States in the US and into the international arena. He was one of the original five board members of The Competitiveness Institute (TCI), Barcelona, Spain, and VP of the Americas for The Competitiveness Institute during its first two years.

The Tucson region is one of the longest continually occupied areas of the United States, with a history that dates back a few thousand years. Amid a forest of giant Saguaros, petroglyphs from earlier cultures are preserved in the west unit of *Saguaro National Park*, shown here.

Photo Courtesy of Brian Anderson

Thin Film Interference

James C. Wyant

If you have ever noticed a spectrum of colors produced by a soap bubble, you have observed the colors produced by thin film interference. Other common examples of thin film interference are the colors seen looking at the oily film on a water puddle in a parking lot or the streaks of color on a car windshield shortly after a windshield wiper has swiped it. Thin film interference occurs when incident light waves reflected by the upper and lower surfaces of a thin film interfere with one another. The thin film interference pattern gives information about the surfaces from which the light waves are reflected including the thickness of the film and the refractive index of the film. Thin films have many commercial applications including anti-reflection coatings on camera or eyeglass lenses and optical filters.

A thin film is a layer of material in the sub-nanometer to micron range. When the light wave strikes the top surface of the film part of the light wave is transmitted and part is reflected. Light that is transmitted reaches the bottom surface and once again part of the light wave is transmitted and part is reflected. The splitting continues as the light makes many passes through the film. The light reflected from the top and bottom surfaces of the thin film will interfere. The reflected light waves from the two surfaces will produce constructive interference when the light waves are in phase and destructive interference when the light waves are exactly out of phase. The degree of constructive or destructive interference between the light waves depends on the difference in their phase. This phase difference in turn depends on the thickness of the thin film, the refractive index of the film, and the angle of incidence of the light wave on the film. In addition, a phase shift may be introduced upon reflection at a thin film surface. The pattern of light that results from this interference can appear either as light and dark bands, or as colorful bands, depending upon the source of the incident light.

When the light incident on a thin film is monochromatic the resulting reflected interference patterns appear as light and dark bands. Light bands correspond to regions at which constructive interference is occurring between the reflected waves and dark bands correspond to destructive interference regions. If the thickness of the film varies from one location to another, the interference may change from constructive to destructive.

The interference patterns that result when the thin film is illuminated with white light are much more interesting. The white light is composed of many different colors where each color has its own wavelength. While the thickness of a film at a given location may be just the correct amount for one wavelength to have constructive interference, other wavelengths will have either complete, or at least partial, destructive interference. The result is that some colors will be enhanced and other colors are diminished. The result is often a very colorful pattern, especially if the thickness of the thin film varies, but never becomes too thick. An excellent example of this is a soap film and soap bubbles.

If a soap film is held vertically as shown in Figure 1, its weight makes it thicker at the bottom than at the top. If the thickness of the soap film is one-fourth the wavelength of the light in the film then the round trip path length in the film is a half wavelength. You might expect the ray reflected from the second surface would return to the front surface 180° out of phase with the light reflected from the front surface and the two waves would cancel each other, but when a transverse wave is reflected from a medium in which its speed is slower (larger refractive index), the wave is inverted and a phase shift of 180° is introduced. As a result, for the soap film the ray reflected from the first surface (air-soap film boundary) is inverted and the ray reflected from the

second surface (soap film-air boundary) is not inverted. Thus, if the thickness of the soap film is one-fourth the wavelength of the light in the film, the two reflected waves are in phase and we have constructive interference.

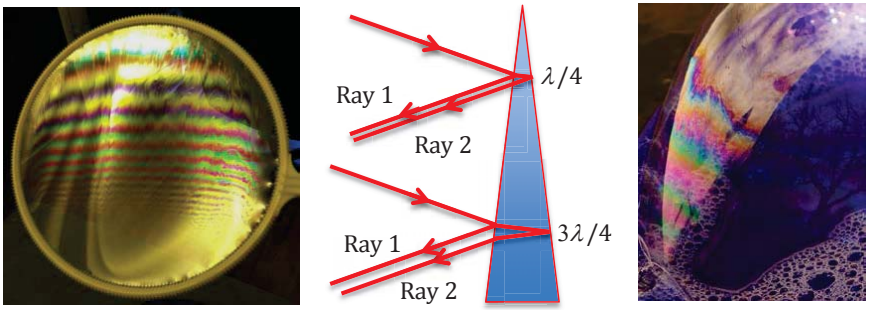

Figure 1: Two soap films with varying with varying thickness. There is constructive interference for thicknesses of $\lambda/4$, $3\lambda/4$, $5\lambda/4$, etc.

If λ is the wavelength of the light in the film and the film thickness, d, satisfies the requirement $d = \lambda/4$, then the color of the light with that wavelength will be most strongly reflected. Since different colors of light have different wavelengths, if the film thickness varies the wavelength requirement will be met at different thickness for different wavelengths. The result is a rainbow of color. Where the film is too thin to produce constructive interference for any wavelength of visible light, the film appears black. If the thickness of the thin film varies the colors that appear on the film repeat. When the film thickness is $3\lambda/4$, the round trip path difference is $6\lambda/4$ and constructive interference occurs for light with a wavelength λ again. Any thickness equal to $1\lambda/4$, $3\lambda/4$, $5\lambda/4$ and so on satisfies the condition for constructive interference for a given wavelength. As the thickness increases it is possible for more than one wavelength to have constructive interference and the colors become less pronounced. Coherence theory is related to how the interference fringe visibility depends on the spectrum of the source and the path difference between the two interfering beams and as the colors become less pronounced we would say that the path difference between the two beams exceeds the coherence length of the source (Hecht).

A thin film is said to be iridescent since the colors we see depend upon the angle of illumination and the angle of viewing. It can be shown that as our viewing angle increases from normal incidence, the wavelength of the pattern we see goes from red to blue (Hecht) because the effective thickness of the thin film decreases as the cosine of the angle from normal incidence.

Figure 2 shows the beautiful colors of a soap bubble. The iridescence of a soap bubble is a result of the light striking the bubble from varied angles. Since the path length varies with the angle of incident light there are varying path differences for the internally and externally reflected rays at different points on the bubble. Thus, even if the soap film is of uniform thickness, different colors can be seen.

It is fun to watch the colors of a soap bubble as they change with time. The colors of a bubble are dependent on the thickness of the film. A bubble becomes thinner and thinner as it dries out (due to evaporation), before finally popping. As the surface film of the bubble becomes increasingly thinner, a change in overall color can be seen. As the bubble film gets very thin

shorter wavelengths are cancelled until finally the film becomes so thin that even the blue wavelength range disappears. Against a black background the bubble surface could appear black.

Whether a wave is inverted depends on the refractive indexes of the mediums involved. If both waves are traveling from a lower to a higher index of refraction, they will both be inverted. If both waves are traveling from a higher to a lower index of refraction, neither will be inverted. In both of these cases the film thickness for constructive interference would be $\lambda/2$, λ, $3\lambda/2$, and so on.

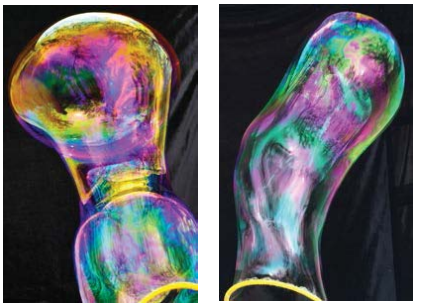

Figure 2. Examples of beautiful colors produced by thin film interference for a soap bubble.

In everyday life we see many examples of thin film interference. Another common example where we see various colors resulting from thin film interference from a thin oily film on a water puddle in a driveway or parking lot as shown in Figure 3. It is interesting to see how the colors change as we move around to change our viewing angle.

There are many examples of thin film interference in nature. For example, light interference occurs in the outer layer of the shells of many beetles as shown in Figure 4 for a Tiger Beetle. The shimmering green is a result of reflection from thin, parallel layers of different materials that differ in refractive index. These thin film parallel layers can be observed using electron microscopes. Many other beetles and butterflies, as well as gemstone opal, exhibit similar thin film interference effects.

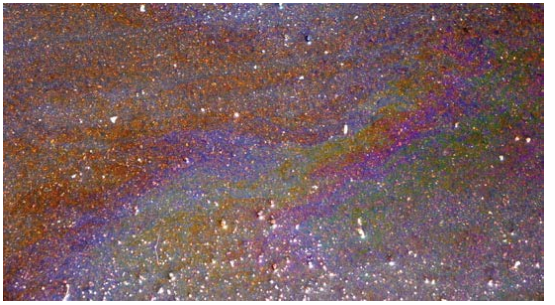

Figure 3. Oil film on water.

Figure 4. Tiger Beetle.

Another example I see nearly every day is shown in Figure 5. A former colleague of mine, Dave Cushing, was an expert in depositing thin films inside a vacuum chamber for making optical filters used in optical systems. Dave also liked to make thin film art by depositing multi-

layer thin films on Mylar, when he purposely caused the thin films to have thickness variations. The example shown in Figure 5 is from a framed sample he gave me that I have on the wall behind my desk. As I walk around my office the colors vary in a spectacular way. This is a great example of art and optics.

There are many applications of thin-films. Thin films are commonly used in anti-reflection coatings, mirrors, and optical filters. They can be engineered to control the amount of light reflected or transmitted at a surface for a given wavelength. These films are created through deposition processes to selectively choose which wavelengths are allowed to transmit through the device. Typical thin film coatings consist of many thin layers of different materials having different refractive indices.

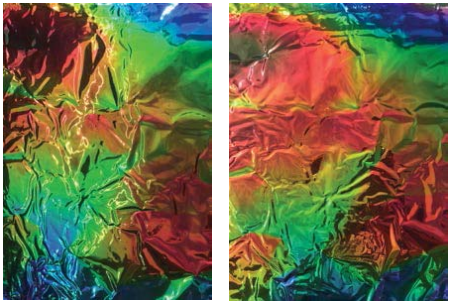

Figure 5. Multilayer thin film as viewed from two different angles.

1. Eugene Hecht, "Optics", Addison-Wesley, 4th edition, 2001.
2. David H. Cushing, "Enhanced Optical Filter Design, Volume: PM201, SPIE Press, 2011.

James C. Wyant is professor emeritus at the *College of Optical Sciences* at the University of Arizona, where he was Director (1999-2005), Dean (2005-2012), and a faculty member since 1974. He received a B.S. in physics from Case Western Reserve University, and M.S. and Ph.D. in Optics from the University of Rochester. He was a founder of the WYKO Corporation and served as its president and board chairman from 1984 to 1997, and he was a founder of the 4D Technology Corporation and currently serves as its board chairman. Wyant is a member of the National Academy of Engineering, a Fellow of OSA (Optical Society of America), SPIE (International Society of Optics and Photonics), and the Optical Society of India, an honorary member of the Optical Society of Korea, and former editor-in-chief of the OSA journal Applied Optics. He was the 2010 president of OSA and the 1986 president of SPIE. He has been a member of the Board of Trustees of Case Western Reserve University since 2010 and the University of Rochester since 2012. Wyant has received several awards for his technical work, including the OSA Joseph Fraunhofer Award; SPIE Gold Medal; SPIE Technology Achievement Award; SPIE Chandra Vikram Award; and four R&D 100 awards. He received the University of Rochester College of Engineering Distinguished Alumnus Award and a Doctorado Honoris Causa from the Instituto Nacional de Astrofisica, Optica y Electronica in Puebla, Mexico. For his entrepreneurial activities, Wyant has received several awards, including Arizona's "Innovator of the Year" Product Award; the Tom Brown Excellence in Entrepreneurship Award; the University of Arizona Technology Innovation Award; and the Arizona Technology Council William F. McWhortor Award.

Kayakers on the mighty Rillito River, as it flows west through the city. Most of the year, the Rillito is completely dry, and even in the rainy season the river usually sustains a trickle. But once every few years, enough rain falls in the mountains in a short period of time, eventually leading to an amazing spectacle that might last only for a day or two. When this happens, kayaking is certainly not a recommended activity, but visiting the river during these events is nevertheless a unique and worthwhile experience.

Photo Courtesy of Brian Anderson

WYKO Corporation

James C. Wyant

There have been many companies started by the College of Optical Sciences personnel. One very successful one was the WYKO Corporation founded on December 27, 1982 to design, manufacture, sell, and service metrology instruments. The founders were two OSC graduates, Chris Koliopoulos and Steve Lange, OSC post-doc Keith Prettyjohns, and one OSC professor, myself, Jim Wyant. For me, starting, growing, and selling WYKO was an unbelievable experience that was more fun than I ever dreamed anything could be.

WYKO grew out of the research my students and I did at the Optical Sciences Center, but its origins actually go back earlier to the Itek Corporation where I went to work in 1968 right after graduate school. At Itek I got involved in what is now called adaptive optics (then called active optics), and in the process I developed ideas for what we now call phase-shifting interferometry. I will not discuss what phase-shifting interferometry is, but for the purpose of this story it is a very good way of getting interferogram data into a computer. At the time I was at Itek, phase-shifting interferometry could not be implemented well with the technology present at the time and it was essentially useless until personal computers and detector arrays became available, so I nearly forgot about it for several years until about 1980.

In 1974 I joined the faculty of the Optical Sciences Center at the University of Arizona and began building a research group. In about 1981 I visited the Union Carbide Y-12 plant in Oak Ridge, Tennessee where they were making diamond-turned mirrors and I saw they were using several interference microscopes to determine the surface finish of the diamond turned mirrors. They would take Polaroid pictures of the interference fringes and then several people analyzed the interferograms using a ruler and pencil to determine how straight the interference fringes were. I figured there had to be a better way of determining the surface finish and I was able to get funding from Los Alamos Scientific Labs to develop an instrument for measuring surface finish. I found a brilliant student, Chris Koliopoulos, to work on the project for his PhD dissertation.

By this time some Reticon detector arrays were available and the Z80 microprocessor had just come on the market, so after a little fumbling and borrowing some interference microscope parts we were able to put together a crude phase-shifting interference microscope system. We had a lot of trouble doing the electronics until a recent PhD graduate from Sheffield University in England, Keith Prettyjohns, contacted me asking for a postdoc position. Keith knew electronics and he had done some work interfacing Reticon solid-state detector arrays to computers. I quickly gave him a postdoc position so he could do the electronics for us and it turned out that Keith was fantastic.

At about the time we got the microscope system to work, a wonderful IBM engineer, Bharat Bhushan, contacted me to see if we had any technology for measuring the surface roughness of magnetic tape. I thought the phase-shifting interference microscope system we had for measuring diamond turned mirrors would work, and it worked so well IBM wanted to buy a system. We told Bharat that we did not want to build another system at the university, but we had started a company called WYKO (WY from my name and KO from Chris Koliopoulos's last name) and that we would sell IBM a system for $100,000, but we needed $60,000 up front to buy the parts. He said OK. (Note that we should have worried about the university owning the IP and we should have gotten permission from the university to sell the system through our company, but in 1982 we didn't worry about such things!)

In December 1982 we received a $60,000 check from IBM as down payment for our first sale. I rushed off to the bank to cash the check but I found out we had a problem. I had told Bharat that we had formed a company *WYKO Optical, Inc*., but we had never actually formed the company. The check was made out to *WYKO Optical, Inc*. and we could not cash the check. We formally started WYKO on December 27, 1982 so we could cash the check.

We rented a small office off campus and our WYKO goals were to have fun and make money. Unfortunately neither was happening. We were not having fun and the money was not flowing in through the door. The problem was that we could not make the IBM system work. We were able to make simpler

systems for other customers so we had some income, but the system using the two dimensional detector array that we sold to IBM would not work well enough for us to deliver it to IBM. Every month I would send a letter to the IBM purchasing person telling him that we were unable to ship that month, but we would ship the next month. The next month I would change the date on the letter and send it again. IBM was extremely nice and they gave us more time and they did not ask for the deposit to be returned. Finally in September 1984 I knew that things had to change. WYKO could not continue this way. We made several changes, but one major change was that I stopped doing research at the university and I went to 20% time at the university (teaching one or two classes per year) and I went to WYKO full time, or at least 80 hours per week. I thought this change would be for 2–5 years, but it continued for 13 years. John Hayes, who had just finished his PhD working for me, also joined WYKO at that time and he was excellent at designing real products.

WYKO changed rapidly. We were able to deliver the system to IBM and we were able to develop an extremely successful phase-shifting-interference microscope, TOPO-3D, shown below. I loved the TOPO-3D so much I have a large photo of it in my living room. I found that by putting my full effort into WYKO I was able to get others to put their full effort into WYKO. People will work extremely hard for you as long as you work as hard as you ask them to work.


TOPO-3D phase-shifting interference microscope.

By then we had moved to a larger second location. Since our name was *WYKO Optical, Inc*., we had a lot of people stopping in to buy eyeglasses. We decided to change the name of the company to *WYKO Corporation*.

Sales and profits were excellent so we developed more products and we moved to our third location that was across the street from the university so I could easily walk to the university to teach a class, and university students could easily work for us. University students make great employees. They are smart and they work hard. It gives you a great opportunity to learn more about the students and you can easily hire the best after they graduate.

During this time the business grew well and we purchased a 110,000 sq ft building that had previously been occupied by IBM. We won several awards such as the SPIE Technology Achievement Award, R&D 100 Award, and several Photonics Spectra Awards. While measuring magnetic media remained our largest market, we added instruments for the automotive and semiconductor industry. It was a great time and we were having so much fun and making so much money!

By the time 1996 came along I was 53 years old and I knew it was time to sell WYKO. While I was still having fun with WYKO, I wanted to go back to the university full time before I became too old and I was tired. I had been working essentially 7 days a week since 1984 and I needed a rest. We talked with 4 companies about buying WYKO and we finally decided to sell to Veeco. Essentially every manufacturer of hard disk drives in the world was using our equipment for evaluating the hard disks and the recording heads and they were using Veeco's process equipment for manufacturing the disks and heads, so it seemed like a good match. We worked out a deal where we would trade WYKO stock for Veeco stock in a tax-free swap. The $60,000 IBM gave us as the down payment on the first system sold was used to fund the starting of WYKO and we never had to go to outside investors. Thus, we owned the company and we did not have to split the profits with investors. We were so lucky! So in July 1997 we completed the deal and I went back to the university.

Starting and growing a company is not for everyone, but for the right people it can be an extremely rewarding experience and I strongly recommend it. In fact doing companies is so much fun that in 2002 John Hayes and I with two friends from California, James Millerd and Neal Brock, started another interferometer company, *4D Technology* (http://www.4dtechnology.com). There are many OSC graduates and students working at 4D. Doing companies is so much fun!

Glass sculpture at the entrance to the College of Optical Sciences. The sculpture was created by Don Cowen from a block of unannealed Pyrex, a portion of a pour by *Corning Glass Works* (circa 1935).

Photo Courtesy of Chris Summitt

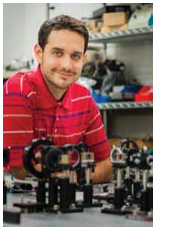

Chris Summitt is a PhD candidate at the College of Optical Sciences. He received his B.S. degrees in Optical Sciences and Applied Mathematics, and his M.S. in Optical Sciences from the University of Arizona. Currently he works with Prof. Yuzuru Takashima in the field of microlithography. Outside of the lab he is a professional photographer with interests ranging from astrophotography to portraiture.

A Student's Experience at the College of Optical Sciences

Kali Wilson

The people I interact with at the *College of Optical Sciences*, both my professors and fellow students, have defined my graduate school experience. From my very first classes, the quality of teaching exceeded my expectations. I am impressed by the time my professors devote to their classes, and the care they take to teach, not only their subject matter, but also the craft of being a scientist. Their willingness to take time away from research to mentor me has made me feel that I, as an aspiring scientist, am a part of the intellectual community rather than simply a cog in the laboratory machine. Even now when I no longer take classes, I have a number of professors with whom I interact on a regular basis to discuss my career aspirations, research directions, and recommendations for good hiking trails.

Student interactions are equally important. My fellow graduate students are my friends and study partners; without whom I would not have survived the gauntlet of the comprehensive exam. In addition, given the wide span of research at the college, I have found my fellow graduate students to be a valuable resource when brainstorming solutions to challenges that arise in the lab. There are two student groups that facilitate this community, providing an environment for both formal and informal student interactions. The Student Optics Chapter (SOCk), affiliated with the *Optical Society of America* (OSA) and the *International Society for Optics & Photonics* (SPIE), runs the biweekly Community Speakers program where topics include anything from modeling zombie population dynamics to presentations of student research. Women in Optics (WiO) hosts informal brownbag lunches with speakers from both industry and academia, and recently hosted a career panel in conjunction with the Industrial Affiliates meeting. SOCk sponsors an annual camping trip to Mount Graham to tour the Large Binocular Telescope and escape the last of the Tucson summer heat. A number of students participate in intramural sports and our soccer teams are often in the finals.

As I progress in the graduate program, I have learned to take advantage of the breadth of expertise found in the college, and have benefited from professors and graduate students taking the time, outside of formal courses, to answer questions about their area of expertise. In addition, as a student of optical physics who strongly considered Physics Ph.D. programs, I have found that the flexibility of the course requirements has allowed me to supplement the breadth of the optics curriculum with a number of physics courses, and to take advantage of the resources of the *Physics Department* in addition to those of the *College of Optical Sciences*.

Science outreach has been a sustaining part of my Optical Sciences experience. In addition to the college's outreach class, both WiO and SOCk offer multiple opportunities for participating in outreach. Once a year, SOCk turns the Optical Sciences building into a science museum for Laser Fun Day, opening the doors to Tucson families for a day of optics demos and lectures. For longer-term outreach, the Adopt a School Mentor program, run by Prof. Scott Tyo, connects student mentors with a teacher at a local bilingual elementary school. Mentors work with the teacher and their class for an entire school year.

Last but not least, the mountain ranges ringing Tucson provide an essential complement to the laboratory and coursework. Mount Lemmon, in particular, provides a year-round playground; as the temperatures in Tucson soar, we hike, bike, climb, and play at higher elevations.

U.A. campus view from the 8th floor patio of the College of Optical Sciences

Photo courtesy of Chris Summitt

College of Optical Sciences
THE UNIVERSITY OF ARIZONA®

The Giant Saguaro cactus is an icon of Tucson and the Sonoran Desert. Here, one of the many trails in the east unit of *Saguaro National Park*, at the eastern edge of Tucson, leads past one striking specimen.

Photo Courtesy of Brian Anderson